Atlas of Endoscopic Ultrasonography

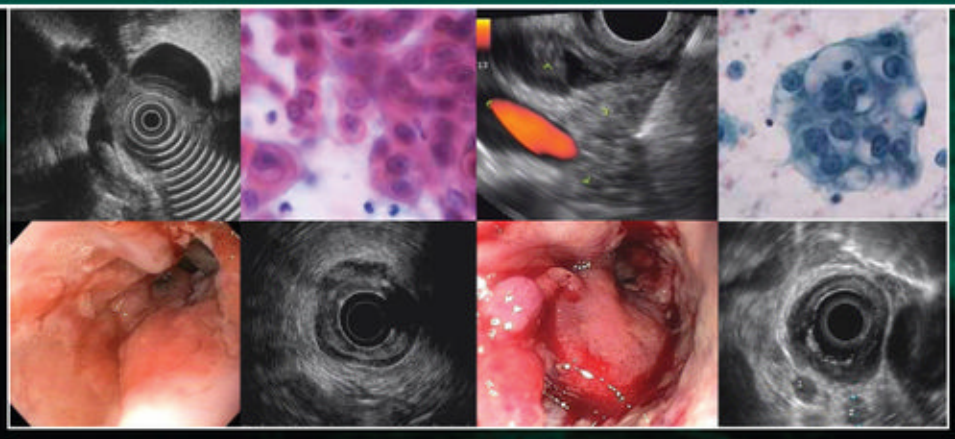

EDITED BY
Frank G. Gress, Thomas J. Savides,
Brenna C. Bounds, and John C. Deutsch

with website

WILEY-BLACKWELL

Atlas of Endoscopic Ultrasonography

Companion DVD-ROM

This book is accompanied by a companion DVD with:

- A database of videos showing procedures described in the book.
- A search feature.
- All videos are referenced in the text at the end of each chapter.

All figures from the book are available for downloading at:
www.wiley.com/go/gress/ultrasonography.

We dedicate this to our families whose support and love allowed us to create this atlas.

Atlas of Endoscopic Ultrasonography

EDITED BY

Frank G. Gress MD, FACP, FACG

Professor of Medicine
Chief, Division of Gastroenterology and Hepatology
State University of New York Downstate Medical Center
Brooklyn, NY, USA

Thomas J. Savides MD

Professor of Clinical Medicine
Division of Gastroenterology
University of California, San Diego
La Jolla, CA, USA

Brenna Casey Bounds MD, FASGE

Director of Endoscopic Training
Massachusetts General Hospital
Harvard Medical School
Boston, MA, USA

John C. Deutsch MD

Essentia Health Care Systems
Duluth, MN, USA

WILEY-BLACKWELL

A John Wiley & Sons, Ltd., Publication

This edition first published 2012 © 2012 by Blackwell Publishing Ltd

Blackwell Publishing was acquired by John Wiley & Sons in February 2007. Blackwell's publishing program has been merged with Wiley's global Scientific, Technical and Medical business to form Wiley-Blackwell.

Registered office: John Wiley & Sons, Ltd, The Atrium, Southern Gate, Chichester, West Sussex, PO19 8SQ, UK

Editorial offices: 9600 Garsington Road, Oxford, OX4 2DQ, UK
The Atrium, Southern Gate, Chichester, West Sussex, PO19 8SQ, UK
350 Main Street, Malden, MA 02148-5020, USA

For details of our global editorial offices, for customer services and for information about how to apply for permission to reuse the copyright material in this book please see our website at www.wiley.com/wiley-blackwell

Library of Congress Cataloging-in-Publication Data

Atlas of endoscopic ultrasonography / edited by Frank G. Gress ... [et al.].
p.; cm.
Includes bibliographical references and index.
ISBN-13: 978-1-4051-5721-6 (hardcover: alk. paper)
ISBN-10: 1-4051-5721-6 (hardcover: alk. paper)
1. Endoscopic ultrasonography–Atlases. 2. Gastrointestinal system–Diseases–Diagnosis–Atlases. 3. Gastrointestinal system–Ultrasonic imaging–Atlases. I. Gress, Frank G.
[DNLM: 1. Endosonography–Atlases. 2. Digestive System–ultrasonography–Atlases. 3. Digestive System Diseases–ultrasonography–Atlases. WN 17]
RC804.E59A85 2011
616.07'543–dc23

2011014520

A catalogue record for this book is available from the British Library.

This book is published in the following electronic formats: ePDF 9781444346275; Wiley Online Library 9781444346305; ePub 9781444346282; Mobi 9781444346299

Set in 9/12pt Meridien by Toppan Best-set Premedia Limited

01 2012

Contents

Part 4 How to Section, 133

Companion DVD-ROM

This book is accompanied by a companion DVD with:

- A database of videos showing procedures described in the book.
- A search feature.
- All videos are referenced in the text at the end of each chapter.

All figures from the book are available for downloading at:
www.wiley.com/go/gress/ultrasonography.

List of Contributors

Douglas G. Adler MD, FACG, AGAF, FASGE
Associate Professor of Medicine
Director of Therapeutic Endoscopy
Gastroenterology and Hepatology
University of Utah School of Medicine
Salt Lake City, UT, USA

Aman Ali MD
Gastroenterology Fellow
Massachusetts General Hospital
Boston, MA, USA

Everson L. A. Artifon MD, PhD, FASGE
Associate Professor of Surgery
University of São Paulo, São Paulo, Brazil
Director, Pancreatic-biliary Endoscopy
Ana Costa Hospital, Santos, Brazil

Andrew J. Bain MD
Clinical Instructor
Division of Gastroenterology
University of California, San Diego
La Jolla, CA, USA

Cynthia Behling MD, PhD
Pacific Rim Pathology Group
Sharp Memorial Hospital
Voluntary Associate Professor of Pathology
University of California, San Diego
San Diego, CA, USA

Manoop S. Bhutani MD, FASGE, FACG, FACP, AGAF
Professor of Medicine, Experimental Diagnostic Imaging and Biomedical Engineering
Director, Endoscopic Research and Development
University of Texas MD Anderson Cancer Center
Houston, TX, USA

Brenna Casey Bounds MD, FASGE
Director of Endoscopic Training
Massachusetts General Hospital
Harvard Medical School
Boston, MA, USA

William R. Brugge MD
Director, Gastrointestinal Endoscopy
Massachusetts General Hospital
Professor of Medicine
Harvard Medical School
Boston, MA, USA

Jonathan M. Buscaglia MD
Director of Advanced Endoscopy
Assistant Professor of Medicine
Stony Brook University Medical Center
State University of New York
Stony Brook, NY, USA

Marc F. Catalano MD
Clinical Associate Professor of Medicine
Medical College of Wisconsin
Pancreatobiliary Services
St. Luke's Medical Center
Milwaukee, WI, USA

Indraneel Chakrabarty MD, MA
Clinical Associate of Medicine
Tufts University School of Medicine
Division of Gastroenterology
Lahey Clinic Medical Center
Burlington, MA, USA

Kenneth J. Chang MD
Professor of Clinical Medicine
Division Chief, Gastroenterology
University of California, Irvine
Irvine, CA, USA

Suresh T. Chari MD
Professor of Medicine
Division of Gastroenterology
Mayo Clinic
Rochester, MN, USA

Silvio Wanderley de Melo Jr. MD
Assistant Professor
Division of Gastroenterology and Hepatology
University of South Alabama
Mobile, AL, USA

John C. Deutsch MD
Essentia Health Care Systems
Duluth, MN, USA

John DeWitt MD, FACG, FACP, FASGE
Associate Professor of Medicine
Co-director, Endoscopic Ultrasound Clinical Program
Division of Gastroenterology and Hepatology
Indiana University Medical Center
Indianapolis, IN, USA

Vinay Dhir MD, DNB
Director Clinical Research and Chief of Endosonography
Institute of Advanced Endoscopy
Mumbai, India

Christoph F. Dietrich MD
Professor, Second Department of Internal Medicine
Caritas-Krankenhaus
Bad Mergentheim, Germany

Christopher J. DiMaio MD
Associate Director, Advanced Endoscopy Fellowship
Gastroenterology and Nutrition Service
Memorial Sloan-Kettering Cancer Center
New York, NY, USA

Mohamad A. Eloubeidi MD, MHS, FASGE, FACP, FACG, AGAF
Professor of Medicine
American University of Beirut School of Medicine
Beirut, Lebanon

Richard A. Erickson MD, FACP, FACG, AGAF
Director, Division of Gastroenterology
Scott and White Clinic and Hospital
Professor of Medicine
Texas A&M Health Science Center
Temple, TX, USA

Douglas O. Faigel MD, FACG, FASGE, AGAF
Professor of Medicine
Division of Gastroenterology and Hepatology
Mayo Clinic College of Medicine
Scottsdale, AZ, USA

Syed M. Abbas Fehmi MD, MSc
Clinical Assistant Professor of Medicine
Division of Gastroenterology
Department of Medicine
University of California, San Diego
La Jolla, CA, USA

David G. Forcione MD
Associate Director of Interventional Endoscopy
Massachusetts General Hospital
Harvard Medical School
Boston, MA, USA

Carlos K. Furuya Jr. MD, MSc
Assistant Professor of Medicine
University of São Paulo School of Medicine
São Paulo, Brazil

Adam J. Goodman MD
Assistant Professor of Medicine
Division of Gastroenterology and Hepatology
State University of New York Downstate Medical Center
Brooklyn, NY, USA

Frank G. Gress MD, FACP, FACG
Professor of Medicine
Chief, Division of Gastroenterology and Hepatology
State University of New York Downstate Medical Center
Brooklyn, NY, USA

Nalini M. Guda MD, FASGE
Clinical Associate Professor of Medicine
University of Wisconsin, School of Medicine and Public Health
Pancreatobiliary Services
St. Luke's Medical Center
Milwaukee, WI, USA

Kapil Gupta MD, MPH
Associate Director, Pancreatic and Biliary Diseases
Interventional Endoscopy
Division of Gastroenterology
Cedars-Sinai Medical Center
Los Angeles, CA, USA

Michael D. Harris MD
Division of Gastroenterology and Hepatology
Department of Medicine
State University of New York at Stony Brook
Stony Brook University Medical Center
Stony Brook, NY, USA

Sammy Ho MD
Assistant Professor of Medicine
Director of Pancreaticobiliary Services and Endoscopic Ultrasound
Division of Gastroenterology
Montefiore Medical Center/AECOM
Bronx, NY, USA

Joo Ha Hwang MD, PhD
Associate Professor of Medicine
Division of Gastroenterology
Department of Medicine
University of Washington
Seattle, WA, USA

Ann Marie Joyce MD
Assistant Professor of Medicine
Tufts University School of Medicine
Director of Endoscopy
Lahey Clinic Medical Center
Burlington, MA, USA

Michel Kahaleh MD, FACG, FASGE
Associate Professor of Medicine
Director Pancreatico-biliary Services
Division of Gastroenterology and Hepatology
University of Virginia Health System
Charlottesville, VA, USA

Sandeep Lakhtakia MD, MNAMS, DM
Consultant
Asian Institute of Gastroenterology
Hyderabad, India

Thuy Anh Le MD
Gastroenterology Fellow
Division of Gastroenterology
University of California, San Diego
La Jolla, CA, USA

Michael J. Levy MD
Consultant
Division of Gastroenterology and Hepatology
Mayo Clinic
Rochester, MN, USA

Jennifer Maranki MD
Clinical Instructor
Division of Gastroenterology and Hepatology
University of Virginia Health System
Charlottesville, VA, USA

Ravinder K. Mittal MD
Professor of Medicine
Division of Gastroenterology
University of California, San Diego
La Jolla, CA, USA

V. Raman Muthusamy MD, FACG, FASGE
Director, Gastroenterology Fellowship Program
Health Sciences Associate Clinical Professor of Medicine
Division of Gastroenterology
Department of Medicine
University of California, Irvine
Irvine, CA, USA

Satish Nagula MD
Director of Endoscopy
Assistant Professor of Medicine
Division of Gastroenterology and Hepatology
State University of New York Stony Brook School of Medicine
Stony Brook, NY, USA

David J. Owens MD
Clinical Instructor
Division of Gastroenterology
University of California, San Diego
La Jolla, CA, USA

M. Babitha Reddy DO, MPH
Gastroenterology Fellow
Lenox Hill Hospital
New York, NY, USA

David H. Robbins MD, MSc
Associate Director
Center for Advanced Therapeutic Endoscopy
Lenox Hill Hospital
New York, NY, USA

Sarah A. Rodriguez MD
Assistant Professor of Medicine
Oregon Health and Science University
Portland, OR, USA

Lucio G. B. Rossini MD
Assistant Professor
Santa Casa of São Paulo School of Medicine
Coordinator, Brazilian–French Center of EUS Research
São Paulo, Brazil

Thomas J. Savides MD
Professor of Clinical Medicine
Division of Gastroenterology
University of California, San Diego
La Jolla, CA, USA

James T. Sing Jr. DO, FACG, AGAF
Assistant Professor of Medicine
Texas A&M University Health Science Center
Director, Endoscopy
Department of Medicine
Scott and White Clinic and Hospital
Texas A&M University Health Science Center
Temple, TX, USA

Raymond S. Tang MD
Clinical Instructor
Division of Gastroenterology
University of California, San Diego
La Jolla, CA, USA

Shyam Varadarajulu MD
Director of Endoscopy
University of Alabama at Birmingham Medical Center
Birmingham, AL, USA

Michael B. Wallace MD, MPH
Professor of Medicine
Division of Gastroenterology and Hepatology
Mayo Clinic College of Medicine
Jacksonville, FL, USA

Maurits J. Wiersema MD
Lutheran Medical Group
Fort Wayne, IN, USA

James L. Wise MD
Essentia Health Care Systems
Duluth, MN, USA

Richard C. K. Wong MD, FASGE, FACG, AGAF, FACP
Professor of Medicine
Case Western Reserve University;
Medical Director, Digestive Health Institute Endoscopy Unit
University Hospitals Case Medical Center
Cleveland, OH, USA

Sam Yoselevitz MD
Clinical Associate of Medicine
Tufts University School of Medicine
Division of Gastroenterology
Lahey Clinic Medical Center
Burlington, MA, USA

Preface

Learning to perform and interpret endoscopic ultrasound (EUS) requires both didactic learning and repetitive exposure to images. We presented detailed aspects of the didactic part of learning in the Gress and Savides textbook *Endoscopic Ultrasonography*. The purpose of this atlas is to allow aspiring endosonographers to visualize numerous examples of images and videos as they improve their pattern recognition of pathologic conditions. Additionally, expert authors have been asked to write a brief, less than 1000 words narrative without references, about the important concepts related to their topics.

This atlas will be of interest not only to those learning EUS, but also those who already perform EUS and want to quickly update their daily use of EUS in terms of diagnosis and therapy. Additionally, the images and videos are in a form which can be easily downloaded from the accompanying DVD in order to give presentations to others.

We are lucky to have added two expert teachers of endosonography, Brenna Bounds and John Deutsch. They bring expertise in EUS video training to the project, as well as contributing significantly from their collections. Without them, this project would not have been possible.

Our contributors are either the "first-generation" pioneers of endosonograpy or "second-generation" protégés of those pioneers. Their collective experience in applying endoscopic ultrasonography in the management of gastrointestinal diseases is unsurpassed. A tremendous amount of effort on the part of each individual author has led to this new atlas. We are deeply grateful to them for their outstanding collaboration.

Frank G. Gress
Thomas J. Savides

1 Normal EUS Anatomy

1 Normal Human Anatomy

John C. Deutsch
Essentia Health Care Systems, Duluth, MN, USA

Introduction

The Visible Human Project at the University of Colorado has generated large volumes of human anatomy data. The original information is captured by slowly abrading away frozen human cadavers in a transaxial manner and capturing the anatomy by digital imaging. The digital data is compiled and then over the years is manipulated by scientists at the University's Center for Human Simulation to allow access to identified cross sections in any plane as well as to models which can be lifted from the data set. Details regarding the Visible Human Project and its applications to gastroenterology and endosonography have been previously described.

This atlas is fortunate to be able to use the interactive anatomy resources developed by Vic Spitzer, Karl Reinig, David Rubenstein, and others to create movies that help explain what takes place during endoscopic ultrasound (EUS) evaluations. Since EUS is a "real-time" examination, it seems reasonable to present this section primarily as "real-time" videos. The videos can be viewed over and over, allowing endosonographers to look not only at the highlighted structures, but also at structures they might visualize during EUS that are not specifically identified on the selected video.

This chapter uses the terms "radial array orientation" to describe planar anatomy which would be found perpendicular to a line going through the digestive tract (as would be generated by a radial array echoendoscope, Figure 1.1) and "linear array orientation" for planar anatomy generated parallel to a line going through the digestive tract (as would be generated by a linear array echoendoscope, Figure 1.2).

Normal EUS anatomy from the esophagus

Radial array orientation (Video 1.1)

Video 1.1 starts with Visible Human Models of the left atrium (purple), trachea and bronchi (light blue), aorta and pulmonary arteries (red), vena cava (dark blue), and the esophagus (brown). A plane is shown passing through the esophagus. This plane contains the transaxial cross-sectional anatomy images which then follow, starting in the oropharynx and going caudally. The upper esophageal sphincter (UES) is identified. As the images proceed distally, the trachea and esophagus can be followed to a point where the brachiocephalicn left carotid and left subclavian arteries are evident just above the aortic arch. Below the aortic arch is the aortopulmonary window. The azygous arch can be seen exiting the superior vena cava (SVC). This occurs just above the tracheal bifurcation. The esophagus, labeled as "E" is surrounded by the descending aorta, the vertebrae, and the trachea. The thoracic duct (not labeled) is visible between the aorta and vertebrae, inferior to the esophagus. Going distally, the pulmonary artery becomes prominent. The region between the right mainstem bronchus (RMB) and left mainstem bronchus (LMB) is the subcarinal space. The video progresses to a level where the left artrium surrounds the superior aspect of the esophagus and then the video ends as the esophagus passes the gastroesophageal junction.

An image plane cross-section of taken from a radial array orientation at the level of the subcarinal space is shown (Figure 1.3).

Linear array orientation (Video 1.2)

Video 1.2 starts with the same models as above (The left atrium [purple], trachea and bronchi [light blue], aorta and

Atlas of Endoscopic Ultrasonography, First Edition. Edited by Frank G. Gress, Thomas J. Savides, Brenna Casey Bounds, John C. Deutsch.

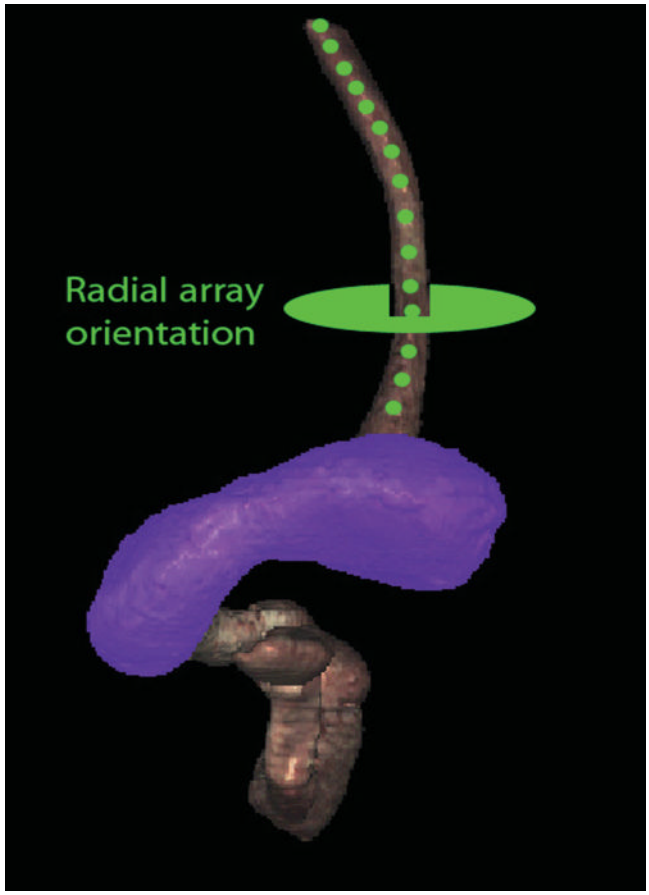

Figure 1.1 Visible Human Model of esophagus, stomach, and duodenum. The green circle shows a plane perpendicular to the axis and is similar to a plane developed during radial array endosonography.

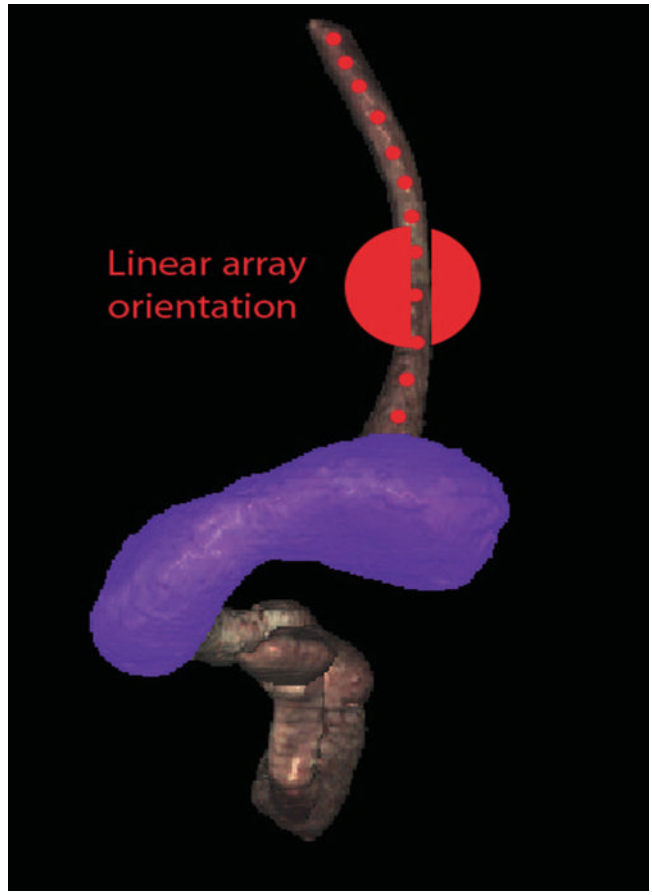

Figure 1.2 Visible Human Model of esophagus, stomach, and duodenum. The red circle shows a plane parallel to the axis and is similar to a plane developed during linear array endosonography.

pulmonary arteries [red], vena cava [dark blue], and the esophagus [brown]). The plane shows potential ways that cross-sectional anatomy can be generated. The video then shows a sagittal image with the descending aorta inferior to the esophagus, much as what is done during linear array EUS. In this orientation the pulmonary artery (PA) and left atrium are superior. The image plane is rotated to bring the left atrium and pulmonary artery to the inferior side of the esophagus. The models are then shown again, and the plane is moved in the caudal and cephalad directions, much as during EUS.

Normal EUS anatomy from the stomach

Radial array orientation (Video 1.3)

Endoscopic ultrasound of the stomach differs from EUS at other sites since the stomach does not constrain the endoscope tightly. It is important to follow anatomical structures (such as in a station approach) to avoid getting lost.

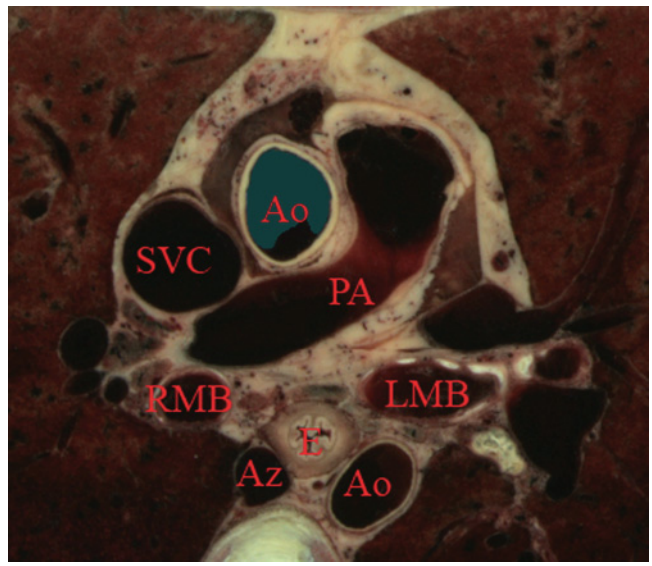

Figure 1.3 Transaxial cross-section of digital anatomy taken at the level of the subcarinal space (Ao = aorta [both ascending, superior in the image, and descending, inferior in the image, are shown]; Az = azygos vein; PA = pulmonary artery; RMB and LMB = right and left main stem bronchi; SVC = superior vena cava).

The video shows models of the stomach, esophagus, duodenum, gallbladder, pancreas (brown), the aorta, splenic artery, hepatic artery and left gastric artery (red), adrenal glands (pink), and splenic, superior mesenteric veins (dark blue) as viewed from behind. A plane is passed that is similar to the image plane generated during radial array EUS. The resultant cross-sectional anatomy starts at the level of the gastroesophageal junction, with the aorta and inferior vena cava (IVC) labeled. The aorta (which is collapsed) is followed, which brings the pancreas and left adrenal gland into view. The first artery that comes off the aorta in the abdomen is the celiac artery. There is a trifurcation into the splenic, hepatic, and left gastric arteries (LGA), although the LGA is generally smaller and difficult to see. It is shown in the video at the "x" just before the bifurcation into the celiac and hepatic arteries as identified.

The superior mesenteric artery (SMA) comes off the aorta just distal to the celiac artery. Various endoscope maneuvers can be used to bring the portal confluence into view, and then the splenic vein can be used as a guide to visualize the pancreas body, left adrenal, kidney, and spleen. The diaphragm can be easily imaged between the kidney and the vertebrae.

Linear array orientation (Video 1.4)

The linear array exam also follows the aorta to the stomach, but, as shown Video 1.4, the image plane across the pancreas is generally obtained through a sweeping motion. The first major gastric landmark is the origin of the celiac artery and SMA from the aorta (Figure 1.4). The superior mesenteric vein (SMV), portal vein, and splenic vein can be used as guides to go back and forth across the pancreas and in the process, the left adrenal, kidney, and spleen can be seen. The splenic artery runs roughly parallel to the splenic vein, but is generally tortuous.

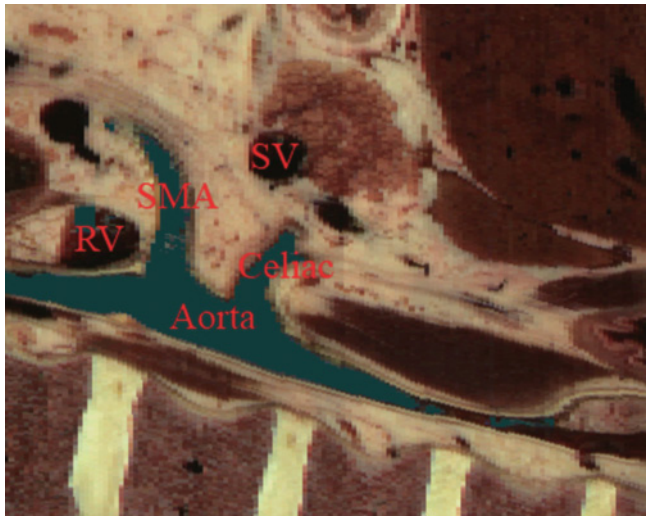

Figure 1.4 Sagital cross-section of digital anatomy at the level of the gastroesophageal junction, similar to a view seen during linear array endoscopic ultrasound (EUS). The celiac and superior mesenteric arteries (SMA) are shown at their insertion into the aorta. The renal vein (RV) is shown adjacent to the SMA and the splenic vein is shown adjacent to the pancreas.

Normal EUS anatomy from the duodenum

Radial array orientation (Video 1.5)

The radial array EUS examination through the duodenum follows a constrained path, but the endoscope can be rotated to put various structures into the inferior aspect of the image plane, as shown in the models of the duodenum, pancreas (brown), portal and superior mesenteric veins (blue), aorta (red), and SMA (silver). There are many structures of interest in a rather small area, and most of the images obtained are from the posterior view, with the liver to the right and the pancreas to the left of the image screen. After leaving the pylorus, the pancreas can be oriented with the tail pointed either to the left or inferiorly, and the splenic vein runs in the same direction as the pancreas. Going through the duodenal bulb, the gastroduodenal artery (GDA) often appears. Without Doppler, the GDA can be confused with the common bile duct (CBD) since these structures are nearly parallel in orientation and are very close to each other. As the apex of the duodenal bulb is reached, the image plane captures a longitudinal view of the CBD and the portal vein. As the descending duodenum is reached, the bile duct is seen in cross-section and the inferior vena cava (IVC) comes into view. As the third part of the duodenum is reached, the image plane rotates in such a way as to give a longitudinal cut through the IVC and then passes underneath the junction of the SMA with the aorta. Branches of the SMV can be found and the renal vein is visible in the "armpit" formed at the insertion of the SMA into the aorta. A special area is then highlighted in Video 1.5. Models show how the gastroduodenal artery and the hepatic artery (in red) relate to the CBD (in orange).

Figure 1.5 shows a model with an image plane and Figure 1.6 shows the resultant planar anatomy, which forms the stack sign – a phenomenon in which the portal vein, CBD, and main pancreatic duct are captured in the same field.

Linear array orientation (Video 1.6)

The linear array exam of the duodenum is an excellent way to see the CBD and pancreatic head. The anatomy is difficult to understand since the endoscope image is tipped into the C-sweep of the duodenum, and then the image plane is swept in various angles, resulting in a cross-sectioning of the CBD and pancreatic duct (PD). The image planes employed can be appreciated from observing the models in the video. The cross-sections obtained can be positioned to first give a

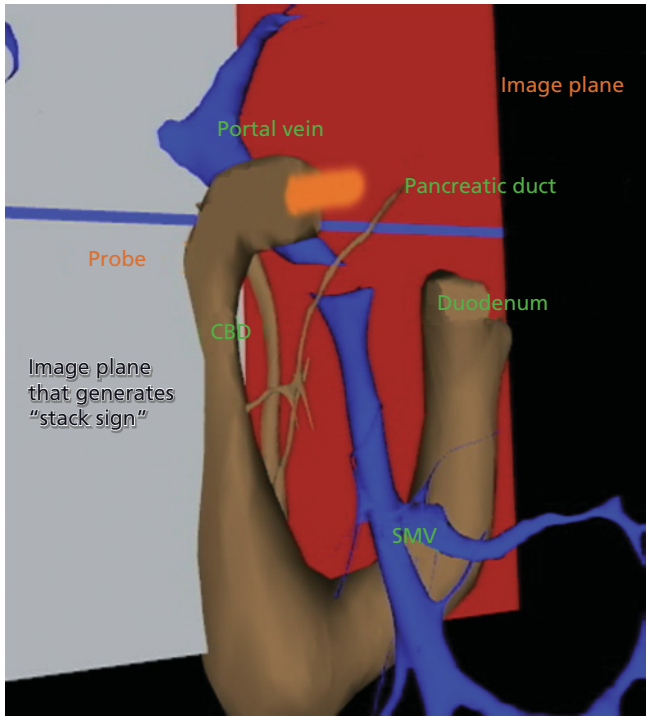

Figure 1.5 Visible Human Model of an image plane that is in the location in which radial array endoscopic ultrasound (EUS) generates the "stack sign", in which the portal vein, common bile duct (CBD), and pancreatic duct are in the same field. A probe in orange is shown going into the proximal duodenum. The superior mesenteric vein (SMV) is also shown.

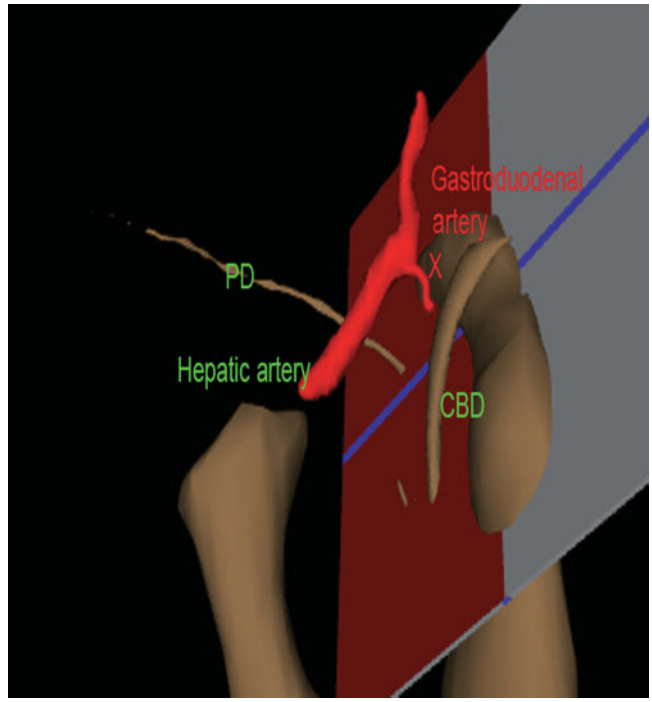

Figure 1.7 Visible Human Model with a plane that is in a location similar to what can be generated during linear array endoscopic ultrasound (EUS), showing the relative position of the gastroduodenal artery, pancreatic duct (PD), hepatic artery, and common bile duct (CBD).

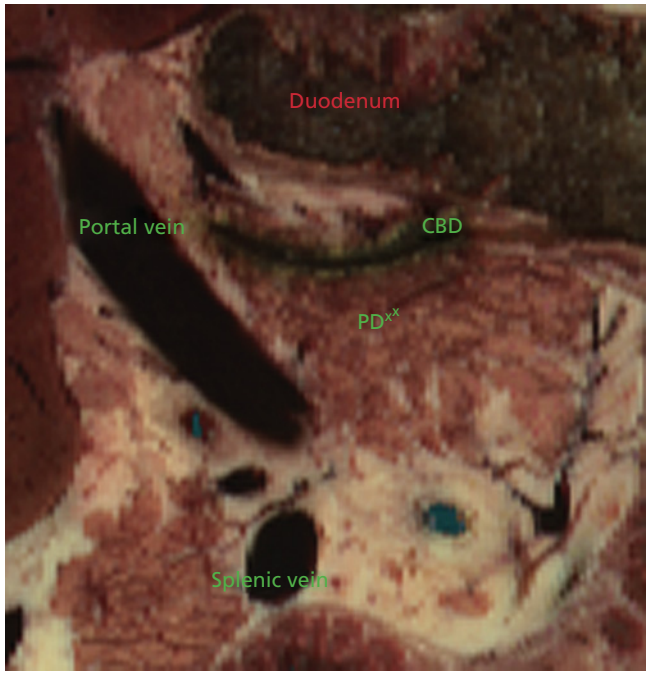

Figure 1.6 The cross-sectional anatomy within the plane shown in Figure 1.3. The common bile duct (CBD), pancreatic duct (PD), and portal vein are all in the same field ("stack sign").

longitudinal view of the CBD and both longitudinal views and cross-sections of the portal vein and SMV.

As seen in the first part of Video 1.6, if the endoscope is in the second part of the duodenum, the bile duct goes to the ampulla away from the transducer and the liver is towards the transducer. If the endoscope is in the duodenal bulb, as shown in the second part of the video, the liver is away from the transducer.

The GDA drapes over the portal vein and can be found most readily using Doppler. Figure 1.7 shows a model and Figure 1.8 the resultant cross-section where the GDA can be found.

Normal EUS anatomy from the rectum

Radial array orientation, male (Video 1.7)

Video 1.7 shows models of various male pelvic structures, starting with the rectum and sigmoid colon, the aorta, and the iliac arteries with internal and external branches. The SMA is included to show the anterior direction of the models. The prostate, bladder, coccyx, and sacrum are added sequentially. A second set of models is then shown which contains the rectum, sigmoid colon prostate, bladder, coccyx,

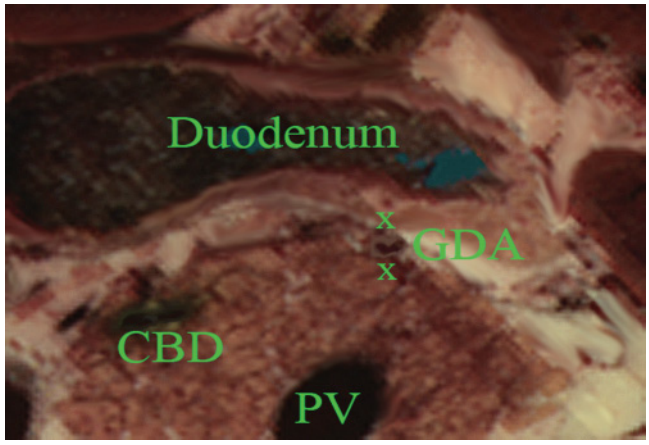

Figure 1.8 Cross-sectional anatomy generated within the plane shown in Figure 1.5. The gastroduodenal artery (GDA) and common bile duct (CBD) are shown with the pancreatic head. The portal vein (PV) is shown near the portal confluence.

sacrum external iliac arteries (red), veins (blue), as well as three-dimensional models of the internal and external anal sphincters. The sphincters and sigmoid colon are then removed.

Planar anatomy in the radial array orientation from the male rectum is then shown, starting distally and moving proximally. The anal sphincters are labeled, followed by the prostate, urethra, levator ani, and coccyx. The sacrum and seminal vesicles are then shown, followed by the right internal iliac artery.

Radial array orientation, female (Video 1.8)

Video 1.8 starts distally at the end of the anal canal. The internal and external sphincters are shown, and residual stool is present in the rectum. Moving proximally, the vagina and urethra are shown, followed by the cervix and bladder.

Linear array orientation, male (Video 1.9)

Video 1.9 starts with a sagittal plane through the pelvis with the body facing the left. The prostate, rectum anal canal, and bladder are identified. The plane is rotated, and the seminal vesicles and internal anal sphincter are labeled. The coccyx and sacrum are apparent at the start and end of the video but are unlabeled.

Linear array orientation, female (Video 1.10)

Video 1.10 starts with a sagittal plane through the pelvis with the body facing the left and slightly face down. The anal canal, rectum, uterus, and bladder are identified. Stool is present in the rectal vault. The plane is rotated, and towards the end of the video the internal anal sphincter (IS) and external anal sphincter (ES) are identified.

Vascular videos

Arterial (Video 1.11)

Video 1.11 shows models of some of the main arteries that are visulaized during endosonography. A close-up view shows the celiac artery with its branches (hepatic, splenic, and left gastric arteries). The gastroduodenal and pancreaoduodenal arteries are shown coming off the hepatic artery. The internal and external iliac arteries are then identified, followed by identification of the arteries associated with the aortic arch (left subclavian, left carotid, brachiocephalic) and the branches of the brachiocephalic (right subclavian and right carotid). Various organs are then placed in the model starting with the esophagus, then pancreas, stomach, and duodenum.

Venous (Video 1.12)

Some of the major veins visualized during endosonography are shown. At first, the vena cava and right artrium are identified, after which, the renal veins and azygos veins are added. The portal system with the portal vein, SMV, splenic vein, and inferior mesenteric vein (not labeled) are placed in blue. The systemic veins are then colored and removed. The pancreas is placed on the portal vein and its branches, showing how the head runs parallel to the SMV and the tail runs parallel to the splenic vein.

Endobronchial ultrasound anatomy (Video 1.13)

Extratracheal anatomy is similar to extraesophageal anatomy and many of the structures seen in the extratrachial spaces are the same as what is seen in the extraesophageal spaces. The endoluminal views of the trachea are oriented so that the membranous trachea is inferior and is splayed wider that the cartilaginous trachea at the level of the carina, putting the right mainstem bronchus (RMB) to the right and the left mainstem bronchus (LMB) to the left (Figure 1.9). As one goes right the bronchus immediately branches superiorly towards the right upper lobe (RUL), and continues straight as bronchus intermedius (BI) (Figure 1.10), which then branches towards the right middle lobe (RML) and right lower lobe (RLL) of the lung (Figure 1.11).

Going left from the carina, one goes down the relatively long left mainstem bronchus until it branches towards the left upper lobe (LUL) and left lower lobe (LLL) of the lung (Figure 1.12). An overview of the bronchial tree is shown in Figure 1.13.

Video 1.13 starts with the cervical trachea. All images are in a linear array orientation as endobronchial ultrasound (EBUS) is exclusively linear. The esophagus is inferior and the brachiocephalic artery and vein are superior. The video begins with rotation of the image plane. The superior part of the plane moves left and the inferior part moves right. This moves the esophagus out of view and brings the left

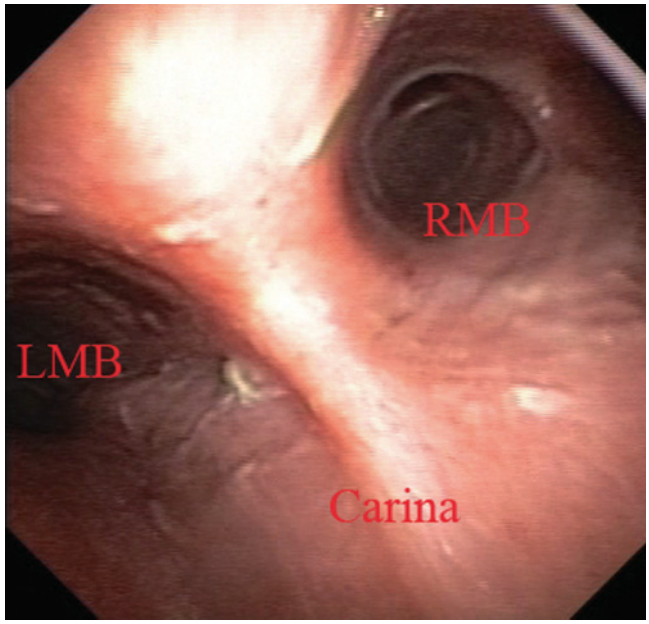

Figure 1.9 Endobronchial view of the carina, showing the right (RMB) and left (LMB) mainstem bronchi.

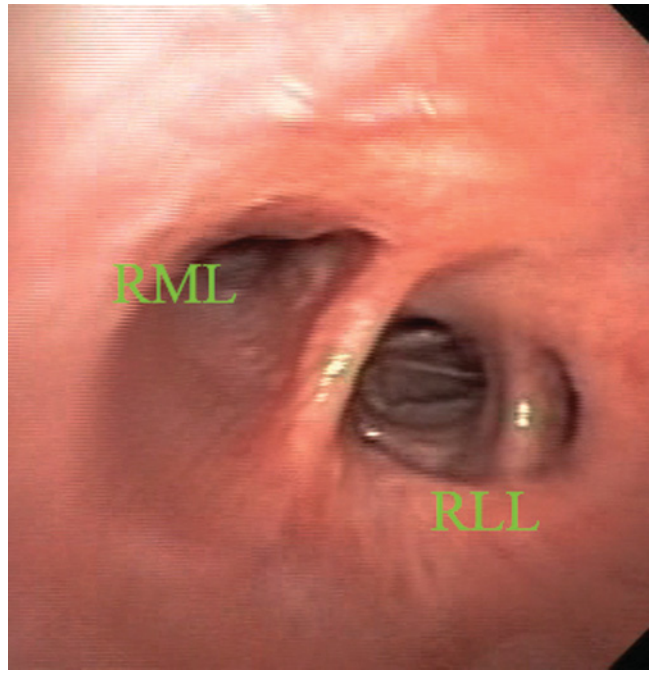

Figure 1.11 Endobronchial view of the bifurcation of the bronchus intermedius towards the right middle lobe (RML) and the right lower lobe (RLL).

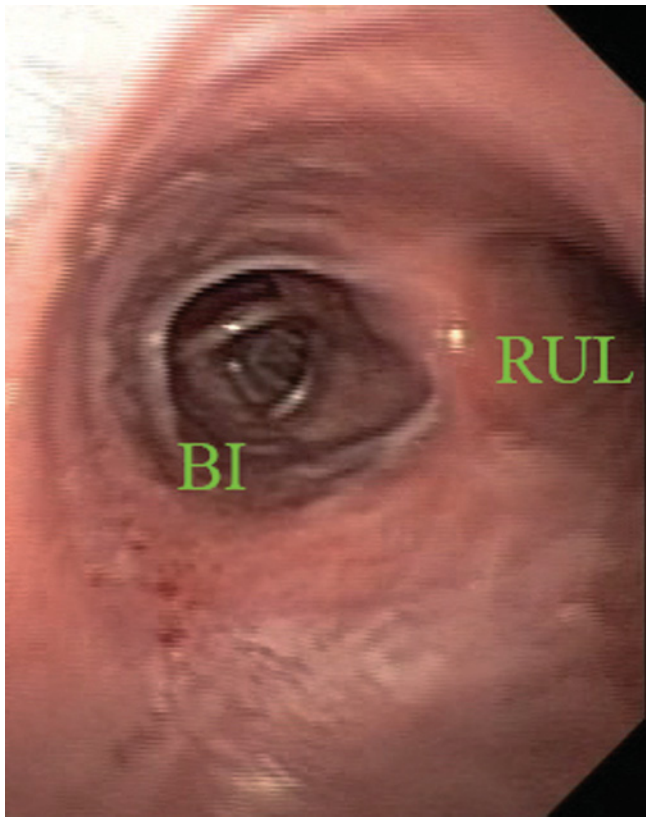

Figure 1.10 Endobronchial view of the first branch of the right mainstem bronchus towards the right upper lobe (RUL) and the bronchus intermedius (BI).

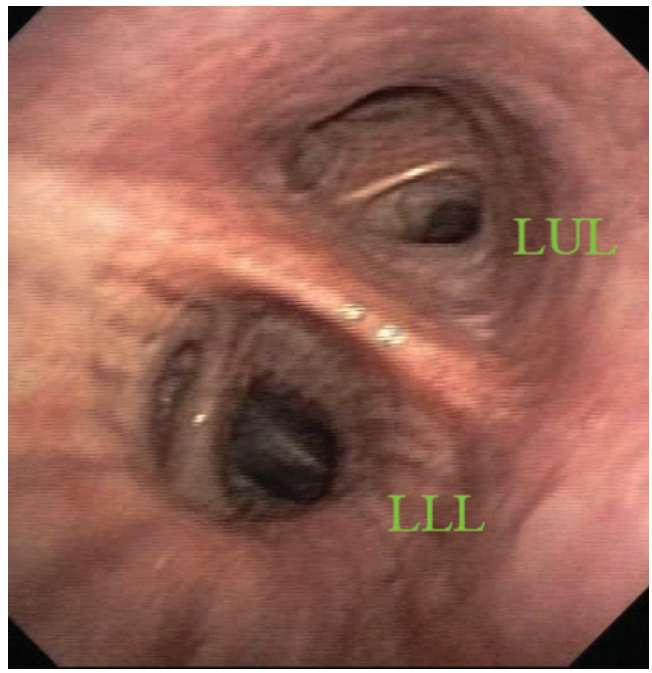

Figure 1.12 Endobronchial view of bifurcation of the left mainstem broncus towards the left upper lobe (LUL) and left lower lobe (LLL).

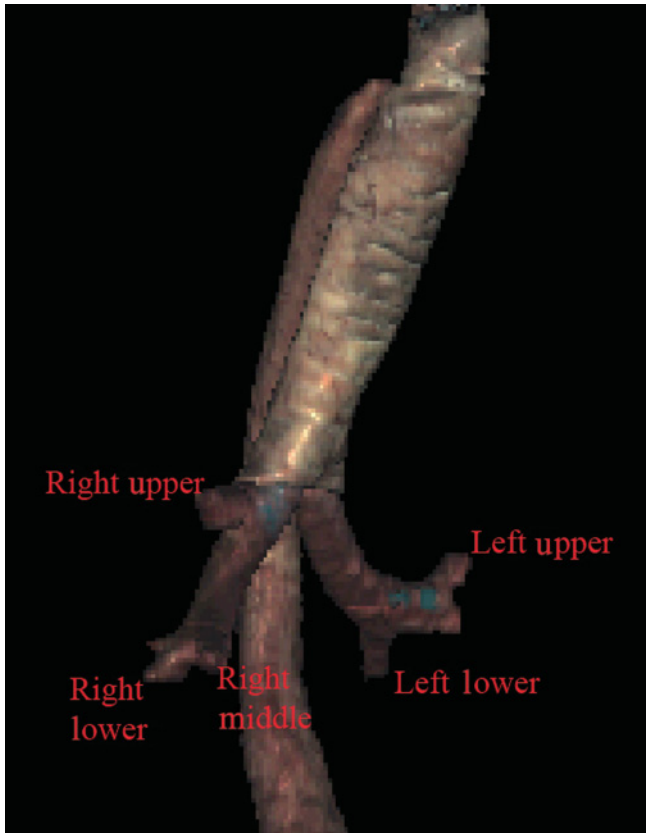

Figure 1.13 A Visible Human Model of the bronchial tree.

subclavian artery and left carotid artery into the inferior part of the image. Eventually, the esophagus is seen in the superior part of the image and, with continued motion, the esophagus again appears inferior to the trachea. At this point, the image plane moves caudally to the carina. The right pulmonary artery, brachiocephalic artery (BA), and left brachiocephalic vein (LBV) are labeled. The plane is again rotated to splay the right (RMB) and left (LMB) mainstem bronchi apart. The plane is then moved to better visualize the right mainstem bronchus, showing the branch to the right upper lobe (RUL), the azygos arch (AzArch), the bronchus intermedius (BI). This same plane shows the relation of the aortic arch (AoArch) and left pulmonary artery to the left mainstem bronchus (LMB). As the plane goes down the right mainstem bronchus/bronchus intermedius (RMB) towards its next bifurcation, the azygos arch (AzAr), right pulmonary artery (RPA), and right pulmonary vein (RPV) are shown.

The plane is brought back to the carina to visualize the left mainstem bronchus (LMB), and the azygous arch (AzAr), aortic arch (AoAr), left pulmonary artery (LPA), and vein (LPV) are identified. The branching to the left upper lobe (LUL) and left lower lobe (LLL) are shown, and the aorta (Ao) and left pulmonary artery are labeled.

Chapter video clips

Video 1.1 Esophageal-related models and cross-sectional anatomy: radial orientation.

Video 1.2 Esophageal-related models and cross-sectional anatomy: linear orientation.

Video 1.3 Gastric-related models and cross-sectional anatomy: radial orientation.

Video 1.4 Gastric-related models and cross-sectional anatomy: linear orientation.

Video 1.5 Duodenal-related models and cross-sectional anatomy: radial orientation.

Video 1.6 Duodenal-related models and cross-sectional anatomy: linear orientation.

Video 1.7 Male rectum-related models and cross-sectional anatomy: radial orientation.

Video 1.8 Male rectum-related cross-sectional anatomy: linear orientation.

Video 1.9 Female rectum-related cross-sectional anatomy: radial orientation.

Video 1.10 Female rectum-related cross-sectional anatomy: linear orientation.

Video 1.11 Arterial models.

Video 1.12 Venous models.

Video 1.13 Bronchial anatomy in a linear orientation.

2 Esophagus: Radial and Linear

James L. Wise and John C. Deutsch
Essentia Health Care Systems, Duluth, MN, USA

Layers of the esophageal wall

Staging the depth of involvement of tumors and the layer of origin of subepithelial masses is an important component of competency in endoscopic ultrasonography (EUS). An intimate knowledge of the normal layers of the esophageal wall is critical for this to be done accurately. The wall of the esophagus has four readily appreciable layers by EUS using standard operating frequencies (5–12 MHz). The layers are seen in concentric, alternating rings of hyper and hypoechoic structures emanating out distally from the tip of the endoscope. Starting with the layers closest to the scope tip, they are as follows:

- Interface echo between the superficial mucosa and water (hyperechoic).
- Deep mucosa (hypoechoic).
- Submucosa plus the acoustic interface between the submucosa and muscularis propria (hyperechoic).
- Muscularis propria minus the acoustic interface between the submucosa and muscularis propria (hypoechoic).

If a higher resolution frequency probe is used, greater number of layers could be visualized as detailed in Chapter 4. The esophagus lacks an obvious fifth layer as there is no serosa.

In our opinion, visualization and discernment of the layers of the esophageal wall is usually best accomplished using radial compared to linear instruments.

Figure 2.1 (a and b) shows the esophageal walls using radial and linear instruments. To help separate the layers, these images include a muscularis mucosae leiomyoma that was subsequently resected. Images show subepithelial hypoechoic lesion in echolayer II as well as in the other defined layers of the esophageal wall.

Normal radial extraesophageal anatomy

Standard examination of the esophagus and mediastinum begins with advancing the radial instrument to the gastroesophageal (GE) junction at or near the squamocolumnar junction. At this level the aorta is seen as an anechoic circular structure in the 5 o'clock position. The descending aorta is kept in this position as all radial mediastinal imaging will then correlate quite nicely with cross-sectional imaging. Other structures visible at the level of the GE junction are the inferior vena cava (IVC) seen between 7 and 9 o'clock and the liver between 6 o'clock and 12 o'clock surrounding the IVC (Figure 2.2).

As the scope is withdrawn, the vena cava moves clockwise and superiorly into the right atrium. The spine soon comes into view adjacent to the descending aorta at 6 o'clock.

Further withdrawal upward to usually around 30–35 cm reveals the anechoic chamber of the left atrium in the 12 o'clock position (Figure 2.3). With this field, relatively slight movement of the scope will reveal the mitral valve (Figure 2.4), aortic root, and the aortic valve (Figure 2.5). In the inferior portion of the field the descending aorta, the spine, the thoracic duct, and a relatively prominent azygos vein can be seen.

As the scope is withdrawn the bronchi come together at the carina. At or just proximal to this level the azygos arch (Figure 2.6) can be identified traveling superiorly and laterally into the superior vena cava. This is also the area of the aortopulmonary (AP) window at approximately 2 o'clock.

The endoscope can be pushed down from here or pulled up slightly from the position of the left atrium to reach the subcarinal space. Of interest in the subcarinal space are the right and left main-stem bronchi seen emanating out as ribbed-

Atlas of Endoscopic Ultrasonography, First Edition. Edited by Frank G. Gress, Thomas J. Savides, Brenna Casey Bounds, John C. Deutsch.

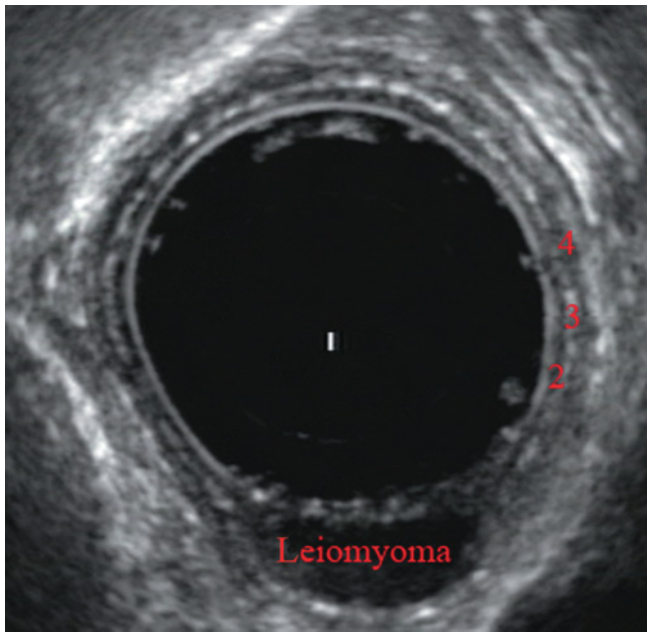

(a)

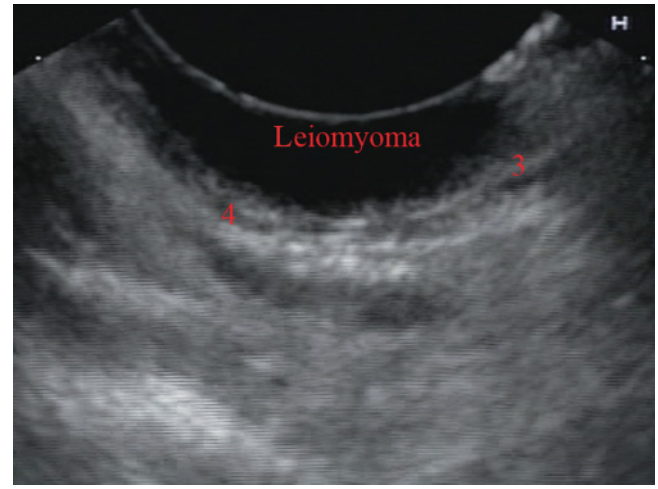

(b)

Figure 2.1 (a) Radial array image of esophageal wall with small echolayer II leiomyoma. (b) Linear array image of esophageal wall with small echolayer II leiomyoma.

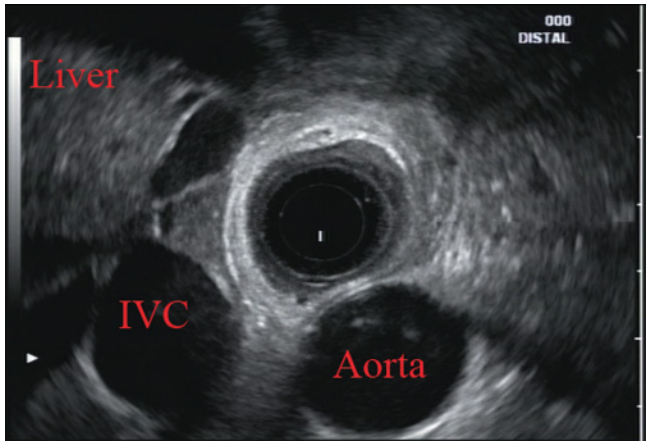

Figure 2.2 Radial array image at gastroesophageal (GE) junction (IVC = inferior vena cava).

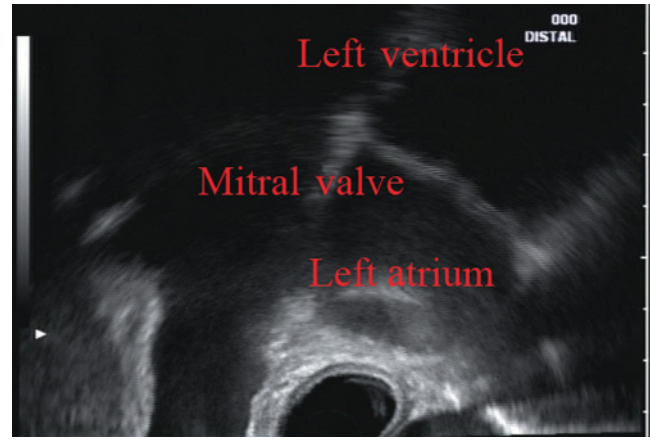

Figure 2.4 Radial array image at the level of the mitral valve.

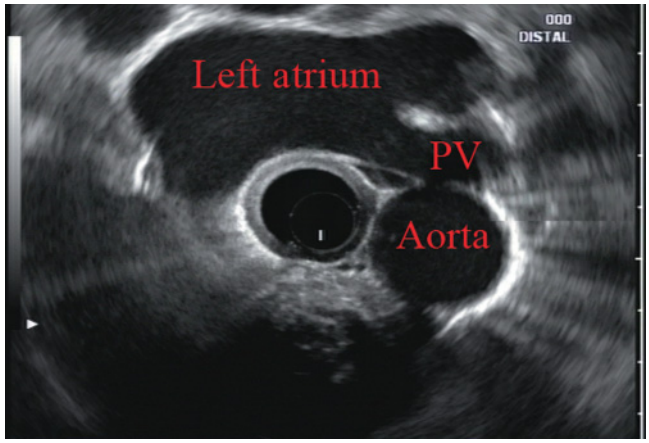

Figure 2.3 Radial array image at the level of the left atrium (PV = pulmonary vein).

Figure 2.5 Radial array image at the level of the aortic root.

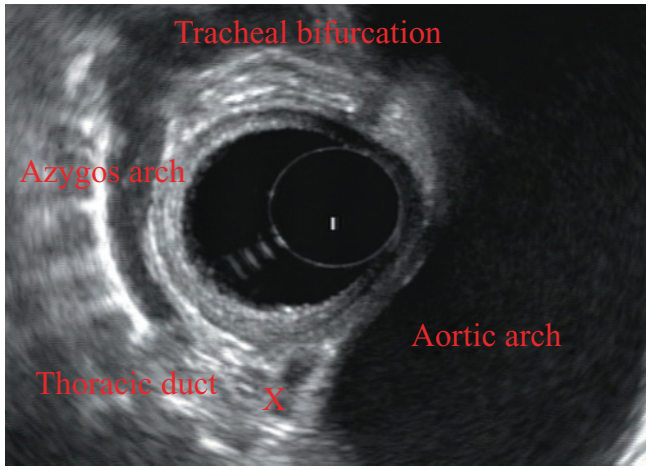

Figure 2.6 Radial array image at the level of the azygos arch.

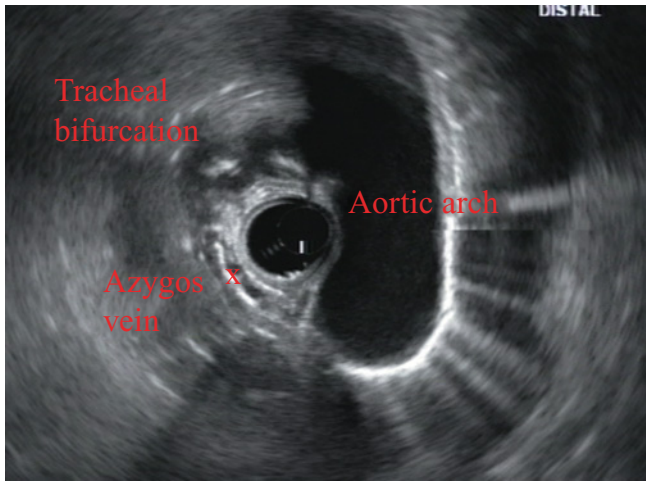

Figure 2.7 Radial array image at the mid aortic arch.

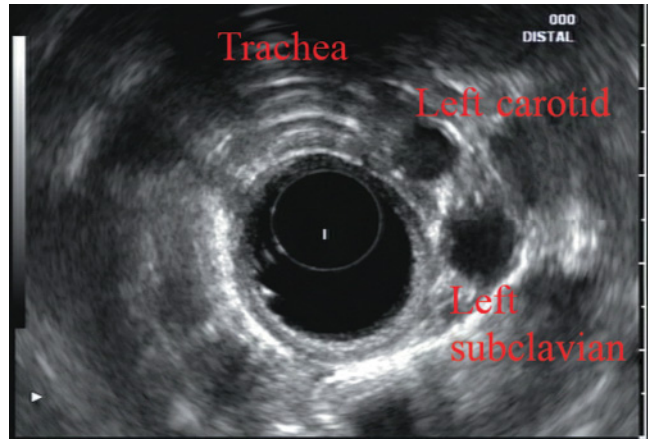

Figure 2.8 Radial array image at the level of the left carotid and subclavian arteries.

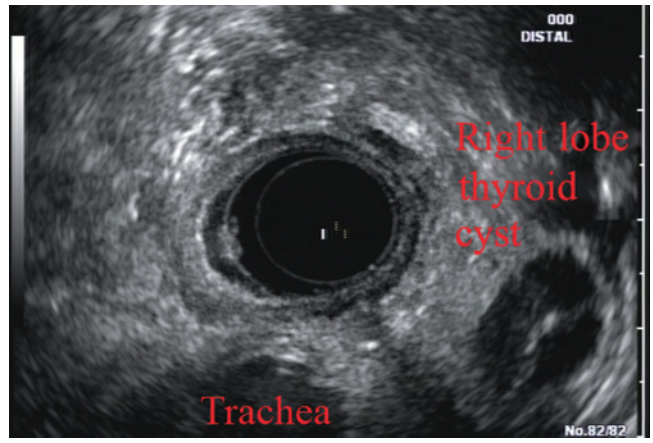

Figure 2.9 Radial array image at the level of the thyroid.

like air-filled structures. As many have suggested, these can be imagined to have the appearance of two headlights.

More proximally from the area at the AP window the aorta elongates and forms the aortic arch (Figure 2.7). This usually creates a semicircle on the entire right side of the image correlating to the left-sided arch. However, with usual orientation the aorta should not cross the midline. The left carotid and left subclavian artery can easily be seen to leave the aortic arch as small round structures on the right side of the image (Figure 2.8). The brachiocephalic artery can some times be seen as well superior to the carotid on the right. As the scope is withdrawn the thyroid comes into view. For example, on the image to the right a prominent thyroid can be seen with a cystic structure within it (Figure 2.9).

Normal linear thoracic anatomy

The linear scope is advanced to the GE junction by following the descending aorta from the level of the arch downward (Figure 2.10). In order to follow this path, the scope is usually torques clockwise 90–180 degrees and, as the aorta is followed down, the scope is gently rotated counterclockwise to stay on the aorta. As seen in the accompanying video, the thyroid is visualized briefly and the scope is then advanced to the level of the GE junction.

The origin of the celiac artery (Figure 2.11) is identified and then the scope can be withdrawn. This is the standard reference point for the beginning of the exam during withdrawal. Examination of the extraesophageal and thoracic structures is more time consuming than the radial approach as this echoendoscope's narrow focal point has to be torqued back a further 180 degrees to cover the same field of examination. This is done by withdrawing the scope at increments with constant back and forth torque.

As the scope is withdrawn 3–5 cm back from the GE junction, the scope will need to be rotated 180 degrees off the aorta to see the left atrium and cardiac structures. The cardiac structure can be discerned quite readily using the linear scope. The mitral valve is just adjacent to the aortic

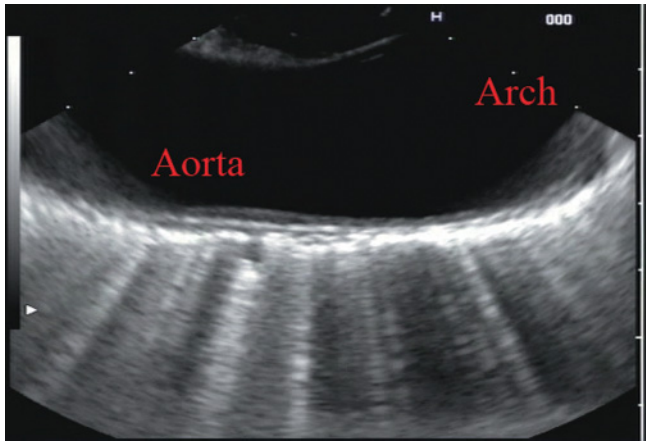

Figure 2.10 Linear array image at the mid aorta.

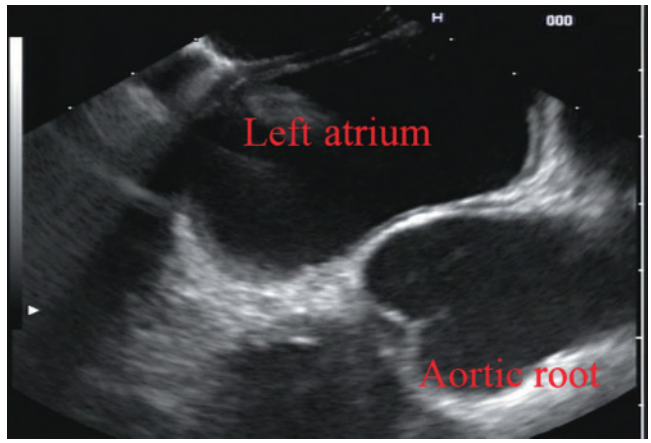

Figure 2.12 Linear array image at the aortic root.

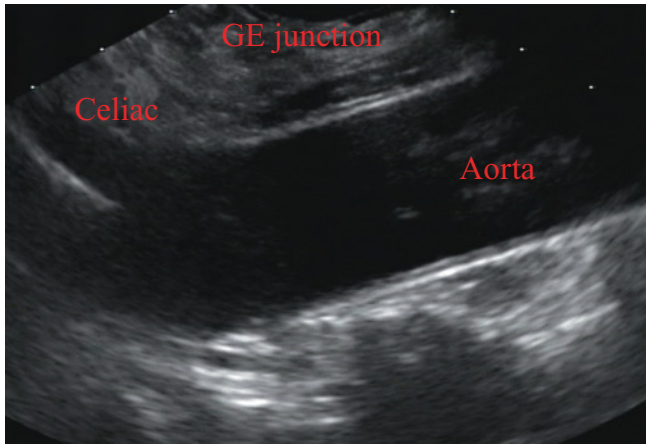

Figure 2.11 Linear array image at the level of the celiac artery.

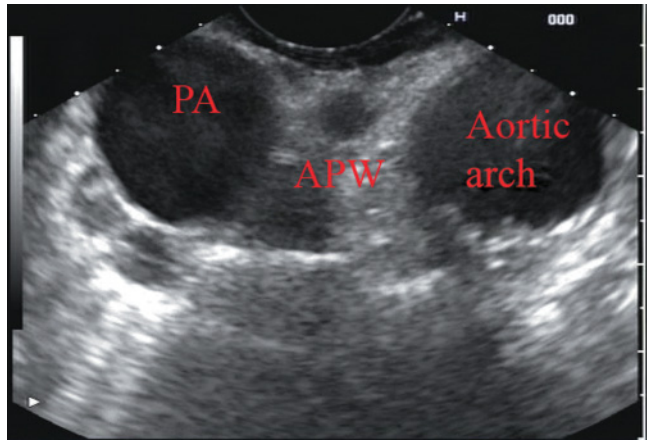

Figure 2.13 Linear array image at the aortopulmonary window (APW) (PA = pulmonary artery).

root, which is just at clockwise rotation from the mitral valve. The aortic valve can be visualized at various angles with appropriate endoscopic manipulation given its position relative to the esophagus (Figure 2.12).

Withdrawing from the level of the left atrium by 1–2 cm reveals the subcarinal space. This is the area between the pulmonary artery and the left atrium. The bifurcation of the trachea is by definition occurring at this level as well.

The AP window is just proximal to this area by several centimeters orientation and is slightly clockwise torque from the subcarinal space. The space between the aortic arch and the pulmonary artery make up this region. This is below the level of the aortic arch by a few centimeters. There is a small node seen on the image which could be readily sampled via endoscopic ultrasound-guided fine needle aspiration (EUS-FNA) (Figure 2.13).

The azygos arch is also visualized around this area, just at or slightly below the aortic arch. The azygos vein can be followed distally along the spine, as in the accompanying Video 2.2. Occasionally intercostal veins are visible.

Chapter video clips

Video 2.1 Radial array examination of the extraesophageal spaces.

Video 2.2 Linear array examination of the extraesophageal spaces.

3 Normal Mediastinal Anatomy by EUS and EBUS

Silvio Wanderley de Melo Jr.[1] and Michael B. Wallace[2]

[1] University of South Alabama, Mobile, AL, USA
[2] Mayo Clinic College of Medicine, Jacksonville, FL, USA

Introduction

The mediastinum is a common anatomical location for lymph node (LN) metastases in lung cancer as well as many other malignant and inflammatory conditions. The presence and specific location of mediastinal lymph node metastases in non-small cell lung cancer (NSCLC) dictates therapy with surgery for localized disease, combination therapy when contralateral LNs are involved, and palliative therapy when contralateral LNs and metastases are encountered. Unfortunately, cross-sectional imaging with computed tomography (CT), magnetic resonance imaging (MRI), or positron emission tomography (PET) alone is not adequate to confirm a diagnosis; thus, a tissue sample is preferred. Recently, it has been suggested that the use of endoscopic ultrasound-guided fine needle aspiration (EUS-FNA) associated with endobronchial ultrasound-guided transbronchial fine needle aspiration (EBUS-TBNA) can adequately sample LNs in the mediastinum avoiding the need for a futile surgery.

The purpose of this chapter is to provide the basic anatomical information as well as technical maneuvers used to investigate the mediastinum successfully.

Anatomical definitions

The LNs in the mediastinum were classified in different stations based on surgical and anatomical landmarks for the purpose of staging lung cancer but this schema is now widely used in other chest diseases (Figure 3.1). The LNs with their respective stations and corresponding anatomical locations can be seen in Table 3.1.

EUS-FNA usually is best suited to sample LNs adjacent to the esophagus which runs posterior to the trachea. Because of ultrasound artifacts created by the air-filled trachea, lesions immediately anterior to the trachea are not well seen. Endoscopic ultrasound-accessible stations include: 2L, 2R, 4L, 4R, 5, 7, 8, 9, and, sometimes depending of the size, station 6. On the other hand, EBUS-TBNA can target LN either anterior or lateral to the trachea to the level of the carina, and alongside the left and right bronchial tree including stations 2L, 2R, 4L, 4R, 7, 10, and 11. Although both procedures overlap in stations 2 L/R, 4 L/R, and 7, in other stations they are complementary, and in combination, allow nearly complete mediastinal access.

Equipment

Radial and curvilinear array echoendoscopes are available (Figure 3.2), with scanning radius ranging from 270–360 degrees for radial to 100–180 degrees for the linear echoendoscope. These scopes have standard accessory channels (2.0–2.8 mm) and larger accessory channels (3.7 mm) capable of delivering needles and other therapeutic devices such as a 10 French (Fr) plastic stent.

EUS has several types of needles: 19 gauge (G), 22 G, and 25 G for FNA, as well as Tru-cut needles for core biopsy. The needle is occluded with stylet during passage through the gastrointestinal tract wall and bronchial wall to minimize the contamination from passage through those structures.

EBUS equipment is a curvilinear array echoendoscope with an outer diameter of 6.7 mm and a biopsy channel of 2 mm. The ultrasonic frequency is 7.5 MHz with a penetration depth of 4–5 cm, making it well suited for FNA of LNs and lung masses through the trachea and bronchi (Figure 3.2). A 22 G needle is used to perform TBNA in the same manner as in the EUS. Both systems have integrated, oblique viewing optics to guide intubation and limited inspection.

Atlas of Endoscopic Ultrasonography, First Edition. Edited by Frank G. Gress, Thomas J. Savides, Brenna Casey Bounds, John C. Deutsch.
 Published 2012 by Blackwell Publishing Ltd.

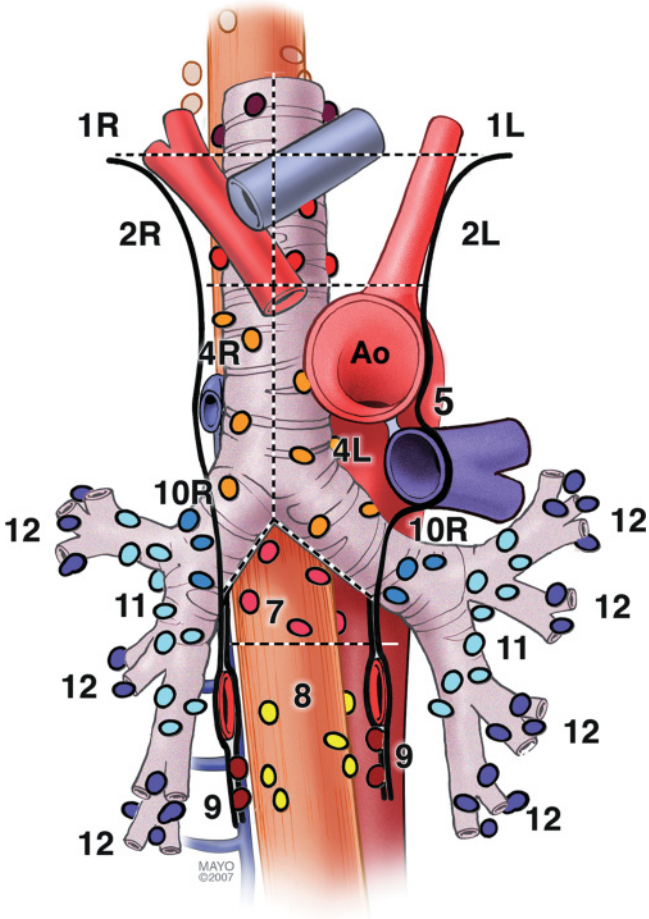

Figure 3.1 Mediastinal lymph nodes stations.

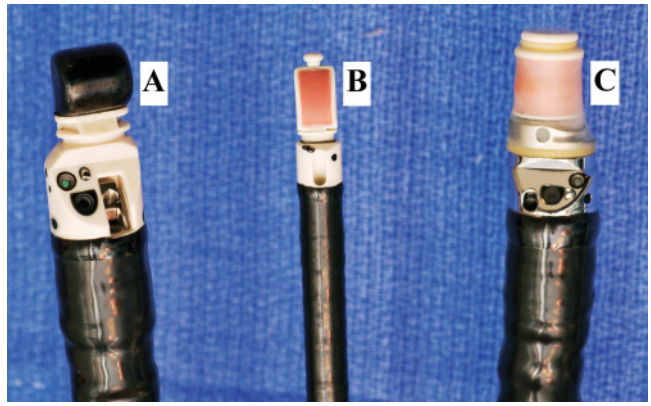

Figure 3.2 Types of echoendoscopes.

Table 3.1 Mediastinal lymph node stations with their anatomical correlations.

Level	Anatomical correlation
Superior mediastinal lymph nodes	
1	Highest mediastinal
2	Upper paratracheal
3	Prevascular and retrotracheal
4	Lower paratracheal (including azygos nodes)
Aortic lymph nodes	
5	Aortopulmonary window (AP) or subaortic
6	Para-aortic (ascending aorta and phrenic)
Inferior mediastinal lymph nodes	
7	Subcarinal
8	Paraesophageal (below carina)
9	Pulmonary ligament
N1 lymph nodes	
10	Hilar
11	Interlobar
12	Lobar
13	Segmental
14	Subsegmental

Technique

Endoscopic ultrasound

The initial examination can be performed with either the radial or linear array echoendoscope; however, the linear scope is required to perform FNA. Given the obvious efficiencies, we prefer to use a single linear echoendoscope for both imaging and FNA. The technique described below refers to linear EUS imaging.

The balloon should be deflated or inflated only slightly to provide good acoustic coupling with the tissue. The mediastinum is imaged by first finding the descending aorta starting at the cardia. The examination can be performed by rotating 360 degrees from the cardia, then withdrawing the shaft 4–5 cm and performing another rotation. Alternatively, one can survey from the cardia to the cervix then rotating 90 degrees and repeating the maneuver until the whole mediastinum is examined. It is useful to use the following five stations as described by Deprez.

Inferior posterior mediastinum

The descending aorta is a large echo-poor longitudinal structure on linear array with a bright, deep wall due to the air interface with the left lung. Clockwise rotation will image sequentially: left lung, left pleura, left atrium, right lung, right pleura, azygous vein, and spine. The azygous vein can be localized by rotating approximately 30 degrees counterclockwise from the descending aorta. It's a thin echo-poor structure that can be followed proximally to its union with the superior vena cava. This is the area of LN stations 8 and 9 (Figure 3.3).

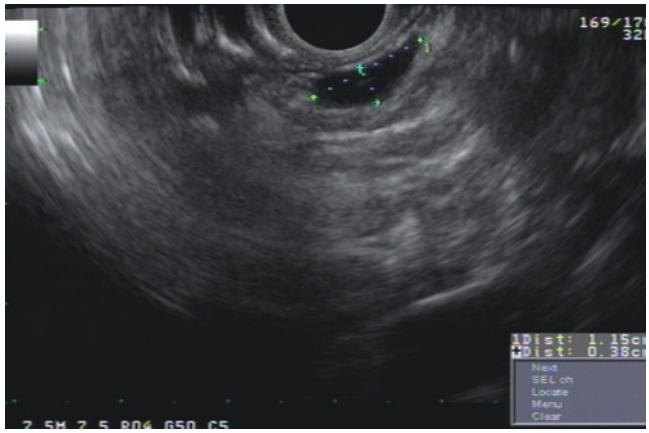

Figure 3.3 Lymph node at station 8 (between calipers).

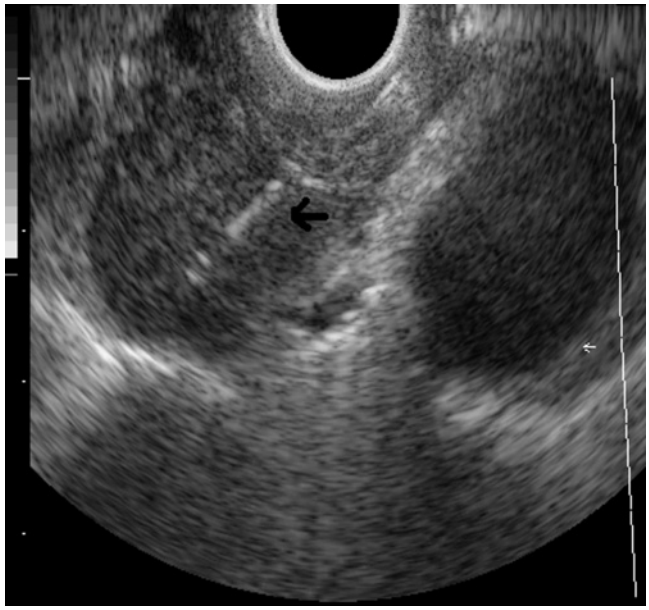

Figure 3.4 Subcarinal lymph node fine needle aspiration (FNA) (black arrow).

Subcarinal area

At approximately 30 cm the subcarinal area is easily recognized by finding the left atrium, a large hypoechoic structure with cardiac motion, and pulling back until it disappears it seen in the left edge of the screen. Then one should have the pulmonary artery at the right portion of the screen (Figure 3.4). Slight movements to the right and to the left have to be performed to completely interrogate this station.

Aortic arch area

The azygous arch is located at 24–25 cm from the incisors. The aortopulmonary (AP) window (station 5) is situated between the aortic arch and the pulmonary artery. The AP window is found by following the aorta cephalad until its

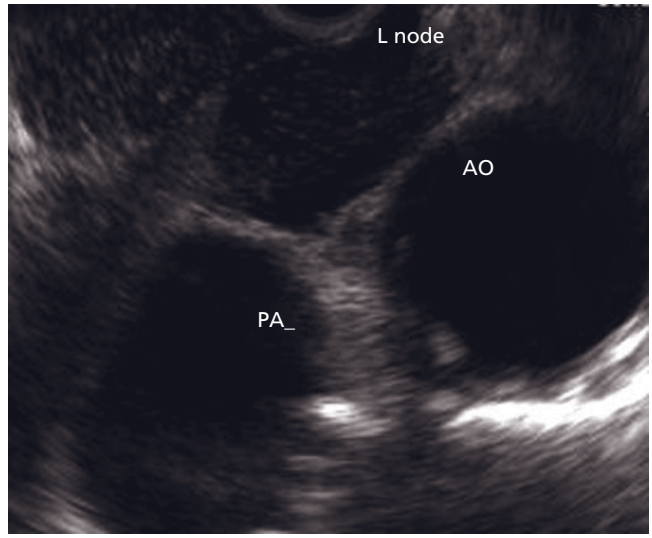

Figure 3.5 Aortopulmonary window station (Ao = aorta; L node = lymph node; PA = pulmonary artery).

arch, rotating clockwise approximately 90 degrees, then advancing 1–2 cm with slight tip up of the echoendoscope. The aorta will be the echo-poor structure on the right and the pulmonary artery will be to the left; the AP window is the space between the two just outside the AP ligament (which is not seen by EUS). The 4L region is immediately medial (close to the esophagus and EUS scope) to the AP window. Alternatively, from the subcarinal area, rotating 90 degrees counterclockwise, crossing the left main bronchus and pulling it back 2–3 cm will put you in the same location. Further withdrawal of the echoendoscope with slight rotation will show the origin of the left subclavian artery. Occasionally, the left carotid artery can be seen above the brachiocephalic (innominate) vein (Figure 3.5).

Cervical area

Between 22 and 24 cm from the incisors, the superior part of the lungs can be imaged along with the trachea, cricoid bone, jugular veins, and carotid arteries.

Thyroid gland

At 17–20 cm from the incisors, the inferior thyroid gland can be imaged as well as cervical LNs, which can be targeted for FNA.

Radial scanning

For radial scanning, one should enter the stomach, inflate the balloon, and pull back the scope until the GE junction. The aorta with be visualized as a large round echo-poor structure. The aorta should be rotated to the 5 o'clock position, the spine will be at 7 o'clock with the azygous vein in the middle. Then the balloon should be deflated and a slow pull back is performed observing all the mediastinal areas.

It is important to note that, for a complete lung cancer staging with both radial and linear, the celiac axis, the left adrenal, and the left lobe of the liver should be surveyed. This is easily accomplished with a slight tip down on the echoendoscope and then pushing it into the stomach: the celiac take-off can be seen and the left adrenal can be seen at the 6 to 4 o'clock position with its usual seagull appearance. For the liver, one goes to the gastric antrum, aspirates all the air, inflating the balloon, and then tip up with a slow pull back.

Endobronchial ultrasound

Just like EUS, EBUS can be performed with conscious sedation, deep sedation, or general anesthesia. The tip of the scope is placed under direct visual contact in different positions starting from the segmental bronchi to the trachea scanning 360 degrees every 1–2 cm. EBUS-TBNA is performed under the same principles as EUS-FNA. As mentioned before, this technique is particularly useful for LN stations 2, 4, 7, 10, and 11 (Figure 3.6).

Stations 10 and 11

The hilar region is best seen by impacting the EBUS scope at the distal most aspect of the bronchial tree. The diameter of the EBUS scope (6–7 mm) precludes passage beyond the third-generation bifurcation corresponding to the main lung lobes. Lymh nodes in the region are seen by 360-degree rotation at this distal-most point.

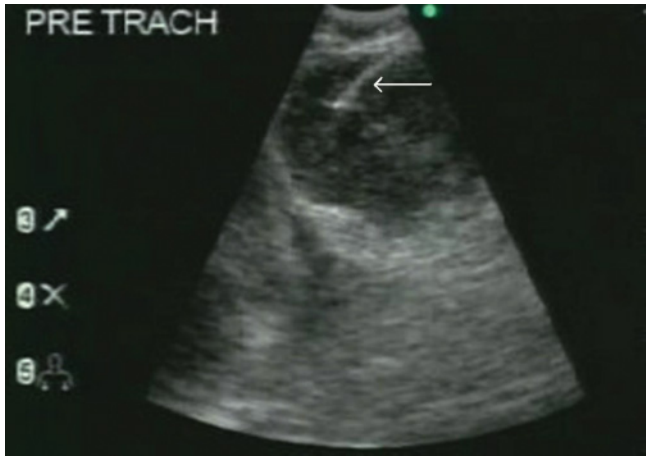

Figure 3.6 Endobronchial ultrasound (EBUS) showing fine needle aspiration (FNA) pretracheal lymph node (white arrow).

Subcarina (station 7)

Station 7 is best seen from the proximal left or right main bronchus. For an endosocopist, hold the instrument in the left hand (it is easiest to do this from the left main bronchus with medial [clockwise] rotation).

Aortopulmonary window: left paratracheal stations

The left paratrachal region is seen from the trachea beginning 1–2 cm above the carina and rotating counterclockwise. The view of the AP window is very similar to that seen by the EUS scope with the aortic arch on the right and pulmonary artery on the left (see Figure 3.5). The 2L region is seen immediately cephalad of the innominate artery.

Right paratracheal stations (4R, 2R)

These stations are seen similary to the left side but with clockwise rotation from the carina.

Complications and safety

EUS-FNA and EBUS-TBNA are highly safe procedures in experienced hands with a complication rate of 0.8%. A major safety precaution with FNA is to visualize the entire length of the needle and to use color Doppler to avoid any blood vessels in the needle path.

Conclusions

EUS-FNA and EBUS-TBNA are complementary procedures with a high degree of sensitivity and specificity to diagnose/stage benign and malignant diseases of the chest. Careful attention to technique must be applied in order not to miss important clinical information. This chapter provided a description of the techniques used to image the mediastinum with EUS and EBUS.

Chapter video clips

Video 3.1 Pretracheal lymph node EUS-FNA.
Video 3.2 Pretracheal lymph node EBUS-FNA.
Video 3.3 Subcarinal lymph node EUS-FNA.
Video 3.4 Subcarinal lymph node EBUS-FNA.

4 Stomach: Radial and Linear

Joo Ha Hwang
University of Washington, Seattle, WA, USA

Endoscopic ultrasound (EUS) examination of the stomach is often performed to evaluate subepithelial lesions, staging of mucosa associated lymphoid tumor (MALT) lymphomas, staging of gastric cancer, and evaluation of thickened gastric folds. Examination can be performed using mechanically scanning or electronic array echoendoscopes, or with ultrasound catheter probes.

The basic technique for performing EUS imaging of the gastric wall initially requires clearing the gastric lumen of any mucous or debris. The lumen should be thoroughly irrigated with water and suctioned. If there are excessive amounts of bubbles in the gastric lumen, a small amount of simethicone can be added to the irrigating water and suctioned. Once the gastric lumen has been cleared the gastric lumen should be decompressed and then filled with clean water. Ideally, degassed water should be used to fill the gastric lumen; however, this is often not available and clean water typically is sufficient. However, efforts should be made to minimize the presence of bubbles within the water as this will degrade the image quality. It is important to make sure that all air is aspirated from areas where imaging is to be performed. When filling the gastric lumen with the patient on their left side, the fundus and body will fill preferentially due to gravity. If the area of interest is in the antral wall, positioning the patient on their right side may be necessary to safely fill the gastric lumen with water for imaging. Filling of the gastric lumen with water places the patient at risk of aspiration; therefore, precautions should be taken to protect against an aspiration event.

After aspirating the air out of the lumen and distending the gastric lumen with water, the gastric wall can be surveyed with a radial scanning echoendoscope by starting the exam with the ultrasound probe in the antrum and slowly withdrawing the probe (Figure 4.1). If only a focal area needs to be examined, the use of a water-filled balloon can be used, especially for evaluating non-mucosal lesions such as subepithelial tumors. However, the use of a water-filled balloon creates an additional interface echo impacting the image quality at the balloon–mucosa interface. Therefore, a water-filled balloon should not be used to provide acoustic coupling to mucosal lesions.

It is also important to perform imaging within the focal region of the transducer. The mechanical radial scanning echoendoscopes and catheter probes have a fixed natural focus where the best image resolution is obtained. The focal distance can easily be determined by adjusting the distance of the transducer from the gastric wall. The best resolution will be seen when the area of interest is at the focus of the imaging transducer. Electronic array echoendoscopes (radial and curvilinear) have the ability to electronically adjust the location of the focal region; therefore, when imaging the gastric wall, the focal region should be adjusted accordingly.

For imaging superficial lesions, the use of a catheter probe through a double-channel endoscope allows for visual guidance of probe placement. The use of a double-channel endoscope allows for one channel to be used for the ultrasound catheter probe and the other channel to be used for injecting water into the gastric lumen and suctioning water and air from the gastric lumen. Ultrasound catheter probes come in frequencies of 12, 20, and 30 MHz. The image resolution increases with increasing frequency; however, penetration (depth of imaging) decreases as frequency increases.

The stomach has a well-developed five-layered wall structure (Video 4.1). This is easily visualized when water is placed in the lumen. The second layer is often prominent because of the relatively thick columnar mucosa and glands (Figure 4.2). The fourth layer is often thicker in the distal stomach compared to the proximal stomach. The fifth layer generally corresponds to surrounding structures and perigastric fat as the serosa is too thin to be resolved with endoscopic ultrasound. EUS imaging of the gastrointestinal (GI)

Atlas of Endoscopic Ultrasonography, First Edition. Edited by Frank G. Gress, Thomas J. Savides, Brenna Casey Bounds, John C. Deutsch.

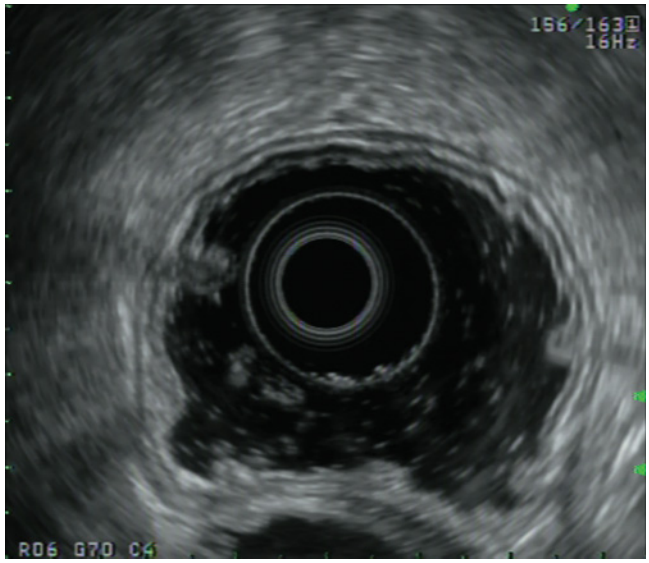

Figure 4.1 Circumferential image of the gastric wall after filling and distending the gastric lumen with water. Image is taken with an electronic radial array echoendoscope at 5 MHz.

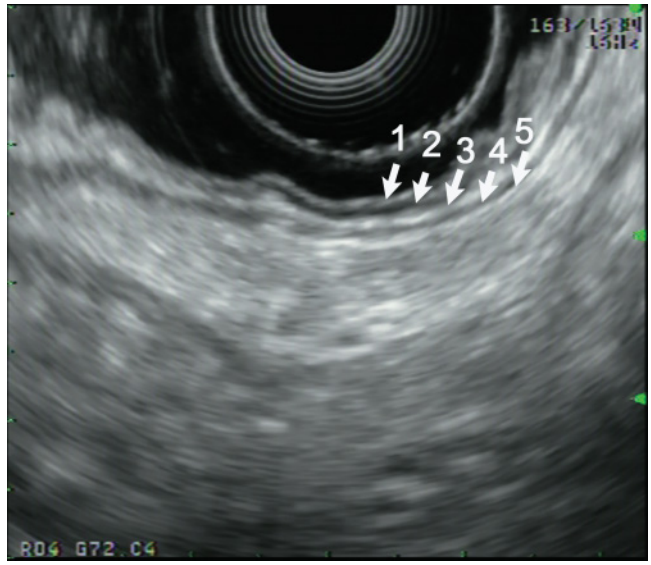

Figure 4.3 Five-layer structure of the gastric wall obtained with an electronic radial array echoendoscope at 5 MHz.

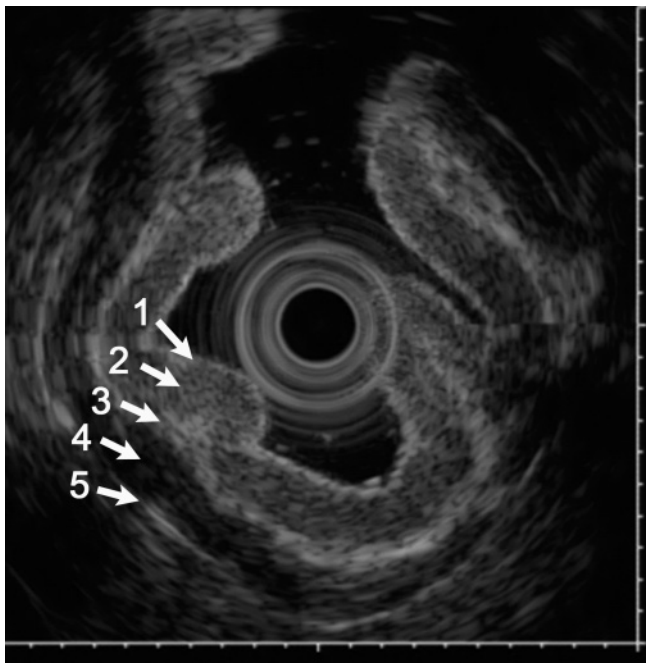

Figure 4.2 Five-layer structure of the gastric wall demonstrating a relatively thick mucosal layer (layers I and II). Image is taken with a 20 MHz catheter probe.

tract wall typically exhibits five layers; however, seven or nine layers can be resolved if imaging is performed at higher frequencies depending on the region of the GI tract being examined. Initial interpretation of the EUS images assumed direct correspondence of the layers seen on EUS to those seen on histology. It was presumed that the first echogenic layer represented the mucosa, the second echolucent layer represented the muscularis mucosae, the third echogenic layer represented the submucosa, the fourth echolucent layer represented muscularis propria, and the fifth echogenic layer represented the serosa and subserosal fat. However, it was later proven that this was an incorrect interpretation of the EUS images of the GI tract wall. In fact, it was demonstrated that the five layers seen on EUS imaging correspond to the following (Figures 4.2 and 4.3):

1. Interface echo between the superficial mucosa and water (hyperechoic).
2. Deep mucosa (hypoechoic).
3. Submucosa plus the acoustic interface between the submucosa and muscularis propria (hyperechoic).
4. Muscularis propria minus the acoustic interface between the submucosa and muscularis propria (hypoechoic).
5. Serosa and subserosal fat (hyperechoic).

If a high-frequency (10 MHz or greater) transducer is used, seven or nine layers can potentially be identified on EUS imaging. These nine layers corresponding to the following (Figure 4.4):

1. Epithelial interface (hyperechoic).
2. Epithelium (hypoechoic).
3. Lamina propria plus the acoustic interface between the lamina propria and the muscularis mucosae (hyperechoic).
4. Muscularis mucosae minus the acoustic interface between the lamina propria and muscularis mucosae (hypoechoic).
5. Submucosa plus the acoustic interface between the submucosa and inner muscularis propria (hyperechoic).

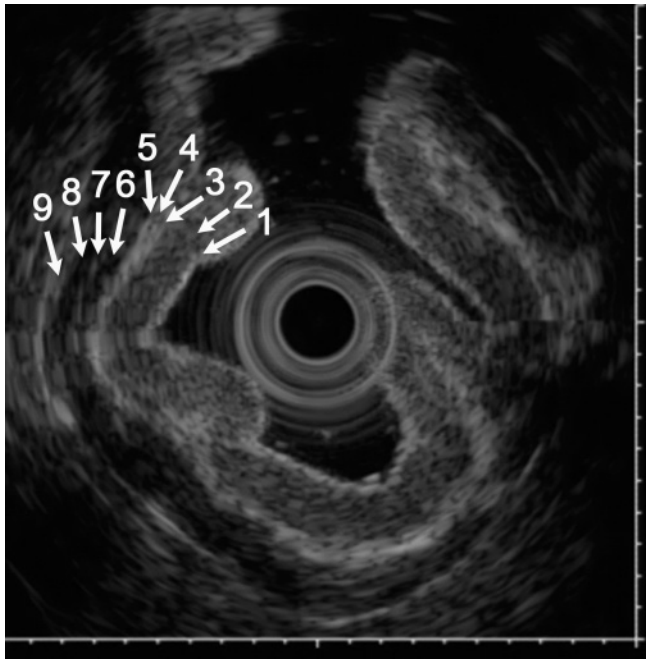

Figure 4.4 Nine-layer structure of the gastric wall obtained with a 20 MHz catheter probe. The image is the same as Figure 4.2 except additional layers are identified.

6. Inner muscularis propria minus interface between the submucosa and inner muscular propria (hypoechoic).
7. Fibrous tissue band separating the inner and outer muscularis propria layers (hyperechoic).
8. Outer muscularis propria (hypoechoic).
9. Serosa and subserosal fat (hyperechoic).

An important aspect of EUS imaging in the stomach is to maintain orientation of the imaging plane to avoid tangential imaging especially when evaluating mucosal lesions. Tangential imaging can result in overstaging of lesions.

In conclusion, the only available *in vivo* method for examining the full thickness of the GI wall, beyond the mucosal surface, is EUS. It provides gastroenterologists with a valuable diagnostic tool to assess pathology in the GI tract to help guide clinical management of the patient. Selection of the correct transducer and using good technique are important in obtaining high-quality images. When imaging the wall of the GI tract, the method of acoustic coupling is critical. Without good acoustic coupling to the mucosal surface, high-quality images cannot be obtained. The highest frequency available should be used to image the wall of the GI tract since deep penetration is not necessary unless imaging a large tumor arising from the wall. Using a higher frequency transducer will result in better resolution and allow for better identification of the layers involved. Lower frequencies may be required to identify the size of a mass and if there is involvement with any adjacent structures (T-staging), and to assess nodal involvement (N-staging).

Chapter video clip

Video 4.1 Layers of the gastric wall.

5 Bile Duct: Radial and Linear

Kapil Gupta
Cedars-Sinai Medical Center, Los Angeles, CA, USA

Normal bile duct anatomy

Endoscopic ultrasound provides excellent imaging of the biliary tree and gallbladder. Using radial and linear echoendoscope, visualization of the bile duct is performed from two main stations, from the duodenal bulb and from the second portion of the duodenum. The gallbladder is usually seen from the duodenal bulb or the antrum of the stomach. As the entire biliary tree can be visualized only using linear echoendoscope, more endosonographers are primarily using linear echoendoscope for evaluating bile duct anatomy.

Normal anatomy of the bile duct and gallbladder with radial echoendoscope

The echoendoscope is advanced through the pylorus into the duodenal bulb. To achieve this, the scope is usually in a long position along the greater curvature. The big wheel is then turned downwards and the scope is either turned slightly clockwise or the small wheel rotated slightly to the right to deflect the tip of the echoendoscope towards the apex of the duodenal bulb and impacted there. To achieve a stable position the balloon can be inflated, which helps in maintaining the tip of the scope in the bulb.

Here, with slight right and left movement, the liver is oriented at 12 o'clock. In this position the portal vein and the common bile duct can be visualized as two parallel tubular structures to the left of the transducer (Figure 5.1). With slight right rotation the bile duct can be followed towards the head of the pancreas into the ampulla where a thin pancreatic duct can be visualized below the bile duct (Figure 5.2). With left rotation or slight counterclockwise rotation the bile duct can be followed upwards into the liver (Video 5.1).

The gallbladder usually is visualized along the under surface of the liver (Figure 5.3) and with slight rotation, withdrawing, and pushing the echoendoscope the entire gallbladder can be visualized (Video 5.1).

To visualize the bile duct from the second portion of the duodenum, the transducer is placed along the ampulla and with slight movement the bile duct and the pancreatic duct can be visualized as two round anechoic structures (Figure 5.4) (Video 5.1).

Normal anatomy of the bile duct and gallbladder with linear echoendoscope

The bile duct is visualized with a linear echoendoscope from either the duodenal bulb or the second portion of the duodenum. The transducer of the echoendoscope is advanced across the pylorus. Once in the bulb the balloon can be filled slightly with water to maintain a stable position. Initially the tip of the echoendoscope is impacted at the apex of the bulb; to achieve this, the big wheel is turned downwards. With slightly counterclockwise torque and turning the big wheel down further the bile duct is visualized as a round structure, right in the center of the field (Figure 5.5). The cut section of the visualized bile duct is in the region of the common bile duct or the common hepatic duct. In this view the portal vein is usually visualized below the bile duct, and also the inferior vena cava (IVC) can be seen to the right of the field (Figure 5.5). The common hepatic artery can also be visualized coursing in between the bile duct and the portal vein towards the left of the bile duct. From this view the inward impacted position of the tip of the transducer is maintained. By rotating the transducer in a counterclockwise manner the bile duct is followed towards the hilum into the liver and the bifurcation at the porta hepatis can be visualized. Cystic duct take-off can also be visualized by tracing the bile duct.

Atlas of Endoscopic Ultrasonography, First Edition. Edited by Frank G. Gress, Thomas J. Savides, Brenna Casey Bounds, John C. Deutsch.
 Published 2012 by Blackwell Publishing Ltd.

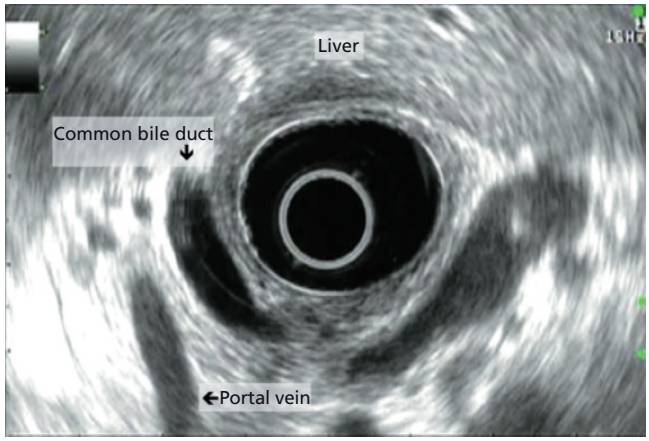

Figure 5.1 Bile duct as visualized from the duodenal bulb (radial echoendoscope).

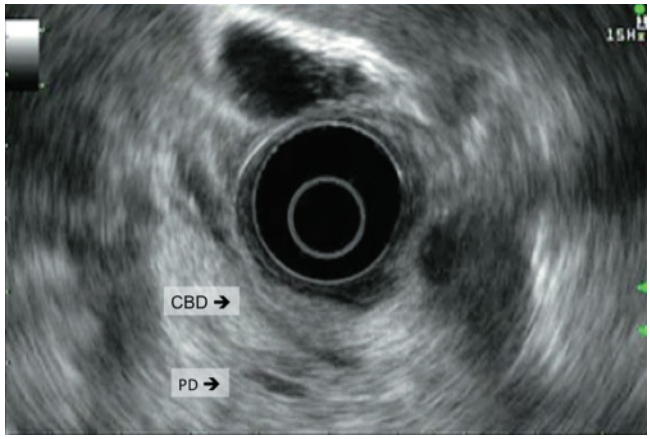

Figure 5.2 Bile duct followed towards the head of the pancreas from the duodenal bulb (radial echoendoscope) (CBD = common bile duct; PD = portal vein).

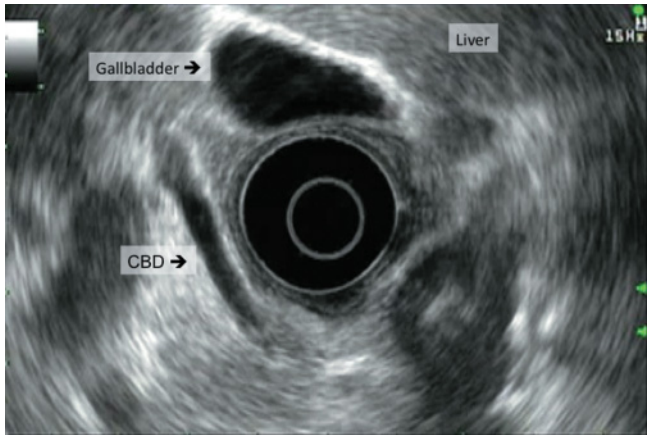

Figure 5.3 Gallbladder from the duodenal bulb (radial echoendoscope) (CBD = common bile duct).

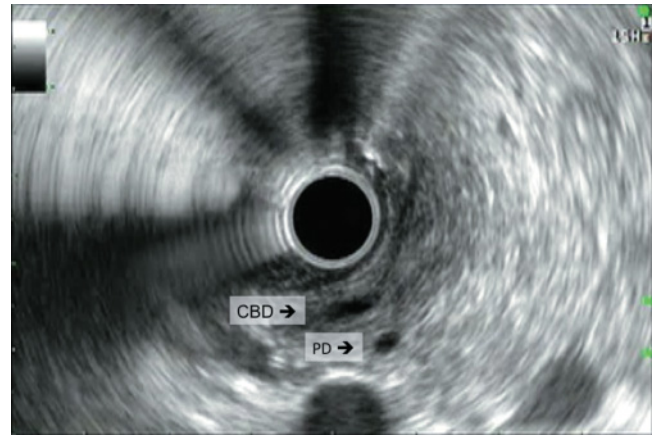

Figure 5.4 Bile duct and pancreatic duct from the second portion of the duodenum (radial echoendoscope) (CBD = common bile duct; PD = portal vein).

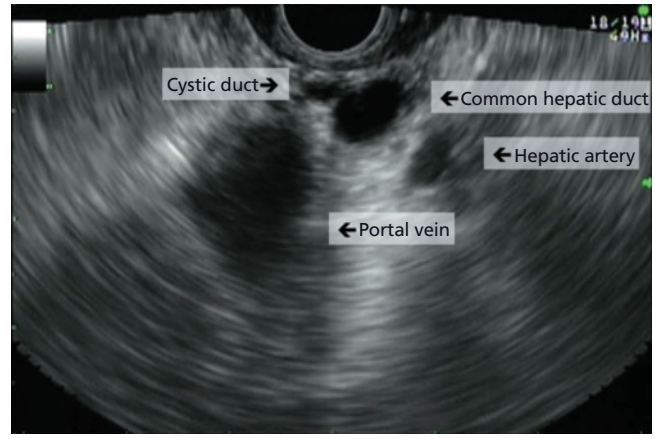

Figure 5.5 Common hepatic duct and cystic duct as visualized from the duodenal bulb (linear echoendoscope).

Undoing the counterclockwise rotation, and rotating the scope to the right, the transducer is rotated to follow the bile duct in the intrapancreatic portion towards the papilla. With this maneuver the entire bile duct can be followed. In most of the instances the bile duct can be traced downstream all the way to the point where it joins the pancreatic duct into the ampulla. Just below the bile duct, in the intrapancreatic portion, the pancreatic duct can be visualized (Video 5.1).

For visualizing the gallbladder the transducer is impacted in the bulb and the big wheel is turned up and the scope rotated counterclockwise so the transducer now faces the under surface of the liver; by turning the small wheel to the right and left the gallbladder can be seen in the subhepatic region. Moving the big wheel up and down, and turning the small wheel right and left, the entire gallbladder can usually be scanned. Sometimes the scope is slightly withdrawn to visualize the entire gallbladder (Video 5.1).

Care should be taken when advancing the echoendoscope into the second portion. By slight inward push, turning the big wheel down and the small wheel to the right, the scope tip usually points in the axis of the second portion of the duodenum. Carefully moving the big wheel up and down the scope tip falls into the second portion of the duodenum. At this point the small wheel is kept turned towards the right and the scope is reduced to a short position to align the transducer along the papilla.

The transducer is kept in close apposition with the major papilla. With slight right and left torque while withdrawing the scope, the bile duct is visualized as a long tubular structure closer to the duodenal wall, and deep to it lays the pancreatic duct (Figure 5.6). The bile duct can then be followed towards the liver with continued slow withdrawal of the scope and slight right and left torque. Usually the bile duct can be followed to the common hepatic duct portion when the scope tends to slip back into the stomach; to prevent this scope is again pushed inwards with counterclockwise rotation to gain a position similar to one in the duodenal bulb (Video 5.1).

Combining views from both the stations, that is the duodenal bulb and the second portion of the duodenum, the entire biliary tree can be visualized.

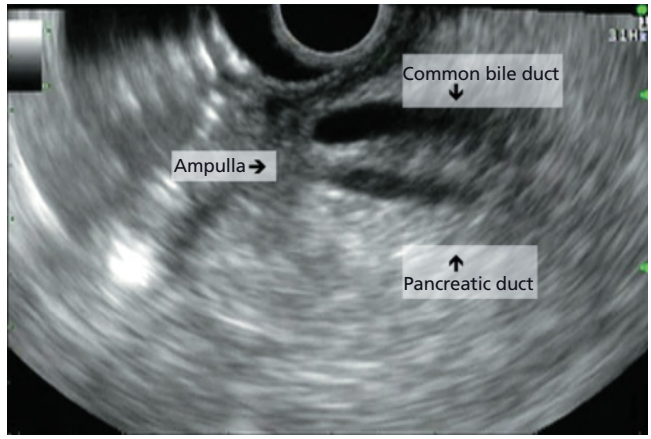

Figure 5.6 Bile duct and pancreatic duct from the second portion of the duodenum (linear echoendoscope).

Chapter video clip

Video 5.1 Radial and linear array images of the bile duct from the duodenum.

6 EUS of the Normal Pancreas

Richard A. Erickson and James T. Sing Jr.
Scott and White Clinic and Hospital, and Texas A&M Health Center, Temple, TX, USA

Radial examination of the pancreas

In radial examination of the pancreas, the organ is usually first encountered with the instrument in the mid to upper body of the stomach. On entering the stomach, the abdominal aorta can be followed a few centimeters distally to the take-off of the celiac artery. From there, advancing the scope just a few centimeters more distally will result in it crossing the neck/body of the pancreas (Figure 6.1). The confluence of the portal vein (PV) and splenic vein (SV) should appear deep to the pancreas neck with some minor manipulations of the orientation of the echoendoscope tip. The superior mesenteric artery (SMA) can be seen in cross section deep to the confluence surrounded by the echogenic fat of the retroperitoneum. The portal/splenic vein confluence has been described as looking like a golf club with the portal vein being the head of the club, the splenic vein the shaft and the superior mesenteric artery the golf ball (Figure 6.2). By continuing to follow the pancreas and splenic vessels towards the patients left and slightly withdrawing the echoendoscope, the tail of the pancreas is imaged (Figure 6.3). Following the splenic vessels to the left will lead to the hilum of the spleen, which is an important landmark as it marks the leftward limit of the tail of the pancreas. It is important to not forget that the tail of the pancreas may move deep from the stomach wall nestled between the left kidney and spleen (Figure 6.4). If this area is not examined carefully, pancreatic tail lesions can be easily missed. From the confluence of the portal/splenic vein gently advancing the tip of the echoendoscope forward and angulating the tip of the echoendoscope posterior one can view the pancreatic neck (Figure 6.5). Again, if this area is not examined carefully, pancreatic neck lesions may go unnoticed.

On advancing the echoendoscope deep into the duodenum, the side-by-side cross sections of the inferior vena cava and abdominal aorta come into view. On withdrawing the echoendoscope from the deep duodenum, the most caudad portion of the ventral pancreas will usually come into view just to the patients left (counterclockwise) of the abdominal aorta (Figure 6.6). On gentle withdrawal, the ampulla can usually be located by identifying the first visible portions of pancreatic duct in the ventral pancreas (VP) and following the course of the duct by slow withdrawal towards the duodenal wall and ampulla (Figure 6.7). The triangular-shaped ventral pancreas may appear more echolucent than the dorsal pancreas (DP) in about 75% of normal people and should not be mistaken for an echolucent tumor (Figure 6.6). The echolucency of the ventral pancreas can occasionally even be seen in views of the organ through the stomach. Further withdrawal reveals more of the pancreatic head where longitudinal views of the pancreatic duct may occasionally be seen (Figure 6.8). The confluence of the superior mesenteric vein with the portal vein and splenic vein are seen deep to the pancreatic head (Figure 6.9). This is an important view for examining splanchnic venous involvement by pancreatic head malignancies. As the echoendoscope comes around the junction of the second and first portion of the duodenum, small changes in orientation of the tip will result in major shifts in views. Sometimes the best views of the head of the pancreas are obtained when the echoendoscope first enters into the duodenal bulb with the scope in a long position. It is this orientation which most commonly provides a "stack sign" of the common bile duct (CBD) running parallel to the deeper main pancreatic duct (Figure 6.10). A stack sign can be demonstrated in >80% of patients with normal pancreatic ductal anatomy. When pancreas divisum exists (3–7% of normal people), a stack sign can only be demonstrated in about one third of patients. Instead of not seeing a stack sign, in pancreas divisum may see the more specific crossed duct sign. The crossed duct sign results from the CBD being seen in cross section while the pancreatic duct, draining to the minor ampulla, is seen in longitudinal section.

Atlas of Endoscopic Ultrasonography, First Edition. Edited by Frank G. Gress, Thomas J. Savides, Brenna Casey Bounds, John C. Deutsch.

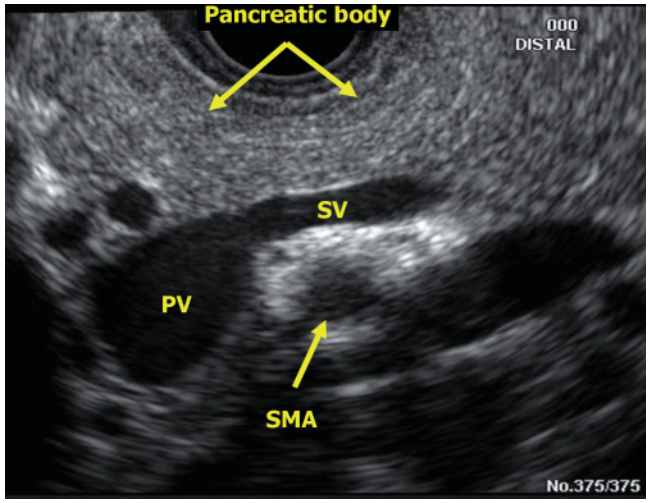

Figure 6.1 Radial endoscopic ultrasound (EUS): pancreatic body, confluence (PV = portal vein; SMA = superior mesenteric artery; SV = splenic vein).

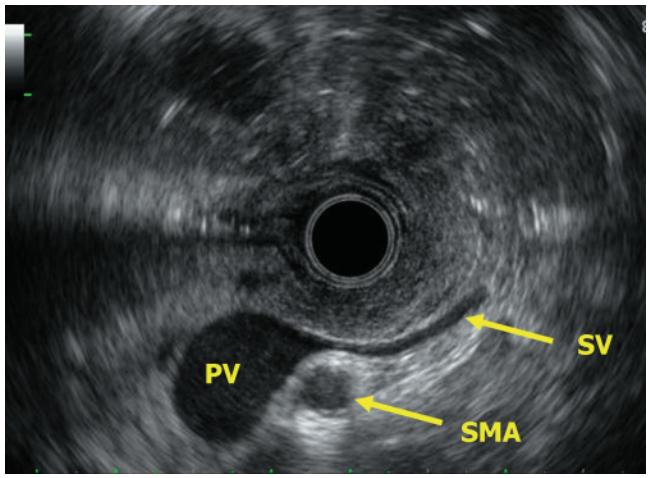

Figure 6.2 Radial endoscopic ultrasound (EUS): PV confluence (PV = portal vein; SMA = superior mesenteric artery; SV = splenic vein).

Linear examination of the pancreas

The linear endosonographic examination of the pancreas through the stomach differs fundamentally from the radial examination in that complete imaging of the pancreas must be provided by rotating the shaft of the scope. Since the retroperitoneal structures are all posterior to the stomach, clockwise (rightward) rotation of the echoendoscope will point the echoendoscope towards the patient's left and counterclockwise (leftward) rotation towards their right side. To find the pancreas in the stomach, one starts at the abdominal aorta near the gastroesophageal junction and follows it course distally until the take-off of the celiac artery is visible. Usually, the more oblique take-off of the superior

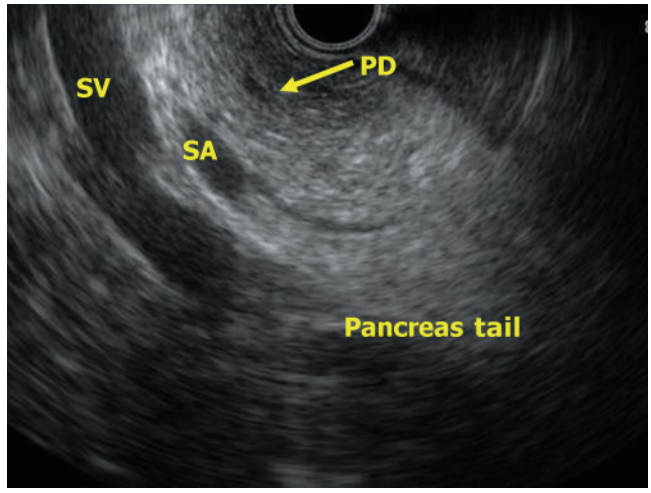

Figure 6.3 Radial endoscopic ultrasound (EUS): pancreas tail (PD = pancreatic duct; SA = splenic artery; SV = splenic vein).

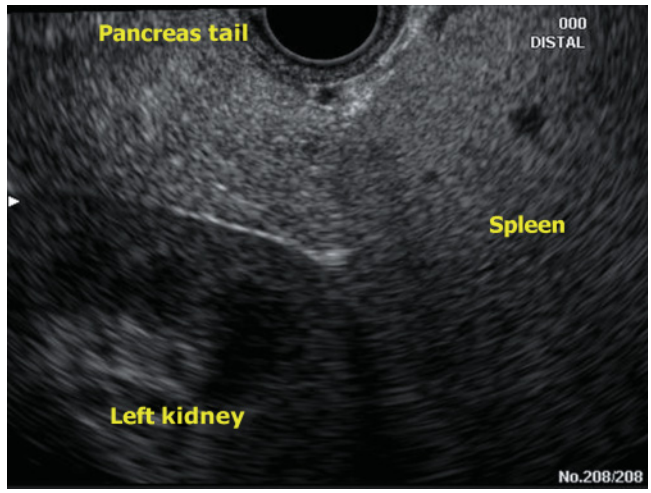

Figure 6.4 Radial endoscopic ultrasound (EUS): pancreas tail.

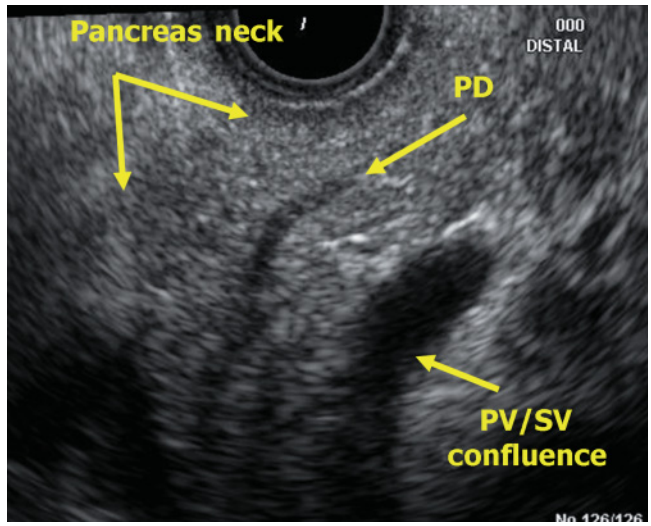

Figure 6.5 Radial endoscopic ultrasound (EUS): pancreas neck (PD = pancreatic duct; PV = portal vein; SV = splenic vein).

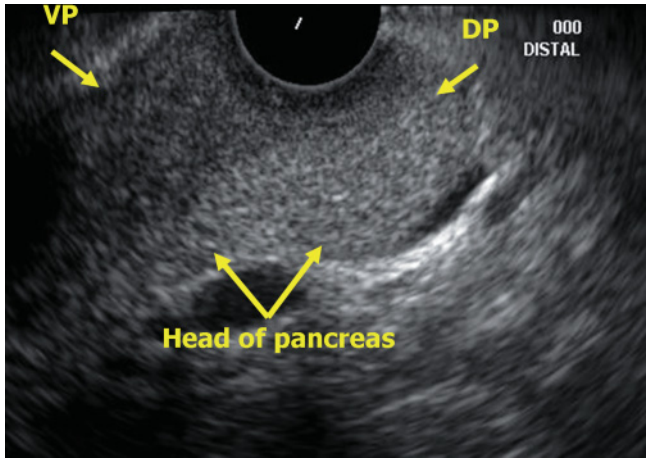

Figure 6.6 Radial endoscopic ultrasound (EUS): head of pancreas (DP = dorsal pancreas; VP = ventral pancreas).

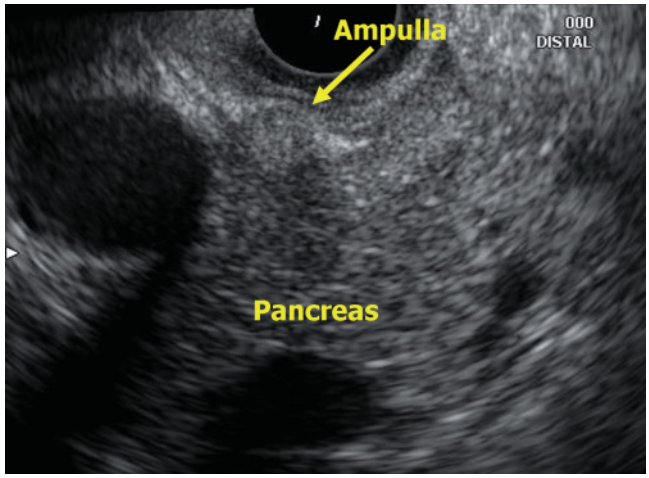

Figure 6.7 Radial endoscopic ultrasound (EUS): ampulla.

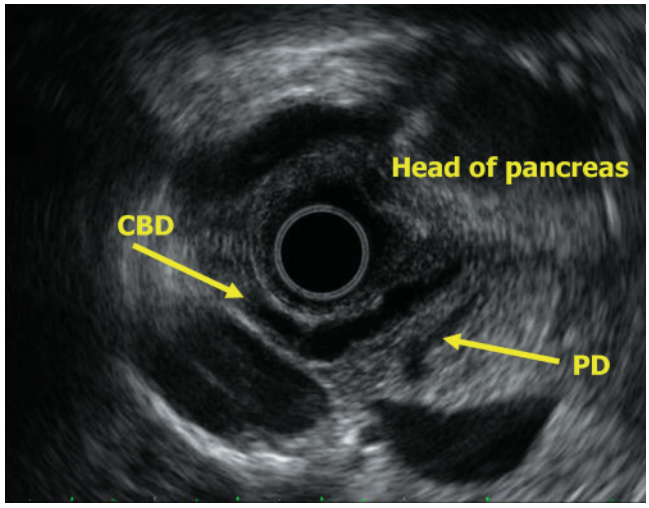

Figure 6.8 Radial endoscopic ultrasound (EUS): head of pancreas (CBD = common bile duct; PD = pancreatic duct).

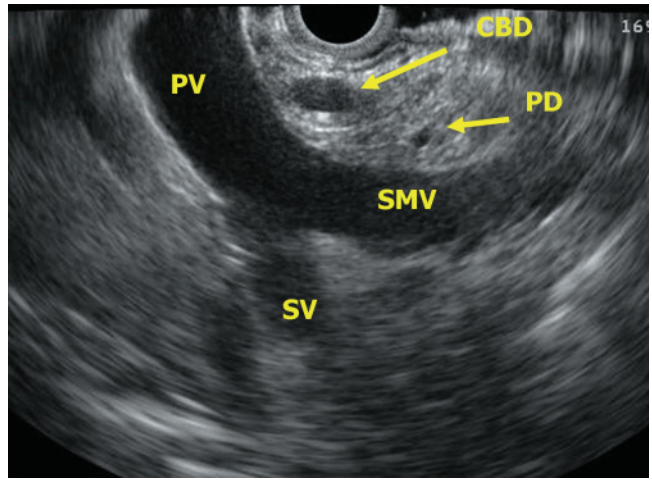

Figure 6.9 Radial endoscopic ultrasound (EUS): head of pancreas, vasculature (CBD = common bile duct; PD = pancreatic duct; PV = portal vein; SMV = superior mesenteric vein; SV = splenic vein).

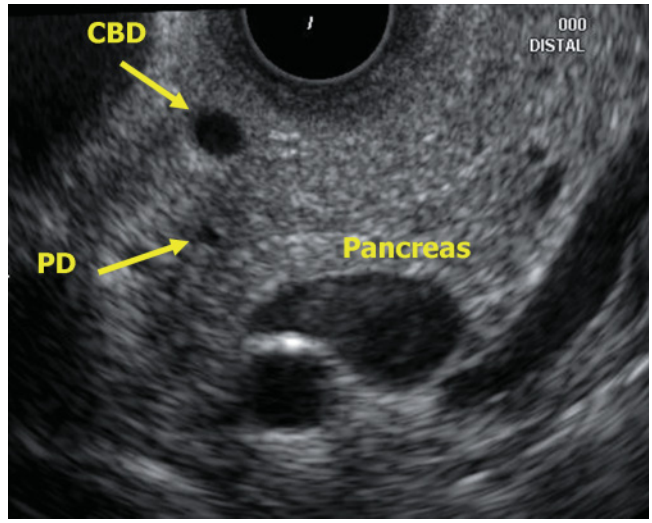

Figure 6.10 Radial endoscopic ultrasound (EUS): head of pancreas (CBD = common bile duct; PD = pancreatic duct).

mesenteric artery is apparent just distal to this. Further advancement of the instrument distally will find the pancreas neck/body nestled between the "V" of the celiac and superior mesenteric artery. The splenic artery will course tortuously in and out of the pancreas body/tail, but the splenic vein usually has a straight course and is the larger, deeper and more ovoid of the two vessels (Figure 6.11). The pancreas is interrogated sequentially from the neck to the body and tail through the stomach at this level by rotating the echoendoscope to the right (clockwise) with slight withdrawal following the splenic vein and splenic artery as they run into the hilum of the spleen. The pancreas neck, body, and tail will appear be the tissue found between the splenic vein and the posterior gastric wall. The pancreatic duct is

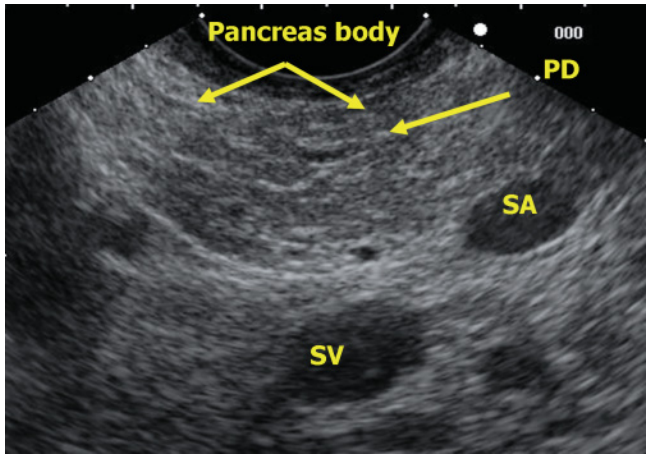

Figure 6.11 Linear endoscopic ultrasound (EUS): pancreas body (PD = pancreatic duct; SA = splenic artery; SV = splenic vein).

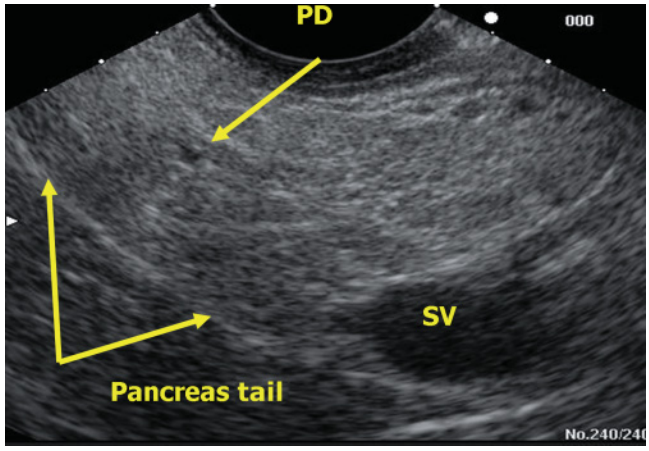

Figure 6.12 Linear endoscopic ultrasound (EUS): pancreas tail (PD = pancreatic duct; SV = splenic vein).

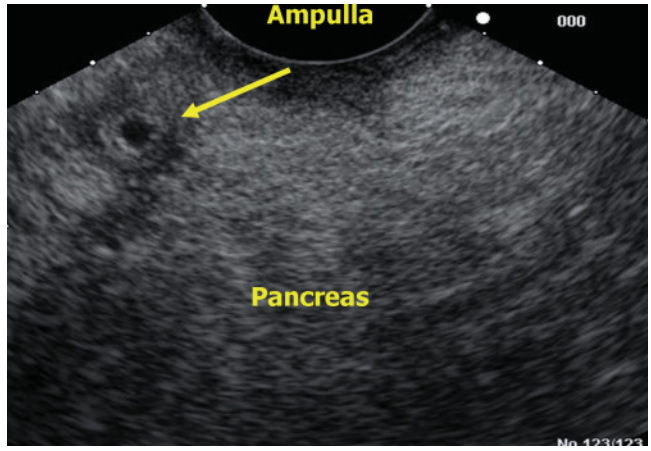

Figure 6.13 Linear endoscopic ultrasound (EUS): ampulla.

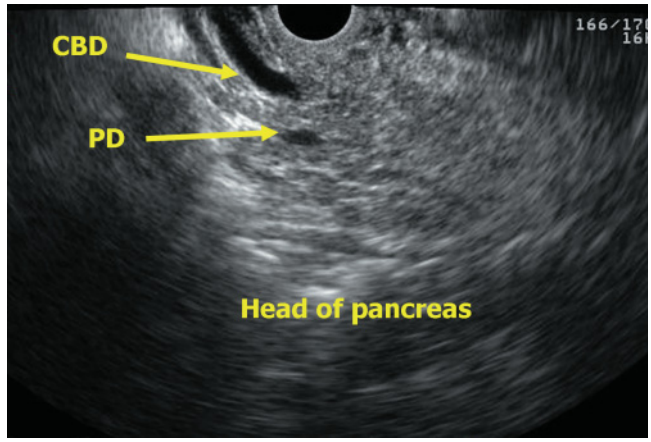

Figure 6.14 Linear endoscopic ultrasound (EUS): head of pancreas (CBD = common bile duct; PD = pancreatic duct).

usually seen in cross section through the stomach (Figure 6.12). A normal caliber duct will appear as a small, sometimes difficult to see, echolucent dot in the middle of the pancreatic parenchyma. Rotation to the left at the level of the celiac axis and body of the pancreas brings into view the pancreatic neck with the portal vein confluence deep to it. The splenic vein merges into the confluence from the patient's left and the superior mesenteric vein runs caudad from the portal vein confluence. A little further leftward rotation of the echoendoscope may produce views of the right border of the pancreatic neck looking down towards the pancreatic head. Sometimes, longitudinal views of the pancreatic duct can be obtained from this view.

As with radial endosonography, the linear duodenum presents the endosonographer with the most variability in endosonographic relationships of vessels, ducts, and peridu-odenal organs. There is a marked transition in the direction of the scope tip and therefore anatomic views between entering the duodenal bulb in a "long position", where the scope tip is pointing cephalad and posterior, and a "short position" when withdrawing from the second portion of the duodenum, where the scope tip is pointing caudad. Generally, we try to start by inserting the linear echoendoscope deep into the second portion of the duodenum. With the echoendoscope in a short position in the second portion of the duodenum, the scope is designed to be facing the medial wall of the duodenum near the region of the ampulla (Figure 6.13). On slightly rotating the scope right or left with very gentle withdrawal, usually the pancreatic duct will be seen first traveling relatively perpendicularly away from the transducer. The CBD will be seen to originate from the ampulla between the duodenal lumen and the pancreatic duct (Figure 6.14). The pancreatic parenchyma seen at the level of the ampulla represents primarily the ventral pancreas. The relative echolucency of the ventral anlage commonly seen by radial endosonography may be less apparent

by linear endoscopic ultrasound (EUS). At this level, if vessels are seen deep to the pancreatic head they are usually the superior mesenteric vein and artery. If one inserts the echoendoscope deeper into the third portion of the duodenum, one may see the uncinate portion of the pancreas nestled among the vessels of the mesenteric root may be seen. Because this is a difficult view to get with a radial instrument, this view using a linear instrument is sometimes the only way in which deep uncinate tumors may be seen. From the ampullary region, further gradual withdrawal and rotation to the left (counterclockwise) will follow the course of the tubular structures of the porta hepatis. The pancreatic head will appear as the tissue between the superior mesenteric vein/portal vein and the duodenal wall.

Endosonographic appearance of the normal pancreatic parenchyma

There is considerable variability in the endosonographic appearance of the pancreatic parenchyma. Classically is has a homogeneous, fine, "salt and pepper" appearance with echogenicity similar to the spleen. The ventral anlange is more echolucent because of its different embryologic origin and its lesser content of echogenic fat. In the elderly, the pancreas can get more nodular with courser echogenicity. In obese patients, the pancreas becomes infiltrated with fat and can almost disappear into the retroperitoneal fat. Fortunately, any pathologic pancreatic lesions, such as dilated ducts, cysts, or neoplasms will be easily visible in the bright background of retroperitoneal fat. Thin patients typically offer particularly detailed imaging of the pancreas.

Chapter video clips

Video 6.1 Linear array EUS head of pancreas.

Video 6.2 Linear array EUS of the pancreas neck to tail.

Video 6.3 Radial array EUS head of pancreas.

Video 6.4 Radial array EUS of the pancreatic neck to tail.

7 Liver, Spleen, and Kidneys: Radial and Linear

Nalini M. Guda[1] and Marc F. Catalano[2]

[1] University of Wisconsin, School of Medicine and Public Health, Pancreatobiliary Services, St. Luke's Medical Center, Milwaukee, WI, USA

[2] Medical College of Wisconsin, Pancreatobiliary Services, St. Luke's Medical Center, Milwaukee, WI, USA

Introduction

This chapter describes the endosonographic features of the major organs of the abdomen: the liver, spleen, kidneys, and adrenal glands. Ultrasound features of the pancreas and bile duct are described elsewhere.

The liver, spleen, kidneys, and adrenal glands (left side) are visualized from the stomach (Videos 7.1 and 7.2).

Liver

Radial endosonography

As the radial probe is advanced through the esophagus into the gastric cardia, the liver is the predominant organ visualized. When positioning the abdominal aorta at the 6 o'clock position, the left lobe of the liver is seen anteriorly and medially to the right (Figure 7.1). The aorta, with a dark hypoechoic band which is the diaphragmatic crux, is seen immediately adjacent to the probe. In this position, near the hiatus, the hepatic veins are seen as anechoic structures, entering the inferior vena cava (IVC). In this position, possibly with left tip deflection, the spleen can be seen on the right of the screen. As the aorta is traced distally, maintaining its 6 o'clock position, the liver may still be seen anteriorly. Vascular structures can be differentiated from ductal structures by a thicker (echogenic) wall and the presence of flow.

When advancing the echoprobe towards the antrum, the gallbladder is often visualized as an oval-shaped anechoic structure. In this position, the porta hepatis can be seen with subtle tip deflection upwards.

Linear endosonography

With the probe at the level of the diaphragmatic hiatus, the longitudinal aorta and celiac artery origin are the most recognizable reference points (Figure 7.2), demonstrated as tubular longitudinal structures. Here, rotation of the probe counterclockwise will bring into view the liver parenchyma and its vascular structures (Figure 7.3).

Advancing the probe at the level of the pylorus and duodenal bulb, clockwise rotation and superior tip deflection brings into view the porta hepatis along with several vascular structures. Use of Doppler can differentiate arterial from venous structures as well as biliary structures.

The entire liver is not visualized by endoscopic ultrasound (EUS). Despite this limitation, it is useful to carefully examine the liver since metastatic processes can be easily identified and biopsied and could lead to a change in clinical staging and management of a suspected tumor.

Spleen

The spleen appears as a homogeneous structure seen between the tail of the pancreas, left kidney, and gastric wall. With a radial scope it is imaged from the gastric cardia. It is similar to liver in echogenicity except that it is devoid of any ducts and vessels (Figure 7.4). It can be easier to follow the splenic vein after visualizing the pancreas from the gastroesophageal (GE) junction. The splenic artery, vein, renal vein, and the left adrenal are usually visualized as well while attempting to scan the spleen. The splenic vein can be easily traced along the inferior aspect of the body and tail of the pancreas; however, the splenic artery is tortuous and it is difficult to follow its course to the celiac trunk. With a linear

Atlas of Endoscopic Ultrasonography, First Edition. Edited by Frank G. Gress, Thomas J. Savides, Brenna Casey Bounds, John C. Deutsch.

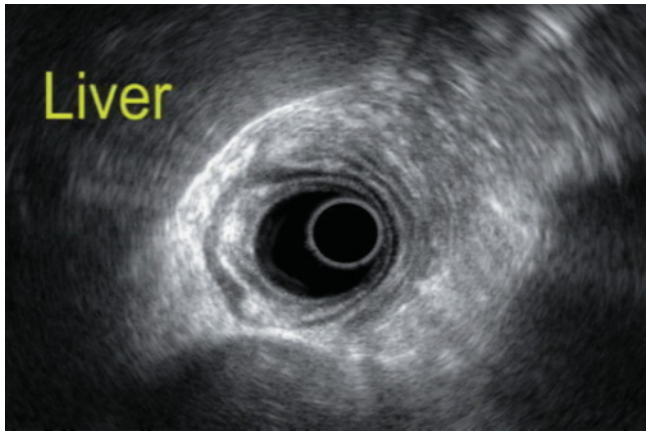

Figure 7.1 Image of the liver scanned by radial ultrasound.

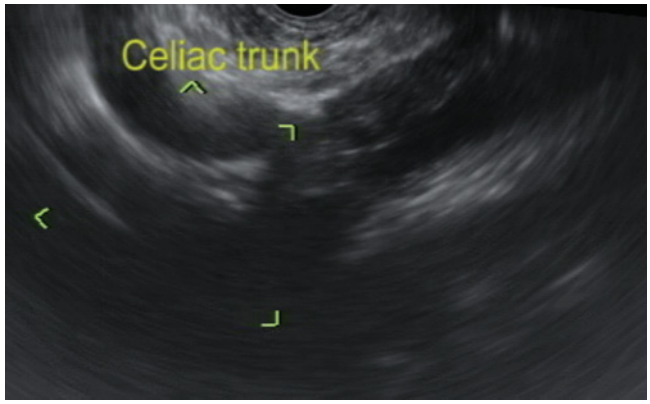

Figure 7.2 Celiac artery imaging by linear ultrasound.

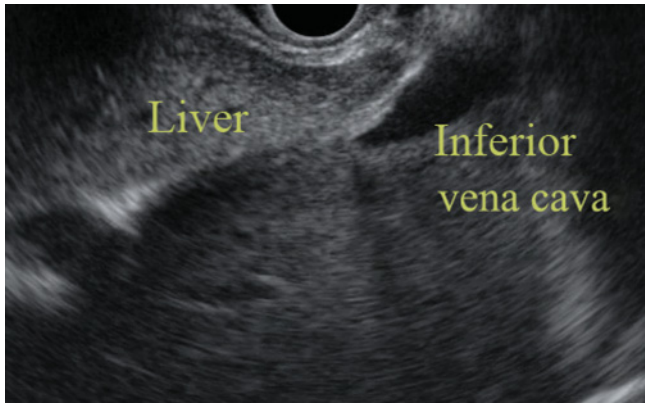

Figure 7.3 Image of liver by linear ultrasound.

scope one has to scan inferior to the left kidney and laterally to visualize the spleen (Figure 7.5).

Kidney

Both the right and left kidneys can be visualized by EUS. The left kidney is readily identified from the fundus of the stomach. It has a complex echogenicity with hypoechoic parenchyma and hypertonic areas within representing the calyceal system.

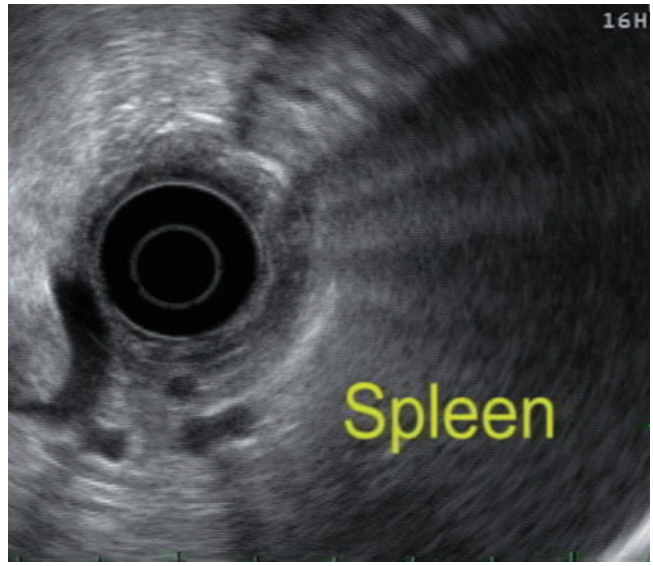

Figure 7.4 Image of spleen by radial ultrasound.

Figure 7.5 Image of spleen by linear ultrasound.

Radial endosonography

With the echoendoscope in the gastric cardia the left kidney is readily visualized. One can see the calyceal system and the renal vessels (Figure 7.6). To visualize the right kidney the echoscope is placed in the D-3 position. Visualization of the IVC and aorta provide easily identifiable landmarks. Upon slow withdrawal, the image brings into view the right kidney immediately right of the probe along with the right renal vein and artery. As the kidney is traced proximally, lateral deflection of the tip may bring into view the right adrenal gland.

Linear endosonography

With a linear scope one can withdraw the scope in the fundus posteriorly towards the pancreas until the tail is visu-

Figure 7.6 Image of left kidney by radial ultrasound.

Figure 7.7 Image of left kidney by linear ultrasound.

alized and then push the scope inferiorly to see the left kidney (Figure 7.7). To view the right kidney, the probe is placed just below the level of the papilla and counterclockwise rotation brings into view the right kidney and its vascular structures. Slow withdrawal allows for visualization of the right adrenal glands.

Adrenal glands

Radial endosonography

With the probe in the gastric fundus, the left adrenal gland can be found immediately proximal to the celiac artery and

Figure 7.8 Image of left adrenal gland by radial ultrasound.

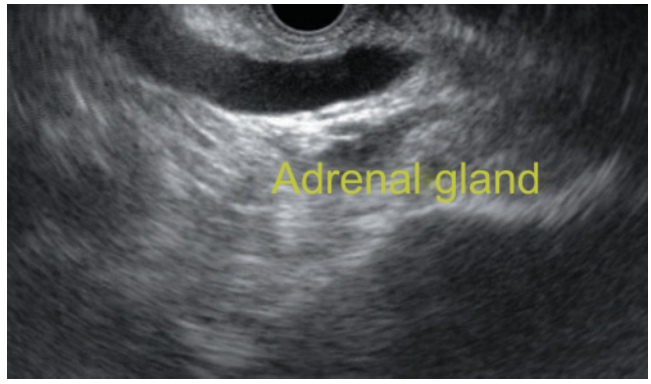

Figure 7.9 Image of left adrenal gland by linear ultrasound.

left of the aorta. It is seen as an echo-poor, thin strip of tissue ("seagull" shaped). The left adrenal gland can also be located by tracing the left kidney cephalad, located medial to the upper pole of the kidney (Figure 7.8).

Linear endosonography

With the probe at the level of the celiac trunk take-off, slight clockwise rotation brings into view the left adrenal gland seen as a thin echo-poor structure (Figure 7.9).

Chapter video clips

Video 7.1 Normal imaging of liver, spleen, kidney, and adrenal by radial ultrasound.

Video 7.2 Normal imaging of liver, spleen, kidney, and adrenal by linear ultrasound.

8 Anatomy of the Anorectum: Radial and Linear

Christoph F. Dietrich
Caritas-Krankenhaus, Bad Mergentheim, Germany

Introduction

Radial and also longitudinal endorectal ultrasound (ERUS) allows precise imaging of the rectal wall in multiple planes and detailed information about the surrouding structures. The same is true for the generally not well known but effective anorectal ultrasound using a conventional transabdominal transducer technique (PNUS: perineal ultrasound). A transversal section with a 360-degree transducer is most helpful for orientation and, therefore, for the examination of the anal canal, whereas for examination of more orally located structures (flexible or stiff) radial as well as sector scanners can be used. Sagittal, frontal and transverse, and other variable longitudinal sections have to be considered.

The anatomical relationship between the internal anal sphincter (IAS), external anal sphincter (EAS), levator ani and puborectal muscles, and ischiorectal fossa can be reconstructed by the examiner's anatomical knowledge and his or her capability of a multidimensional imagination. Reproducible documentation and imaging can be also done using three-dimensional (3D) techniques or real-time 3D technique (also called 4D).

Examination technique

A comprehensive categorization of the anal canal and distal rectum can be achieved by examining at different levels. From a didactic point of view, a step-by-step approach by retracting the transducer indicating the distance from the anocutaneous level in centimeters seems to be helpful. A pushing forward technique may also be done but is less often used due to less reproducibility. Orientation is achieved by identification of the surrounding leading structures (bladder, prostate, vagina, puborectal muscle, etc.) and details are best seen with appropriate focussing and instrument adjustment (Video 8.1).

Retracting the transducer corresponding sections at 4–6 cm (perirectal tissue, prostate, seminal vesicles, cervix, vagina), at 2–4 cm (IAS, EAS, puborectal muscle), and at a superficial level at 0–2 cm (EAS with continous fibers radiating into the subcutaneous fat) are visualized.

Orientation

Reporting of the anatomy and findings should always use the clock-orientation as a reference (i.e. the pubic symphysis is always at the 12 o'clock position).

Normal anatomy

Anatomical remarks

The anal canal is covered by a columnar epithelium below the anal crypts. The mucosa is a transitional cell epithelium and begins at the height of the anal crypts. It can, however, be only inconstantly visualized as a faintly dark layer with scattered echos of medium echogenicity. The transitional epithelium disappears in the first echo-rich border area dependend on the type and frequency of the ultrasound probe. The dentate line and the anorectal crypts are of importance with respect to fistula formation but often cannot be seen mainly due to the compression of the anal canal by the endorectal probe. The hemorrhoidal plexus normally is virtually not visible, unless very thin probes are used or thrombosis is present. Important anatomical details are summarized in Table 8.1.

Rectal wall

The rectum can be examined at any level by endoscopic and/or visual orientation. The echogenicity of the various mural

Atlas of Endoscopic Ultrasonography, First Edition. Edited by Frank G. Gress, Thomas J. Savides, Brenna Casey Bounds, John C. Deutsch.

layers in the anal canal is similar to that in the gastrointestinal tract elsewhere and characterized by different, well separated bands when imaged from the lumen. Above the transition zone the typical sonographic features of the five (or nine) layered rectal wall are found. The typical five layers comprise the echo-rich borderline between the probe and the mucosa, the echo-poor mucosa, the echo-rich submucosa, the echo-poor muscularis propria, the echo-rich serosa and the border area to the perirectal fat tissue. Using highly sophisticated equipment up to nine layers can be displayed, including the two parts of the muscle's proper layer differentiating the stratum circulare (inner ring layer) and the stratum longitudinale (outer ring layer) separated by a connective tissue-like septum. A further differentiation of the inner layers yields additional layer separation in the mucosa and submucosa. In addition, it is relevant that these layer structures are important in staging rectal cancer according to the TNM classification.

Table 8.1 Anatomical structures and abbreviations.

ARUS	Anorectal endosonography (alternative: PNUS – perineal ultrasound)
ERUS	Endorectal endosonography
C	Cutis (skin)
Muc	Mucosa
IAS	Internal anal sphincter. Musculus sphincter ani internus (inner [ring] muscle fibers of the rectum radiating into M. sphincter ani internus)
EAS	External anal sphincter. M. sphincter ani externus
LAM	Levator ani muscle (M. puborectalis, M. ischiococcygeus, M. iliococcygeus, M. pubococcygeus; endosonographic separation of the muscle layer is not always possible)
LM	Longitudinal muscle, M. corrugator ani (longitudinal muscle fibers of the rectum radiating into M. sphincter ani externus)

Level of the prostate or cervix uteri

The standardized approach starts at a level of 4–6 cm above the anocutaneous line (ab ano) by delineating the seminal vesicles, prostate, and urethra in man, whereas at this level the cervix uteri and vagina can be displayed in women, and the urinary bladder in both. The internal iliac vessels cross the rectosigmoid colon just proximal to this region, but definite determination of the edge between the rectum and sigmoid colon is endosonographically still an unsolved problem. The surrounding bones and muscles of the pelvic floor (levator ani muscles (mm. ischiococcygeus, iliococcygeus, and pubococcygeus) including the V-shaped puborectal muscle) (Figure 8.1) should be identified since the anal canal ends at this level and the rectum begins. This funnel-like structure of the levator ani muscle separates the extraperitoneal pelvis into an infraperitoneal or pelvirectal and a subcutaneous or ischiorectal space. The lateral border of the pelvic floor corresponds to the M. obturatorius internus with the foramen obturatorium.

External anal sphincter level

The second section at 2–4 cm ab ano shows as a leading structure the prominent external anal sphincter as a 5–10 mm broad layer characterized by often concentrically arranged echo-rich and sometimes inhomogeneous series of lines (Video 8.1 and Figure 8.2) depending on the examination technique used (criteria: radial or linear probes, diameter of the probe, transducer frequency, tissue harmonic imaging, focus zone).

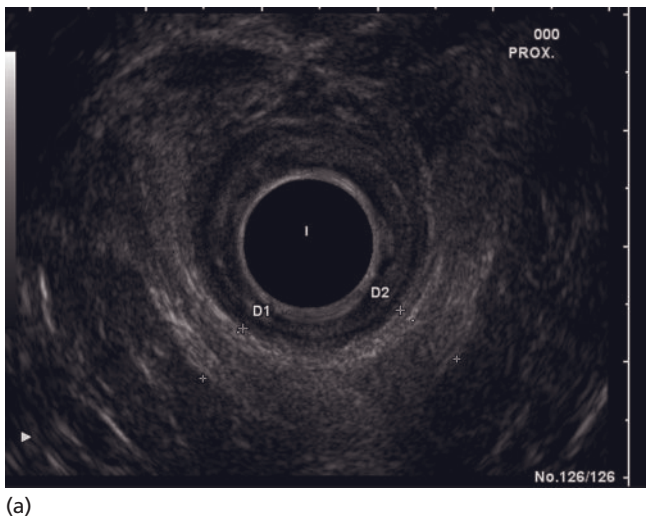

(a)

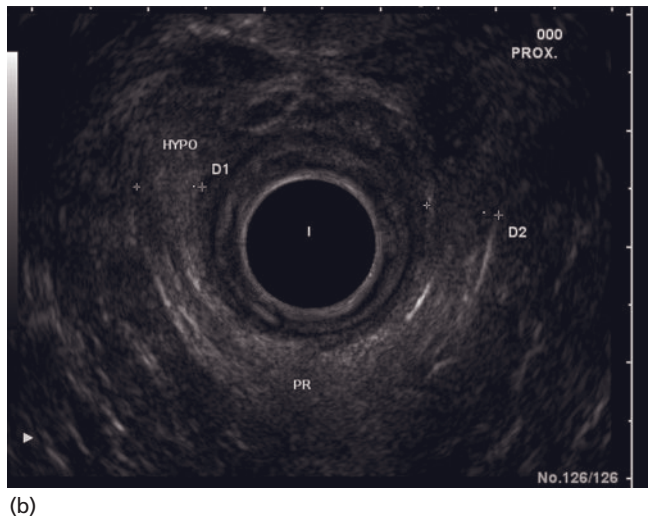

(b)

Figure 8.1 Levator ani muscle with the puborectal part (PR) in between markers (a). The more distant parts of this muscles often show a more inhomogenous and hypoechoic appearance (Hypo) (b).

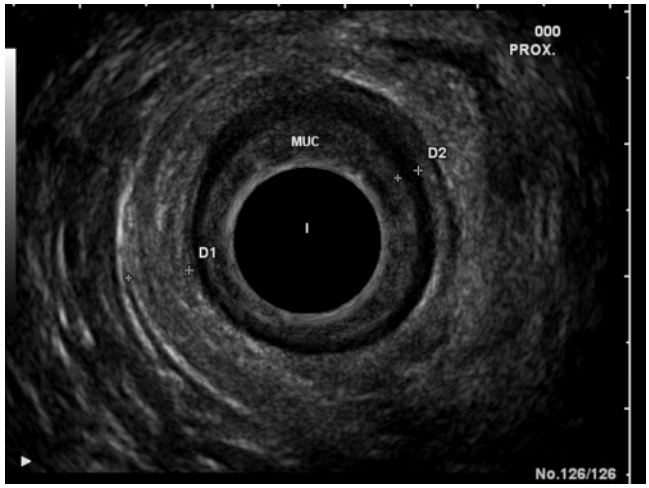

Figure 8.2 Internal anal sphincter (echo-poor) and external anal sphincter (echo-rich). The superficial layer of the anal canal is also indicated (MUC).

The EAS is composed of three more or less separated parts, i.e. the subcutaneous (pars subcutanea), the superficial (pars superficialis), and the deep (pars profunda) components which are confluent with each other. It is of great importance to understand that the shape and configuration of the EAS differs significantly between males and females. The EAS continues into the puborectal muscle (PRM) at the cranial margin of the anal canal which is of importance for the delineation of ischiorectal and pelvirectal fossae. More orally the muscular structures are no longer vertically imaged so that this part of the muscle yields a weaker and less defined image (Video 8.1). At this level the os coccygeum with the coccygeous ligament can be also delineated. Ventrally this broad muscle layer reaches the inferior part of the pubic bone with inclusion of the urethra and the inferior part of the prostate or the vagina, respectively.

Coming back to gender differences, one has to keep in mind that the anal canal is generally 0.5–1.0 cm longer in males and the three different parts of the EAS are configured cylindrically around the anus, which means that the muscle shape and length is roughly the same ventrally and dorsally. In contrast, the three sections of the EAS are fused to a narrow band ventrally at the level of the pars superficialis in females. The notion of this anatomical difference is of importance in order not to misinterpret normal anatomical findings.

Normal sphincter values are highly dependent on age, sex, and examination technique parameters (Table 8.2). The less pronounced echo-poor IAS can be visualized more distally than the PRM and EAS (see below).

Internal anal sphincter level

The IAS can regularly be seen as a homogeneous echo-poor layer with a thickness of 2–4 mm without any relevant gender-dependent differences a little more distally than the EAS (Figure 8.2). The anal mucosa and the IAS muscle are considered the continuation of the inner rectal ring muscle. The measured thickness, however, depends on the probes used as an increasing probe diameter will lead to a thinning of the surrounding structures. The echo texture and thickness of the IAS tend to increase with age. The normal thickness, however, does not exceed 4 mm even in the elderly.

Table 8.2 Normal sphincter values. This is highly dependent on age, sex, and probe diameter, since the measured thickness depends on the probes used as an increasing probe diameter will lead to a thinning of the surrounding structures.

M. sphincter ani internus	1.5–4.0 mm
M. sphincter ani externus	5–10 mm

The intersphincteric space with fibers of the corrugator (or longitudinal) muscle as a continuation of the rectal external longitudinal muscle layer is seen endosonographically as a thin echo-poor layer containing echo-rich connective tissue septa representing the border areas of the echo-poor IAS and the first less echogenic layer of the EAS. It can be identified a little above 2 cm from the anocutaneous line. At this level the fossa ischiorectalis, the anococcygeal ligament, and the os coccygeum can be visualized. Additional points of orientation at this level are the radix penis with the ischiocavernosus muscle and the ramus ossis ischii. At this level also the echo-rich border area between the ultrasound probe and the mucosa (or the anal cutis), the echo-poor, extremely thin mucosa, which often cannot be recognized as a defined layer due to a lacking muscularis and its very thin diameter, the echo-rich submucosa (and subcutis) can be differentiated leading to the structures of the lowest level.

Cutis and subcutis

The last section shows the cutis, the transitional epithelium, and the subcutis with the transition to the submucosa and more orally the IAS surrounded by the superficial and profound transverse perineal muscle and the fossa ischiorectalis as described above. The submucosa and the subcutaneous connective tissue appear as a homogeneous echogenic layer increasing in thickness from the superior to the inferior margin of the anal canal. The transversus perinei profundus and superficialis muscles and the ischiocavernosus muscle can also be imaged by ERUS.

Chapter video clips

Video 8.1 Radial array EUS of the distal rectum and anal canal in a male subject.

2 Upper and Lower GI EUS

9 Esophageal Cancer

Syed M. Abbas Fehmi
University of California San Diego, La Jolla, CA, USA

Introduction

In 2005, according to the American Cancer Society, there were 14 520 new cases of esophageal cancer in the United States. Most were adenocarcinoma, and 13 570 deaths were associated with this malignancy. This represents a 300–500% increase in esophageal cancer incidence over the last 30 years. In the last 10 years, the role of endoscopic ultrasound (EUS) has evolved in the management of esophageal cancer with EUS currently essential for accurate loco regional staging and addressing the key management question of operability.

American Joint Committee on Cancer staging guidelines for esophageal cancer 2010 and implications for endosonographer

The former guidelines from the American Joint Committee on Cancer (AJCC) were based on simple orderly increasing T, then N, and then M classifications. This classification was not optimal for esophagus due to its unique lymphatic anatomy, permitting lymph node (LN) metastasis quite early from superficial cancer (one of the only places in the gastrointestinal [GI] tract to have lymphatics in lamina propria). An advanced T stage cancer with no or few LNs involved may have better prognosis than an early T stage cancer with a higher number of positive LNs. Similarly, the biologic activity of tumor reflected by histology (well differentiated to undifferentiated) was not incorporated in older staging. The new staging system addresses these issues (Table 9.1).

The important changes affecting the endosonographer in daily practice includes simplification of tumor location with the location of primary tumor defined by upper end of cancer in centimeters from the incisors (cervical esophagus 15 cm to <20 cm; upper thoracic esophagus 20 cm to <25 cm; middle thoracic esophagus 25 cm to <30 cm; and lower esophagus 30 cm to 40 cm). In addition, cancers whose epicenter is in the lower thoracic esophagus, esophagogastric junction (EGJ), or within the proximal 5 cm of the stomach (cardia) that extend into EGJ are stage grouped similar to adenocarcinoma of esophagus.

The guidelines of TNM classification now have a redefined Tis, T4, N, and M component (details reviewed below). Lastly, stage groupings are now separate for squamous cell cancer and adenocarcinoma.

Role of EUS in staging of esophageal cancer

The loco regional staging of esophageal cancer is most accurately done by EUS when compared to any other imaging modality (including computed tomography [CT], positron emission tomography [PET] scans, or magnetic resonance imaging [MRI]). Accurate staging helps predict the prognosis, optimal management strategy, and provides a standard platform for comparison of patients for research purposes.

EUS can examine the different wall layers of the esophagus, which forms the basis for its superiority over other imaging modalities. Wall-layer examination is extremely important for the "T" staging component of TNM and G classification system proposed by the AJCC.

The reported accuracy of EUS for T staging is 80–90%. The role of EUS in the setting of Barrett's esophagus or Tis lesion (now defined as "high grade dysplasia" and includes all non-neoplastic epithelium formally referred to as carcinoma in situ) is to exclude periesophageal

Atlas of Endoscopic Ultrasonography, First Edition. Edited by Frank G. Gress, Thomas J. Savides, Brenna Casey Bounds, John C. Deutsch.

Table 9.1 American Joint Committee on Cancer (AJCC) staging of esophageal cancer, 2010 (seventh edition).

TX	Primary tumor cannot be assessed
T0	No evidence of primary tumor
Tis	High grade dysplasia
T1	Tumor invades the lamina propria, muscularis mucosae, or submucosa
T1a	Tumor invades the lamina propria or muscularis mucosae
T1b	Tumor invades the submucosa
T2	Tumor invades the muscularis propria
T3	Tumor invades the adventitia
T4	Tumor invades adjacent structures
T4a	Resectable tumor invading the pleura, pericardium, or diaphragm
T4b	Unresectable tumor invading the other adjacent structures such as aorta, vertebral body, trachea, etc.
NX	Regional lymph nodes cannot be assessed
N0	No regional lymph node metastasis
N1	Metastasis in 1–2 regional lymph nodes
N2	Metastasis in 3–6 regional lymph nodes
N3	Metastasis in 7 or more regional lymph nodes
M0	No distant metastasis
M1	Distant metastasis (no longer M1a and M1b)

Additional changes
Esophagogastric junction (EGJ) cancers are redefined, separate stage groupings for adenocarcinoma and squamous cell carcinoma, Histologic grade is factored into stage groupings, tumor location included in staging for squamous cell carcinoma

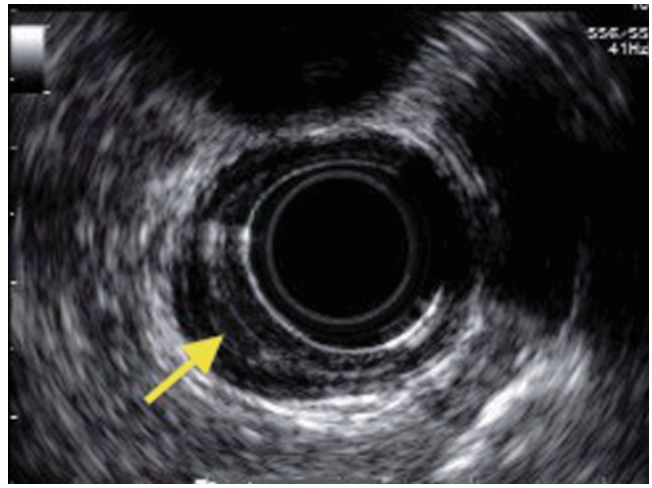

Figure 9.1 Endoscopic ultrasound (EUS) picture of upper thoracic esophageal squamous cell cancer. T1a lesion (yellow arrow), submucosa is intact.

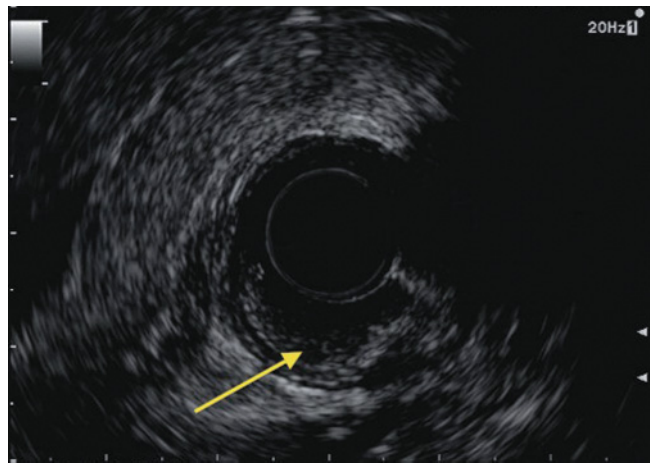

Figure 9.2 Endoscopic ultrasound (EUS) picture of lower thoracic esophageal adenocarcinoma. T1a lesion (yellow arrow), surgery showed no involvement of submucosa.

lymphadenopathy or a mass. T1 lesions can be divided into T1a or T1b depending if tumor is limited to mucosa (Figures 9.1 and 9.2) versus submucosal invasion (Figures 9.3 and 9.4, and Video 9.1). If the tumor is observed to have progressed to invade the fourth layer (muscularis propria [MP] or proper muscle layer), the tumor is classified as T2 (Figures 9.5 and 9.6, and Video 9.1). When the tumor invades through the MP into the adventitia, it is classified as a T3 lesion (Figures 9.7 and 9.8, and Video 9.1). If invasion or involvement of any of the mediastinal structures is observed, it will then be classified as a T4 lesion. Structures to be examined for involvement during EUS exam include pleura, diaphragm, and pericardium – all now staged as T4a (Figure 9.9) (thought to be potentially resectable), versus aorta, trachea, vertebral body, etc. – all now staged as T4b (Figure 9.10) (thought to be unresectable).

For N staging, EUS has an accuracy of 75–80%. Endoscopic ultrasound-guided fine needle aspiration (EUS-FNA) can improve accuracy, but care has to be taken that the needle does not go through the area of the tumor for concerns of false positive results. The positive predictive value of four subjective endosonographic features of LNs (round, hypoechoic, sharp edges, and size 1 cm or more) is about 90%. If these are present, the need to do biopsy is less. With the revised TNM classification, the N component has been subclassified according to the number of regional LNs containing metastasis (N1 meaning metastases in 1–2 regional nodes; N2 meaning 3–6 nodes; and N3 meaning 7 or more). M1 disease is now defined as metastasis to non-regional LNs or distant sites and the M1a/M1b subclassification has been abolished as it was found not be helpful.

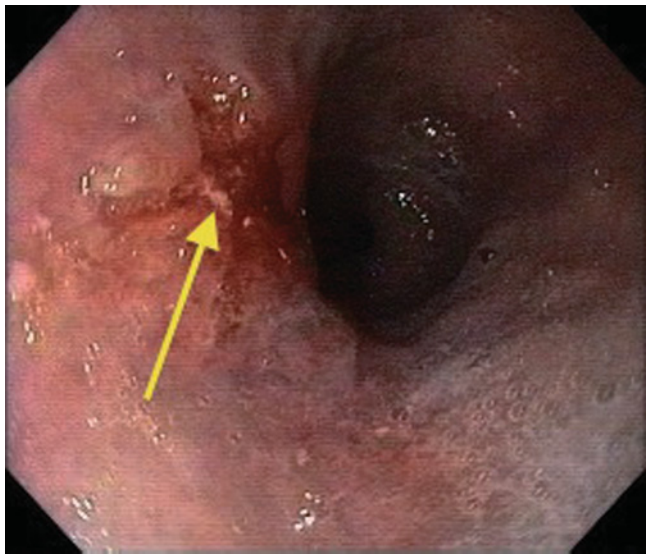

(a)

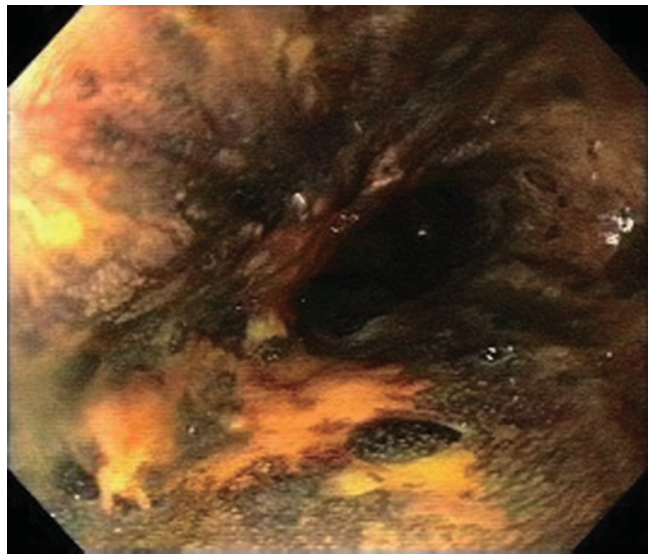

(b)

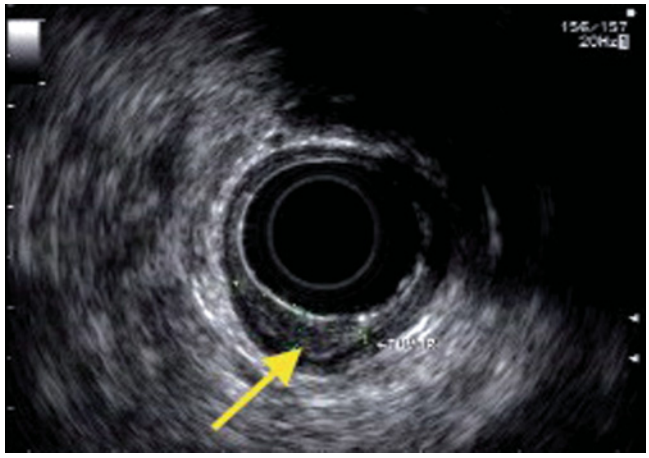

(c)

(d)

Figure 9.3 T1b lesion, squamous cell cancer with nodularity in lower thoracic esophagus shown by yellow arrow (a); Lugols staining (b); endoscopic ultrasound (EUS) image showing submucosal invasion but no involvement of muscularis propria (MP) by yellow arrow (c); endoscopic mucosal resection to confirming submucosal invasion (d).

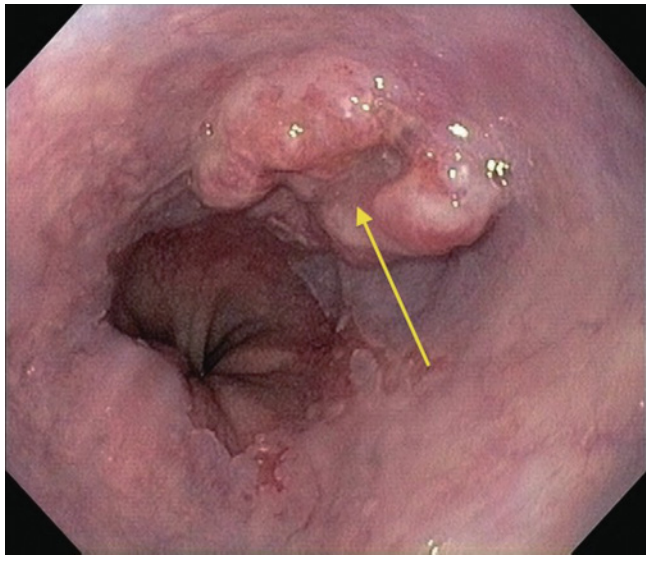

(a)

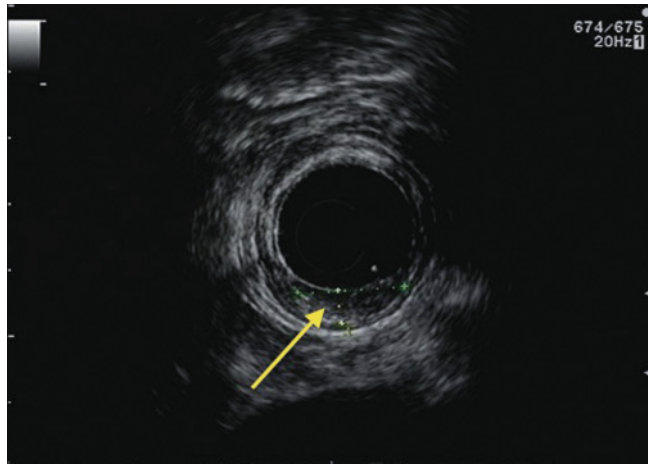

(b)

Figure 9.4 T1b lesion, adenocarcinoma in lower thoracic esophagus with central depression shown by yellow arrow (a); endoscopic ultrasound (EUS) image showing submucosal invasion but no involvement of muscularis propria (MP) shown by yellow arrow (b).

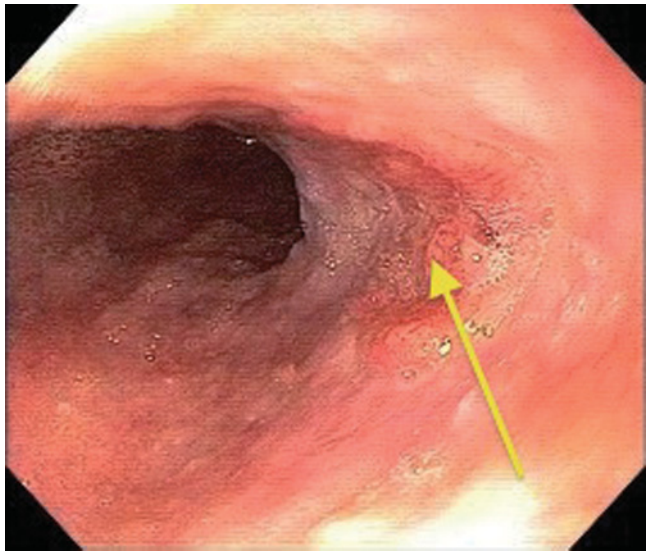

(a)

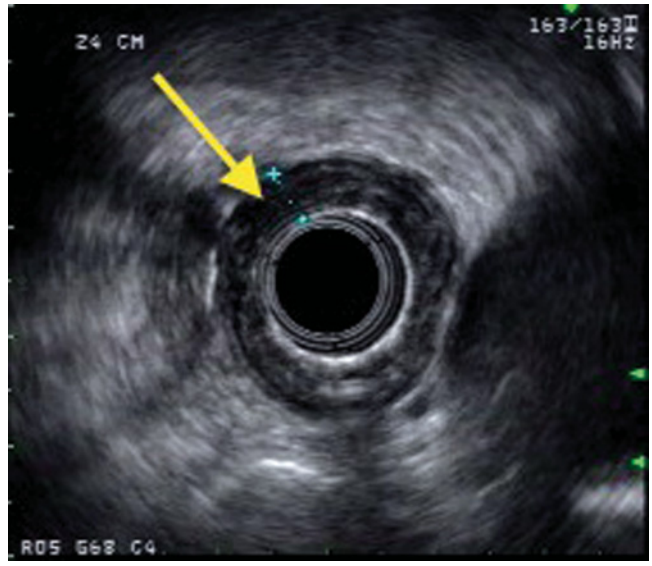

(b)

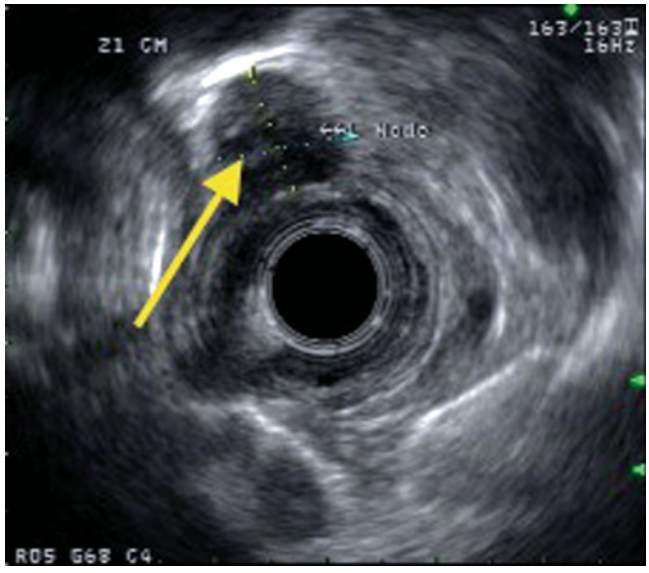

(c)

Figure 9.5 T2N1Mx lesion, squamous cell cancer with ulceration 24 cm from incisors shown by yellow arrow (a); endoscopic ultrasound (EUS) image showing invasion of muscularis propria (MP) but not through the MP shown by arrow (b); malignant appearing paratracheal lymph node also observed and marked by arrow (c). This has all four concerning features suggesting malignant involvement (fine needle aspiration [FNA] proven though not necessary). Since a total of two or less lymph nodes are observed during exam, lesion classified as N1 according to the new American Joint Committee on Cancer (AJCC) classification system.

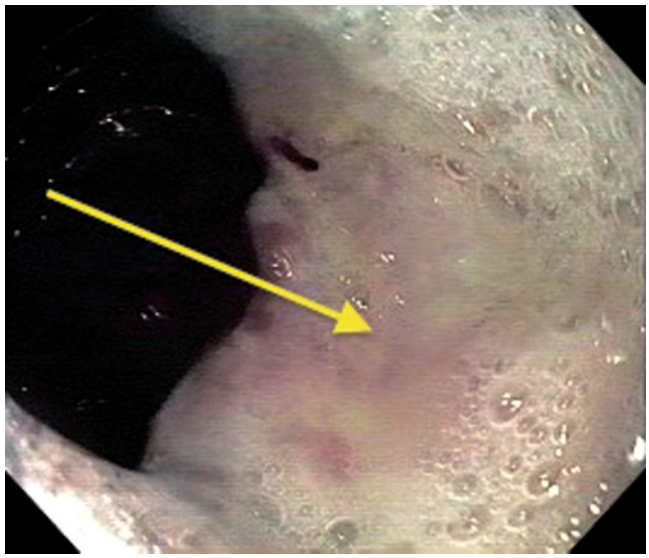

(a)

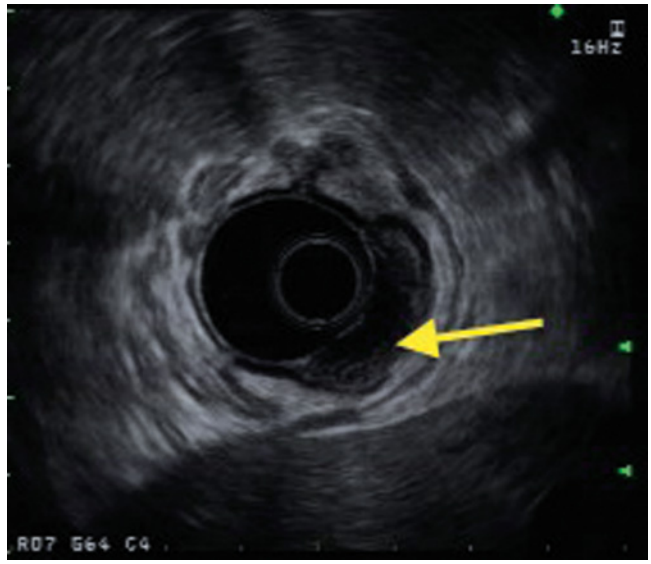

(b)

Figure 9.6 T2N0Mx lesion, adenocarcinoma of lower thoracic esophagus involving gastroesophageal junction (EGJ) marked by arrow (a); endoscopic ultrasound (EUS) image showing invasion of muscularis propria (MP) but not through the MP marked by arrow (b).

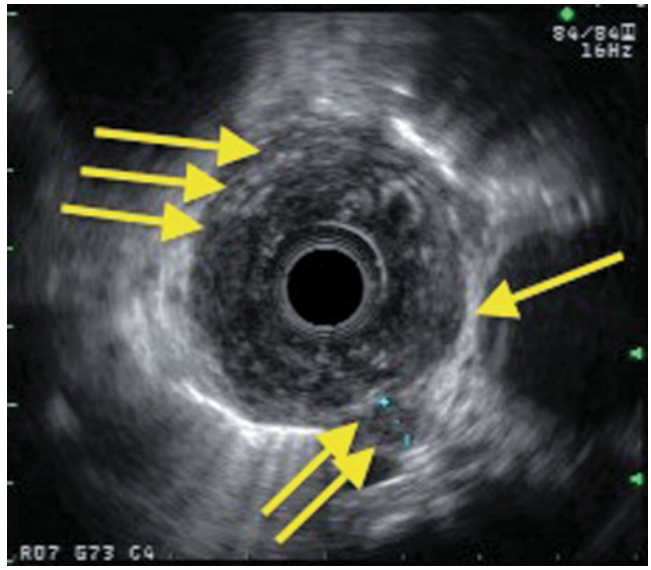

Figure 9.7 T3N3Mx lesion, adenocarcinoma involving the lower thoracic esophagus, lesion invades through the muscularis propria (MP) into the periesophageal fat marked by three arrows. Note malignant appearing lymph node (LN) marked by double arrows: a total of eight such LNs were observed during the exam making this a N3 lesion (according to the new American Joint Committee on Cancer [AJCC] guideline). Note also the intact plane between the lesion and aorta marked by single arrow.

Limitations

It is important to note that edema, cellular infiltration, and neoplastic masses can produce an endosonographic image of a thickened esophageal wall upstaging early disease. EUS is considerably less accurate (40%) for restaging of disease after chemo-radiation therapy secondary to the associated fibrosis and inflammation. EUS-FNA for restaging of loco regional lymphadenopathy may have a role and is undergoing evaluation.

Impact of EUS staging on management

The management for early disease may differ somewhat between institutions, but the treatment outcome for patients is highly stage dependant. For early stage disease, operability is the key question that heavily depends on the accurate T staging by EUS. Currently for Tis or T1a disease in absence of any LNs, endoscopic approach is the usually the preferred option. Even for T1b disease, endoscopic mucosal resection (EMR) has usually been done to confirm

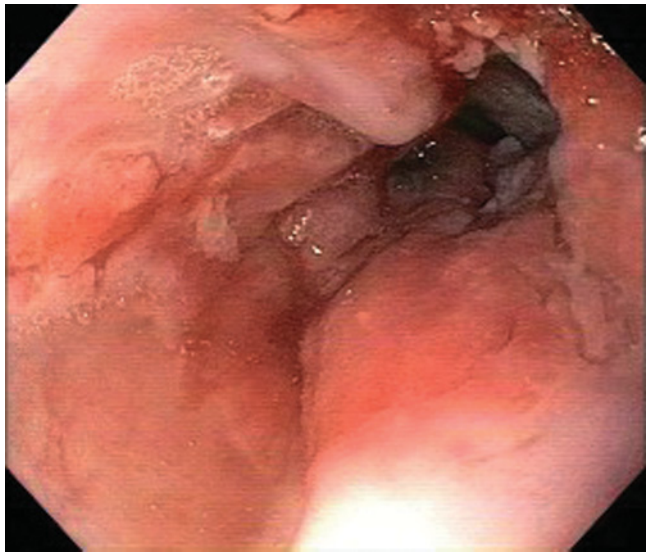

(a)

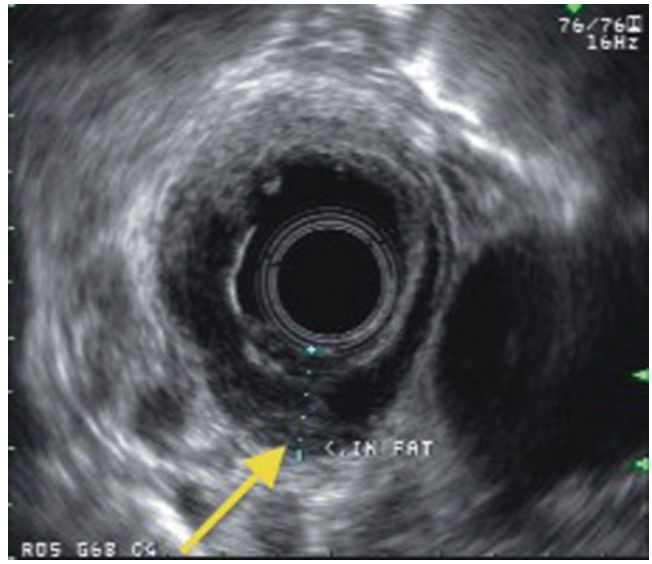

(b)

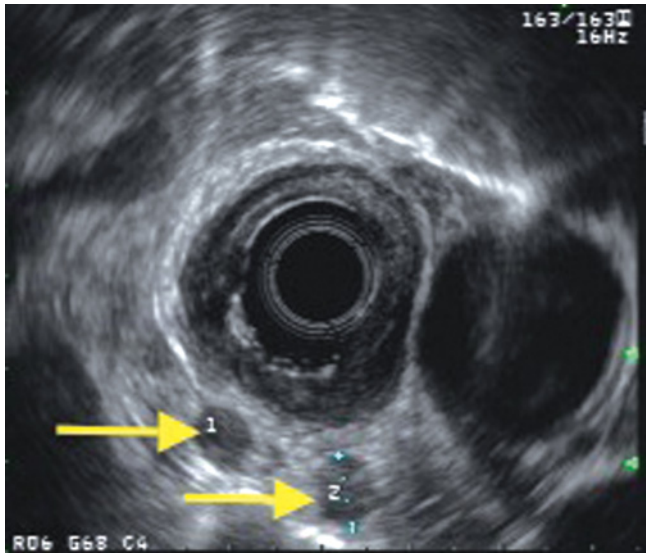

(c)

Figure 9.8 T3N2Mx lesion, adenocarcinoma partially obstructing lower thoracic esophagus, traversed after dilation to complete endoscopic and endosonographic examination (a); endoscopic ultrasound (EUS) image showing lesion invades through the muscularis propria (MP) into the periesophageal fat marked by arrow (b). A total of four malignant appearing lymph nodes were observed during the examination (N2 lesion), two shown in the EUS picture marked by arrows (c).

submucosal invasion. In some poor surgical candidates more aggressive endoscopic therapy with cryoablation may also be offered. Outcomes data is being gathered. Usually for T2 disease with no obvious LN involvement, surgery is done. However, if LN involvement is suspected or it is a T3 disease, neoadjuvant therapy followed by surgery is usually the preferred option. The use of neoadjuvant therapy with subsequent surgery is becoming increasingly popular. T4 disease is usually unresectable with no surgical opportunity for cure. Lastly, EUS in combination with PET–CT has been shown to result in more accurate staging with improved survival and reduction in the number of unnecessary operations (down from 44% to 21%).

Technique

The endosonographer must be familiar with the patient's history (specifically the presence and degree of dysphagia) and the impact of EUS findings on management. It is advis-

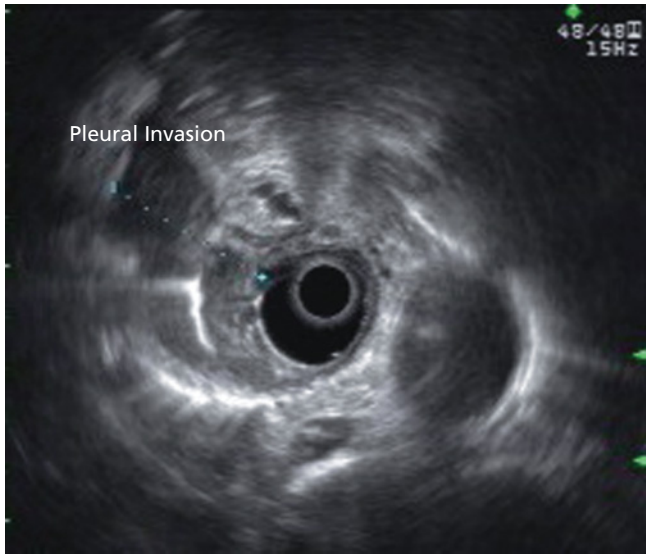

Figure 9.9 T4a lesion, adenocarcinoma in lower thoracic esophagus invading through the muscularis propria (MP) and the periesophageal fat into the right pleura (note made of loss of echogenic plane between lesion and right pleura). According to the new American Joint Committee on Cancer (AJCC) guideline, this is a potentially resectable lesion staged as T4a.

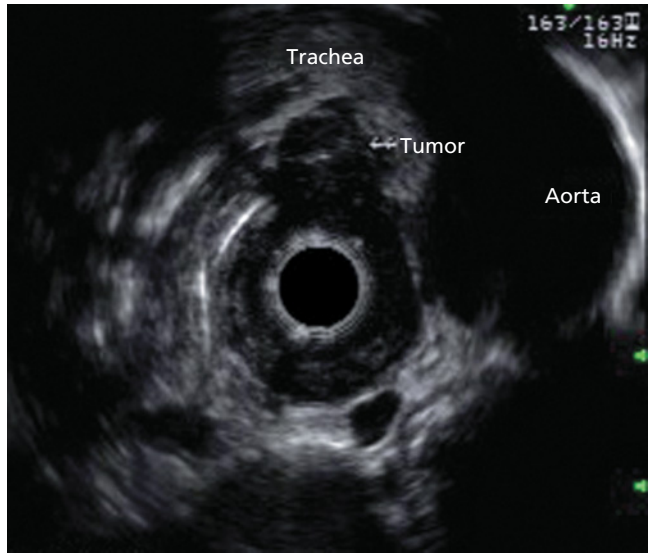

Figure 9.10 T4b lesion, squamous cell cancer in upper thoracic esophagus invading through the muscularis propria (MP) and the periesophageal fat into the aorta and trachea (note made of loss of echogenic plane between lesion and the aorta and trachea). According to the new American Joint Committee on Cancer (AJCC) guideline, this is an unresectable lesion staged as T4b.

able to perform an esophagogastroduodenoscopy (EGD) before EUS in patients to confirm the proximal extent of lesion (for accurate staging) and to assess for need of dilation. In some centers surgery is being offered for staging with an initial approach being minimally invasive; in most centers though, EUS is used. The radial array echoendoscope is most frequently used due to its 360-degree imagining and ease of use. The standard technique is to do multiple pull-backs from the stomach into proximal esophagus paying close attention to the wall layers and periesophageal LNs. Effort should be made to evaluate the liver for metastasis and examine the celiac axis for adenopathy. For stenotic tumors not allowing passage of the usual 13 mm tip echoendoscopes, dilation to 15 mm or 45 Fr is usually required. Risks of dilation need to be weighed against perceived benefits of any additional information gained by passing the endoscope distal to stenosis. Some strategies include use of thin non-optic probes or endobronchial scopes versus embedding the tip of a regular EUS scope in the proximal aspect of tumor and trying to obtain as much information as possible (T3 lesion or N1). Non-optic probes with high frequency can also be used to distinguish T1a and T1b lesions with high accuracy. However, with newer electronic EUS scopes and improved processors, imaging has improved so that high frequency probes are not routinely used in the United States. In addition, EMR is being increasingly utilized for better histologic assessment for mucosal versus submucosal involvement (Figure 9.3d).

Chapter video clip

Video 9.1 Esophageal cancer endosonography.

10 Esophageal Motility Disorders

Thuy Anh Le and Ravinder K. Mittal
University of California, San Diego, La Jolla, CA, USA

Esophageal motility

At first glance, the esophagus appears to be simple in design – composed of two layers of muscle, flanked by upper and lower sphincters. A deeper look however reveals the complexities of the interconnected parts, which must work in a coordinated, peristaltic fashion to provide the most basic human function of eating and delivery of a food into the stomach. Using manometry, the function of the circular muscle (CM) and related pressures were evaluated in normal subjects and patients with disease during the last 50 years. But this was only a partial view of the intricate relationship between two muscle layers of the esophagus. Study of the longitudinal muscle (LM) and its role in esophageal motility disorders were limited due to difficulty with recording its function. With the advent of catheter-based high frequency intraluminal ultrasound (HFIUS), a new door was opened to the understanding of the longitudinal muscle layer.

Catheter-based ultrasound imaging

Since its first use in the early 1990s by Miller and associates, HFIUS imaging has become a powerful tool to study esophageal motility *in-vivo* in humans. Catheter-based ultrasound probes can image at higher frequencies than dedicated EUS scopes, between 12 and 20 MHz. The higher frequencies allow higher resolution with less depth of penetration. HFIUS images recorded simultaneously and continuously with manometry, pH, and impedance provides a unique way to study the complex, dynamic physiologic and pathophysiologic events of the esophagus. An intravascular ultrasound catheter is placed through the core lumen of a manometry catheter and this assembly can be placed through the nose to record pressure and ultrasound images of the esophagus (Figure 10.1). Manometric measures of the amplitudes of esophageal contractions reflect the force of CM contraction, whereas HFIUS images showing the change of the cross sectional area at the peak of contraction is a measure of the force of LM contraction.

Increased muscle thickness in esophageal motor disorder

Some of the earliest studies using the HFIUS modality explored the relationship between esophageal muscle thickness and pressures in primary esophageal motility disorders. Baseline muscle thickness was found to be significantly larger in patients with esophageal motility disorders compared to healthy subjects. The increase in baseline muscle thickness of both the circular and longitudinal layers, thought to be due to increased tone of the LM or hypertrophy of the two muscle layers, is graded in the spastic esophageal motility disorders: greatest for achalasia, then diffuse esophageal spasm (DES), and then nutcracker esophagus (NCE) (Figure 10.2). The degree of muscle hypertrophy may determine the severity of motor disorders since achalasia is most severe, DES moderate, and NCE mildest in clinical symptoms and functional changes. Furthermore, baseline muscle thickness is greater in the distal esophagus compared to proximal, which is similar to pressures from manometry (Figure 10.3).

Ultrasound imaging to detect longitudinal muscle contraction under physiology and pathophysiology

Early observations of superimposed esophageal pressures and muscle cross-sectional area (CSA) tracings suggest that muscle CSA begins to increase 1–2 seconds before the increase in manometric pressures, peaks at the same time, and then return to baseline 2–3 seconds after the end of contraction (Figure 10.4). However, later observations found

Atlas of Endoscopic Ultrasonography, First Edition. Edited by Frank G. Gress, Thomas J. Savides, Brenna Casey Bounds, John C. Deutsch.

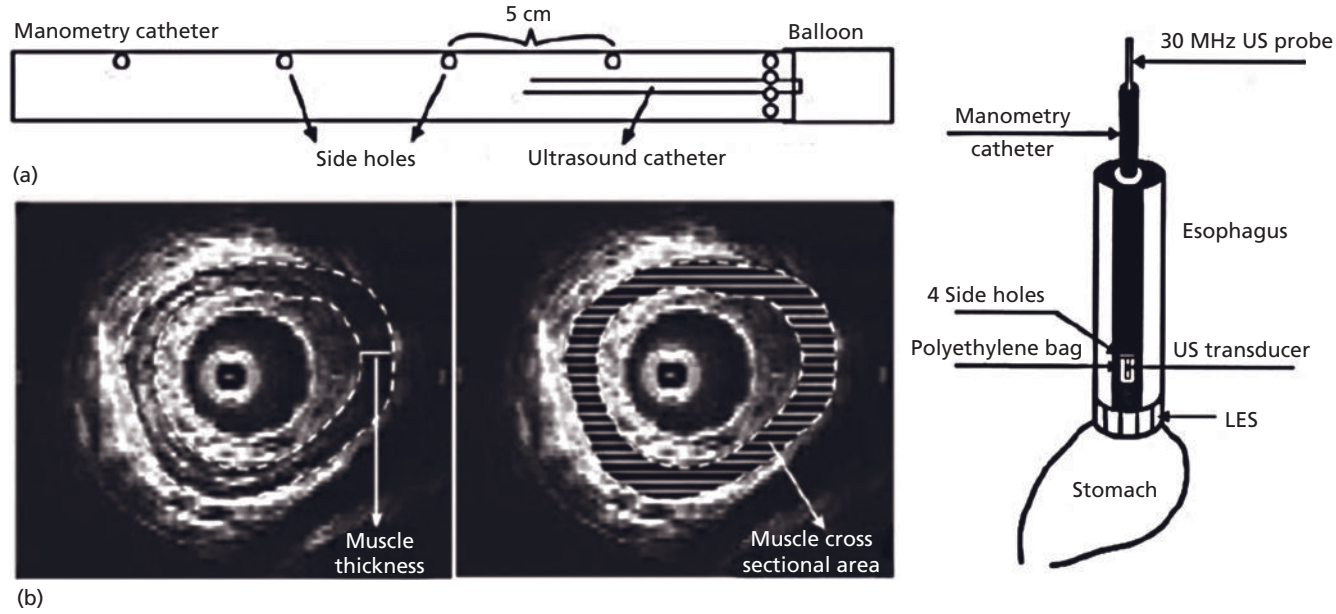

Figure 10.1 (a) Schematics of the catheter system to record pressure and ultrasound images. The ultrasound transducer is located just distal to the tip of the catheter, 2–3 mm distal to the four pressure recording sites. The catheter/ultrasound acquisition system allows capturing of a 360-degree view of the esophagus. (b) Muscle cross-sectional area is obtained by subtracting areas from the outer and inner rings (outer ring is the outer border of the esophagus and inner ring is the outer border of the esophageal mucosa). (Source: Dogan *et al*. 2007. *The American Journal of Gastroenterology*, 102(1): 138, with permission from the Nature Publishing Group.)

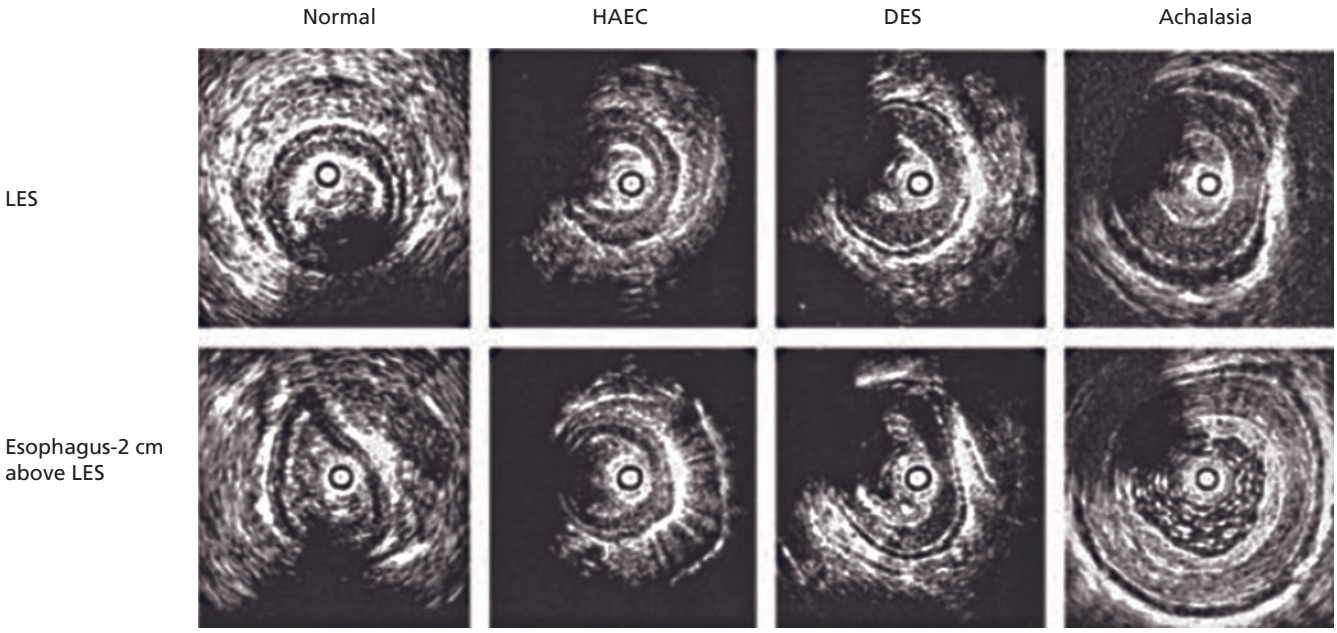

Figure 10.2 Ultrasound images of the lower esophageal sphincter (LES) and esophageal body in healthy subjects and patients with high-amplitude esophageal contractions (HAEC), diffuse esophageal spasm (DES), and achalasia of the esophagus. The LES image is from the center of the LES. The esophageal images are from a time when there was no esophageal contractile activity, which was observed through manometry. Note the differences in the muscle thickness in four subjects, with the thickest muscle in patients with achalasia of the esophagus. (Source: Mittal *et al*. 2005. *Gastroenterology*, 128(2): 492, with permission from Elsevier.)

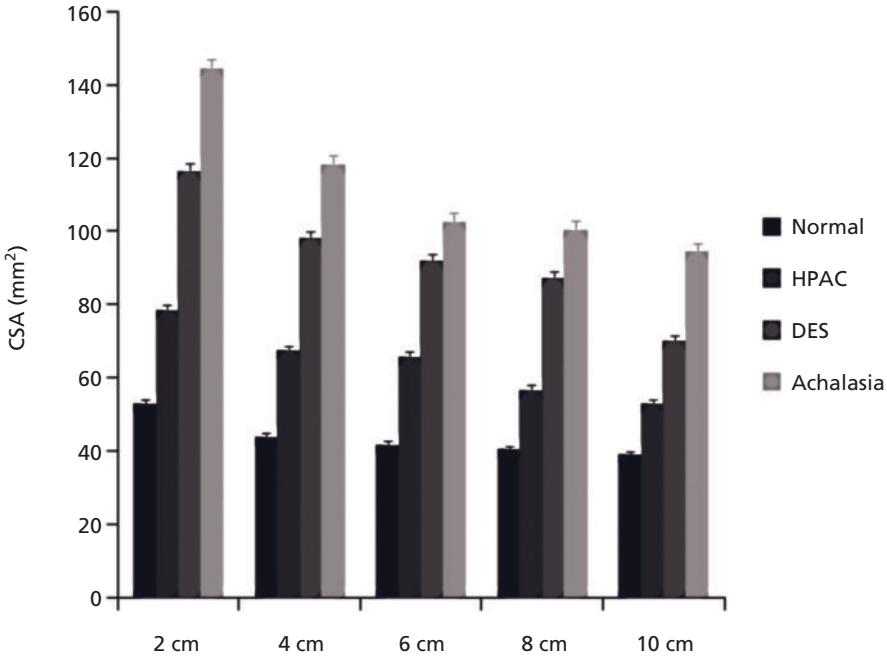

Figure 10.3 Cross-sectional area (CSA) in different motor disorders at different levels in the esophagus. *N* = 10 for each patient category. DES = diffuse esophageal spasm; HPAC = high pressure amplitude contractions. (With permission from Dr. Ravinder Mittal.)

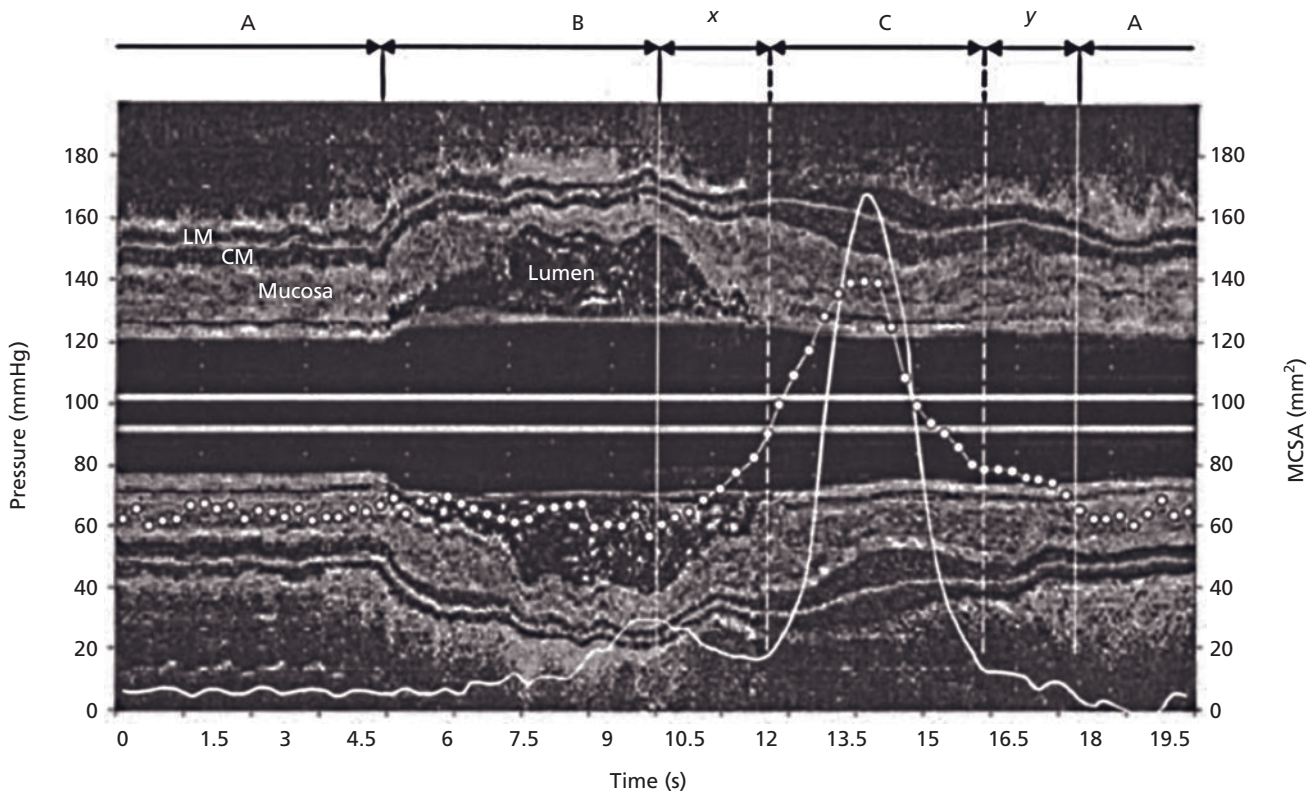

Figure 10.4 M-mode echoesophagograph with a superimposed intraesophageal pressure and muscle cross-sectional area (MCSA) during 5-ml water swallow; the transducer is positioned 2 cm above the lower esophageal sphincter. A, baseline esophagus, before/after swallow; B, bolus-induced distention, bolus pressure, and thinning of mucosa and muscle layers; C, esophageal contraction. Note the dissociation between the increase in MCSA and the increase in intraluminal pressure. The increase in MCSA (—○—) begins before and outlasts the intraluminal pressure wave (——). The difference between the onset of CSA and pressure (*x*) is likely to be due to the delay in recording pressure (circular muscle contraction) by manometry. CM = circular muscle; LM = longitudinal muscle; *y* = time lag between return of pressure and MCSA to baseline. (Source: Mittal *et al*. 2005. *Gastroenterology*, 128(2): 491, with permission from Elsevier.)

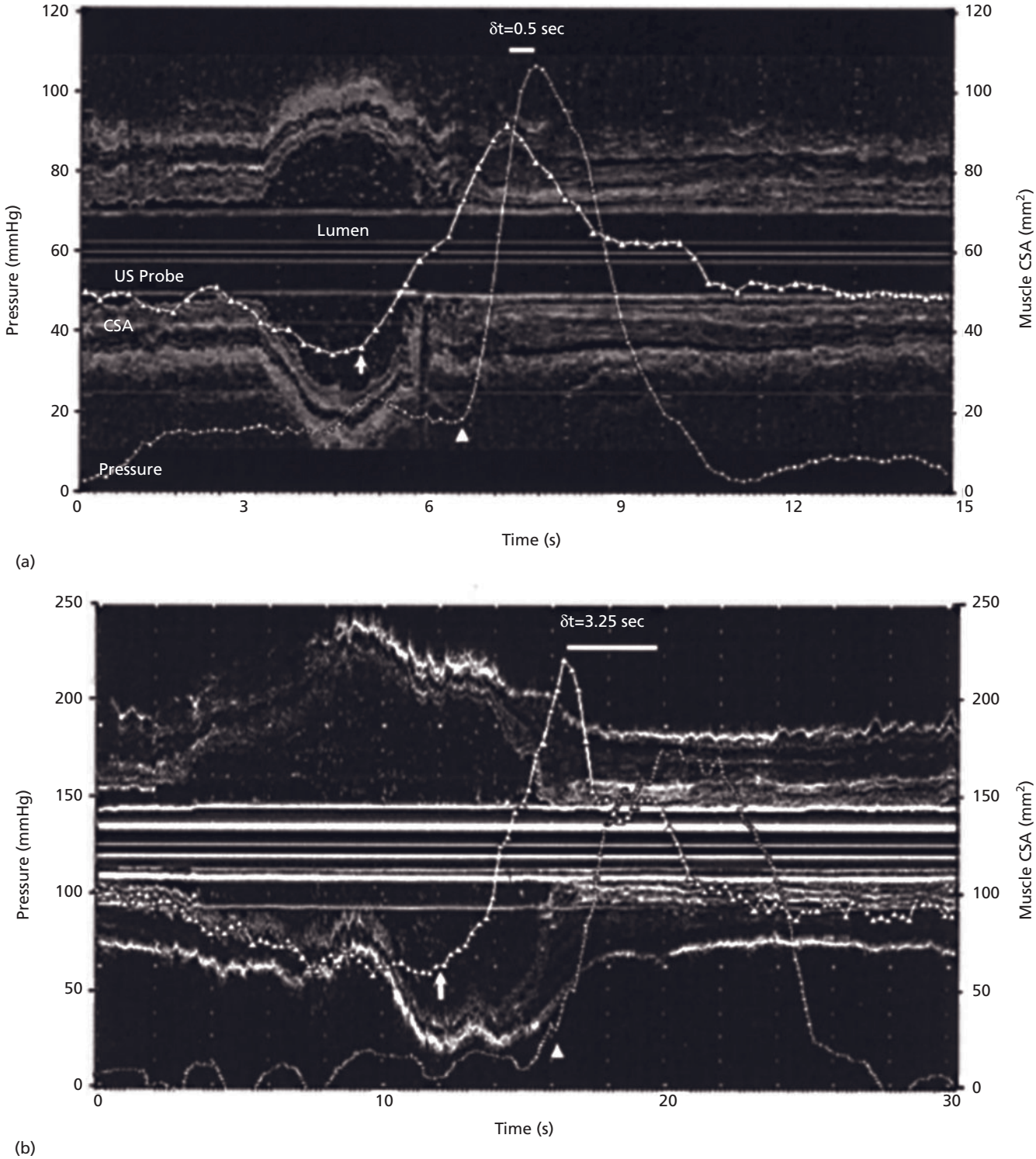

Figure 10.5 (a) Relationship between M-mode ultrasound images, muscle cross-sectional area (CSA), and the pressure wave in a healthy subject. Note that the onset of lumen collapse occurs at the same time as the onset of muscle CSA. Pressure wave occurs at the same time as the first complete collapse of the lumen on the manometric probe. Peak of manometric contraction and peak CSA occurred with a δ–t $\leq$ 0.5 seconds during all 28 swallows at the 2-cm level and all 28 swallows at the 10-cm level. (b) An example of dissociation between circular (cm) and longitudinal (lm) muscle contraction in a patient with nutcracker esophagus. These recordings were obtained 2 cm above the lower esophageal sphincter (LES). Note the disassociation between the peak pressure and peak muscle CSA. (Source: Jung *et al*. 2005. *Gastroenterology*, 128(5): 1182, with permission from Elsevier.)

that if one correlates the onset of lumen collapse (which is a true marker of the onset of CM contraction) with the increase in muscle CSA, then the two muscle layers contract synchronously at onset and peak. Compared to normal subjects who have simultaneous peak of pressure wave and muscle CSA, NCE patients have temporal asynchrony, with peak muscle CSA occurring before peak pressure, with a greater difference at the 2 cm compared to 10 cm level above the lower esophageal sphincter (LES) (Figure 10.5). This asynchrony was reversed with atropine in a dose dependent manner, suggesting that dysfunction in NCE patients are related to a hypercholinergic state (Figure 10.6). Atropine caused a dose-dependent decrease in contraction amplitude and contraction duration as well as peak muscle thickness and duration of muscle thickness.

Simultaneous HIFIUS imaging and manometry has also been used to study other esophageal disease beside primary motility disorders. In patients with eosinophilic esophagitis (EO), continuous HFIUS imaging and manometry during swallow-induced peristalsis shows similar baseline muscle thickness compared to normal subjects, but decreased peak muscle thickness and duration of increase in muscle thickness (amplitude and duration of LM contraction respectively) at the 2 cm and 10 cm level above the LES (Figure 10.7). In response to edrophonium (an acetylcholinesterase inhibitor), normal subjects had significantly greater increase

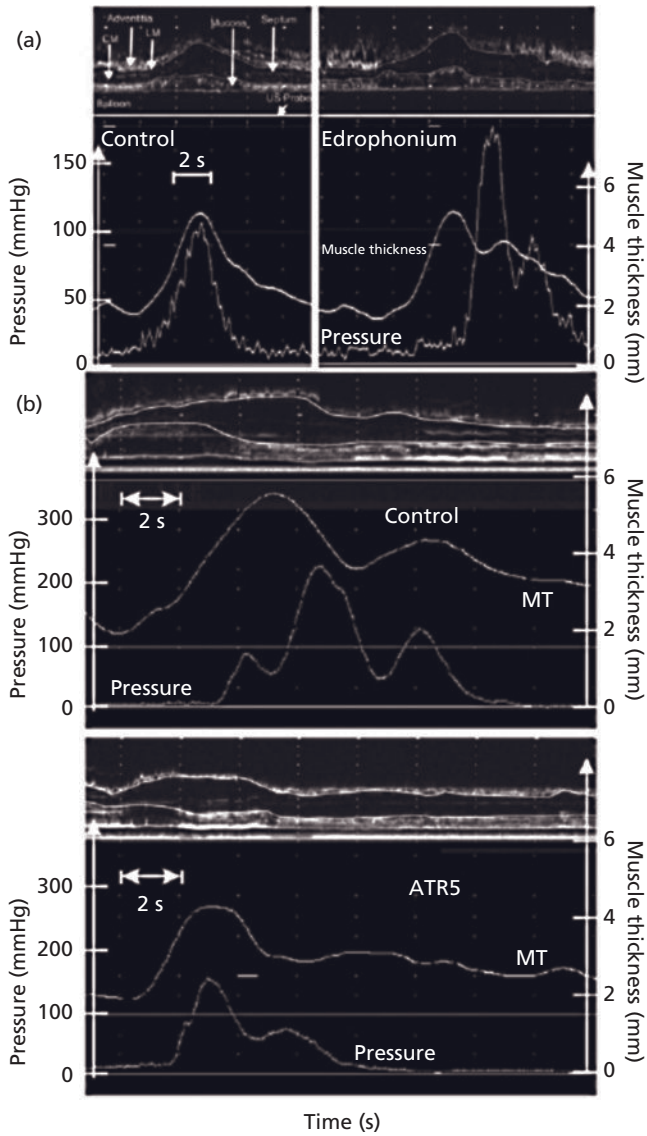

Figure 10.6 (a) M-mode ultrasound images and time-aligned pressure and muscle thickness in a normal subject in control and after edrophonium administration. (b) Same data in a nutcracker esophagus (NCE) patient in the baseline state, after 5 μg/kg, and 10 μg/kg of atropine. (Source: Korsapati *et al*. 2008. *Gastroenterology*, 135(3): 800, with permission from Elsevier.)

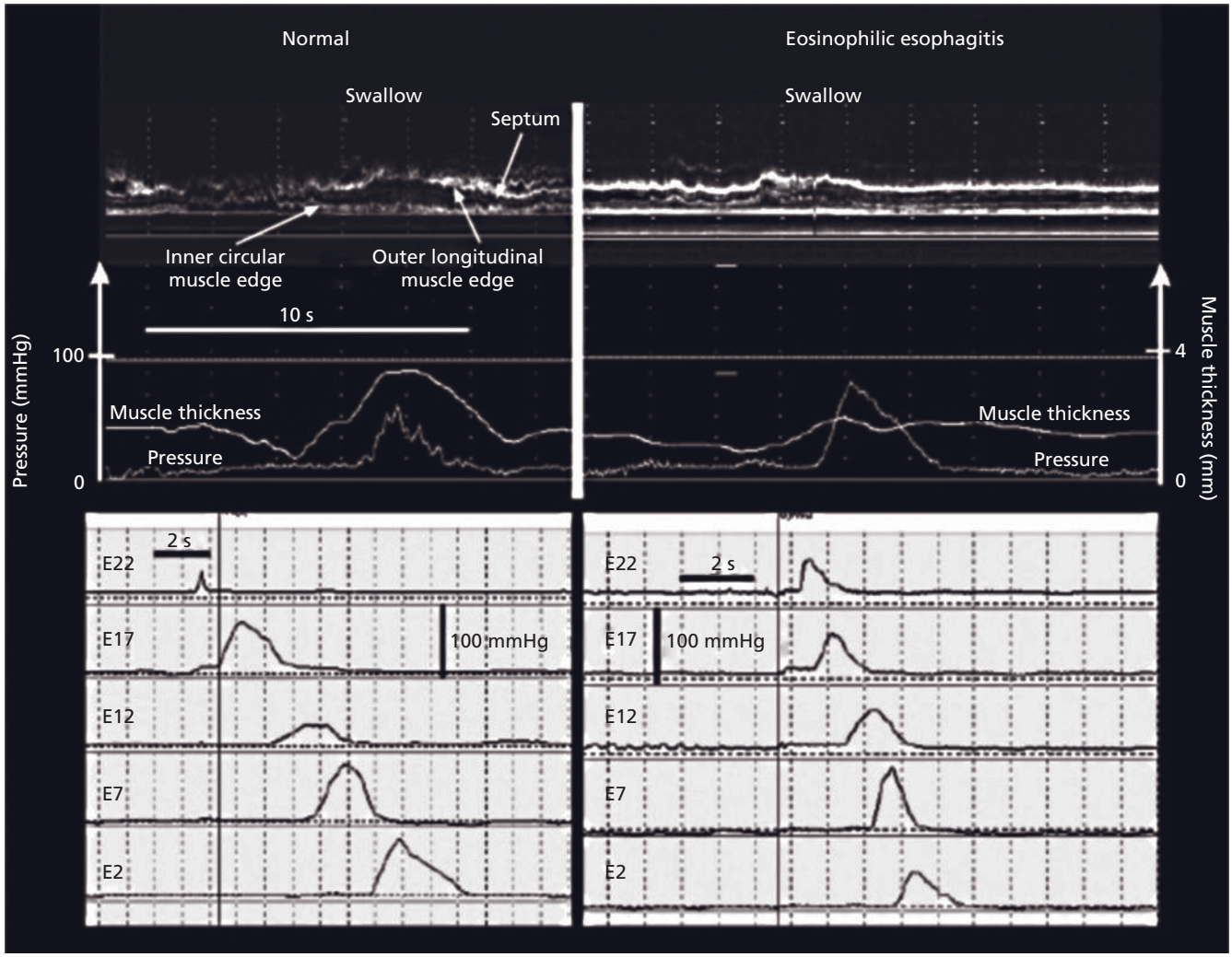

Figure 10.7 Time aligned M-mode ultrasound images, pressure data, and muscle thickness (measured from the M-mode images) in a normal subject and a patient with eosinophilic esophagitis (EO) during a 5 ml swallow. Note that the pressure amplitude and duration are similar in the control and the patient with EO. Also note, the increase in muscle thickness at the peak of the pressure wave in the normal subject, but in the patient with EO the change in muscle thickness is small and the duration of increase in muscle thickness is also small. (Source: Korsapati *et al*. 2009. *Gut*, 58(8): 1058, with permission from the BMJ Publishing Group.)

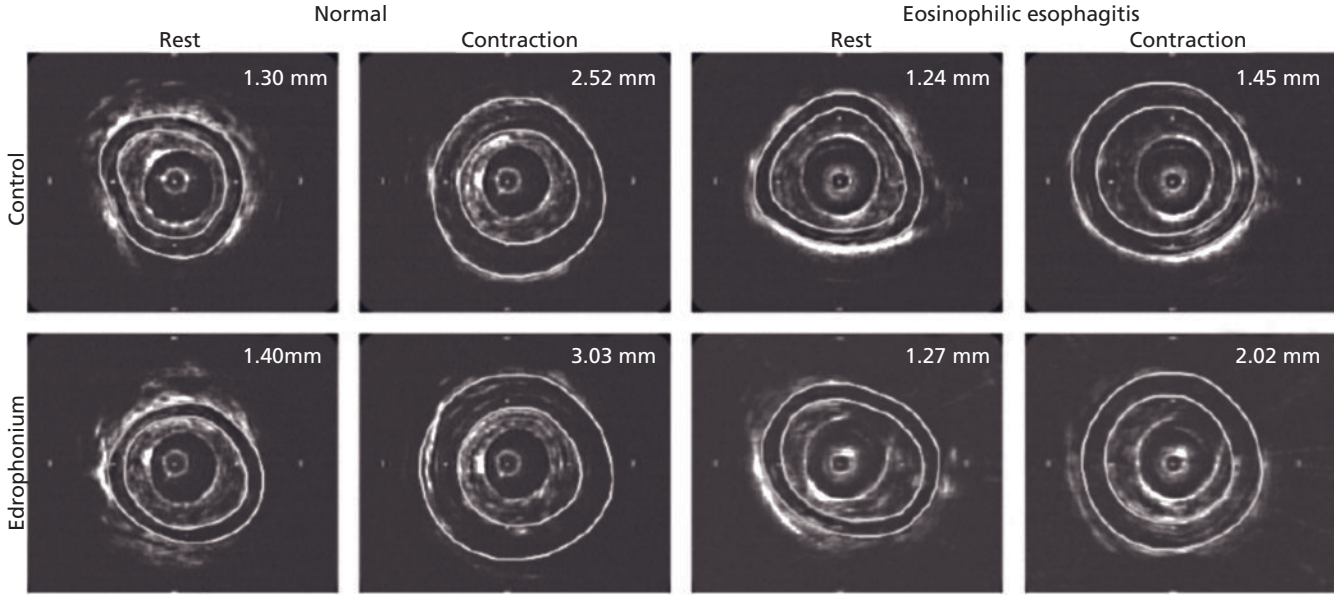

Figure 10.8 B-mode images acquired from a normal subject and a patient with eosinophilic esophagitis (EO) at 2 cm above the lower esophageal sphincter, at rest, at the peak of contraction in the control period, and after edrophonium administration. Both inner circular and outer longitudinal muscle edges are drawn and the muscle thicknesses are shown. These images show a significant increase in the muscle thickness at peak contraction in the normal subject but only a modest increase in the patient with EO. After edrophonium administration, peak muscle thickness increases significantly in both normal subjects and patients with EO, but more so in normal subjects compared with patients with EO. Muscle thickness in millimeters is shown on the top right-hand corner of each panel. (Source: Korsapati *et al*. 2009. *Gut*, 58(8): 1057, with permission from the BMJ Publishing Group.)

in contraction amplitudes and duration (CM contraction) and baseline and peak muscle thickness and duration (LM contraction) compared to patients with EO (Figure 10.8). Because the edrophonium effect on the LM was much more impaired than CM, it was thought that the dysfunction in EO is specific to the LM layer. Similar to findings in patients with nutcracker esophagus, patients with EO have a dissociation between peak LM and CM contraction compared to normal subjects, which did not change with edrophonium suggesting that the dysfunction in EO may be due to LM's inappropriate response to cholinergic stimulation.

LM contraction of the distal esophagus is associated with transient LES relaxation (TLESR), a physiologic event which is the mechanisms of belching, vomiting, and gastroesophageal reflux (GER). Esophageal pressures and HFIUS in healthy subjects during swallow-induced peristalsis and spontaneous TLESR show that the LM contraction starts at the onset of TLESR in the distal esophagus, spreads proximally, and is sustained during entire duration of TLESR (Figure 10.9). The LM contraction during TLESR is temporally associated with an increase in esophageal pressure that is generally stronger than swallow-induced contraction, and may have an important role in the induction of GER.

HFIUS imaging together with esophageal pH and pressure has given new insights to the potential role of LM contraction in relation to chest pain and heartburn. In one study prolonged contraction of the LM with mean duration of 71 seconds, independent of pressure increase or CM contraction, was temporally correlated with the onset of chest pain (Figure 10.10). Sustained LM contraction of lesser duration (32 seconds) was correlated with the onset of heartburn (Figure 10.11). A study which hypothesized heartburn sen-

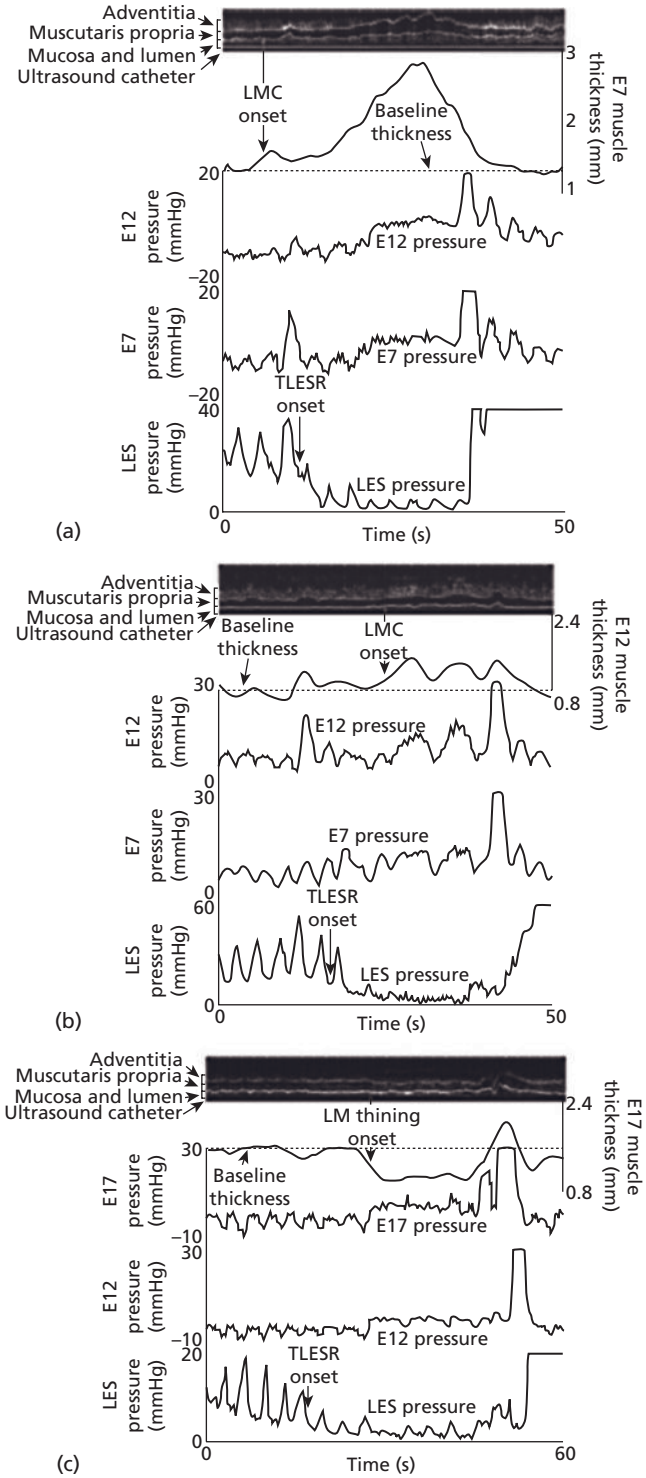

Figure 10.9 Temporal correlation between longitudinal muscle contraction at the 7-, 12-, and 17-cm sites and transient lower esophageal sphincter relaxation (TLESR). Respiration-related changes in muscle thickness were digitally filtered in these records. (a) Note that, at 7 cm, the longitudinal muscle contraction (LMC) starts slowly before the onset of lower esophageal sphincter (LES) relaxation and then accelerates during the TLESR. The LMC lasts during the entire period of TLESR. Also note a close temporal correlation between the increase in esophageal pressure (common cavity pressure) and accelerated LMC during TLESR. (b) Note that, at the 12-cm level, LMC starts after the onset of LES relaxation and lasts until the end of TLESR. Also note a close temporal correlation between the increase in esophageal pressure (common cavity pressure) and the LMC during TLESR. (c) Note a decrease in the muscle thickness during the TLESR at 17-cm site. (Source: Babaei *et al*. 2008. *Gastroenterology*, 134(5): 1326, with permission from Elsevier.)

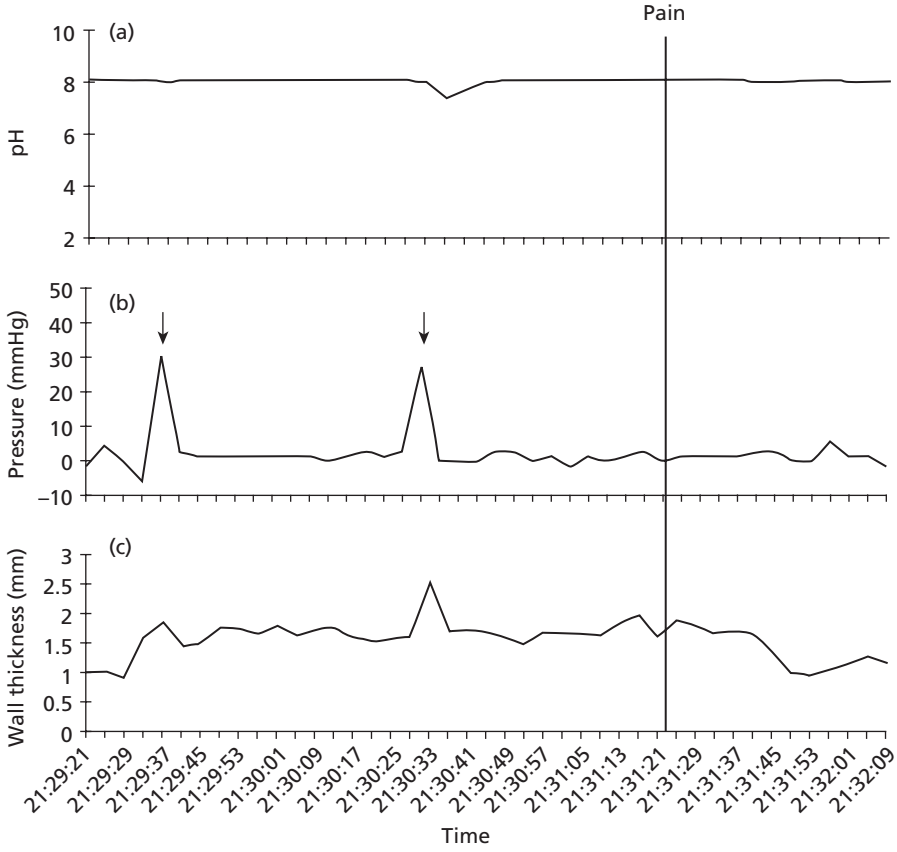

Figure 10.10 Sustained esophageal contraction associated with chest pain. Esophageal pH (a), distal esophageal pressure (b), and esophageal smooth muscle thickness (c) are shown during a 2.5-minute recording interval. The onset of chest pain is depicted by the vertical line (time 0). The onset of sustained esophageal contraction occurs approximately 120 seconds before the onset of pain. The pressure record shows two small contractions (arrows) that are accompanied by brief increases in esophageal muscle thickness during the sustained esophageal contraction. (Source: Balaban *et al*. 1999. *Gastroenterology*, 116(1): 34, with permission from Elsevier.)

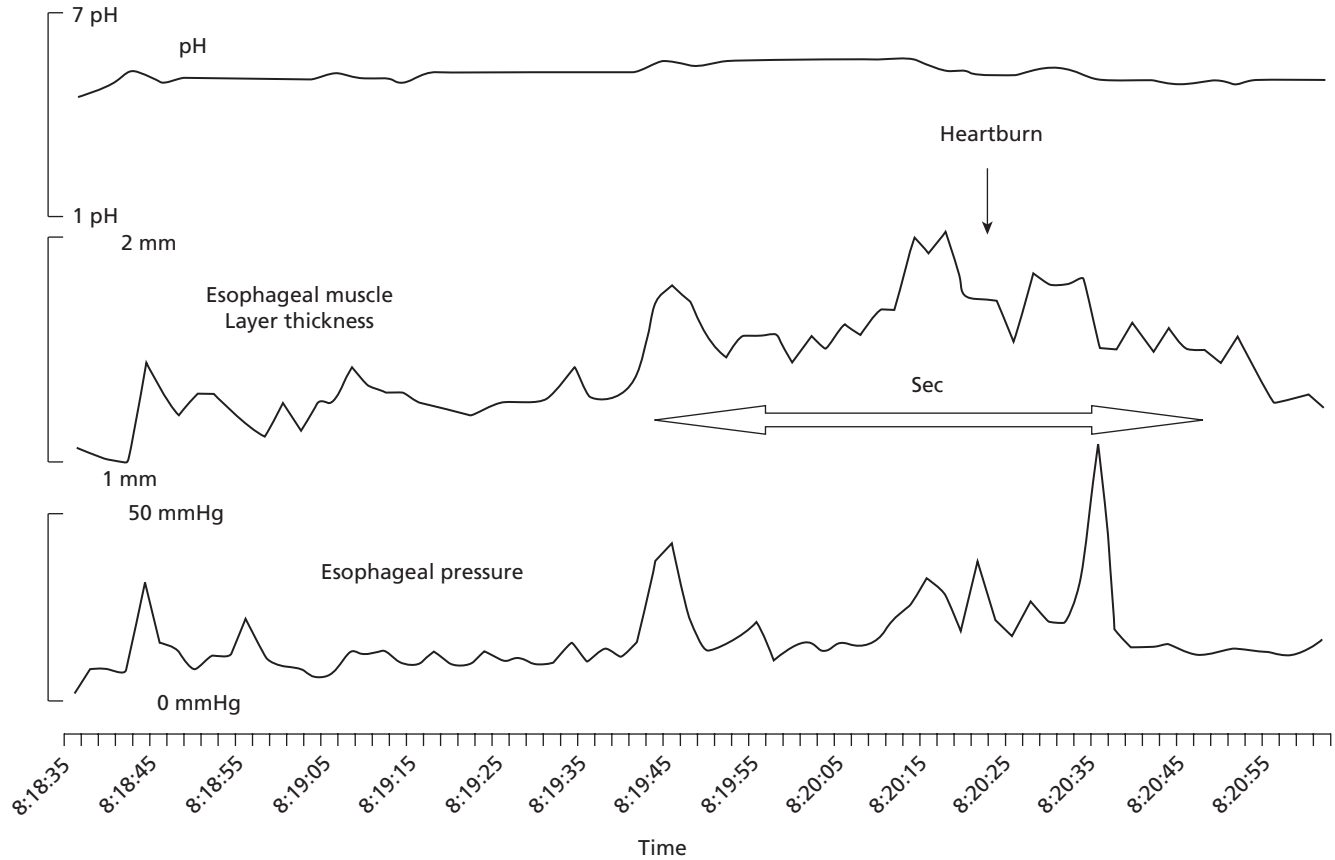

Figure 10.11 Heartburn episode without acid reflux associated with sustained esophageal contraction (SEC). The onset of SEC occurred approximately 54 seconds before the onset of heartburn. Note that phasic contractions of the esophagus were associated with an additional increase in the thickness of esophageal wall during sustained esophageal contraction. (Source: Pehlivanov *et al*. 2001. *American Journal of Physiology. Gastrointestinal and Liver Physiology*, 281(3): G 747, with permission from the American Physiological Society.)

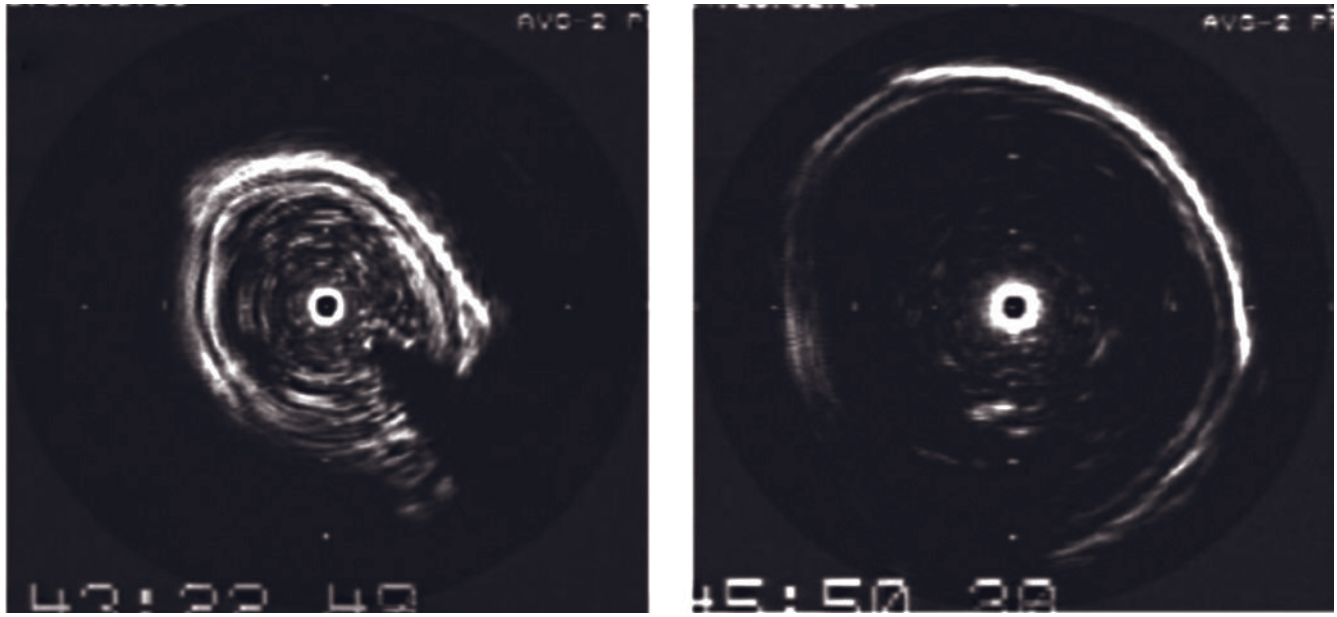

(a) (b)

Figure 10.12 Example of small volume versus large volume gastroesophageal reflux (GER) episodes: (a) asymptomatic GER episode; (b) chest pain symptom. Both GERs were non-acidic and while on treatment with potent acid suppressant. The esophageal lumen cross-sectional area (CSA) at peak GER-induced distension was 268 and 446 mm^2, respectively. (Source: Tipnis *et al*. 2007. *American Journal of Physiology. Gastrointestinal and Liver Physiology*, 293(2): G471, with permission from the American Physiological Society.)

sation to be related to the size of reflux volume and esophageal distention found that though the luminal CSA was greater in GER disorder patients compared to normal subjects, there was no correlation between esophageal luminal CSA and GER episodes that elicited symptoms of heartburn and regurgitation versus episodes that did not produced these symptoms (Figure 10.12).

Chapter video clips

Video 10.1 Three-dimensional endoscopic ultrasound of the esophagus during a swallow.

Video 10.2 Three-dimensional endoscopic ultrasound of the esophagus during an episode of reflux.

11 Malignant Mediastinal Lesions

M. Babitha Reddy[1], David H. Robbins[1], and Mohamad A. Eloubeidi[2]

[1] Lenox Hill Hospital, New York, NY, USA
[2] American University of Beirut School of Medicine, Beirut, Lebanon

Trans-esophageal endoscopic ultrasound (EUS) allows imaging of posterior mediastinal lymph nodes, which is where lung cancer as well as other cancers can metastasize. Additionally, large lung tumors abutting the esophagus can be imaged, as can primary posterior mediastinal lung tumors. EUS-guided biopsies can be performed with either trans-esophageal endoscopic ultrasound-guided fine needle aspiration (EUS-FNA) or endobronchial ultrasound-guided fine needle aspiration (EBUS-FNA).

The EUS characteristics of malignant lymph nodes include short axis diameter greater than 10 mm, round shape, well demarcated, and hypoechoic echotexture. Malignant mediastinal masses are generally greater than 3 cm in short axis diameter.

Staging of lung cancer is based on the American Thoracic Society lymph node map (Figure 11.1). Trans-esophageal EUS can visualize the para-tracheal lymph nodes (station 2), posterior aorto-pulmonic window lymph nodes (station 5),

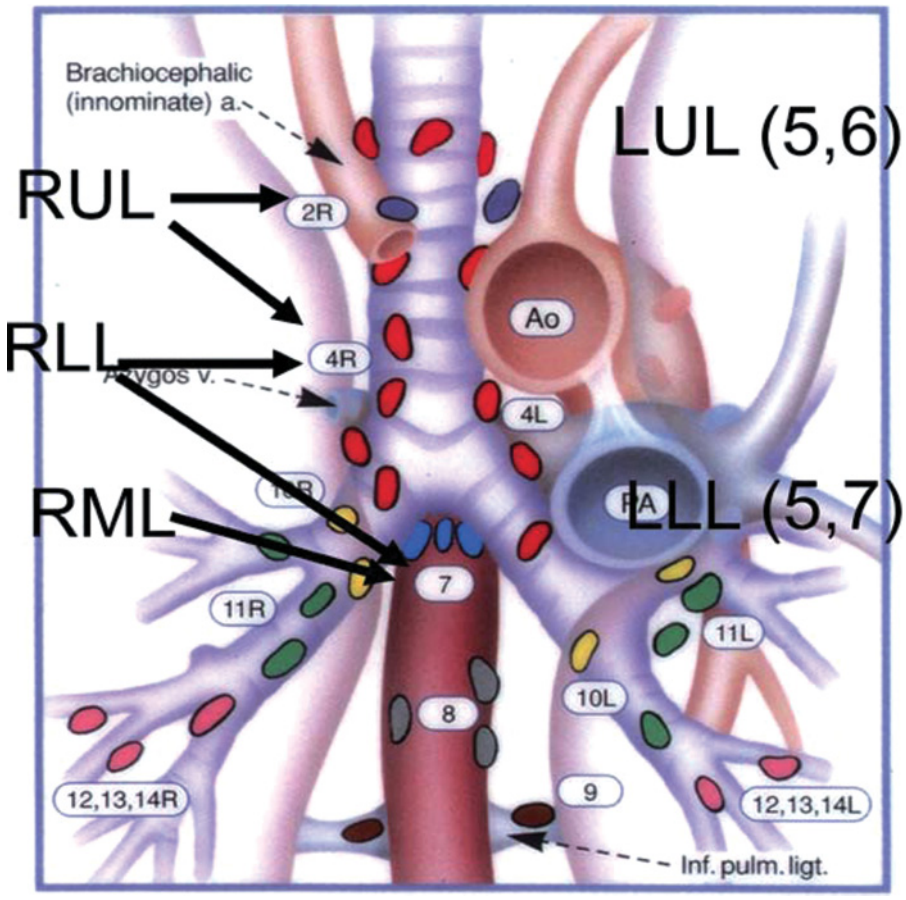

Figure 11.1 American Thoracic Society staging diagram for posterior mediastinal lymph nodes. Note that station 2 is para-tracheal lymph nodes, station 5 is aorto-pulmonic window, station 7 is subcarinal, and station 8 is para-esophageal. The superimposed lung locations show the lymphatic drainage of each part of the lung (LLL = left lower lobe; LUL = left upper lobe; RLL = right lower lobe; RML = right middle lobe; RUL = right upper lobe).

Atlas of Endoscopic Ultrasonography, First Edition. Edited by Frank G. Gress, Thomas J. Savides, Brenna Casey Bounds, John C. Deutsch.

subcarinal lymph nodes (station 7), and para-esophageal lymph nodes (station 8). In addition, trans-esophageal EUS can visualize other sites of metastases such as the left adrenal and the liver. EBUS can visualize stations 1, 2, 3, 4, 7, 10, and 11. Using a combination of both, nearly the entire posterior mediastinum can be visualized and biopsied, which obviates the need in most cases for diagnostic surgical mediastinoscopy.

Intra-pulmonary lung cancer drains to lymphadenopathy at various EUS and EBUS stations depending on the location of the cancer (Figure 11.1). The right upper lobe drains into stations 2R and 4R, accessible by EBUS. The right lower lobe drains into stations 4R and 7 accessible by EBUS and EBUS, EUS respectively. The right middle lobe drains into station 7 which is accessible by EBUS and EUS. Recent case series demonstrated safety in sampling lymph nodes and intra-pulmonary masses at station 6, lateral to the aorta, via the trans-aortic approach. The left upper lobe drains into stations 5 and 6 accessible by EUS and the left lower lobe drains into stations 5 and 7 accessible by EUS and EBUS (Figures 11.2–11.5).

Chapter video clips

Video 11.1 Endoscopic ultrasound-guided fine needle aspiration (EUS-FNA) Tru-cut biopsy of large posterior mediastinal mass.

Video 11.2 Endoscopic ultrasound-guided fine needle aspiration (EUS-FNA) of malignant lymph node in the posterior aorto-pulmonic window (Station 5).

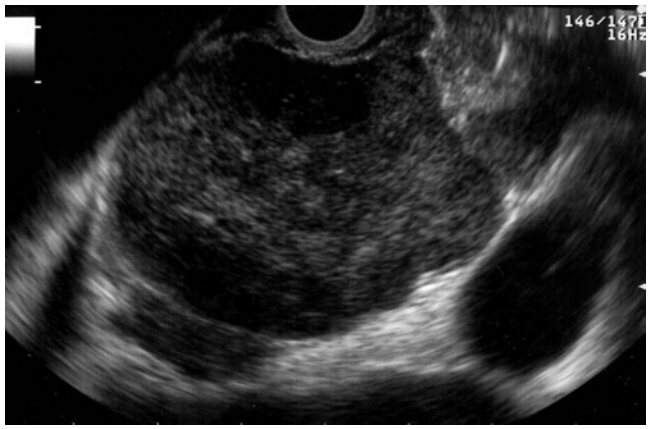

Figure 11.2 Metastatic posterior mediastinal melanoma. Endoscopic ultrasound-guided fine needle aspiration (EUS-FNA) along with immunostains confirmed recurrent metastatic melanoma in the mediastinum.

Figure 11.3 Renal cell cancer metastasis. The lesion was identified slightly above the gastroesophageal junction. Endoscopic ultrasound (EUS) was the only non-surgical approach to reach this lesion.

Figure 11.4 Lung cancer mass. Endoscopic ultrasound-guided fine needle aspiration (EUS-FNA) of a centrally located mass confirmed primary non-small cell lung cancer.

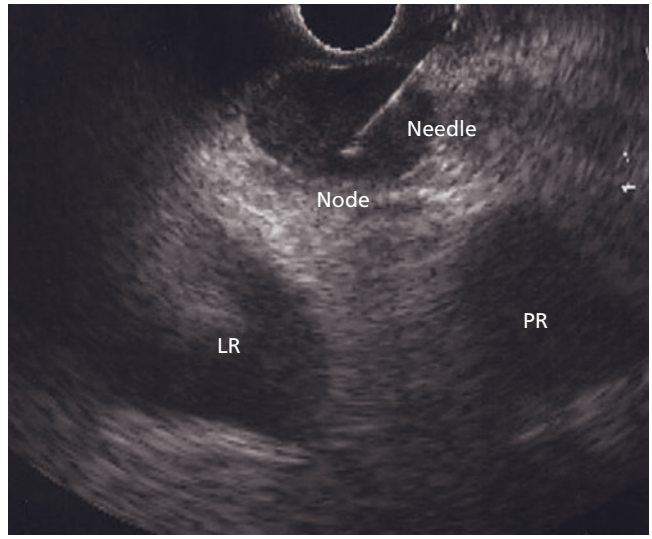

Figure 11.5 Malignant lymph node. The needle is within the rounded, well-demarcated, hypoechoic lymph node (LA = left atrium; PA = pulmonary artery).

12 Benign Mediastinal Lesions

M. Babitha Reddy[1], David H. Robbins[1], and Mohamad A. Eloubeidi[2]

[1] Lenox Hill Hospital, New York, NY, USA
[2] American University of Beirut School of Medicine, Beirut, Lebanon

Benign mediastinal lymphadenopathy is a common incidental finding during endoscopic ultrasound (EUS) (Figures 12.1–12.5). Benign enlarged mediastinal lymph nodes can be reactive lymph nodes from exposure to a pulmonary infection, or granulomatous lymph nodes from sarcoid, histoplasmosis, or tuberculosis. Echogenic features include a crescent or triangular shape. Sometimes there is a central hyperechoic strand suggestive of a blood vessel. The borders are irregular and the short axis is often less than 1 cm. There are often multiple lymph nodes. It is not uncommon to encounter the benign "draping" subcarinal lymph node, which can be ovoid, intermediate in echogenicity, and up to 2 cm in length.

The most commonly found posterior mediastinal cystic lesions are congenital foregut cysts. These are classified as bronchogenic (defined as cystic lesions located away from the esophageal wall) and neuroenteric (found adherent to the esophageal wall such as an esophageal duplication cyst or a neuroenteric cyst). The malignant potential for duplication cysts is exceedingly low and clinical monitoring without intervention is acceptable. Heterogenous echogenicity or internal mass is suspicious finding for malignancy and is an

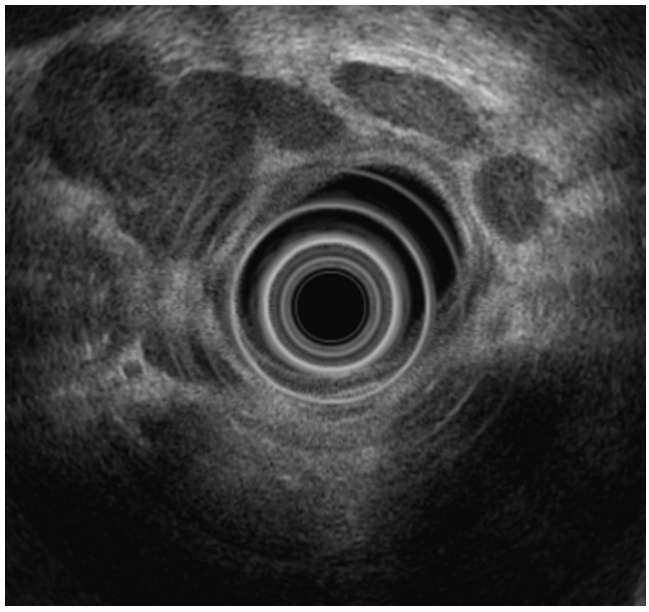

Figure 12.1 Benign subcarinal lymph nodes. Note the oval and triangular-shaped benign-appearing nodes.

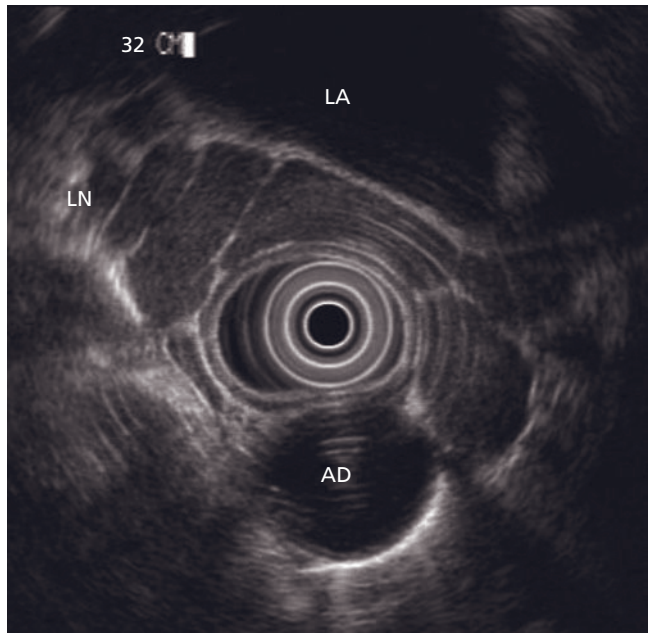

Figure 12.2 Sarcoid lymph nodes. Note the matted together, draping nodes with triangular and rectangular shapes in the subcarinal space. (AO = aorta; LA = left atrium.)

Atlas of Endoscopic Ultrasonography, First Edition. Edited by Frank G. Gress, Thomas J. Savides, Brenna Casey Bounds, John C. Deutsch.

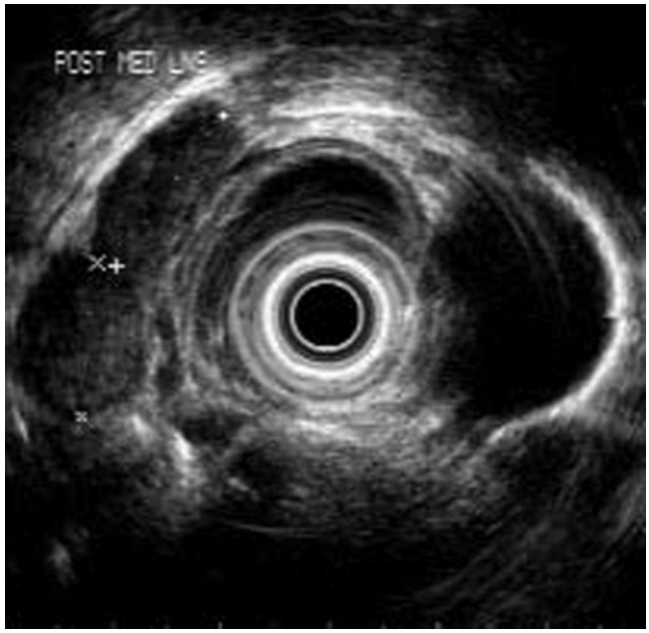

Figure 12.3 Cryptococcal lymph node. These were incidental lymph nodes found in a patient with acquired immunodeficiency syndrome (AIDS). Endoscopic ultrasound-guided fine needle aspiration (EUS-FNA) was important in establishing the diagnosis. (Courtesy of Thomas Savides, MD.)

acceptable indication for surgical resection and/or endoscopic sampling. Hyperechoic reflectors within cystic lesions may suggest thick, tenacious debris which can limit tissue sampling for cytologic evaluation. In addition, intractable symptoms of chest pain, dyspnea, cough, or dysphagia secondary to an enlarging cystic lesion are other acceptable indications for intervention. The risk of infection and mediastinitis can be significant and therefore endoscopic ultrasound-guided fine needle aspiration (EUS-FNA) should be avoided as much as possible in suspected cysts. If FNA is performed due to uncertainty of the diagnosis, antibiotics should be given prior to and after the exam.

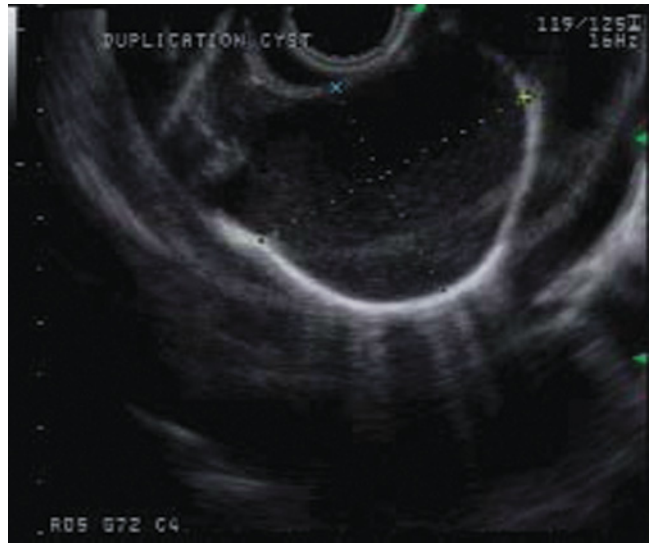

Figure 12.4 Duplication cyst. Note the anechoic appearance with acoustic enhancement of the cyst wall. (Courtesy of Thomas Savides, MD.)

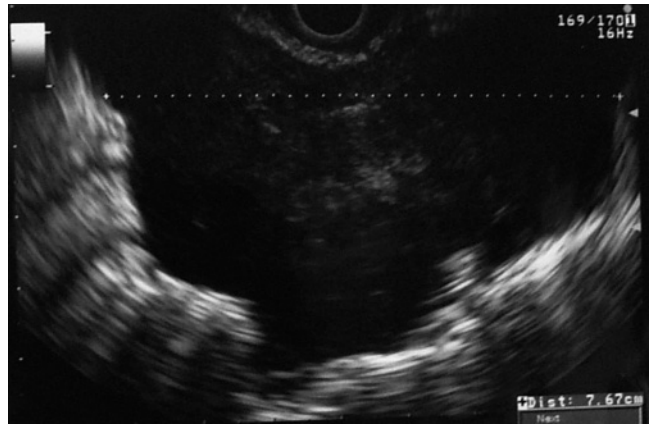

Figure 12.5 Enlarged lymph node due to *Blastocystis hominis* infection. Courtesy of John Deutsch, MD.

13 Gastric Cancer

Douglas O. Faigel[1] and Sarah A. Rodriguez[2]

[1] Mayo Clinic College of Medicine, Scottsdale, AZ, USA

[2] Oregon Health and Science University, Portland, OR, USA

Endoscopic ultrasound (EUS) is frequently employed for the diagnosis and staging of gastric cancers and lymphomas. This chapter will review EUS imaging and staging of these malignancies.

The majority of gastric malignancies are adenocarcinomas. They are staged using the American Joint Commission on Cancer Staging TNM Classification (Table 13.1). These cancers may be either of the intestinal or diffuse type. The intestinal type arises from the mucosa and form discrete tumors. They appear as poorly circumscribed hypoechoic lesions which, at the edges, can be seen to be arising from the mucosal layers. T1 lesions are limited to the mucosa (first and second layers) or may penetrate into the submucosa (third layer) (Figure 13.1). There should be a demonstrable, intact, bright layer of submucosa between the lesion and the dark band of the muscularis propria (fourth layer). T2 lesions extend into but not through the muscularis propria (Figure 13.2). Endosonographically, T2 lesions extend through the bright third layer corresponding to where the tumor penetrates through the submucosa into the muscularis propria. However, the interface at the outer margin of the muscularis where it contacts the serosa (fourth and fifth layers) is smooth and undisturbed by the cancer. In T3 lesions the hypoechoic lesion extends completely through the fourth layer, and the serosa (fifth layer), which would otherwise be smooth, is interrupted and clearly invaded (Figure 13.3). Finger-like projections of tumor, termed pseudopodia, may be seen extending into the extragastric space. If the lesion extends into a local organ (e.g. liver, pancreas, spleen, diaphragm) or large vessel (e.g. aorta, celiac axis) it is classified as a T4-stage lesion (Figure 13.4).

Diffuse type adenocarcinoma (also known as "linitis plastic") are poorly differentiated tumors that infiltrate the stomach wall. Histologically, they consist of single cells or small clusters of cells that contain large mucin vacuoles pushing the nucleus to one side to produce a signet ring appearance. The result of the diffuse infiltration by the cancer cells is a thickened, rigid stomach that has been likened to a leather bottle. Endoscopic ultrasound examination has been found to be exceptionally helpful in evaluating the patient with a suspected infiltrating malignancy. The normal stomach is 3–4 mm in thickness. When an infiltrating cancer is present, the stomach is thickened to greater than 4 mm, and one of two EUS patterns may be seen. In the first, there is complete loss of the normal five-layer pattern, with the markedly thickened wall assuming a homogeneously dark appearance. All layers of the stomach are generally involved and these tumors are stage T3. In the second EUS pattern, the thickened stomach maintains its five-layer pattern, but the muscularis propria (fourth layer) is a prominent, thick, dark band beneath a thickened, bright, third layer (submucosa) (Figure 13.5). Finding either of these patterns should prompt an aggressive search for an infiltrating malignancy. However, this finding is not specific to gastric adenocarcinoma and may be seen in metastatic cancer to the stomach (Figure 13.6) and in gastric lymphoma.

The stomach is the most common site for primary extranodal lymphoma, comprising one-fourth of all extranodal cases and at least half of all primary gastrointestinal (GI) lymphomas. Endoscopically, primary gastric lymphomas usually appear as an exophytic mass, although a more diffuse infiltration can occur, causing a linitis plastica appearance (Figures 13.7 and 13.8). Gastrointestinal lymphomas are staged differently than carcinomas (Table 13.2). Tumors confined to the GI tract are stage IE, and these patients have significantly higher survival rates than those with lymph node involvement or distant spread.

Atlas of Endoscopic Ultrasonography, First Edition. Edited by Frank G. Gress, Thomas J. Savides, Brenna Casey Bounds, John C. Deutsch.
 Published 2012 by Blackwell Publishing Ltd.

Table 13.1 American Joint Committee on Cancer (AJCC) Staging: TNM classification for gastric cancer (with permission from AJCC.)

Tumor (T) stage	
Tx	Primary tumor cannot be assessed
T0	No evidence of primary tumor
T1s	Carcinoma in situ: intra-epithelial tumor without invasion of the lamina propria
T1	Tumor limited to mucosa or submucosa
T2	Tumor invades muscularis propria or subserosa
T2a	Tumor invades muscularis propria
T2b	Tumor invades subserosa
T3	Tumor invades serosa
T4	Tumor invades adjacent structures
Tx	Primary tumor cannot be assessed
Nodal (N) stage	
Nx	Regional lymph nodes cannot be assessed
N0	No regional lymph node metastasis
N1	Metastasis in 1–6 regional lymph nodes
N2	Metastasis in 7–15 regional lymph nodes
N3	Metastasis in more than 15 regional lymph nodes
M: distant metastasis	
Mx	Distant metastasis cannot be assessed
M0	No distant metastasis
M1	Distant metastasis present (e.g. hepatic metastasis, peritoneal dissemination)
Stage grouping	
Stage 0	Tis N0 M0
Stage IA	T1 N0 M0
Stage IB	T1 N1 M0, T2a/b N0 M0
Stage II	T1 N2 M0, T2 a/b N1 M0, T3 N0 M0
Stage IIIA	T2a/b N2 M0, T3 N1 M0, T4 N0 M0
Stage IIIB	T3 N2 M0
Stage IV	T1–3 N2 M0, T4 N1–3 M0, or any T, any N, M1

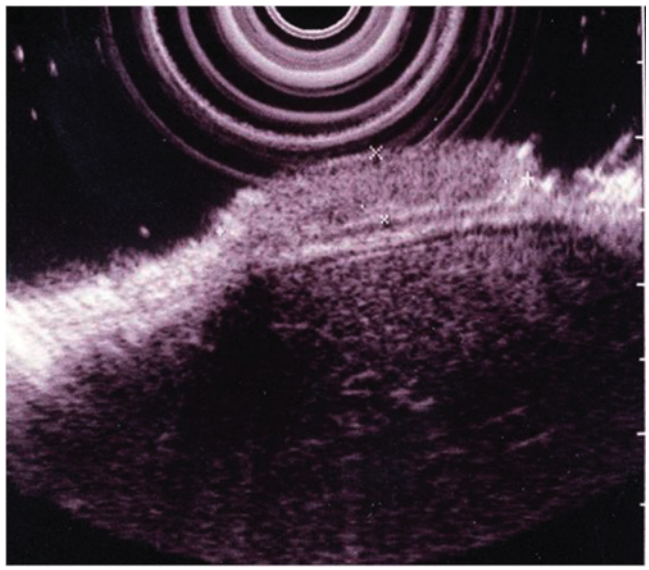

Figure 13.1 T1 gastric cancer. This is a 2.2 × 0.5 cm thick tumor confined to the mucosa without penetration of the muscularis propria.

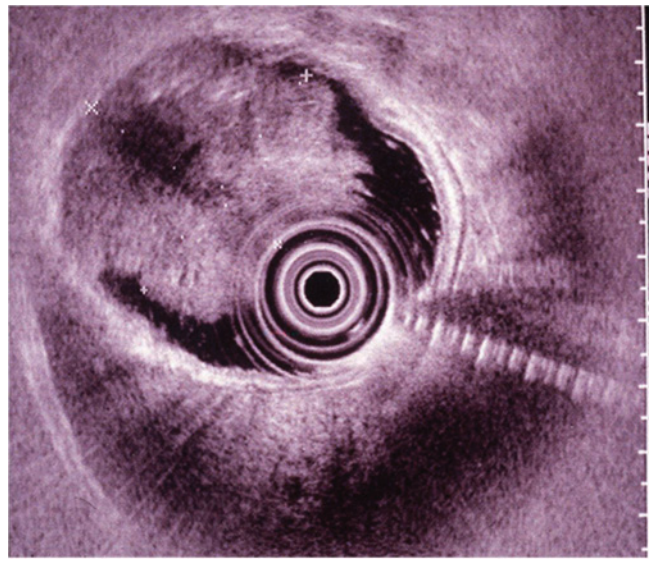

Figure 13.2 T2 gastric cancer. This large 4.2 × 3.6 cm exophytic tumor invades deeply into the gastric wall but does not traverse the serosa. Note the deep margin of the tumor is smooth without deeper pseudopodic extension.

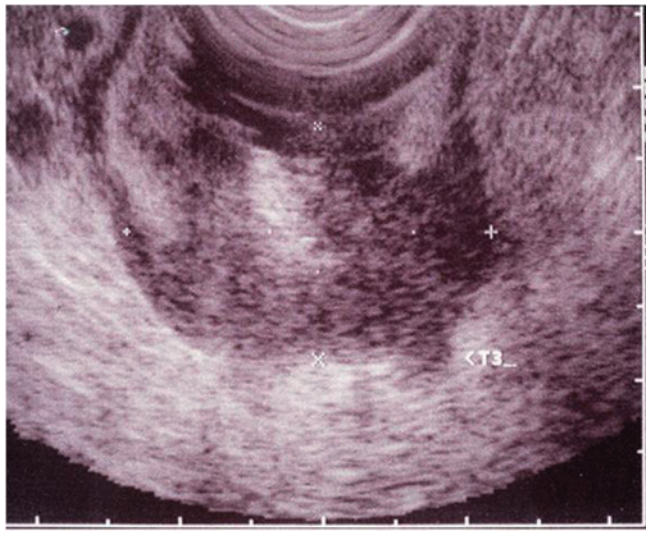

Figure 13.3 T3 gastric cancer. This 2.5 × 1.6 cm tumor invades through all layers of the stomach. A pseudopod of tumor extends through the serosa into the perigastric space (marked by the "<T3").

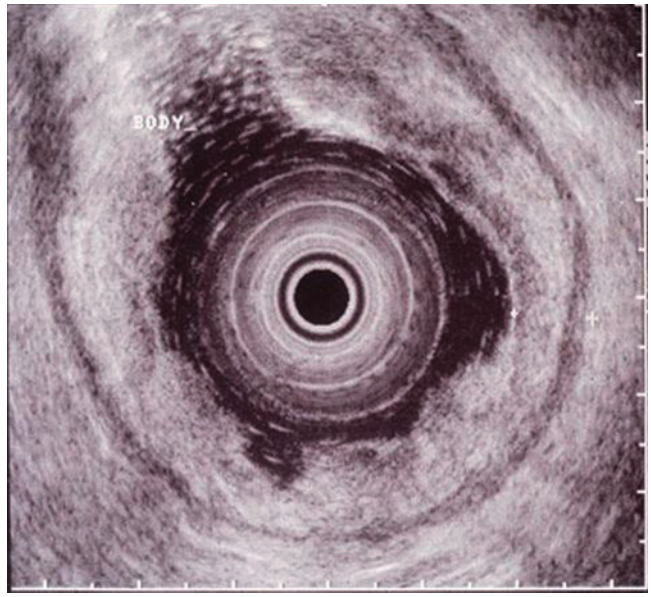

Figure 13.5 Diffuse gastric cancer. The stomach is thickened to 0.8 cm (normal <0.5 cm). The pattern of thickening shows prominence of the bright third layer (submucosa) and dark fourth layer (muscularis propria). This pattern is produced by diffuse infiltration by the signet-ring cell carcinoma.

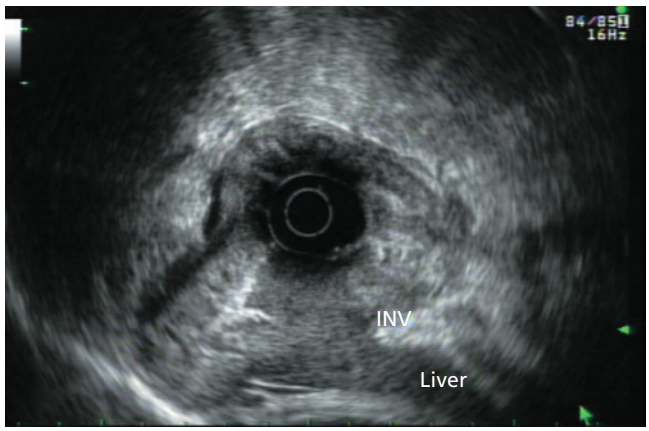

Figure 13.4 T4 gastric cancer. This invasive poorly differentiated cancer invades through the gastric wall to directly involve the adjacent left lobe of the liver. Note the lack of a hyperechoic interface between the gastric tumor and the liver ("INV").

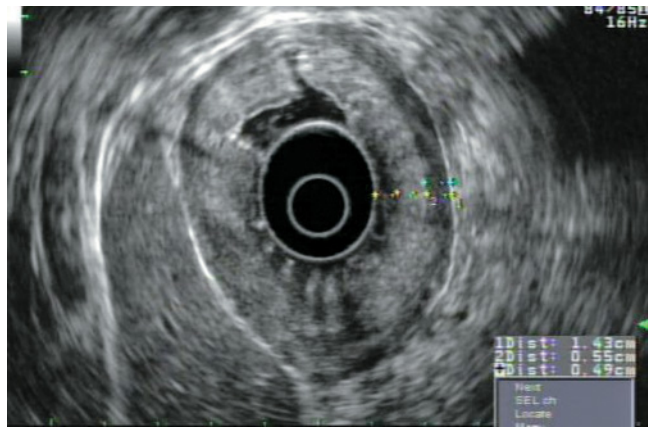

Figure 13.6 Pseudo-linitis plastica. A patient with breast cancer has metastases to the stomach which are infiltrating the wall giving the appearance of linitis plastic. The five-layer pattern is preserved, but the wall is markedly thickened to 14.3 mm (normal <5 mm) and the submucosa (5.5 mm) and muscularis propria (4.9 mm) are prominently thickened. (Source: Gress F, Savides T. *Endoscopic Ultrasonography*, 2nd edn. Oxford: Wiley-Blackwell, 2009.)

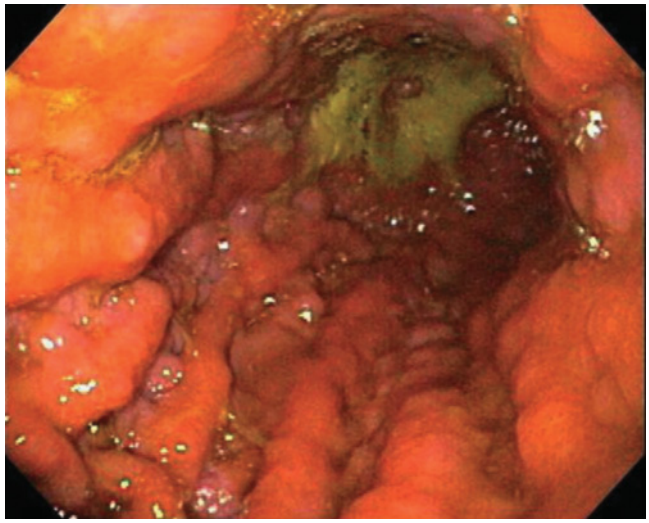

(a)

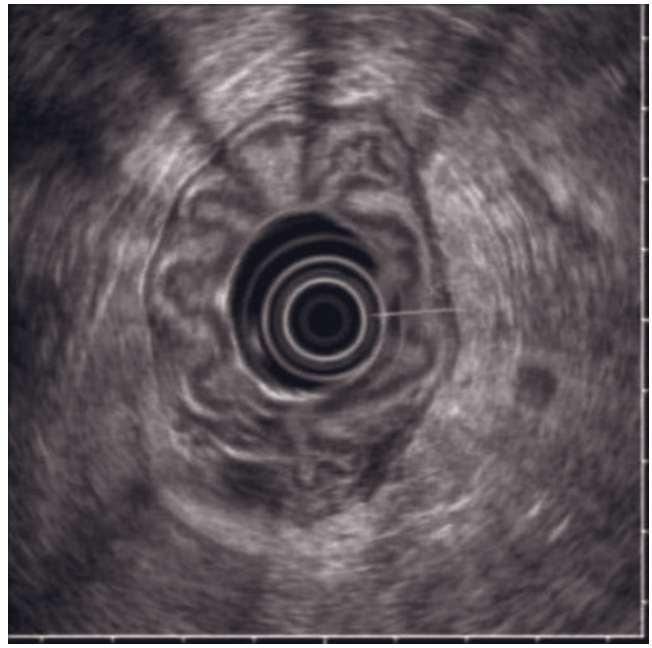

(b)

Figure 13.7 Gastric lymphoma causing a linitis plastic appearance. This patient with a diffusely infiltrating B-cell lymphoma has poorly distensible thickened abnormal-appearing gastric folds on endoscopy (a). On endoscopic ultrasound (b), there is preservation of the five-layer pattern but marked thickening of the gastric wall to 10.9 mm with a thickened muscularis propria to 2.5 mm (normal 1 mm or less).

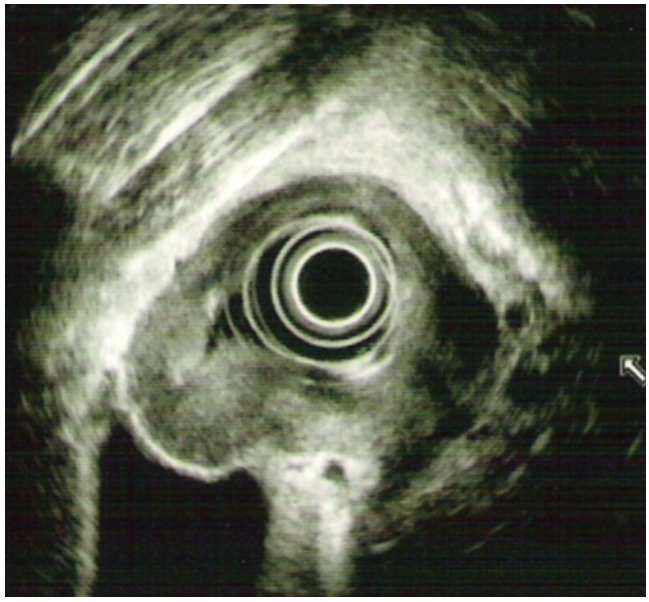

Figure 13.8 Gastric lymphoma. The five-layer wall pattern is obliterated and the gastric wall is markedly thickened. (Source: Gress F, Savides T. *Endoscopic Ultrasonography*, 2nd edn. Oxford: Wiley-Blackwell, 2009.)

Table 13.2 Ann Arbor staging system for gastrointestinal lymphomas. (Adapted from Carbone *et al*. 1971. *Cancer Research*, 31(11): 1860–1, and Lister *et al*. 1989. *Journal of Clinical Oncology*, 7(11): 1630–6, with permission.)

Stage	Sites of involvement
IE	Tumor confined to gastrointestinal tract ("E" designates lymphoma outside of lymph nodes)
IIE_1	Tumor with regional nodal involvement
IIE_2	Tumor with extraregional subdiaphragmatic nodal involvement (e.g. para-aortic, iliac, etc.)
IIIE	Tumor with nodal involvement on both sides of the diaphragm
IVE	Tumor with extranodal disseminated involvement (e.g. bone marrow, lungs, liver, etc.)

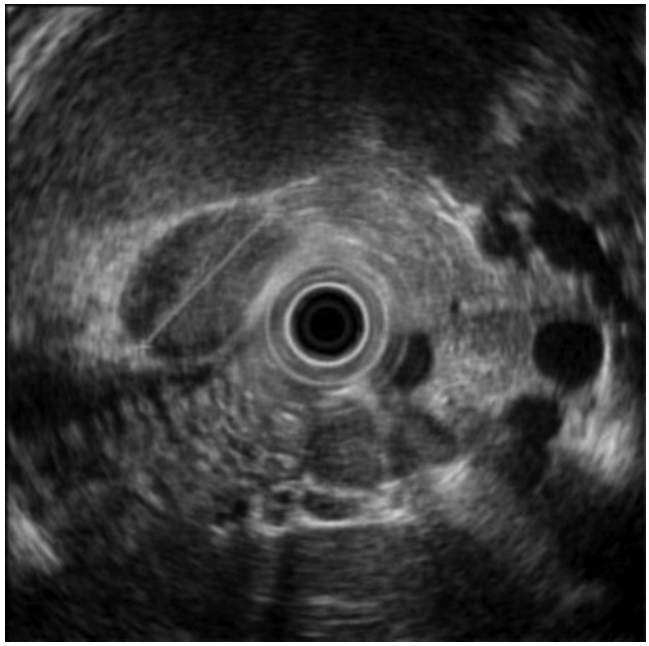

Figure 13.9 Perigastric lymphadenopathy in a patient with primary gastric lymphoma. Note the very large 25.7 × 18.3 mm lymph node. In addition to being large (>1 cm) it has additional malignant features, including a rounded shape with sharp borders, hypoechoic echogenicity, and a homogeneous echotexture.

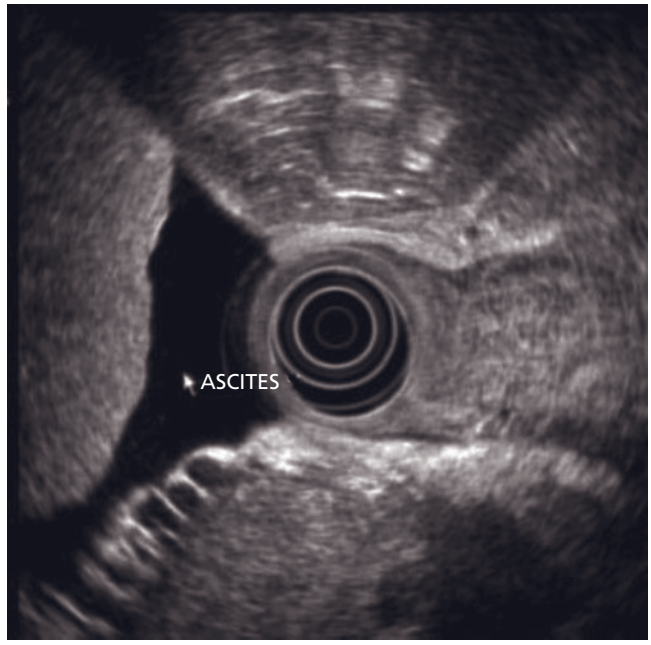

Figure 13.10 Ascites. A large pocket of hypoechoic material is seen next to the liver, located on the left, in a patient with gastric cancer. The ascites was accessed via a 22-gauge needle placed through the duodenum and was positive for malignancy, denoting M1 disease. (Source: Gress F, Savides T. *Endoscopic Ultrasonography*, 2nd edn. Oxford: Wiley-Blackwell, 2009.)

Endoscopic ultrasound evaluation of suspected gastric malignancies should include a thorough search for metastatic lymph nodes, especially in the perigastric, celiac, and gastrohepatic regions (Figure 13.9). The presence of malignant adenopathy is a poor prognostic sign for both adenocarcinoma and lymphoma and may alter management to primary or adjuvant chemotherapy. The presence of ascites raises the likelihood that there is peritoneal seeding (Figure 13.10). Lymph nodes, liver lesions, and ascites may be sampled via EUS-guided fine needle aspiration (FNA) provided that tumor is not traversed (Figure 13.11).

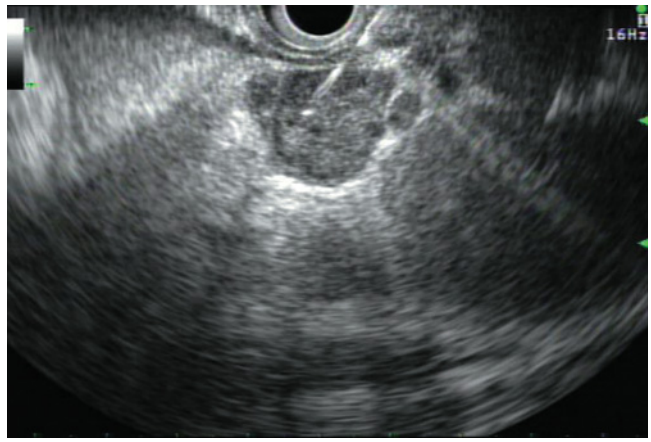

Figure 13.11 Endoscopic ultrasound-guided fine needle aspiration (EUS-FNA) of a perigastric lymph node. This is the same patient as in Figure 13.9 with gastric lymphoma and extensive perigastric lymphadenopathy. The EUS-FNA is performed through normal-appearing stomach into a malignant appearing lymph node. Cytology confirmed the presence of lymphoma within the node.

14 Gastric and Esophageal Subepithelial Masses

David J. Owens and Andrew J. Bain
University of California, San Diego, La Jolla, CA, USA

Introduction

Gastrointestinal (GI) subepithelial masses are lesions that lie underneath normal appearing mucosa. This chapter will focus on subepithelial lesions of the esophagus and stomach. They are usually incidental findings detected during upper endoscopy for other reasons such as heartburn or abdominal discomfort. Most esophageal and gastric subepithelial masses are benign; however, some have malignant potential. Therefore it is important to establish a correct diagnosis and exclude malignancy. Tissue sampling with standard endoscopic techniques is often unsuccessful in establishing a diagnosis due to inadequate biopsy depth. Endoscopic ultrasound (EUS) is important for obtaining a diagnosis by virtue of minimally invasive tissue characterization with ultrasound, determination of wall layer of origin (Table 14.1), and by occasionally allowing fine needle aspiration (FNA) for cytologic diagnosis.

Lipoma

Lipomas are benign growths of mature lipocytes that can be seen in any part of the GI tract. Esophageal lipomas are extremely rare, whereas gastric lipomas are more common. Endoscopically, lipomas appear as smooth masses with normal overlying mucosa with a discernable yellow tint (Figure 14.1a). The "pillow cushion sign", whereby a closed forceps is pressed against the mass leaving a slight indentation, is a reasonably specific endoscopic sign for lipomas. On EUS, lipomas are hyperechoic, homogenous oval masses with smooth borders located in the submucosal layer (Figure 14.1b). Tissue sampling is rarely necessary given the excellent diagnostic accuracy of EUS. Asymptomatic lipomas generally require no additional surveillance.

Carcinoid tumors

Carcinoid tumors are neuroendocrine tumors with malignant potential. They are most commonly found in the appendix and rectum, but can also be found in the stomach, esophagus, and duodenum. Carcinoid tumors arise from the mucosal layer but can invade into the submucosal layer forming a subepithelial mass. Endoscopically, carcinoids appear as smooth, round, yellowish masses (Figure 14.2a) that can display central erythematous depression or ulceration. On EUS, carcinoids appear hypoechoic or isoechoic, homogenous with smooth borders, and are usually located in the mucosa/submucosal layer (Figure 14.2b). Unlike most true submucosal tumors, the diagnosis of carcinoids can often be made with standard biopsy forceps. In general endoscopic resection can be considered for carcinoid tumors less than 1 cm, located within the mucosal or submucosal layer without associated lymphadenopathy. Endosmotically resected carcinoid tumors should be followed periodically with both endoscopy and EUS to assess for local recurrence. Larger tumors should be surgically removed.

Granular cell tumor

Granular cell tumors are rare, generally benign lesions that originate from neural tissue. They are most commonly found on the tongue followed by esophagus, stomach, and colon. Endoscopically, they appear as subepithelial masses with normal overlying mucosa (Figure 14.3a). On EUS, they appear as hypoechoic lesions with smooth margins located in the mucosal or submucosal layer (Figure 14.3b). Granular cell tumors have a low, but not zero risk of metastasizing, and therefore attempts are usually made at resection. Endoscopic mucosal resection (EMR) appears to be an excel-

Atlas of Endoscopic Ultrasonography, First Edition. Edited by Frank G. Gress, Thomas J. Savides, Brenna Casey Bounds, John C. Deutsch.

Table 14.1 Endoscopic ultrasound characteristics of gastric and esophageal subepithelial masses.

Lesion	Wall layer	EUS features
Lipoma	Submucosa	Hyperechoic, homogeneous, oval
Carcinoid tumor	Mucosa/submucosa	Hypoechoic/ isoechoic, homogeneous
Granular cell tumor	Submucosa	Hypoechoic
Duplication cyst	Submucosa	Anechoic, round, acoustic enhancement
Pancreatic rest	Submucosa/mucosa	Hypoechoic, heterogeneous, ductal structure
Varices	Submucosa	Anechoic, tubular, Doppler flow
GIST and leiomyoma	Muscularis propria	Hypoechoic
Extrinsic compression	Outside of wall	Lesion dependent

EUS = endoscopic ultrasound; GIST = gastrointestinal stromal cell tumors.

lent modality for removal of tumors less than 2 cm in diameter. Surgery is most appropriate for lesions greater than 2 cm. Endoscopic ultrasound findings that suggest malignancy include invasion through the intestinal wall and increasing size during surveillance. Repeat esophagogastroduodenoscopy (EGD) with EUS can be used for follow-up surveillance.

Duplication cyst

Duplication cysts arise during embryonic development and can be located anywhere within or adjacent to the luminal GI tract (Figure 14.4a). They are spherical or tubular, contain mucin, possess a smooth muscle layer, and are lined by the same mucosa as the adjacent bowel. They occasionally communicate with the adjacent intestinal lumen. Duplication cysts are usually asymptomatic, but can result in symptoms due to a mass effect, bleeding, or perforation. Duplication cysts rarely have been reported to have malignant transformation. Endoscopic ultrasound of duplication cysts usually reveals a round, anechoic lesion in the submucosa that has acoustic enhancement (increased through transmission of ultrasound signal which gives a bright appearance on the

(a)

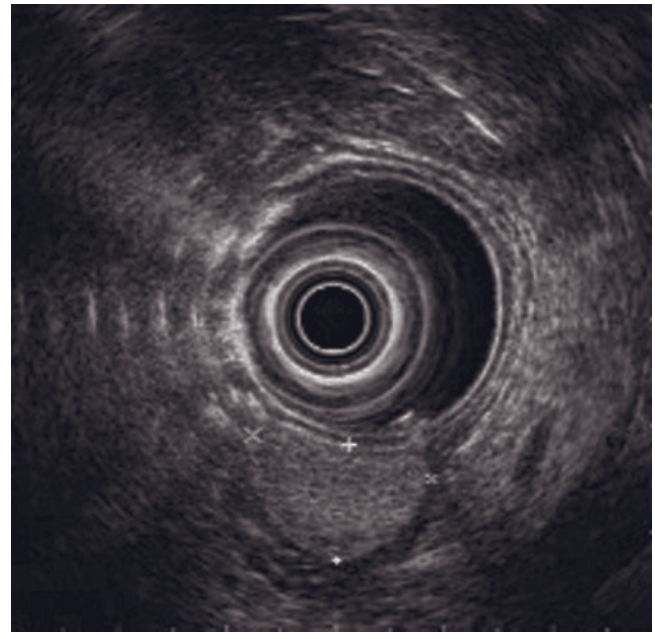

(b)

Figure 14.1 (a) Lipoma with smooth overlying mucosa and discernable yellow tint. (b) Endosonographic view of a lipoma which appears as a 17 × 11 mm homogeneous, hyperechoic oval mass located in the submucosa.

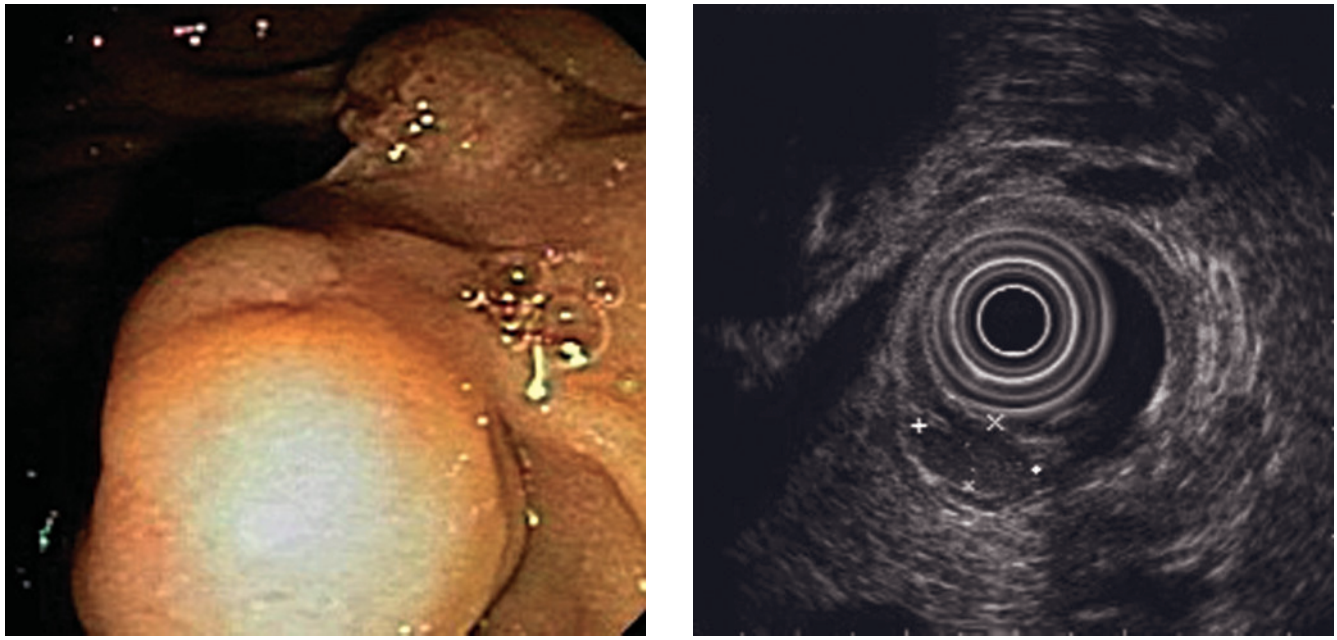

(a) (b)

Figure 14.2 (a) Carcinoid tumor. (b) Endosonographic view of a carcinoid tumor which appears as a 12 × 7 mm oval homogeneous, hypoechoic mass located in the submucosa.

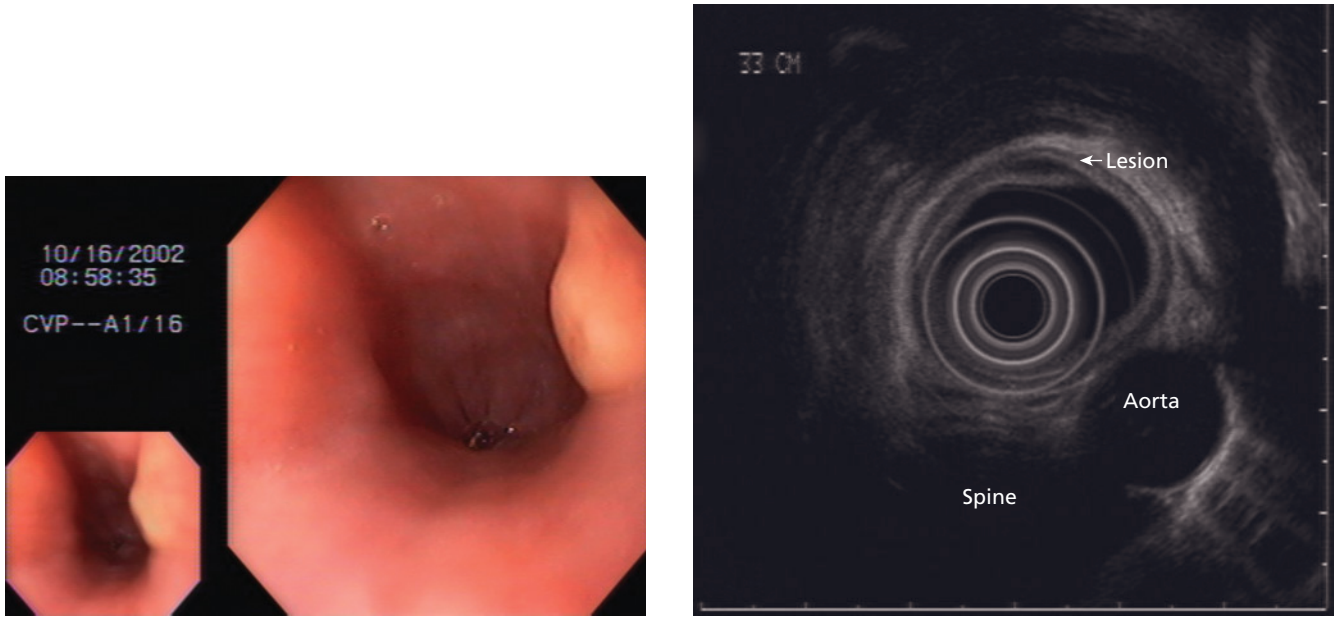

(a) (b)

Figure 14.3 (a) Esophageal granular cell tumor. (b) Endosonographic view of an esophageal granular cell tumor appearing as a very hypoechoic mass located in the submucosal without any acoustic enhancement. Note intact overlying mucosa and underlying muscularis propria.

side distal to the ultrasound transducer, similar to a flashlight effect) (Figure 14.4b). They may have endosonographic findings of echogenic debris which can be mucinous material. The diagnosis can be confirmed with fine needle aspiration of the fluid, although this is not generally necessary and may unnecessarily expose the patient to risk of cyst infection. The optimal management of asymptomatic cysts is unknown. Periodic EUS surveillance to observe for enlargement may be appropriate. Treatment of symptomatic or enlarging lesions has traditionally been surgical resection.

(a)

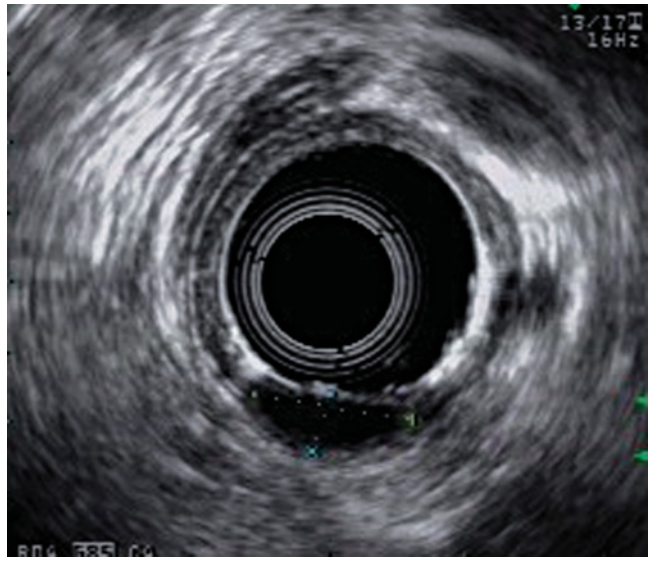

(b)

Figure 14.4 (a) Esophageal duplication cyst. (b) Endosonographic view of an esophageal duplication cyst appearing as an anechoic lesion in the submucosal with mild acoustic enhancement.

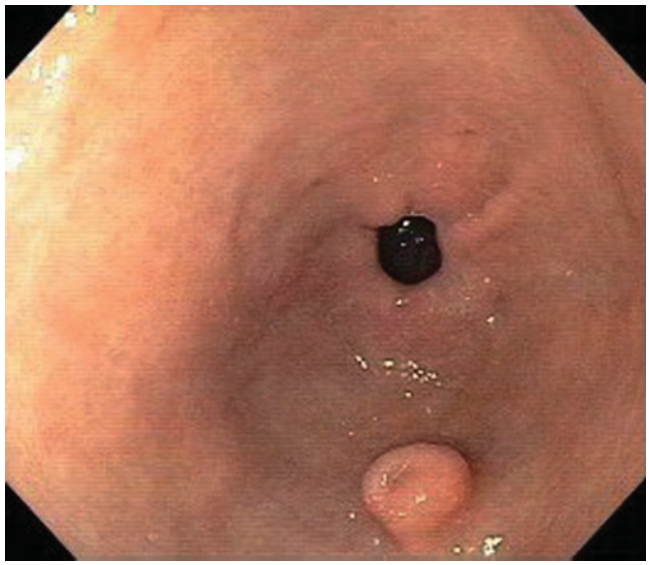

(a)

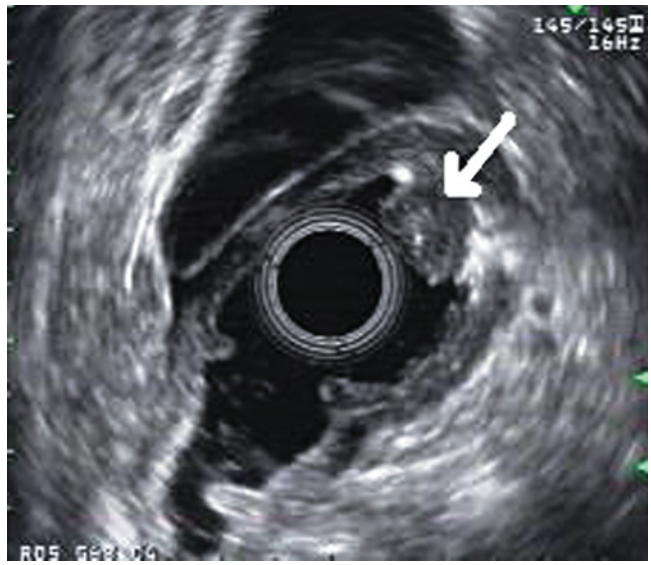

(b)

Figure 14.5 (a) Gastric pancreatic rest. Note the characteristic location in the gastric antrum a few centimeters from the pylorus. This lesion displays central umbilication which is present in the majority of pancreatic rests. (b) Endosonographic view of a pancreatic rest appearing as a heterogeneous mass (arrow) arising from the submucosa.

Pancreatic rest (heterotopic pancreas)

Heterotopic pancreas is any pancreatic tissue that is anatomically unrelated to the pancreas. The majority are 10 mm in diameter, located 1–4 cm from the pylorus in the 6 o'clock endoscopic position in the gastric antrum. Endoscopically, they appear as submucosal masses with smooth overlying mucosa and may display characteristic central umbilication through which secretions drain (Figure 14.5a). On EUS, pancreatic rests are hypoechoic or heterogeneous lesions located in the mucosal/submucosal layer (Figure 14.5b and Video 14.1). Occasionally, EUS can visualize a ductal structure traveling upward to the mucosal surface. Asymptomatic pancreatic rests require no further evaluation or treatment; however, those that are symptomatic, enlarging, or in which the diagnosis is in doubt should be removed endoscopically or surgically.

Varices

Gastroesophageal varices can occur within the submucosal layer (esophageal or gastric varices) or outside the wall as collateral vessels (para-esophageal or para-gastric varices) (Figure 14.6). The EUS appearance is that of tubular anechoic structures which can be traced with the ultrasound probe. Doppler ultrasound allows for easy visualization of varices. For detection of esophageal varices, endoscopy is more sensitive than EUS, but for gastric varices (and perigastric varices) EUS is more sensitive than endoscopy.

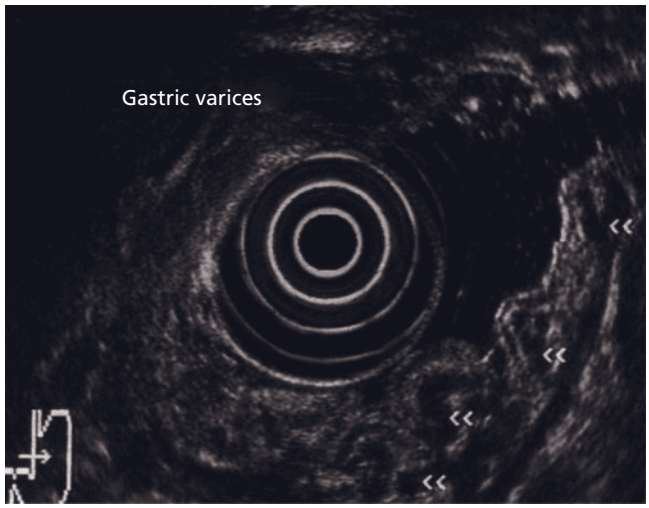

Figure 14.6 Endosonographic view of gastric varices. (Source: Gress F, Savides T. *Endoscopic Ultrasonography*, 2nd edn. Oxford: Wiley-Blackwell, 2009.)

Gastrointestinal stromal cell tumors and leiomyomas

Spindle cell neoplasms are the most common mesenchymal tumors of the GI tract. These include both benign leiomyomas, as well as gastrointestinal stromal cell tumors (GISTs) which have some malignant potential. GISTs are thought to originate from the Interstitial Cells of Cajal. Ninety percent of GISTs are c-KIT positive, which confers a gain of function resulting in cell proliferation and survival. Approximately two-thirds of all GISTs occur in the stomach. Endoscopy reveals a submucosal mass which is often dumbbell shaped and may have mucosal ulceration (Figure 14.7a). Clinically they may present as the source of upper GI bleeding, or as an incidental finding. The EUS appearance of GISTs is usually a hypoechoic mass which originates from the muscularis propria (Figure 14.7b), although occasionally they can arise from the muscularis mucosa. The EUS features associated with risk of metastases for GISTs include a tumor size greater than 4 cm, irregular extraluminal border, echogenic foci (greater than 3 mm), and cystic spaces (greater than 4 mm). Because it is important to differentiate between a GIST and a more benign leiomyoma, EUS-FNA is commonly performed to obtain tissue to confirm spindle cells and for immunohistochemical staining for c-Kit. EUS-FNA does not generally provide sufficient material to comment on the number of mitoses per high powered field, which is also a

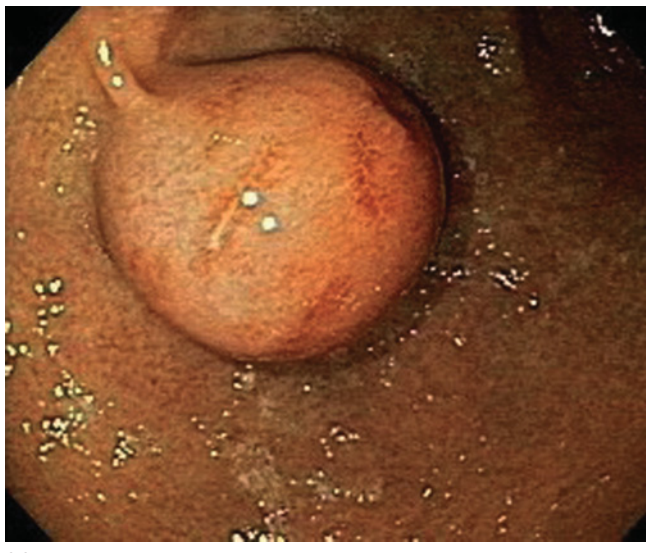

(a)

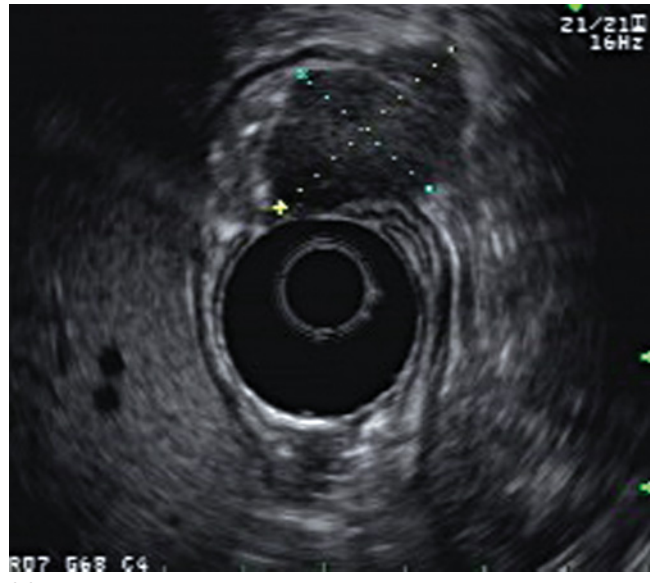

(b)

Figure 14.7 (a) Gastric gastrointestinal stromal tumor (GIST) with surface ulceration. (b) Endosonographic view of a gastric GIST appearing as a hypoechoic mass with irregular borders arising from the muscularis propria.

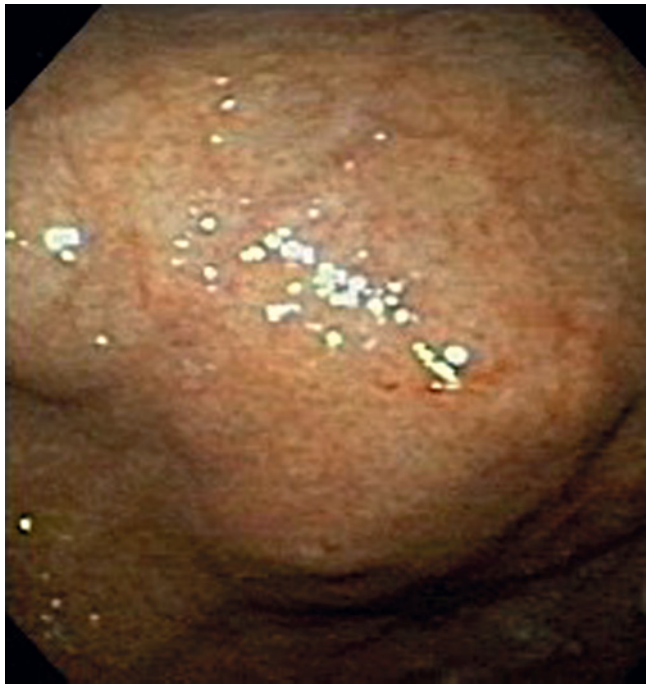

(a)

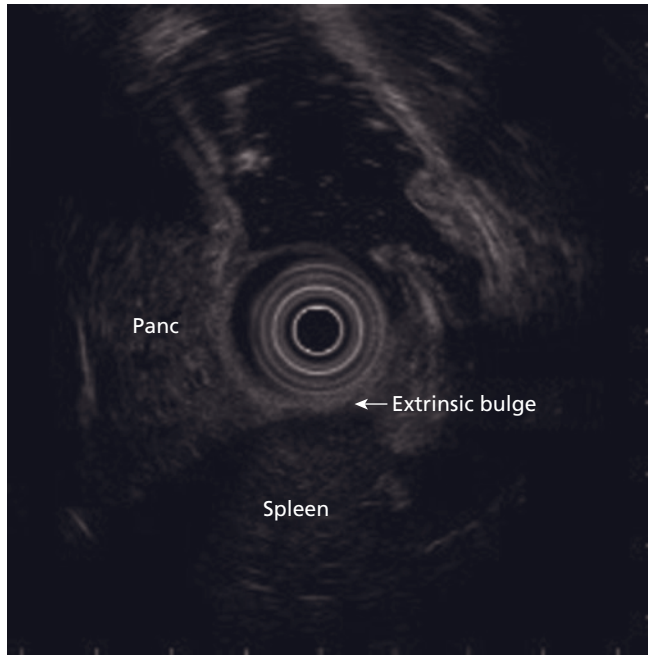

(b)

Figure 14.8 (a) Extrinsic compression from the spleen appearing as a gastric subepithelial mass. (b) Endosonography confirms the extrinsic compression is from the spleen.

marker for metastatic potential. Surgical resection is the treatment of choice for symptomatic or large GISTs, although tumors smaller than 3 cm without EUS features of malignancy can be followed serially with EUS. Metastastic disease is treated with imatinib, a selective inhibitor of certain tyrosine kinases including c-KIT.

Extrinsic compression lesions

Normal abdominal organs can cause indentations in the GI tract which may mimic a submucosal mass (Figure 14.8a). Extrinsic compression can be seen in the esophagus by the aortic arch and left atrium and in the stomach by the left lobe of the liver and the spleen. Pathologic compression may occur from malignant lymph nodes or masses in either the stomach or the esophagus. EUS can identify lesions outside the GI tract exerting mass effect on the intestinal lumen (Figure 14.8b).

Chapter video clips

Video 14.1 Gastric antral pancreatic rest.

15 Anorectal Neoplasia

Manoop S. Bhutani[1] and Everson L. A. Artifon[2]

[1] University of Texas MD Anderson Cancer Center, Houston, TX, USA
[2] University of São Paulo, São Paulo, Brazil and Ana Costa Hospital, Santos, Brazil

Colorectal cancer staging by EUS

Tumor (T) stage

Malignant colorectal tumors by endoscopic ultrasound (EUS) appear as hypoechoic masses. A tumor that by EUS appears to be limited to the mucosa or the submucosa (first three echo layers) is classified as a T1 lesion by EUS (Figure 15.1a & b). A colorectal carcinoma invading into the muscularis propria (hypoechoic fourth EUS layer) but with an intact outer margin of the muscularis propria and with no penetration completely through the muscularis propria will be a T2 lesion by EUS (Figure 15.2a & b). A T3 lesion by EUS penetrates completely through the rectal wall and all the EUS layers, has irregular outer margins, or has tumorous pseudopodia extending beyond the five echo layers (Figures 15.2b and 15.3). A T4 lesion by EUS is a colorectal cancer that is locally invading into an adjacent organ, e.g. the prostate or vagina.

N stage

Lymph nodes during EUS may be seen as round, oval, or sometimes triangular structures that may be hypoechoic, echogenic, or with mixed echogenicity. In addition, if a color Doppler is available on the echoendoscope it may further help in differentiating a vascular structure from a lymph node by observing color flow within a vessel (Figure 15.4). When no lymph nodes are seen during EUS, or if the lymph nodes visualized during EUS are considered reactive and not malignant, the N stage is classified as NO. When lymph nodes visualized during EUS are believed to be malignant, N1 stage by EUS is diagnosed with 1–3 regional lymph nodes and N2 stage is diagnosed with 4 or more regional lymph nodes. In rectal cancer, the size cut-off for lymph nodes considered as suspicious for malignant invasion is 5 mm instead of 10 mm. The application of endoscopic ultrasound-guided fine needle aspiration (EUS-FNA) may be used as an adjunct to accurate lymph node assessment during EUS and it has been applied in patients with rectal cancer (Figure 15.5 and Video 15.1). EUS-FNA of lymph nodes is not an option for lymph nodes that are in the immediate vicinity of the primary tumor since traversing of the EUS-FNA needle through the primary will lead to false positive results.

Endoscopic ultrasound for local recurrence of colorectal carcinoma

Local recurrence of colorectal cancer after attempted curative resection occurs in 2.6–32.0% of patients. Endosonography may be useful in the diagnosis of suspected local recurrence when no lesions arising from the mucosa are seen during conventional endoscopy. Endoscopic ultrasound in such cases may reveal hypoechoic areas (or areas of mixed echogenicity) outside the colorectal wall. (Figure 15.6a–c) Endosonographic alterations due to the primary surgery need to be kept in mind. The risk of recurrence after surgery for rectal cancer is greatest in the first two years after surgery. Detection of local recurrence in a resectable stage provides an opportunity for repeat surgery with curative intent.

Restaging after chemotherapy and radiation

Neo-adjuvant chemoradiation is often utilized for down staging of a rectal cancer prior to surgical resection. Although EUS is very accurate in T & N staging for rectal cancer prior to initiating any treatment, re-staging after chemoradiation is problematic. Inflammation and necrosis after chemoradiation appears hypoechoic and indistinguishable from malignant tissue. This results in the obvious problem of over staging by EUS after radiation and chemotherapy.

Atlas of Endoscopic Ultrasonography, First Edition. Edited by Frank G. Gress, Thomas J. Savides, Brenna Casey Bounds, John C. Deutsch.

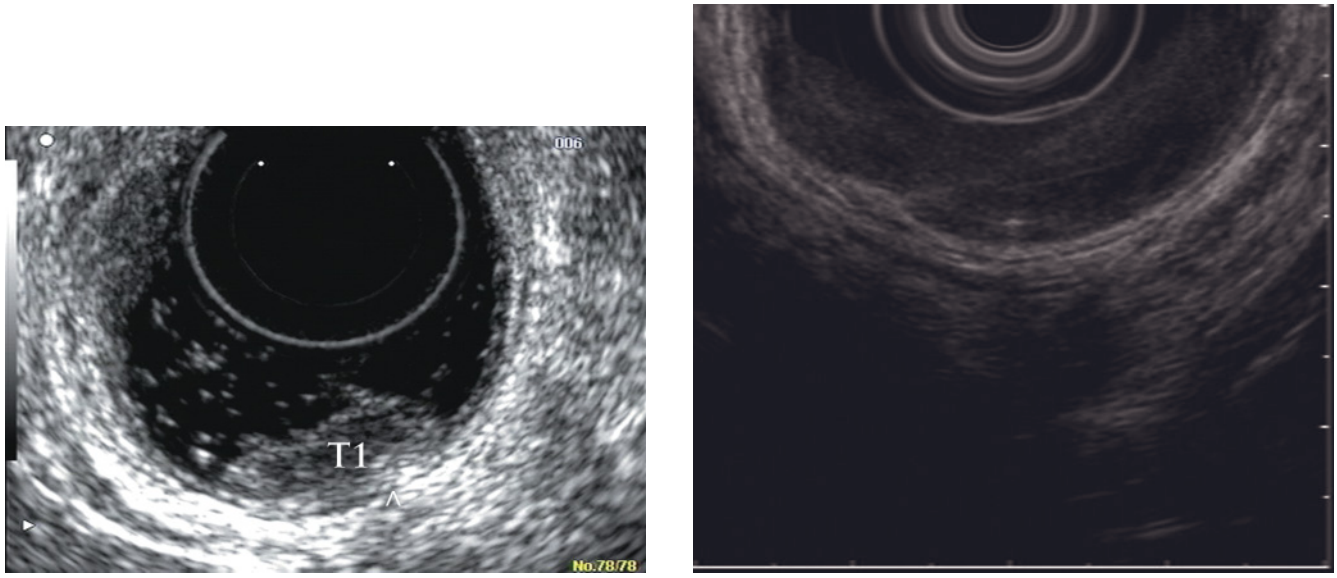

(a) (b)

Figure 15.1 (a) A T1 rectal adenocarcinoma (by radial endoscopic ultrasound) arising in a villous adenoma with an intact submucosa and muscularis propria (arrowhead) underneath. (b) A larger T1 rectal cancer (compared to Figure 15.1a) arising from the mucosa with an intact submucosa underneath the cancer.

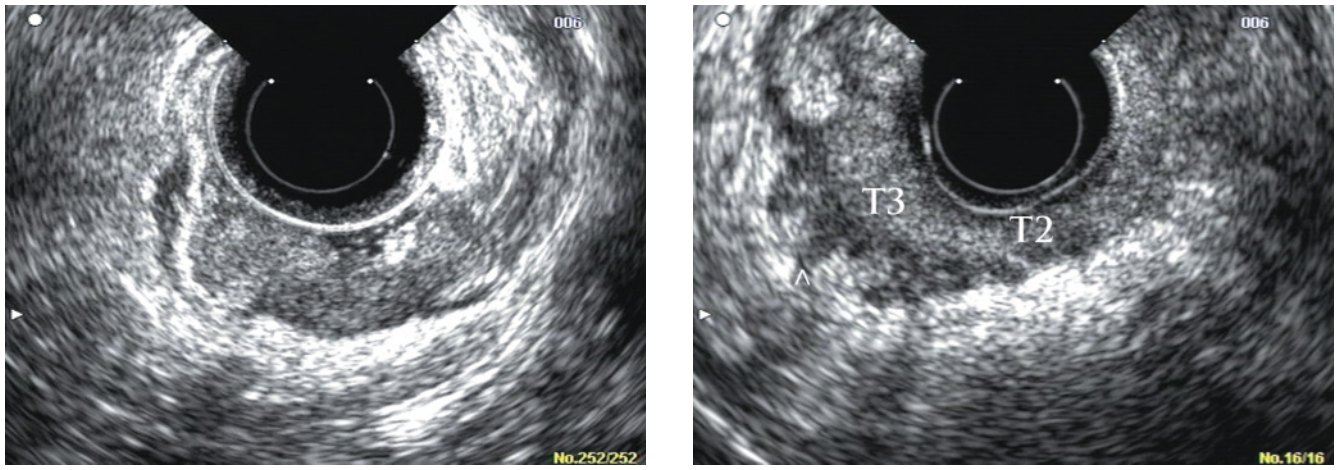

(a) (b)

Figure 15.2 (a) A rectal adenocarcinoma that appears to be T2 (penetration into muscularis propria). (b) Radial endoscopic ultrasound image of a rectal adenocarcinoma that appears to be T2 (penetration into muscularis propria) in one portion and T3 (penetration through the muscularis propria (MP) into peri-rectal fat (arrowheads) in another.

Submucosal tumors of the colorectal wall

It is difficult to predict the cause of an endoscopically visible bulge into the gastrointestinal lumen when the overlying mucosa is normal (Figure 15.7a). A lipoma is characterized by a homogeneous, echogenic lesion that is contiguous with the third echo layer corresponding with the submucosa. Most lipomas are benign and malignant transformation is a rare phenomenon. Thus, there is controversy about the need for endoscopic removal once a lipoma is diagnosed by EUS. However, EUS would be a prerequisite prior to contemplating an endoscopic removal of a lipoma. Endoscopic ultrasound may also help in monitoring this lesion if it is not removed.

A myogenic tumor appears as a hypoechoic mass that is contiguous with the fourth echo layer representing the muscularis propria (Figure 15.7b). The differential diagnosis of

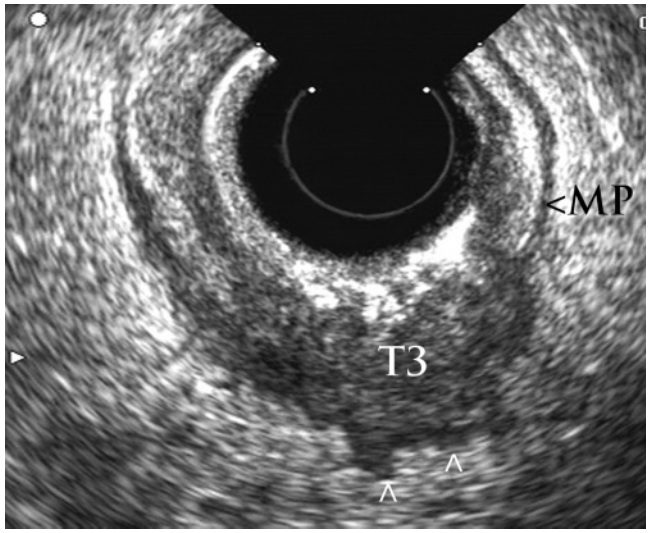

Figure 15.3 Radial endoscopic ultrasound of a T3 lesion showing the primary rectal tumor penetration through the muscularis propria (MP) into peri-rectal fat (arrowheads).

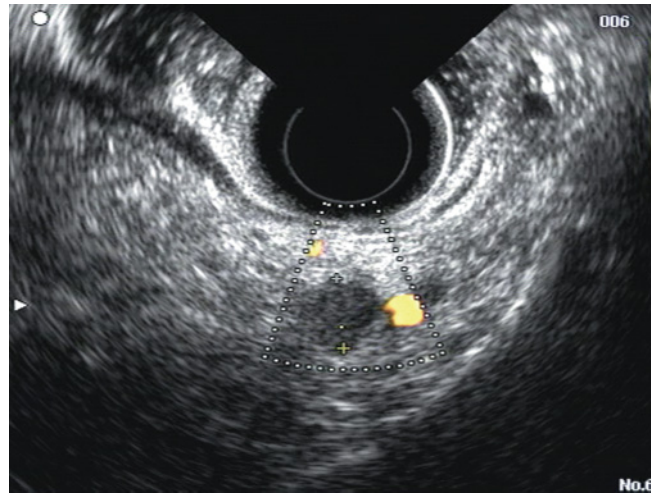

Figure 15.4 Radial endoscopic ultrasound of the patient in Figure 15.3 showing a 7 mm round, peri-rectal, hypoechoic lymph node with no flow on color Doppler with an adjoining vessel nearby with color flow.

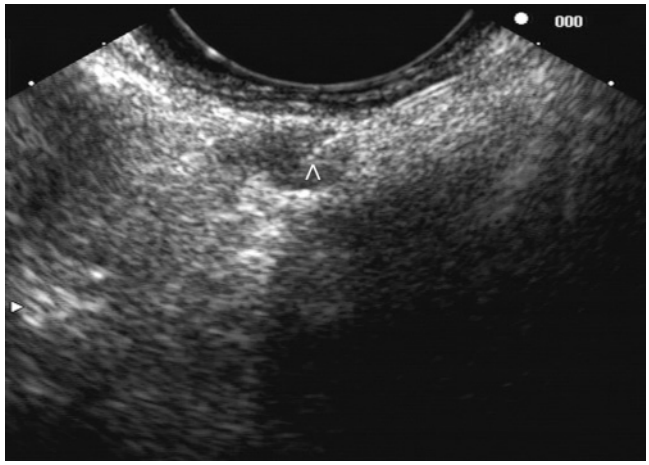

Figure 15.5 Endoscopic ultrasound-guided fine needle aspiration of a peri-rectal lymph node. The tip of the needle is within the lymph node (arrowhead).

a myogenic tumor includes a leiomyomia, leiomyosarcoma, leiomyoblastoma or a gastrointestinal stromal cell tumor (GIST). A myogenic tumor, which is greater than 4 cm in diameter, has an irregular margin, with cystic or echogenic foci is more likely to be a malignant lesion. However, there is overlap between benign and malignant myogenic or GIST lesions, and resection of the entire lesion is the surest way to ensure absence of malignancy. If, however, a decision is made to monitor a myogenic lesion that appears benign, EUS may be useful. Any change in echo features such as size, echogenicity, margins, or appearance of lymphadenopathy may then warrant a surgical resection.

Carcinoid tumors of the rectum are not uncommon. They generally appear as a firm, small, submucosal nodule (Figure 15.8a). By EUS a rectal carcinoid appears as a hypoechoic mass arising from the second echo layer and sometimes compressing or extending to the submucosa (Figure 15.8b).

Colonic lymphangiomas can also produce a submucosal compression. By endosonography they appear as multiple,

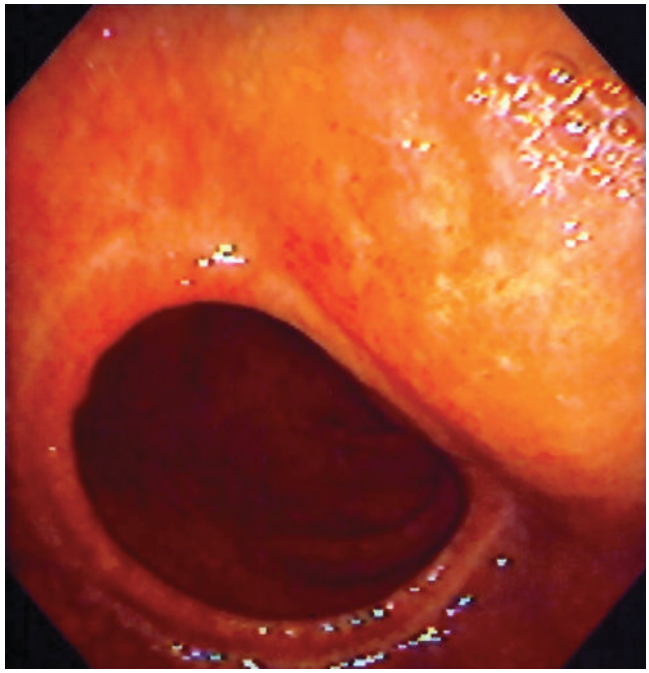

(a)

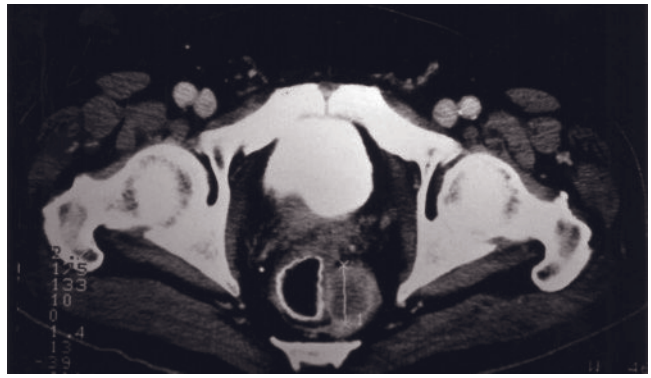

(b)

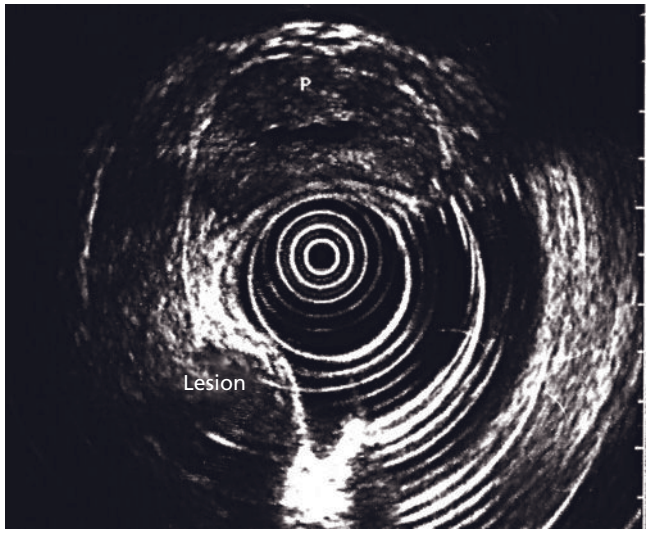

(c)

Figure 15.6 Recurrent rectal cancer. During surveillance colonoscopy in a patient post-sigmoidectomy for colorectal cancer, a bulge was noted at the anastomosis (a). A computed tomography (CT) scan examination (b) and endoscopic ultrasound (c) revealed tumor recurrence at the anastomosis, with involvement of the muscularis propria and submucosa.

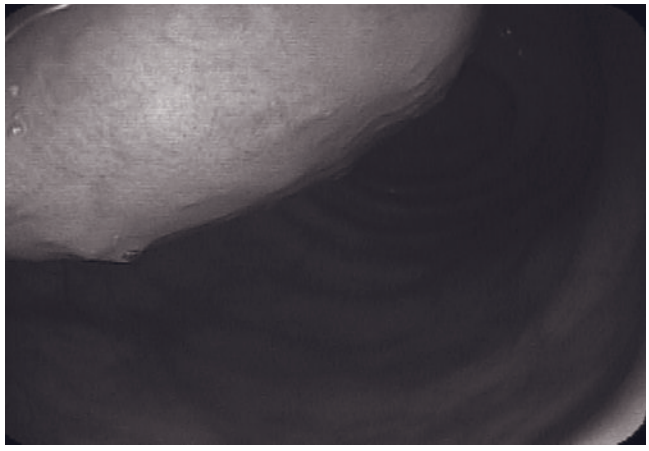

(a)

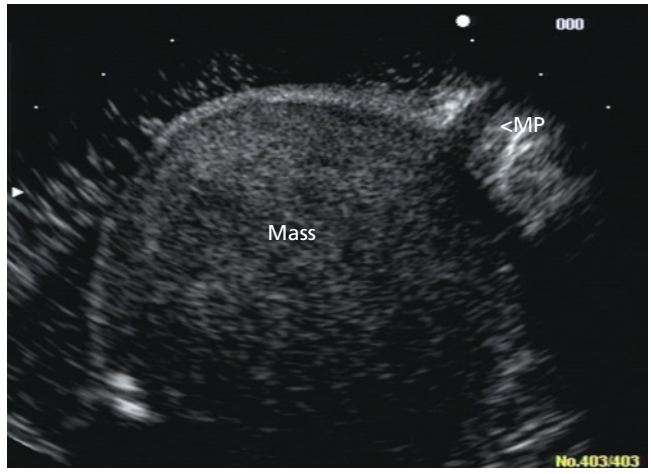

(b)

Figure 15.7 (a) A subepithelial bulge in the rectum from a large intra-mural, subepithelial mass. (b) Endoscopic ultrasound of the mass in Figure 15.7a shows it to be to be a hypoechoic mass (MASS) that is contiguous with the muscularis propria (MP). Endoscopic ultrasound-guided fine needle aspiration revealed it to be a gastrointestinal stromal cell tumor (GIST).

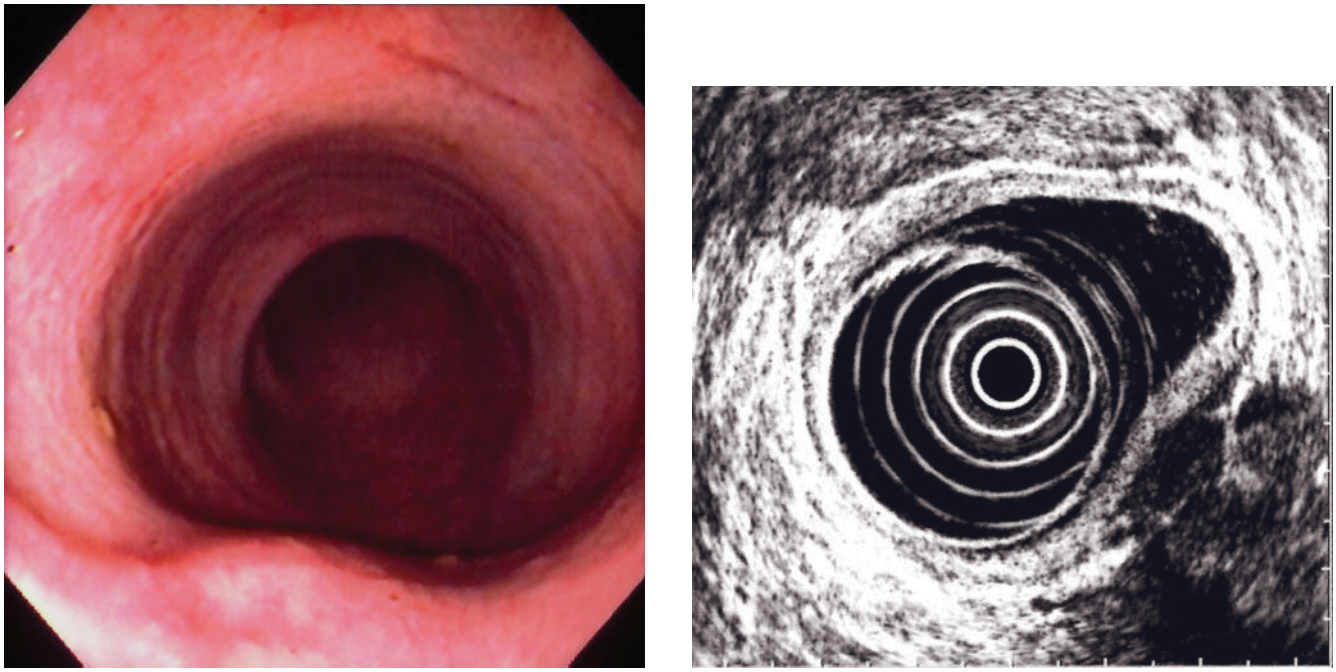

(a) (b)

Figure 15.8 Rectal carcinoid. A rectal bulge was noted during routine colonoscopy (a). Endoscopic ultrasound showed a hypoechoic lesion in posterior rectum, with involvement of the submucosa and muscularis propria (b). Histopathological examination was diagnostic of a carcinoid tumor.

anechoic (cystic) lesions with echogenic septations located within the third echo layer corresponding with the submucosa. These lesions are generally benign and are left alone unless they cause symptoms such as bleeding, intestinal obstruction, or intussusception. The endosonographic image of a rectal lesion–colitis cystic profunda is similar to echo features of colonic lymphangiomas. There has also been isolated case reports of endosonography in colonic pneumatosis cystoids intestinalis and polypoid prolapsing mucosal folds associated with colonic diverticular disease. Recurrence of colorectal carcinoma, malignant lymphoma, and appendical mucocele may also cause submucosal elevation in the colorectum.

Chapter video clip

Video 15.1 Linear endoscopic ultrasound (EUS) -guided transrectal fine needle aspiration (FNA) of an oval, peri-rectal lymph node in a patient with rectal cancer.

16 Anal Sphincter Disease: Fecal Incontinence and Fistulas

Raymond S. Tang and Thomas J. Savides
University of California, San Diego, La Jolla, CA, USA

Introduction

Endoanal ultrasound has become a simple and reliable tool in the evaluation of benign anorectal diseases such as fecal incontinence and anal fistula.

Fecal incontinence

Prevalence

Fecal incontinence can cause significant distress in otherwise functional individuals. Large community studies report a prevalence of fecal incontinence ranging from 1 to 24%. It affects up to 50% of all nursing home residents. The prevalence of fecal soiling is 7% in the US population, affecting men and women equally. Gross incontinence occurs in 0.7% of the US population and is almost twice as common in women as in men. Obstetrical trauma is one of the most common causes of anal sphincter injury leading to fecal incontinence. Fecal incontinence is present in 20% of postpartum women with an anal sphincter defect. Overt anal sphincter damage due to a third-degree or fourth-degree tear occurs in 0.7% of women undergoing vaginal delivery with posterolateral episiotomy.

Etiology of fecal incontinence

Maintenance of fecal continence requires the following: normal functioning of the anal sphincters and puborectalis muscle, intact anorectal sensation, intact cognitive function, and normal stool consistency. Etiologies of fecal incontinence include: (i) weakness of internal or external anal sphincter (e.g. obstetrical trauma from vaginal delivery and episiotomy, prior anorectal surgery, fistula, pudendal neuropathy, diabetes); (ii) weakness of puborectalis muscle (e.g. spinal cord lesion, peripheral neuropathy); (iii) decreased perception of rectal sensation (e.g. diabetes, multiple sclerosis, dementia); (iv) reduced storage capacity (e.g. rectal ischemia, radiation proctitis, inflammatory bowel disease); (v) overflow state with intact sphincter function (e.g. severe diarrhea, fecal impaction).

Assessment of fecal incontinence

Assessment of fecal incontinence begins with a careful history regarding the nature of incontinence, prior history of anorectal diseases and surgeries, obstetrical history in female patients, neuropathies, and neurologic diseases. Physical examination should include perianal inspection at rest and upon straining as if to defecate, digital rectal examination to check for structural lesion, anal sphincter tone at rest and upon squeezing, and ano-perineal sensation. Patients with internal anal sphincter defects have decreased resting sphincter tone, while patients with external anal sphincter defects have decreased voluntary anal canal squeeze.

Diagnostic tests

Further testing of anal sphincter for structural defect or dysfunction may be pursued when etiology of fecal incontinence is uncertain. Flexible sigmoidoscopy or colonoscopy can be used to exclude mucosal inflammation or mass. Pelvic magnetic resonance imaging (MRI) provides a non-invasive way to investigate the structural integrity of the anorectum. Anorectal manometry allows measurement of resting and squeeze anal sphincter pressure. An intra-rectal balloon can be used to assess rectal sensation. Decrease of resting or squeeze sphincter pressure with normal sensory testing suggests mechanical sphincter defect. Pudendal nerve terminal latency testing (PNTL) measures the time to induce external anal sphincter contraction after stimulation of pudendal nerve. About 16% of postpartum women would have a conduction delay. The use of electromyography

Atlas of Endoscopic Ultrasonography, First Edition. Edited by Frank G. Gress, Thomas J. Savides, Brenna Casey Bounds, John C. Deutsch.

(EMG) for anal sphincter mapping, usually poorly tolerated by patients, has diminished as endoanal ultrasound becomes available.

Endoanal ultrasound

Endoanal ultrasound has emerged as a reliable and well-tolerated investigation for defects in internal anal sphincter (IAS) and external anal sphincter (EAS). The accuracy of endoanal ultrasound in detecting anal sphincter defect prior to sphincter repair ranges from 89 to 100% in surgical series. Endoanal ultrasound can be performed with a rigid radial ultrasound probe, or a radial echoendoscope. Figure 16.1 shows a schematic diagram of the anal canal complex. On ultrasound, two rings of tissue can be seen in the normal anal canal (Figures 16.2 and 16.3). The inner hypoechoic ring of tissue corresponds to the IAS, with normal thickness

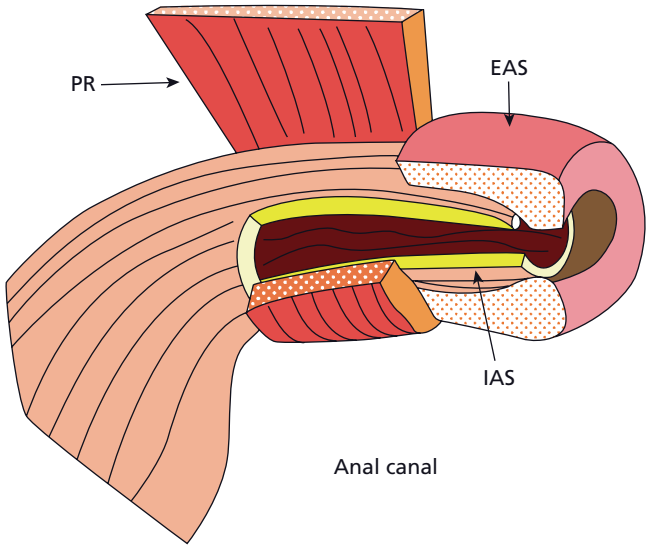

Figure 16.1 Schematic diagram of the anal canal (EAS = external anal sphincter; IAS = internal anal sphincter; PR = puborectalis muscle). (Courtesy of Ravinder Mittal, MD.)

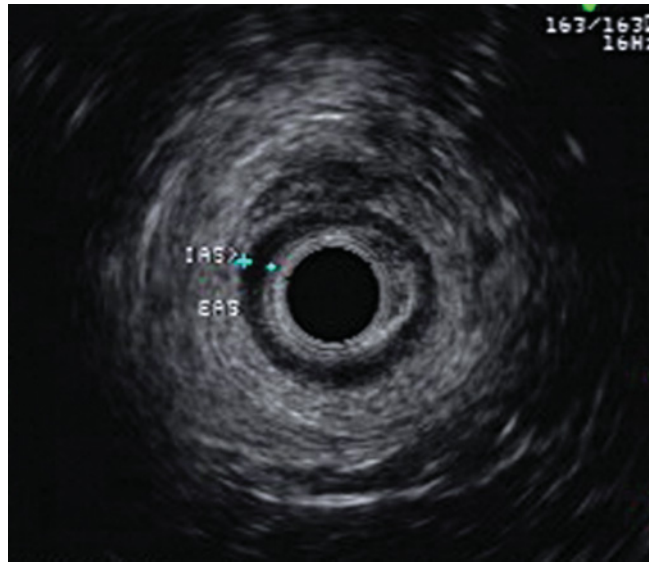

Figure 16.2 Normal anal sphincter complex. The internal anal sphincter (IAS) is black (hypoechoic) and the external anal sphincter (EAS) is white (hyperechoic).

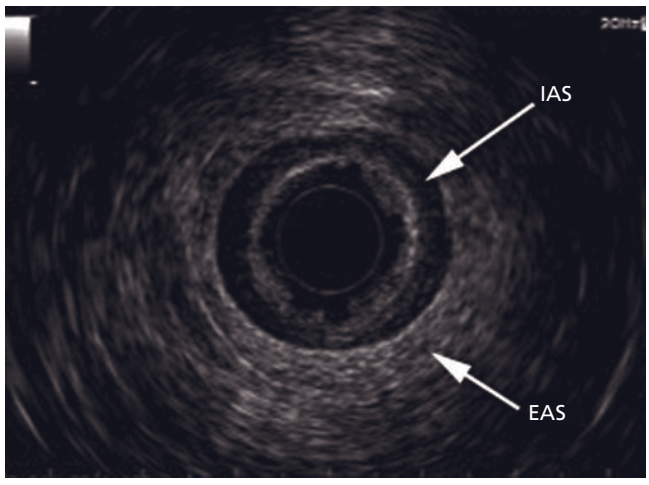

(a)

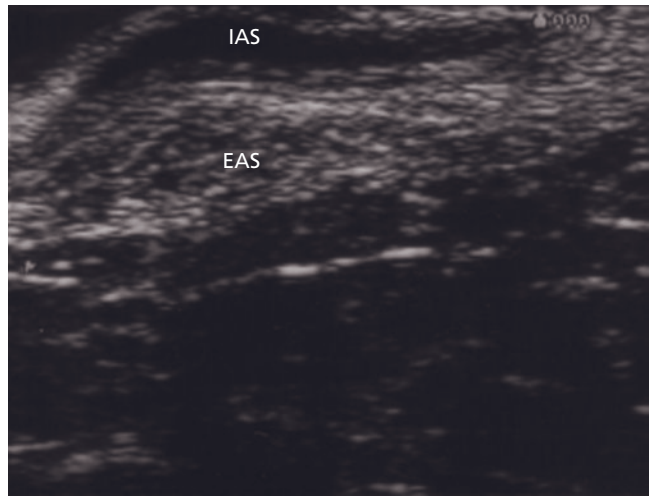

(b)

Figure 16.3 Normal anal sphincter complex. The internal anal sphincter (IAS) is black (hypoechoic) and the external anal sphincter (EAS) is white (hyperechoic). Figure (a) shows the radial array image, and Figure (b) shows the linear array image. (Courtesy of Everson Artifon, MD.)

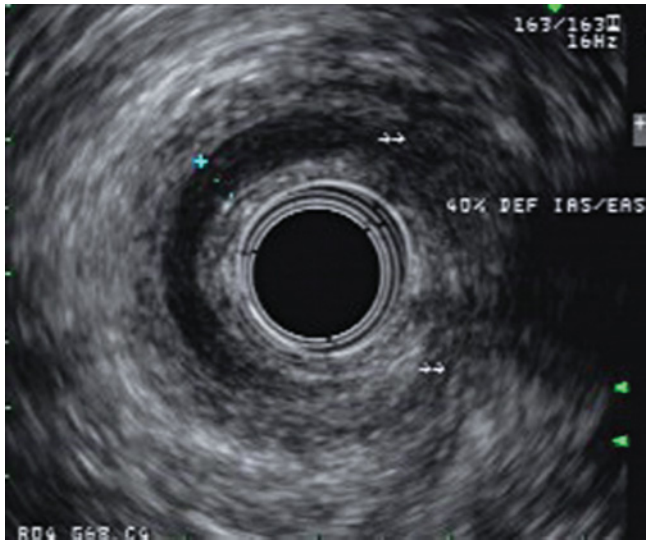

Figure 16.4 Forty percent defect in both the internal hypoechoic anal sphincter (IAS) and the outer hyperechoic external anal sphincter (EAS), likely due to obstetrical trauma.

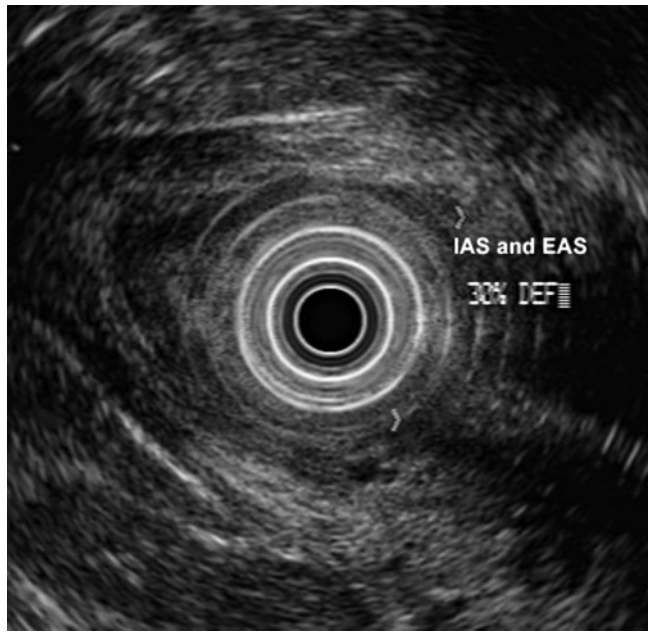

Figure 16.6 Thirty percent defect in both the internal anal sphincter (IAS) and the external anal sphincter (EAS), likely due to obstetrical trauma.

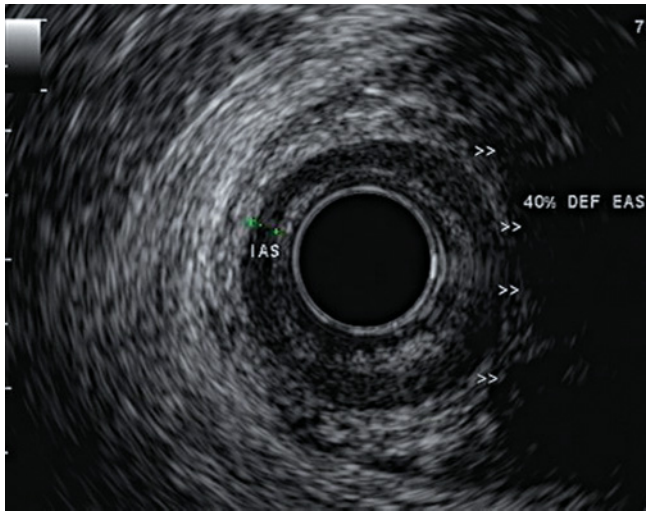

Figure 16.5 Forty percent defect in external anal sphincter (EAS), likely due to obstetrical trauma. Note that the black hypoechoic inner circular muscle layer is circumferentially intact.

of 1–3 mm. The outer hyperechoic ring of tissue represents the EAS, with normal thickness of 6–10 mm. The IAS increases in thickness and becomes more hyperechoic with age, while the EAS becomes thinner with age. The normal anterior part of EAS seems to be shorter and slopes downward in women, which may sometimes be incorrectly identified as an EAS defect. IAS defects appear as hyperechoic breaks in the normally hypoechoic ring, whereas EAS defects appear as relatively hypoechoic areas in the normally hyperechoic ring (Figures 16.4–16.6). Obstetrical trauma usually involves the anterior aspect of the anal sphincters (Video 16.1).

Transperineal ultrasound

Transperineal three-dimensional (3D) ultrasound offers another approach to evaluate the anal sphincter complex. It is less invasive compared to the endoanal approach and allows visualization of the entire sling of the puborectalis muscle, which is often not possible on endoanal ultrasound (Figure 16.7). The length of the anal sphincter complex and the longitudinal size of sphincter defect can be studied using the 3D images (Figure 16.8).

Treatment

Trial of bulk forming agents, anti-diarrheal agents, bowel habit ritualization, and biofeedback is reasonable for initial management of fecal incontinence. If indicated by diagnostic testing or lack of response to conservative management, patients can be referred for surgical management.

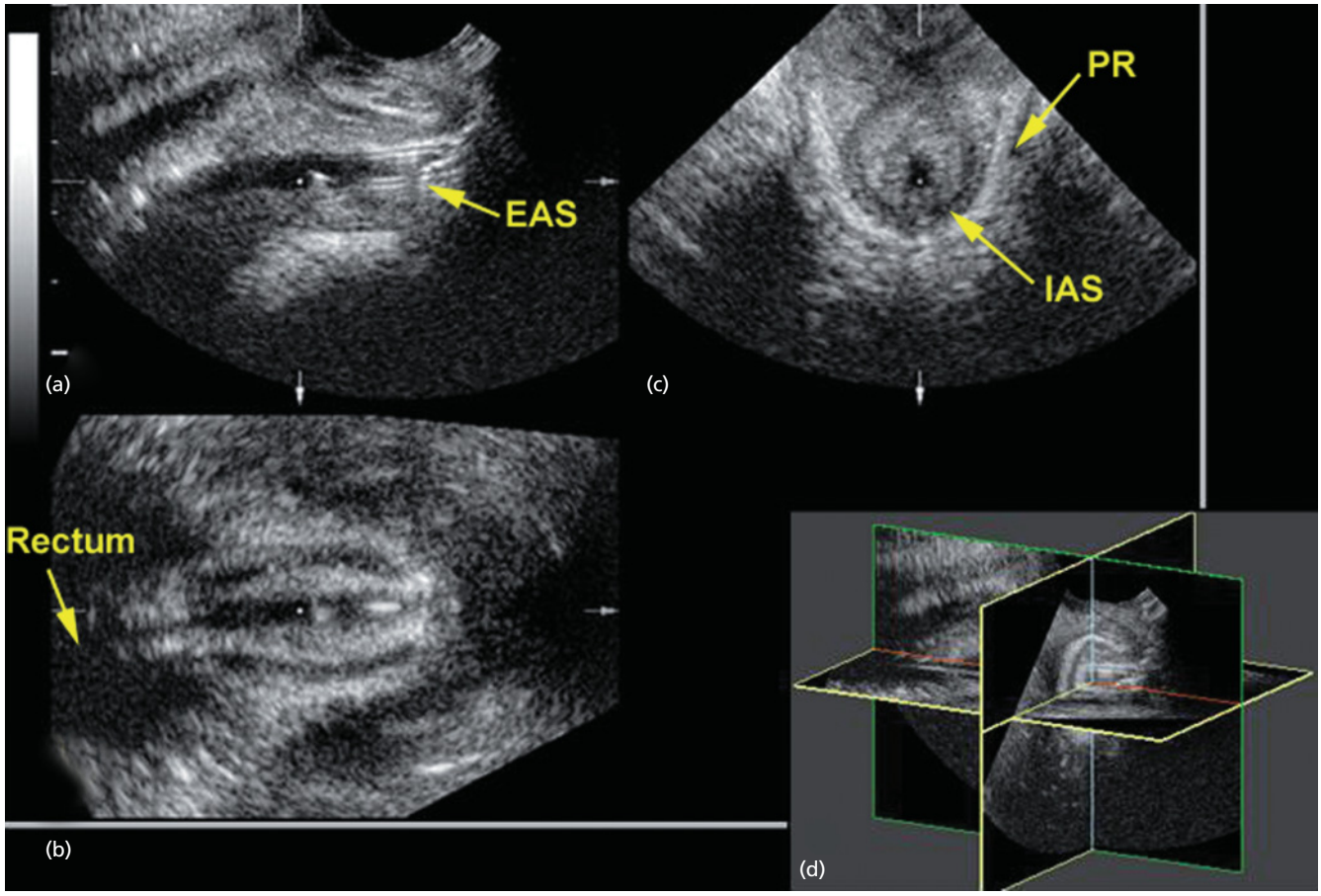

Figure 16.7 Transperineal three-dimensional ultrasound images showing the anal canal in the three orthogonal planes. (a) Sagittal image of the anal sphincter complex (EAS = external anal sphincter). (b) Coronal image of the anal sphincter complex. (c) Transverse image at the proximal anal sphincter showing the internal anal sphincter (IAS) and the puborectalis muscle (PR). (Courtesy of Ravinder Mittal, MD.)

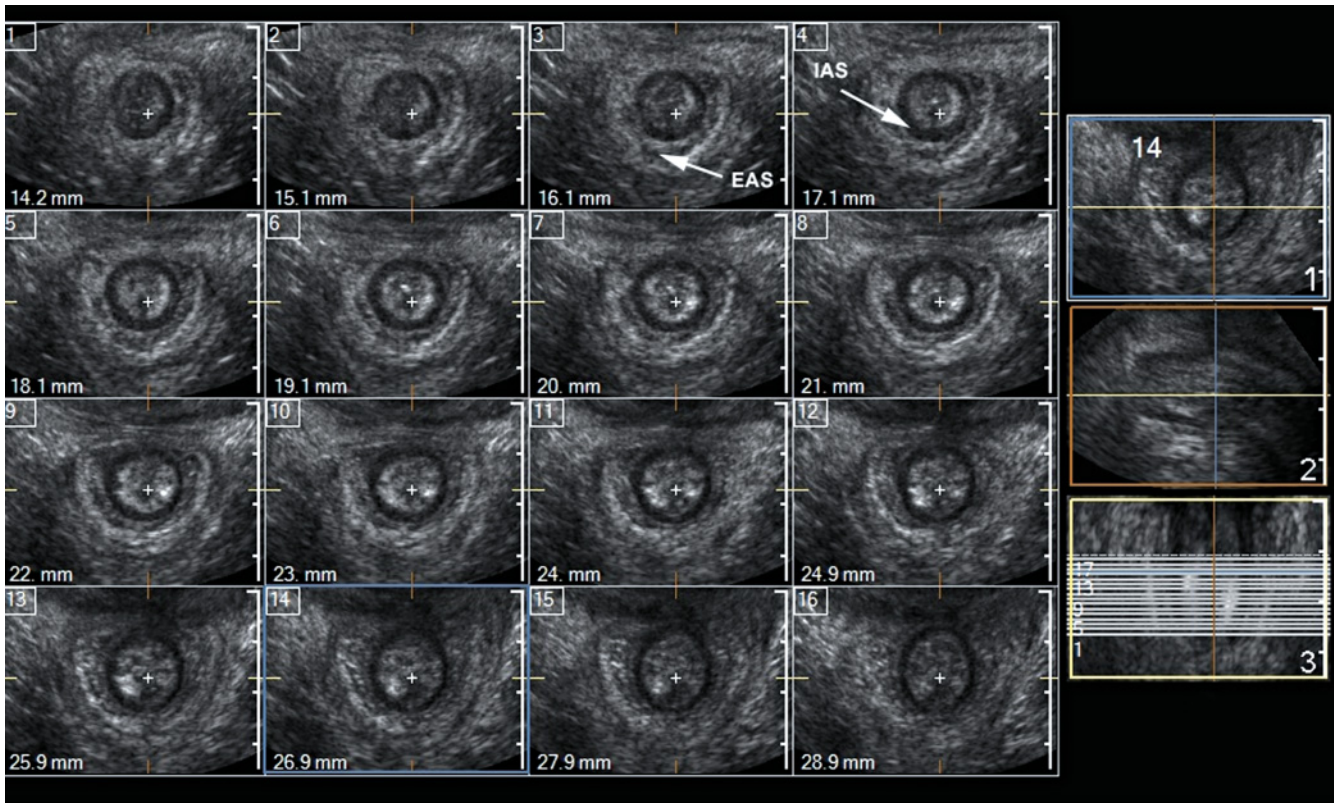

Figure 16.8 Transverse (cross-sectional) 1 mm multislice imaging of the normal anal canal produced by transperineal three-dimensional ultrasound (EAS = external anal sphincter; IAS = internal anal sphincter). (Courtesy of Ravinder Mittal, MD.)

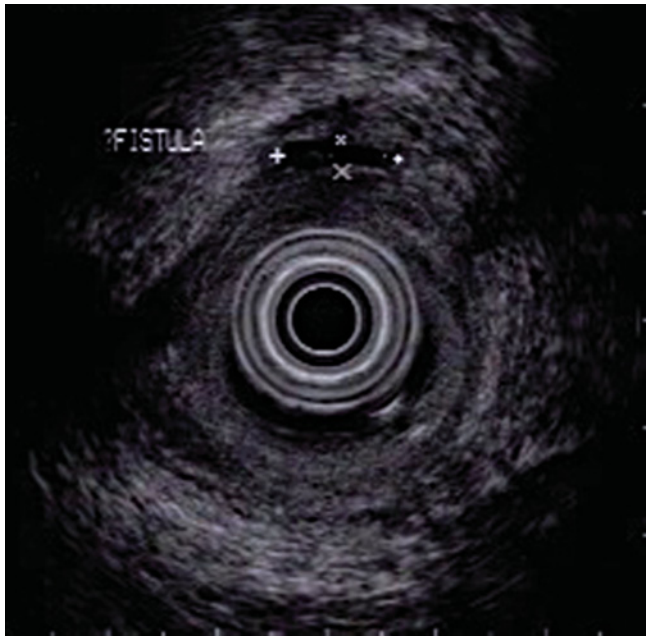

Figure 16.9 Perianal fistula. Note that the anechoic tubular structure is outside of the anal sphincters.

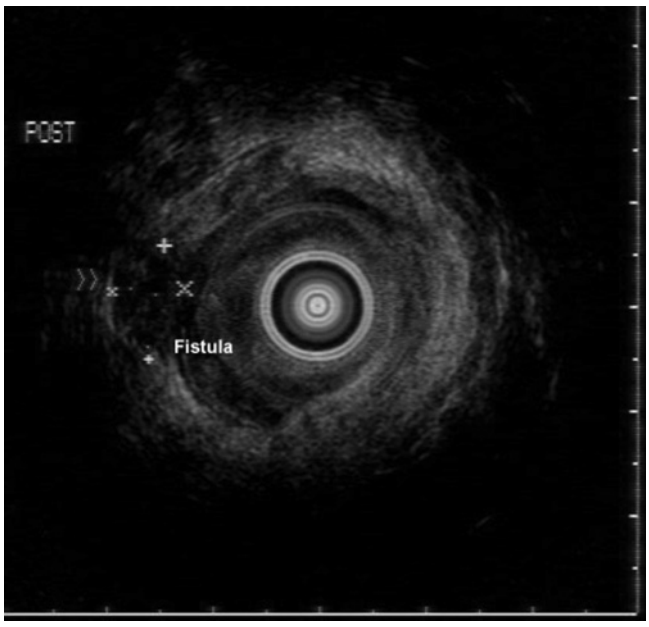

Figure 16.10 Perianal fistula with small perianal abscess measuring 11 × 7 mm.

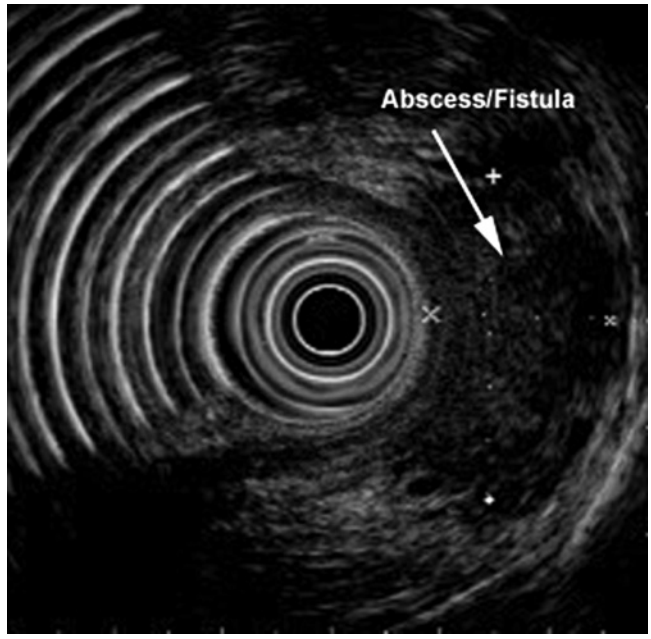

Figure 16.11 Perianal abscess and fistula.

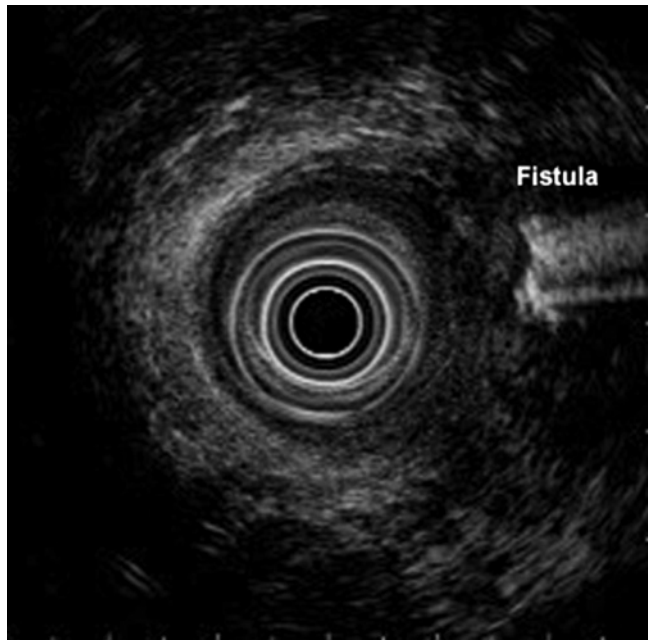

Figure 16.12 Post-hydrogen peroxide injection image of the perianal fistula and abscess shown in Figure 16.11. Note the hyperechoic signal which better delineates the fistula track in the abscess after hydrogen peroxide injection.

Perianal fistula

Perianal fistula can develop secondary to trauma, Crohn's disease, infection, or malignancy. Endoanal ultrasound can be used to study the fistula course and anal sphincter involvement. Fistula tracks are identified as hypoechoic tracts on endoanal ultrasound (Figures 16.9–16.11). Hydrogen peroxide infusion into the fistula generates the formation of small air bubbles, which can enhance visualization of the fistula track by changing it to a hyperechoic structure on ultrasound (Figure 16.12). Additional examples are seen in Figures 16.13–16.16.

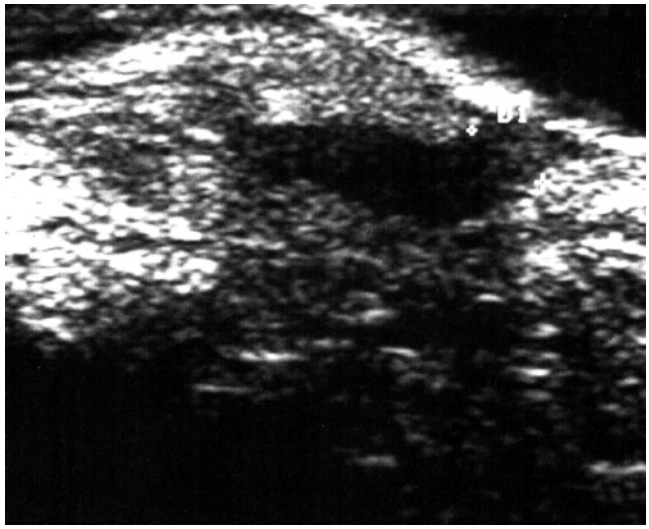

Figure 16.13 Perianal fistula. A hyperechoic path is visible, starting on the skin of the perianal region, and coursing through the hyperechoic band which corresponds to the external anal sphincter (outlined with the + markers). (Courtesy of Everson Artifon, MD.)

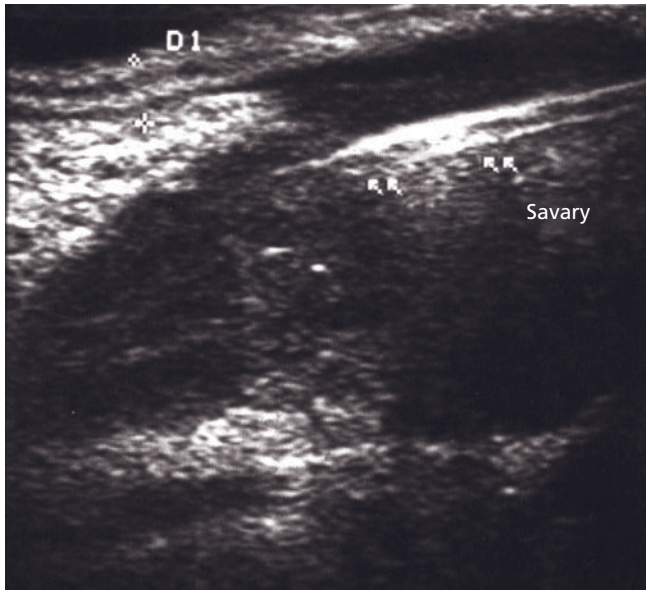

Figure 16.14 The path of a complex perianal fistula is identified by inserting the flexible end of a Savary guidewire through the fistula opening on the skin side. Two hyperechoic lines are seen (Savary wire) which cross the hypoechoic perirectal tissue. (Courtesy of Everson Artifon, MD.)

Chapter video clip

Video 16.1 Endoscopic ultrasound examination of post-obstetrical anal sphincter defect in a patient with fecal incontinence.

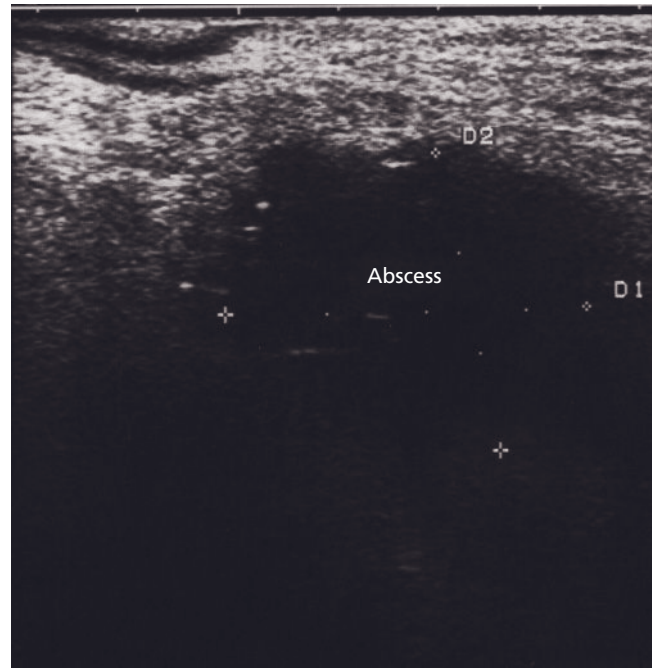

Figure 16.15 Perirectal abscess. A 36-year-old woman with history of Crohn's disease and recurrent perirectal abscesses presented to the hospital with perianal pain and fever. Rectal endoscopic ultrasound was performed under anesthesia, revealing a perirectal abscess (hypoechoic collection) measuring about 36 mm in greatest diameter. (Courtesy of Everson Artifon, MD.)

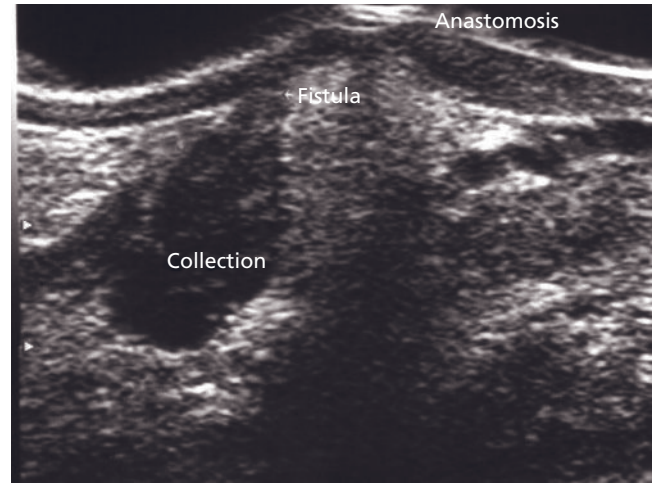

Figure 16.16 Anastomotic abscess. A patient with history of sigmoidectomy for diverticular disease undergoes follow up colonoscopy. Endoscopic examination reveals the presence of an orifice near the anastomosis, which was draining purulent material. Endoscopic ultrasonography with a linear probe was carried out. In the superior aspect of the image, hyperechoic lines can be noted, corresponding to the staple anastomosis. Inferiorly and to the left of the anastomosis, a heterogenous, predominantly hypoechoic collection can be seen, representing an abscess which fistulizes to the intestinal lumen. (Courtesy of Everson Artifon, MD.)

17 Other Pelvic Pathology

Everson L. A. Artifon[1], Lucio G. B. Rossini[2], and Carlos K. Furuya Jr.[3]

[1] University of São Paulo, São Paulo, and Ana Costa Hospital, Santos, Brazil
[2] Santa Casa of São Paulo School of Medicine, São Paulo, and Brazilian–French Center of EUS Research, São Paulo, Brazil
[3] University of São Paulo School of Medicine, São Paulo, Brazil

Endoscopic ultrasound (EUS) can identify much pelvic pathology besides rectal cancer and fecal incontinence. These include endometriosis and prostate cancer (Figures 17.1–17.23).

Transrectal EUS can identify and help stage prostate cancer. Although this is not within the practice of most gastrointestinal (GI) endosonographers, it is important to understand the appearance of some of the structures of the prostate and the appearance of cancer within the prostate.

Pelvic endometriosis is important to recognize as it may affect the GI tract in 3–37% of severe cases. Endometriosis can cause abdominal pain in female patients between 18 and 45 years of age. Rectal EUS can occasionally diagnosis endometriosis involving the GI track wall.

Chapter video clips

Video 17.1 Preoperative histological diagnosis of intestinal endometriosis achieved by fine needle aspiration (FNA) during intestinal endosonography (EUS-FNA).

Video 17.2 Endoscopic ultrasound for prostate cancer: systematization of the procedure.

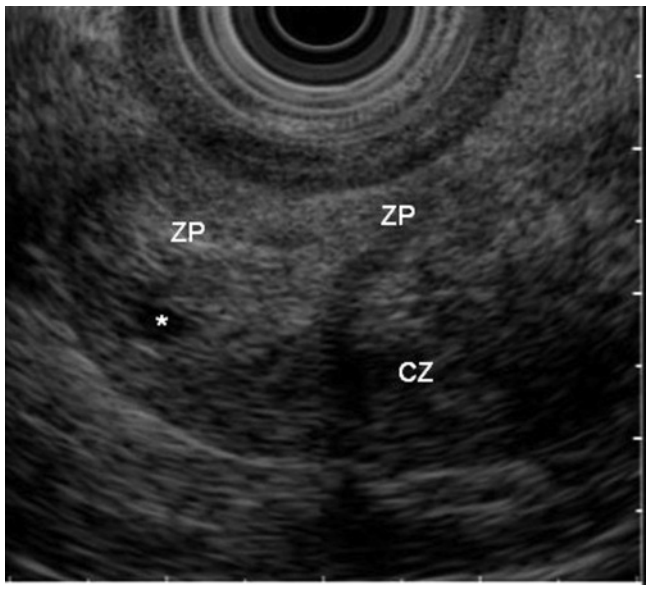

Figure 17.1 Prostate cancer. Radial image demonstrating a hypoechoic lesion in the peripheral zone (ZP) without anatomic capsule invasion (Stage IIA). Center zone (CZ) and adenocarcinoma (*).

Atlas of Endoscopic Ultrasonography, First Edition. Edited by Frank G. Gress, Thomas J. Savides, Brenna Casey Bounds, John C. Deutsch.

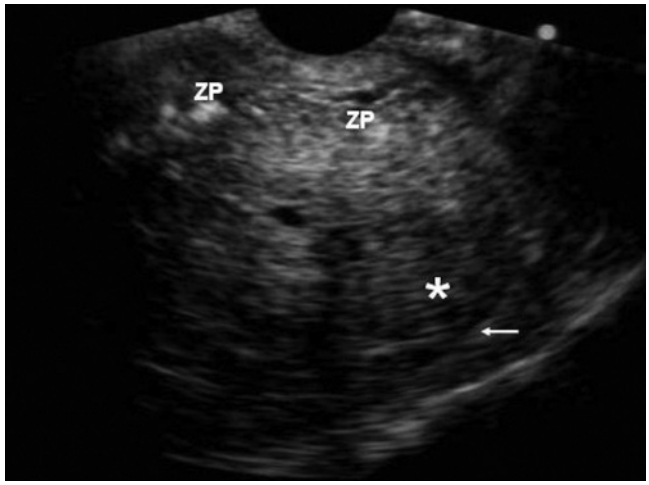

Figure 17.2 Prostate cancer. Linear image demonstrating hypoechoic lesion in the periferic zone invading the anatomic capsule (Stage IIB). Peripheral zone (ZP), lesion (*) and arrow showing the capsule invasion.

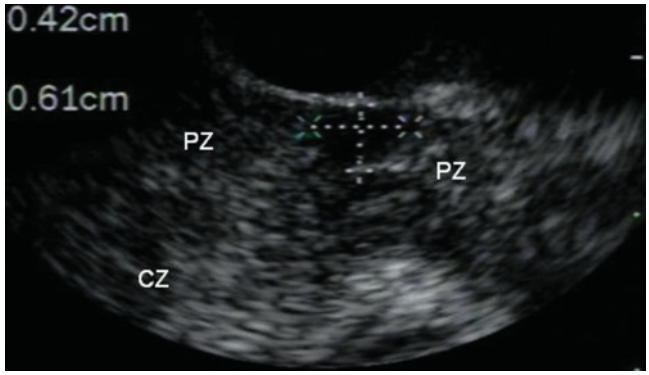

Figure 17.3 Prostate cancer. Linear image demonstrating a hypoechoic lesion in the periferal zone (PZ) without anatomic capsule invasion (Stage IIA). Center zone (CZ).

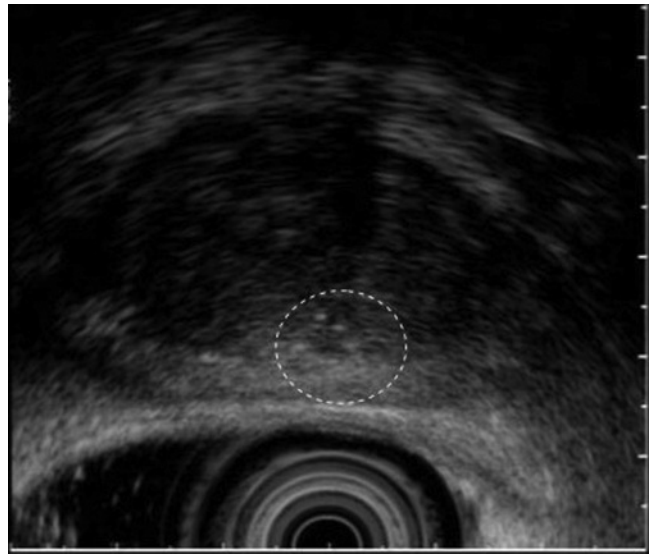

Figure 17.4 Prostate cancer. Radial image showing the Eiffel tower sign, which is the anterior shadowing of the urethra and verumontanum.

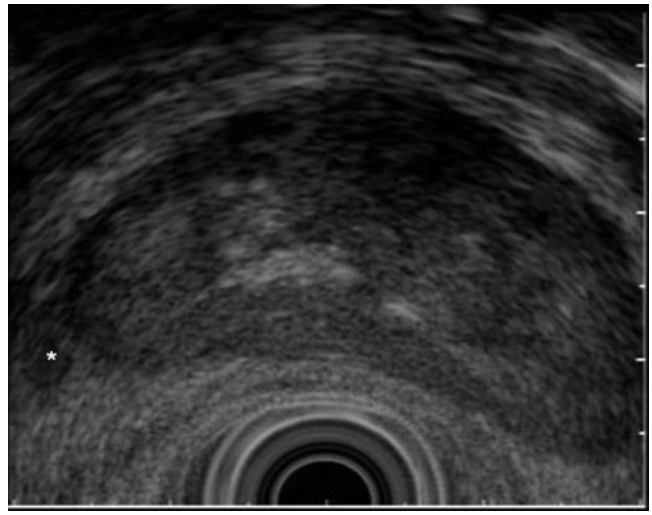

Figure 17.5 Prostate cancer. Radial image demonstrating hyperechoic spots in the left lobe that it appeared after surgery for a T1 adenocarcinoma. Periprostatic node (*).

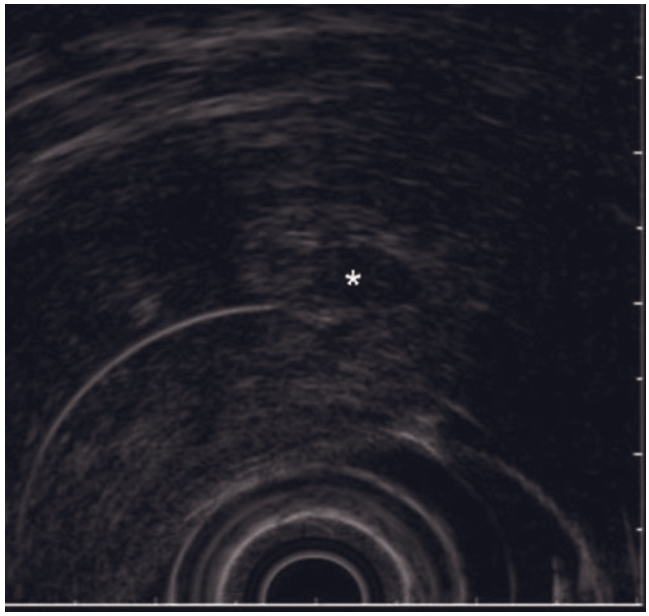

(a)

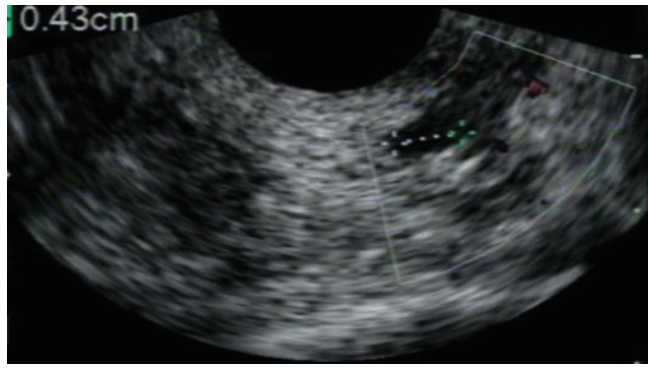

(b)

Figure 17.6 Prostate cancer. Radial (a) and linear (b) image demonstrating a T2A adenocarcinoma.

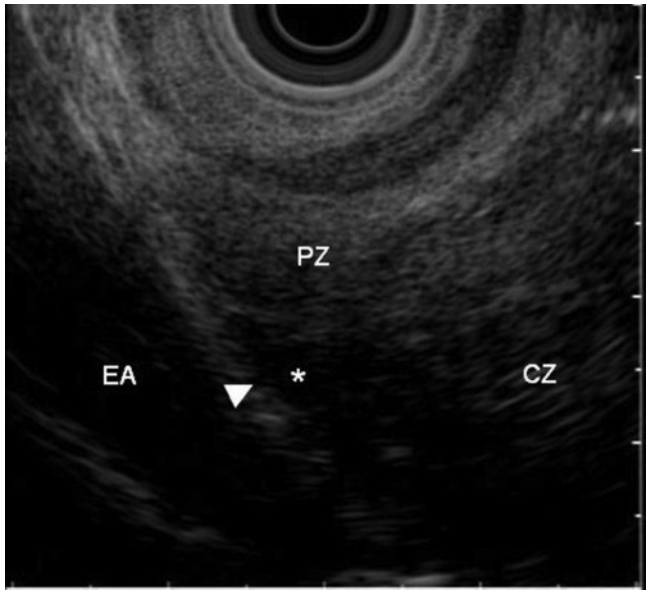

Figure 17.7 Prostate cancer. Radial image demonstrating a adenocarcinoma (T2B). EA = elevator anus; CZ = center zone; PZ = peripheral zone.

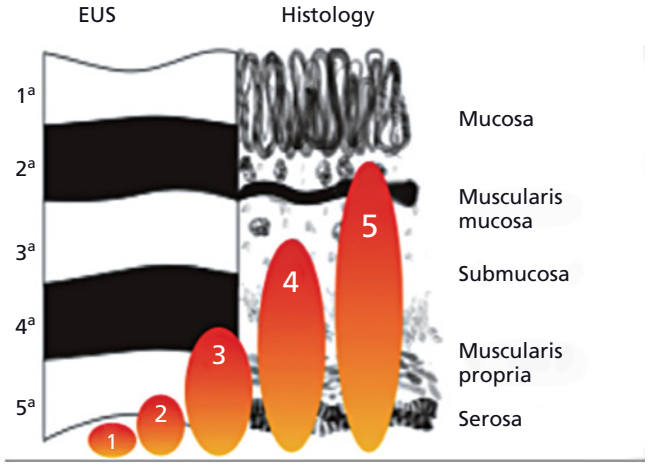

(a)

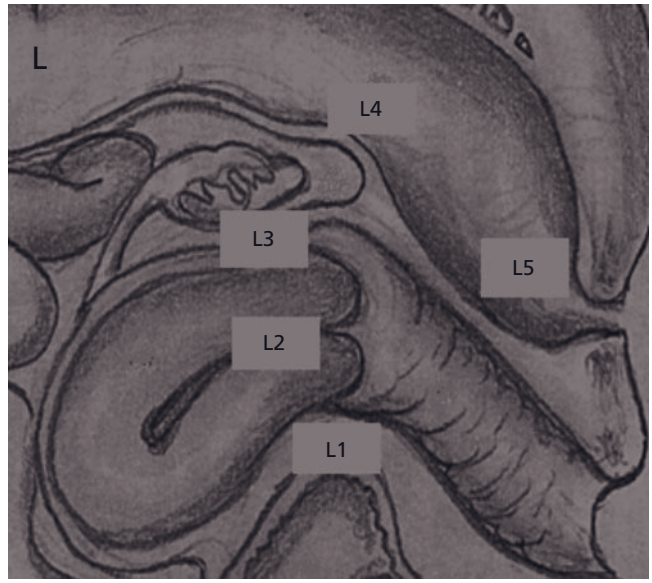

(b)

Figure 17.8 (a & b) Classification of intestinal endometriosis according to Rossini and Ribeiro, 2002. This classification is based on endometriosis involvement of the intestinal wall as noted by endoscopic ultrasound (ueT1–ueT5) and also its location in the pelvis (ueL1–ueL5) (u = ultrasound; e = endometriosis classification; L = location; T = tumor).

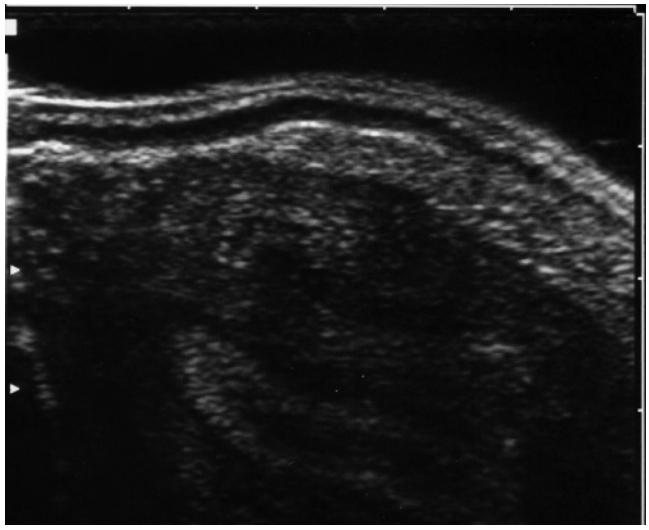

Figure 17.9 Normal anatomy of the intestinal wall (five layers) and uterus, as imaged with a rectal sector probe.

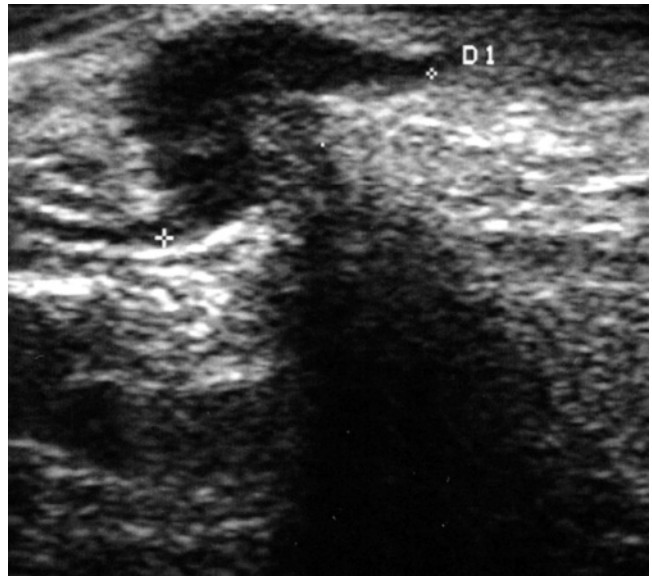

Figure 17.10 Intestinal endometriosis ueT4L3. A heterogenous hypoechoic lesion is noted, with involvement of the serosa and muscularis propria, and with sawtooth involvement of the submucosa (ueT4). The lesion resembles a mushroom, with its stalk (a bit more echogenic) connected to the posterior uterine wall (ueL3), what characterizes the presence of retrouterine block (u = ultrasound; e = endometriosis classification; L = location; T = tumor).

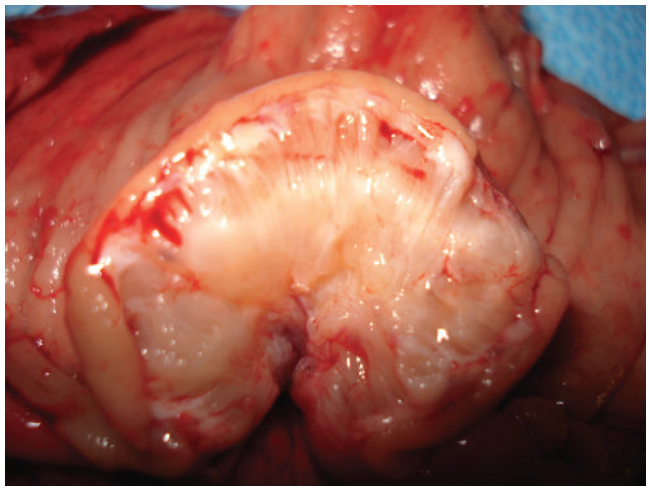

Figure 17.11 Surgical specimen of a focus of intestinal endometriosis, reaching the submucosal layer.

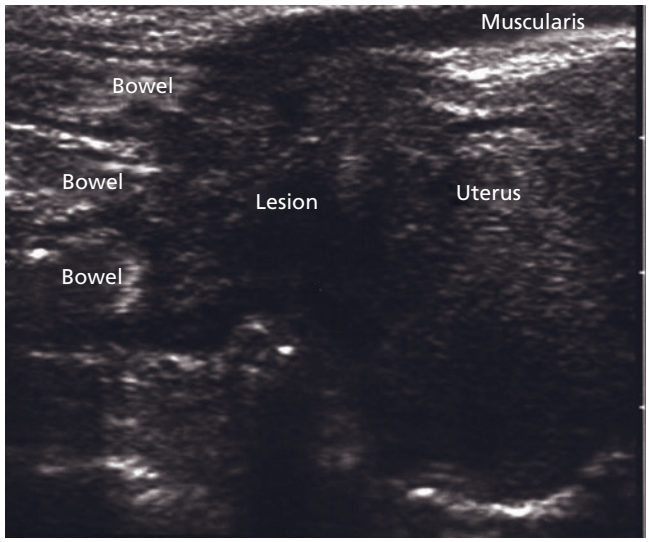

Figure 17.12 Intestinal endometriosis ueT4L3. A large heterogeneous hypoechoic lesion is seen here. The lesion is attached to the uterus and to several loops of bowel in the pelvis.

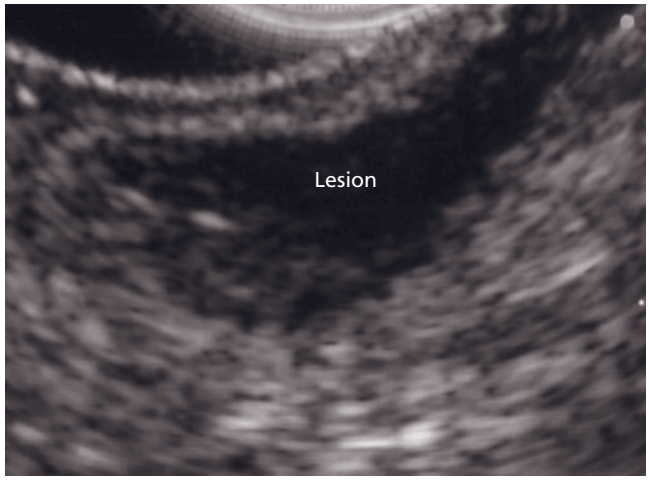

Figure 17.13 Intestinal endometriosis ueT3L3. An heterogeneous hypoechoic lesion is noted, with involvement of the serosa and muscularis propria of the intestinal wall (u = ultrasound; e = endometriosis classification; L = location; T = tumor).

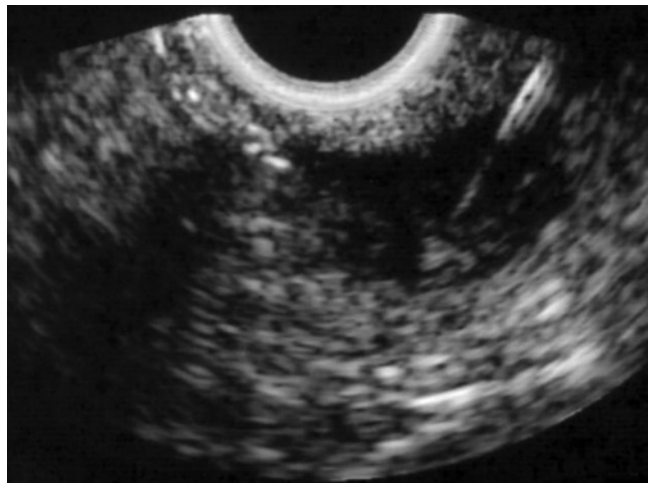

Figure 17.14 Endoscopic ultrasound-guided fine needle aspiration (FNA) of an intestinal endometriosis lesion.

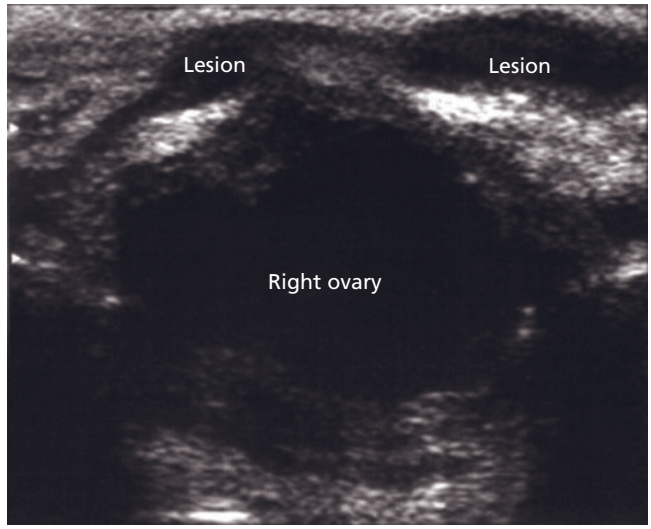

Figure 17.15 Intestinal endometriosis ueT3. Bilobed lesion adherent to the right ovary, with a cystic space within, suggestive of ovarian endometriosis (diagnosis confirmed by histological examination of the surgical specimen) (u = ultrasound; e = endometriosis classification; L = location; T = tumor).

Figure 17.16 Intestinal endometriosis with involvement of all layers of the bowel wall (ueT5L3). The chronic inflammation and scarring led to retraction of surrounding tissue. The hypoechoic involvement in the muscularis propria can be noted, taking a C shape.

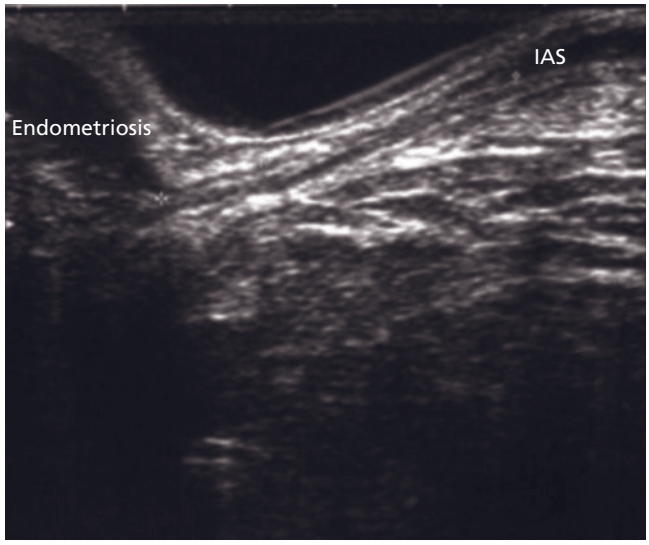

Figure 17.17 Endometriosis in the rectovaginal septum (ueL5). The distance from the endometriosis focus (hypoechoic thickening of the intestinal wall, seen in the left of the image) to the internal anal sphincter (IAS) (hypoechoic layer to the right of the image) is measure in this picture (u = ultrasound; e = endometriosis classification; L = location; T = tumor).

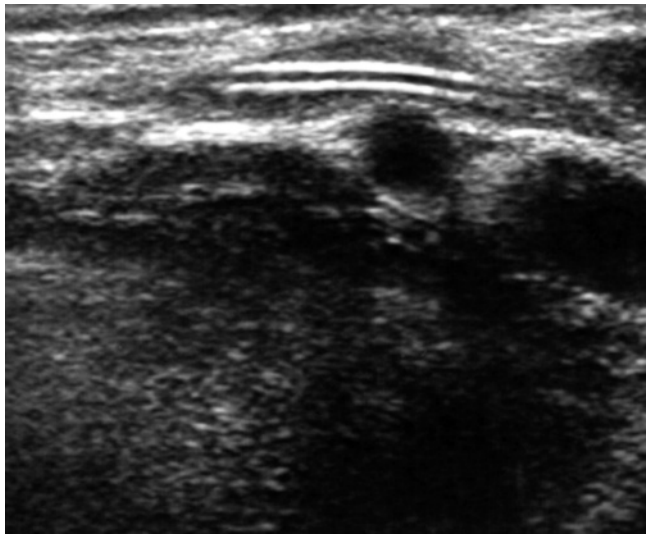

Figure 17.18 Left ureter with internal plastic stent (two parallel hyperechoic lines). The prothesis was inserted in a patient with obstruction of the left ureter due to endometriosis.

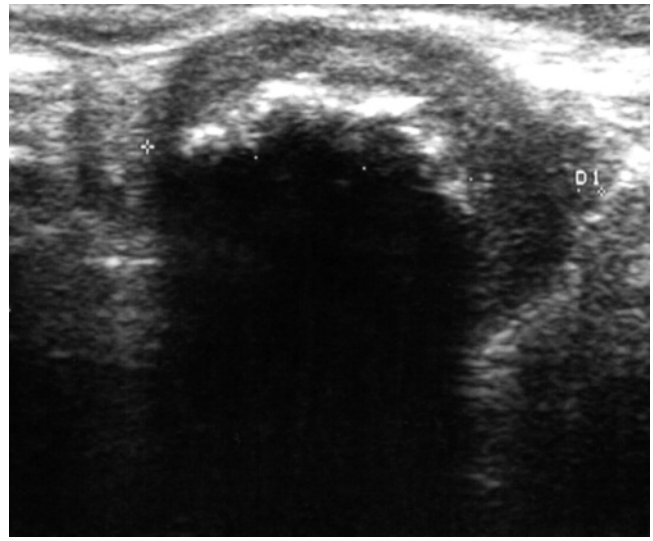

Figure 17.19 Ovarian teratoma with calcification within (note the posterior acoustic shadowing).

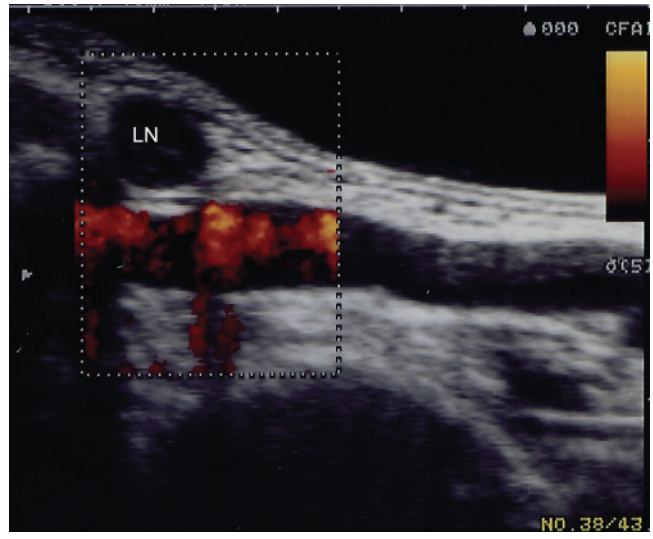

Figure 17.20 Pelvic lymph node. Near the iliac vessels, an oval, well-circumscribed, hypoechoic structure was visualized.

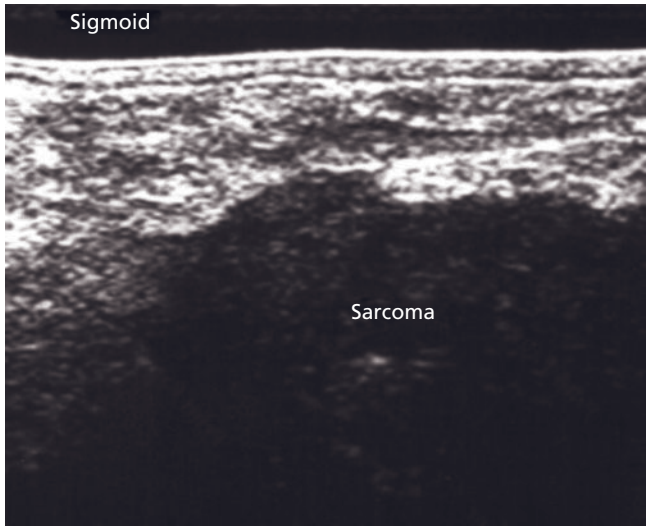

Figure 17.21 Sarcoma. Large hypoechoic lesion in the pelvis, previously noted by computed tomography (CT) scan, in a 67-year-old male with pelvic pain and weight loss. Endoscopic ultrasound-guided fine needle aspiration (FNA) allowed diagnosis of sarcoma.

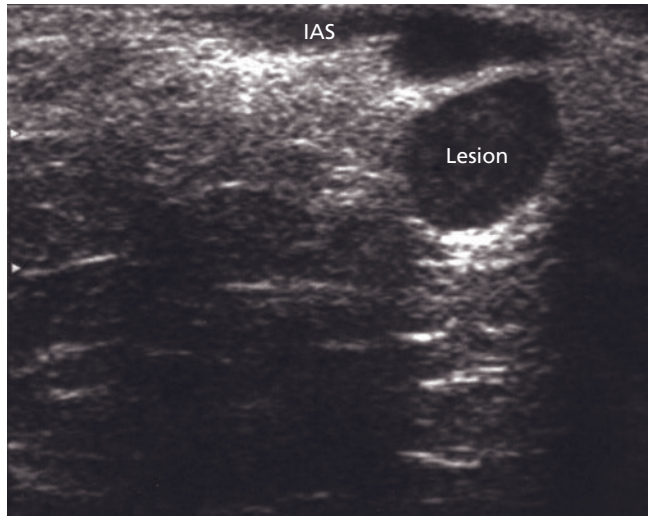

Figure 17.22 Schwannoma. A male patient with history of a schwannoma in the perineal region, which was resected 1 year prior, presented for evaluation of a new perianal nodule. During endoscopic ultrasound examination, an oval, well-circumscribed, hypoechoic lesion (13 mm in greatest diameter) was noted involving the external anal sphincter. Another lesion was noted above the first one, involving the distal portion of the internal sphincter. Both lesions proved to be recurrent schwannoma.

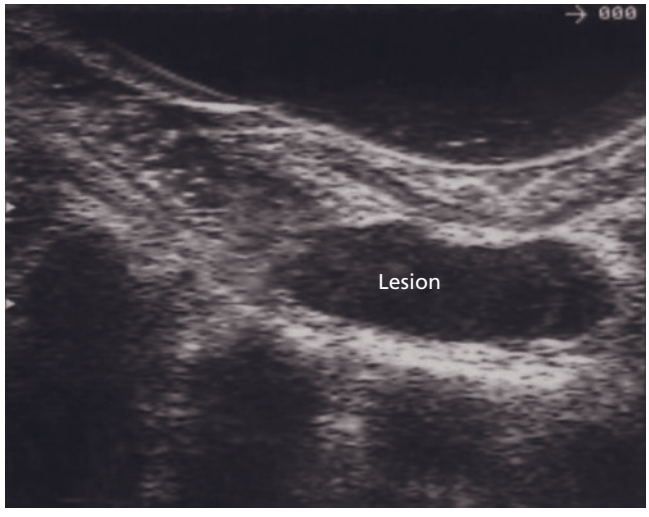

Figure 17.23 Tailgut cyst. A female patient was referred for evaluation of a lesion which was found incidentally during routine gynecological exam. Endoscopic ultrasound revealed an elongated hypoechoic lesion, which measured about 35 mm in greatest diameter. The lesion appeared to be in contact with the sacrum, but not to involve the intestinal wall. Histopathological examination was diagnostic of tailgut. A tailgut is a derivative of the embryonic post-anal gut.

18 Vascular Anomalies and Abnormalities

John C. Deutsch
Essentia Health Care Systems, Duluth, MN, USA

Introduction

Vascular anomalies are often encountered incidentally during an endoscopic ultrasound (EUS) examination. They are frequently ignored as inconsequential (as in the case of atherosclerosis or calcification of the aorta). However, some vascular processes may be responsible for the symptoms which lead to the EUS examination. For example, one may find vascular occlusion of the superior mesenteric artery and celiac artery in a patient with and abdominal pain, or splenic vein thrombosis in a patient with gastrointestinal (GI) hemorrhage ultimately due to isolated bleeding gastric varices. Dysphagia can be causes by aortic arch anomalies ("dysphagia lusoria"). Sometimes an unexpected vascular finding can preclude the original reason for the EUS examination as shown in a case below in which an aortic pseudoaneurysm was identified during an EUS evaluation of early gastric cancer.

This chapter contains images collected during EUS examinations showing a variety of vascular abnormalities that varied from the trivial to important, both symptomatic and asymptomatic. This is not intended to be comprehensive, since there are an unlimited number of conditions which could be described. Rather, this chapter will hopefully help the endosonographer to pay attention to normal and potentially abnormal vascular anatomy, since these features may be pivotal in understanding a patient's condition.

Aortic arch anomalies

Potentially symptomatic aortic arch anomalies are relatively uncommon and occur in a small proportion (1 : 500) of the population. Those which can be easily identified during routine EUS examination include the aberrant right common carotid artery arising directly from the aortic arch. The right subclavian artery (R SCA) arises from the arch distal to the left subclavian artery. The R SCA passes posteriorly to the trachea and esophagus. A right-sided aortic arch can also occasionally be found.

These congenital anomalies can cause swallowing problems (dysphagia lusoria). If the difficulties are severe, one can transect the artery which passes between the esophagus and the vertebrae and reimplant it. After this type of surgery a residual stump can sometimes be identified. Video 18.1 shows an example of an anomalous right subclavian artery. Video 18.2 shows a different patient in whom an anomalous right subclavian artery had been resected and reimplanted. Video 18.3 shows a right-sided aortic arch with a vascular ring formed by an aberrant left subclavian artery, and Video 18.4 shows a different patient with the same features following surgical repair of the vascular ring. As shown in the videos, the aorta is in the right chest (to the left of the vertebrae on the image screen) through its length. At the level of the arch, the left subclavian stump can be seen. An ectatic aorta can sometimes suggest a right-sided aorta (with the aorta in the right chest relative to the vertebrae, but this can usually be sorted out by tracing the aorta for its entire length as in Video 18.5. If the image screen on a radial array instrument is inadvertently flipped, one can also be fooled into thinking structures are on the opposite side of the chest.

There are many different variants (such as double aortic arch) and branching patterns such as the bovine arch. Details concerning these varieties are available on the internet.

Vascular calcification and plaques

These features are extremely common, although the extent of disease varies. Calcification can be seen in any of the

Atlas of Endoscopic Ultrasonography, First Edition. Edited by Frank G. Gress, Thomas J. Savides, Brenna Casey Bounds, John C. Deutsch.

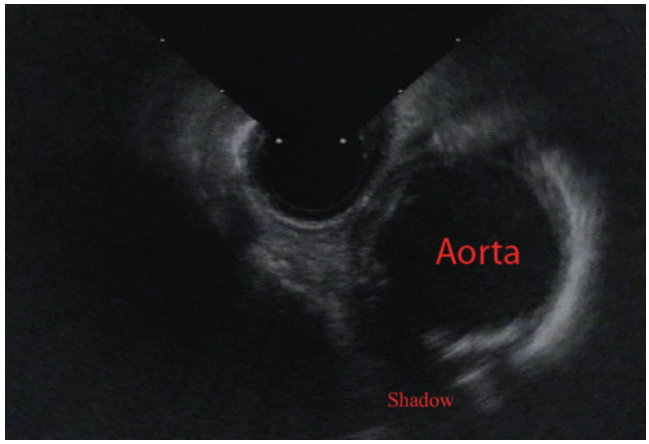

Figure 18.1 A radial array endoscopic ultrasound (EUS) image of a calcific aortic plaque. The area behind the plaque is shadowed out.

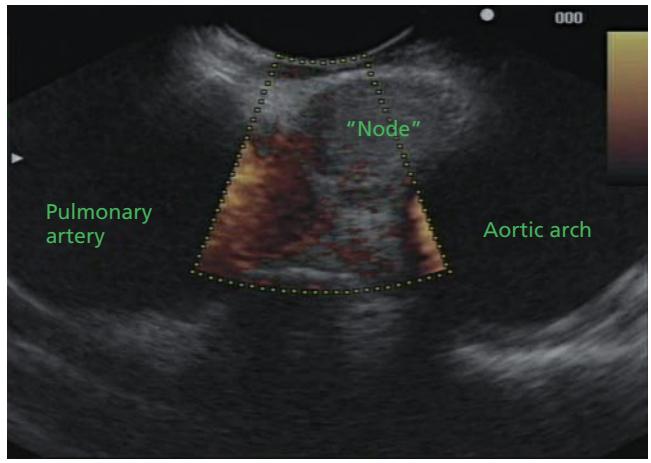

Figure 18.2 A linear array image of the aortopulmonary window with an isoechoic mass that was demonstrated on the video to be a pseudoaneurysm.

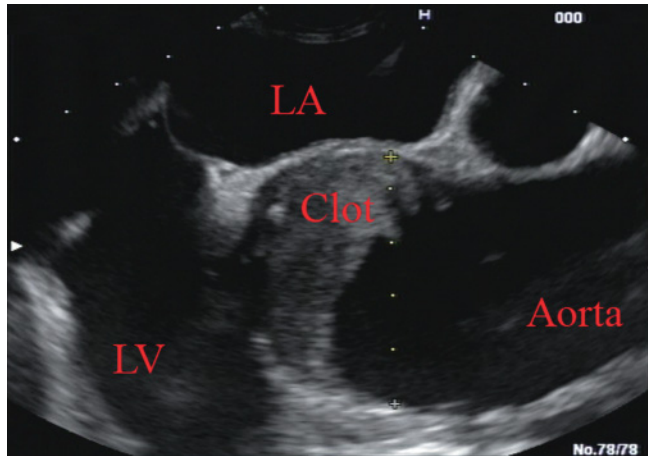

Figure 18.3 A linear array image showing the aortic root with clot due to an unsuspected aortic dissection (LA = left atrium; LV = left ventricle).

arterial structures (Video 18.6). It is usually without symptoms. The echo signal coming off the calcified structures are very bright with acoustic shadowing behind. The shadowing can interfere with visualization of perivascular structures and complicate fine needle aspiration (FNA) of small lesions. The vascular calcifications can sometimes lead to diagnostic confusion (Figure 18.1). Video 18.7 shows the computed tomography (CT) scan of a patient referred to our center for abdominal pain and chronic pancreatitis of unknown cause. Endoscopic ultrasound clearly showed that all calcifications were associated with an artery and that the pancreatic parenchyma was normal. On careful review of the CT scan, this patient appeared to have had a very redundant splenic artery and an accessory splenic artery which was the source of the abnormality seen on CT scan. The abdominal pain appeared to be unrelated to either the pancreas or the calcifications.

However, vascular calcifications can sometimes be the cause of symptoms. The patient shown in Video 18.8 was referred in for marked weight loss and abdominal pain suspected to be chronic pancreatitis. Esophagogastroduodenoscopy (EGD) showed what appeared to be an ischemic stomach. Endoscopic ultrasound showed a normal pancreas but obliteration of the celiac and superior mesenteric artery origins by a calcified plaque. This patient underwent urgent revascularization which corrected her pain and helped her weight return towards baseline. Plaques are not always fixed to the vessel wall. Video 18.9 shows that plaques can sometimes be noncalcified and hypermobile, suggesting a risk of embolism.

Aneurysms and pseudoaneurysms

An aneurysm is expansion of a vessel and all layers of the vascular wall. A pseudoaneurysm occurs when there is disruption of the vascular wall. These features can be subtle. Figure 18.2 and Video 18.10 shows the area near the aortopulmonary window in a person undergoing EUS. This appears to be a pathologically enlarged lymph node. Further evaluation demonstrates this to be a pseudoaneurysm. A dramatic example of an apparent aortic pseudoaneurysm is shown in Video 18.11. This was found during evaluation of an early gastric cancer and took precedence over the evaluation of the tumor. Figure 18.3 shows an example of an aortic root dissection that was first discovered during EUS for abdominal adenopathy suspected to be due to metastatic colon cancer.

Dilation of smaller arteries is more subtle. Video 18.12 was taken from a patient in whom an outside endoscopist found a subepithelial mass and in which "the biopsies were normal". Endoscopic ultrasound revealed a small splenic artery aneurysm. Video 18.13 shows an asymptomatic celiac

artery aneurysm. In addition to degenerative atherosclerotic vascular disease, inflammatory disease such as pancreatitis can cause vascular injury as demonstrated in a patient in whom a splenic artery pseudoaneurysm was found during an exam after a resolved attack of acute pancreatitis. Video 18.14 shows a splenic artery pseudoaneurysm which arose after a bout of gallstone pancreatitis. The vessel was subsequently stented due to risk of hemorrhage.

Venous thrombosis

Thrombosis of the portal vein and its branches are the probably the most common site for endosonographers to detect venous thrombosis. It can occur in patient with portal hypertension as shown in Figure 18.4 and Video 18.15 of a patient undergoing EUS who had cirrhosis from autoimmune liver disease. Splenic vein thrombosis can lead to isolated gastric varices. Video 18.16 shows an endoscopy from a patient referred in for recurrent GI bleeding suspected to be variceal. The endoscopy shows a normal esophagus and possible gastric varicies which were confirmed during EUS. Careful evaluation of the splenic vein revealed venous obstruction from a cystic pancreatic neoplasm near the splenic hilum.

Dieulafoy lesions

Dieulafoy lesions consist of arteries that are ectopically located in the submucosa. These can rupture and cause significant blood loss, but when they are not bleeding they can be very difficult to identify. Endoscopic ultrasound can be used to help identify Dieulafoy lesions as in this case (Video 18.17) in which a pulsatile lesion was seen in the rectal vault.

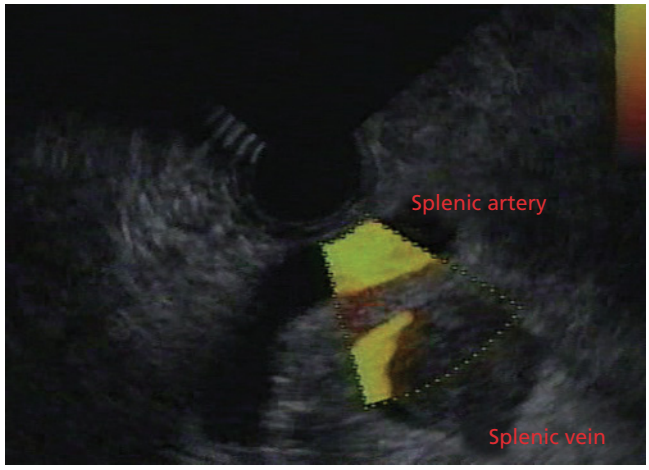

Figure 18.4 Radial array Doppler image of a clot in the splenic vein.

Neoplasms

Neoplastic tumors can extend into blood vessels and can take on the appearance of thrombus. Although rare, there are neoplastic lesions which can arise in the vascular tree and can sometimes be a source of emboli or obstruction. The most common is probably the atrial myxoma but other lesions include leiomyosarcomas and endothelial tumors. An example of a left atrial myxoma is shown in Video 18.18. Figure 18.5 shows an atrial myocardiac metastasis from breast cancer. Figure 18.6 shows a large rhabdomyosarcoma which has infiltrated into the left atrium.

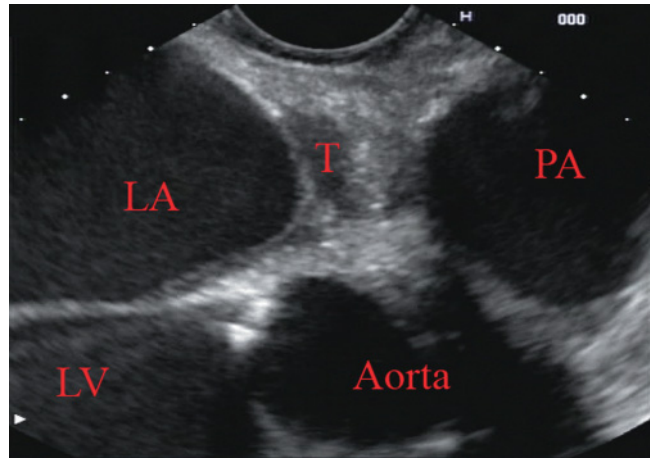

Figure 18.5 A linear array image of a metastasis (T) from breast cancer to the left atrial myocardium. (LA = left atrium; LV = left ventricle; PA = pulmonary artery).

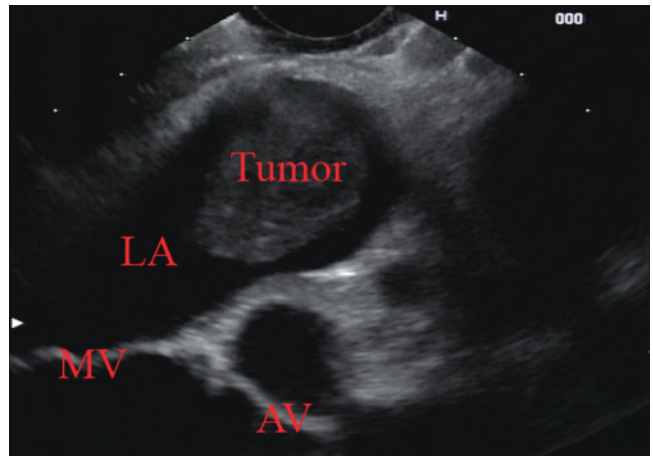

Figure 18.6 A linear array image of a rhabdomyosarcoma infiltrating into the left atrium (LA). The mitral valve (MV) and aortic valve (AV) are shown.

Miscellaneous aberrancies

Arteries can be abnormally long and tortuous resulting in abnormal EUS imaging. An example is shown in Video 18.19 in which a redundant loop of splenic artery is seen. During EUS, the stomach can actually be pushed into the loop resulting in images of the splenic artery surrounding the stomach.

Chapter video clips

Video 18.1 Anomalous right subclavian artery off of left sided aortic arch creating a vascular ring around the esophagus.

Video 18.2 Anomalous right subclavian artery stump created by surgical transaction of anomalous right subclavian artery off of left sided aortic arch.

Video 18.3 Anomalous left subclavian artery off of right sided aortic arch creating a vascular ring around the esophagus.

Video 18.4 Anomalous left subclavian artery stump created by surgical transaction of anomalous left subclavian artery off of right-sided aortic arch.

Video 18.5 Tortuous aorta that is on the right side in the lower chest but crosses midline to the normal left-sided position at the aortic arch.

Video 18.6 Vascular calcification of the brachiocephalic artery and aorta.

Video 18.7 Vascular calcification of anomalous splenic artery that suggested chronic pancreatitis by CT imaging.

Video 18.8 Vascular calcific of celiac and superior mesenteric arteries in setting of gastric ischemia.

Video 18.9 Mobile atheroma.

Video 18.10 Aortic arch pseudoaneurysm that looks like AP window node.

Video 18.11 Aortic pseudoaneurysm.

Video 18.12 Splenic artery bulging into stomach suggestion a subepithelial mass.

Video 18.13 Celiac artery aneurysm.

Video 18.14 Splenic artery pseudoaneurysm.

Video 18.15 Splenic vein thrombosis.

Video 18.16 Splenic vein thrombosis.

Video 18.17 Rectal Dieulafoy lesion.

Video 18.18 Atrial myxoma.

Video 18.19 Tortuous splenic artery creating a loop encircling the stomach.

3 Pancreatico-biliary

19 Duodenal and Ampullary Neoplasia

Brenna Casey Bounds
Massachusetts General Hospital and Harvard Medical School, Boston, MA, USA

German anatomist Abraham Vater (1684–1751) first described a tubular structure which consists of the confluence of the distal common bile duct and main pancreatic duct in the second portion of the duodenum. This convergence is now known as the ampulla of Vater. In about 85% of individuals the pancreatic duct and common bile duct join in the ampulla and form a distal common channel. The normal ampulla starts about 2 mm outside the duodenal wall and penetrates the muscularis propria somewhat more distally, forming an intraduodenal segment 9–25 mm in length.

Tumors of the ampulla of Vater originate from the pancreaticobiliary–duodenal junction, limited by the sphincter of Oddi. Ampullary tumors may present with obstructive jaundice, duodenal obstruction, bleeding, or they may be discovered as an incidental finding at the time of upper gastrointestinal endoscopy or barium radiography for unrelated symptoms. While the presenting symptoms may be very similar to those of pancreatic carcinoma, ampullary malignancies have a much better prognosis. Their evolution appears to follow the adenoma–carcinoma sequence and they are usually discovered at an earlier stage than pancreatic tumors. Ampullary tumors are generally undetectable on transabdominal ultrasound, magnetic resonance imaging (MRI), and computed tomography (CT) scanning due to their small size. Endoscopically they present as polypoid exaggerations of the ampulla. Endoscopic ultrasonography (EUS) provides high resolution images and permits positioning of the ultrasound transducer in close approximation to the tumor in the duodenum. Endoscopic ultrasonography is specifically useful for T- and N-staging, which is important in determining the method of resection and ultimately the prognosis of patients with ampullary carcinomas (Figures 19.1 and 19.2).

Endoscopic ultrasound imaging of ampullary neoplasia is achieved by positioning the echoendoscope directly adjacent to the ampulla itself. Acoustic coupling is aided by a synergy created by positioning the water-filled balloon adjacent to the lesion while water is slowly (to avoid formation of bubbles which will obscure the detail of the images) instilled into the lumen of the duodenum. Particularly in small tumors, it is essential to avoid overfilling the balloon, as the ampullary lesion may be easily compressed by the balloon resulting in impaired visualization or in some cases overlooking the lesion completely. On the other hand, overfilling of the balloon can compress the tumor and underlying wall layers together leading to artifact and misinterpretation resulting in overstaging. The patient is usually in the left lateral position, but in some cases a supine position or right lateral decubitus may improve imaging success especially when the lesions are very small making a stable imaging position challenging. Tumors of the ampulla present as localized wall thickening of the duodenum at the level of the ampulla. The dilated distal common bile duct can be traced into the tumor and neoplastic growth may be seen in the dilated lumen. Smaller tumors are usually echo-homogenous and echo-poor; inhomogeneous internal echoes occur more frequently with increasing tumor size. An adenoma of the ampulla does not involve the duodenal wall layers whereas a more advanced carcinoma infiltrates the duodenal wall layers or the pancreas. Differentiation of a T1 carcinoma (limited to the ampulla) from an adenoma is not possible by means of EUS.

Tumors of the periampullary regions may be either exophytic polypoid or hypoechoic mass lesions in the area of the ampulla that may be indistinguishable from distal pancreatic carcinomas. Although biopsies of the polypoid lesions may only show adenomatous tissue, frequently a small focus of malignancy is present. Endoscopic ultrasound is not capable of differentiating a small focus of malignancy within an otherwise benign adenoma. Only in the case of deep infiltrative growth can the endosonographer discern the presence of a malignancy. A recent sphincterotomy and the resulting inflammatory response to the thermal injury may create artifacts which mimic pseudopodia signifying

Atlas of Endoscopic Ultrasonography, First Edition. Edited by Frank G. Gress, Thomas J. Savides, Brenna Casey Bounds, John C. Deutsch.

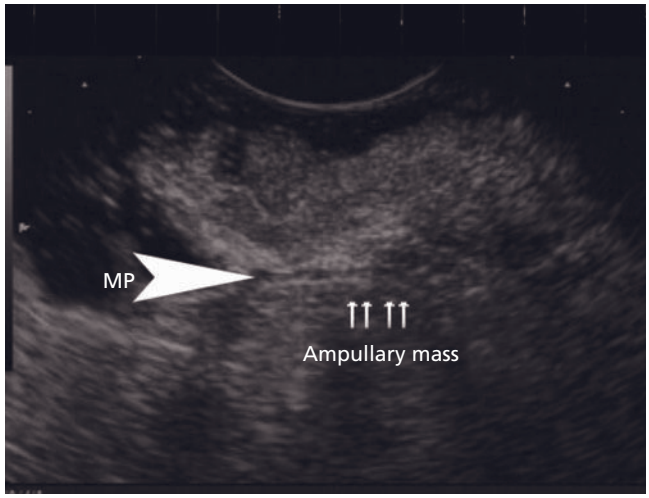

Figure 19.1 The linear array echoendoscope is in the duodenum directly adjacent to the ampulla. There is a large, exophytic, hypoechoic ampullary mass infiltrating the duodenal wall and filling the lumen. The lesion does not penetrate through the muscularis propria (MP, arrowhead).

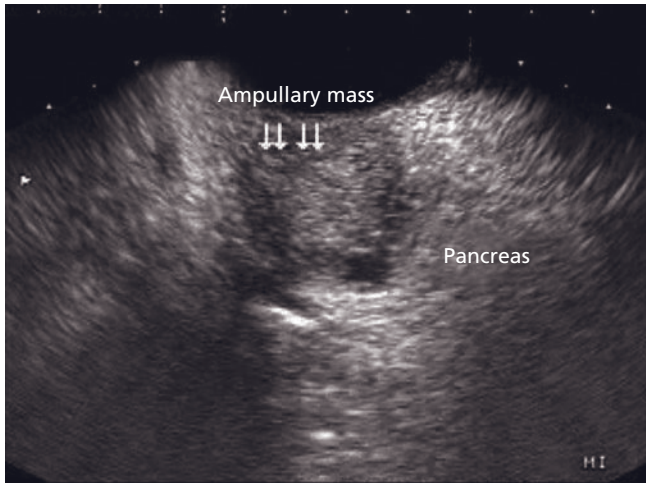

Figure 19.2 A hypoechoic mass is seen here arising from the ampulla. The malignancy is invading through the duodenal wall, surrounding the bile duct and into the pancreas, which makes this lesion a stage T3 ampullary cancer.

inifiltrative growth. Endoscopic ultrasound cannot replace histology and should be used to stage ampullary lesions of known histological status. For villous adenomas of the ampulla of Vater, extension of the villous tissue into the common bile duct can occasionally be seen.

Staging according to the TNM system is as follows:

TX: Primary tumor cannot be assessed
T0: No evidence of primary tumor
T1: Tumor 1 cm or less (tumor limited to ampulla of Vater for ampullary gangliocytic paraganglioma)
T2: Tumor >1 cm
T3: Tumor invades pancreas or retroperitoneum or into non-peritonealized tissues
T4: Tumor invades visceral peritoneum (serosa) or invades other organs

Metastatic lymph nodes are classified using the same uniformly accepted criteria (size or echo pattern).

Accurate local staging is important in centers where endoscopic ampullectomy is performed. However, in most cases local staging does not alter management, as the lesion is removed during a pancreaticoduodenectomy (Whipple procedure). Endoscopic ultrasound detects small ampullary neoplasms when other imaging modalities reveal biliary or pancreatic ductal dilatation in the absence of a detectable mass. It also permits identification of infiltration through the duodenal muscularis propria and invasion into the pancreatic parenchyma. The accuracy of EUS in assessing the depth of tumor invasion and in detecting local lymph node metastases has been reported to be better than 80% for T-stage and 70% for N-stage. Overstaging in stage T1 occurs in up to one-third of cases and depends greatly on operator technique. However, infiltration into the pancreas, which is associated with a poorer prognosis, is detected in nearly 90% of cases using EUS. From a surgical standpoint carcinoma of the ampulla can nearly always be resected unless it infiltrates the peripancreatic vessels, in which case a pancreatic primary infiltrating the ampulla should be considered. Other imaging modalities such at CT, abdominal ultrasound, and MRI, while not useful for T-staging of ampullary carcinoma, are necessary adjuncts for complete N-staging and M-staging prior to surgery and/or initiation of chemotherapy/radiation therapy. Intraductal ultrasound probes are useful for assessing tumor extension into the distal common bile duct in villous or papillary type lesions prior to consideration for endoscopic resection, particularly in those cases in which the limits of the lesion are not clear on cholangiography. Care must be taken to avoid excessive pressure with the duodenoscope elevator on the intraductal ultrasound (IDUS) probe, as well as attention to the acute bend that is formed when the probe leaves the working channel of the duodenoscope and entrance of the bile duct which may lead to poor imaging quality as well as probe breakage.

For elderly patients with locally advanced disease who are not good surgical candidates, palliation of obstructive symptoms may be provided by debulking of the lesion, endoscopic sphincterotomy, and biliary stent placement.

Chapter video clips

Video 19.1 An exophytic ampullary mass is seen on endoscopy and biopsies are obtained for histology which reveal an ampullary adenoma.

20 Biliary Tract Pathology

Brenna Casey Bounds
Massachusetts General Hospital and Harvard Medical School, Boston, MA, USA

Cancer arising in the extrahepatic bile duct is curable by surgery in fewer than 10% of all cases. Prognosis depends in part on the tumor's anatomic location, which determines resectability. Complete resection is possible in 25–30% of lesions that originate in the distal bile duct, whereas the resection rate is much poorer for more proximal sites. Risk factors for bile duct malignancy include a history of primary sclerosing cholangitis, choledochal cysts, or infections with *Clonorchis sinensis*. Patients may present with jaundice, pain, fever, and pruritus.

Endoscopic ultrasonography (EUS) is an invaluable tool for the evaluation of the biliary tract. The close proximity of the echoendoscope transducer to the extrahepatic biliary tree, the lack of radiation, and the low risk of complications makes it an excellent method for examining the common bile duct. The extrahepatic ductal system can be visualized completely by EUS in 96% of patients. The role of EUS in the evaluation of the biliary tract includes biliary obstruction, suspected choledocholithiasis, indeterminate biliary strictures, idiopathic pancreatitis, unexplained right upper quadrant pain, and mass lesions within and adjacent to the biliary tree (Figures 20.1–20.4). Endoscopic ultrasound plays a key role in T-staging of extrahepatic biliary tumors.

TNM staging is as follows:

Primary tumor (T):

TX: Primary tumor cannot be assessed
T0: No evidence of primary tumor
Tis: Carcinoma in situ
T1: Tumor confined to the bile duct histologically
T2: Tumor invades beyond the wall of the bile duct
T3: Tumor invades the liver, gallbladder, pancreas, and/or unilateral branches of the portal vein (right or left) or hepatic artery (right or left)
T4: Tumor invades any of the following: main portal vein or its branches bilaterally, common hepatic artery, or other adjacent structures, such as the colon, stomach, duodenum, or abdominal wall

Regional lymph nodes (N):

NX: Regional lymph nodes cannot be assessed
N0: No regional lymph node metastasis
N1: Regional lymph node metastasis

Distant metastasis (M):

MX: Distant metastasis cannot be assessed
M0: No distant metastasis
M1: Distant metastasis

Differentiating between benign and malignant biliary strictures can be challenging as up to 24% of patients with presumed hilar cholangiocarcinoma are found to have benign disease. Cholangiocarcinoma appears as a round hypoechoic lesion which may arise from a focal point on the bile duct wall or surround the duct wall circumferentially. Endoscopic ultrasound imaging alone is not capable of differentiating inflammatory lesions in the bile duct wall from malignancy and therefore tissue sampling is necessary. Fine needle aspiration cytology may be obtained under EUS guidance using linear array endosonography. In the setting of known malignancy, important staging imaging obtained via EUS should include evaluation of the portal venous system for evidence of tumor invasion.

Intraductal ultrasound (IDUS) is useful in the detection and evaluation of small biliary tumors. Indicators suggestive of malignancy with IDUS include irregular wall thickening, a hypoechoic mass, a papillary projection, disruption of the normal three-layer wall structure of the bile duct. IDUS is ideally suited for imaging of the proximal biliary tree and facilitates imaging of the right hepatic artery, portal vein, and the hepatic duodenal ligament. It has been shown to improve the accuracy of biliary brushings by directing tissue sampling. Limited depth of imaging with IDUS renders it inappropriate for lymph node staging.

Endoscopic ultrasound has emerged as a sensitive and specific precursor to endoscopic retrograde cholangiopancreatography (ERCP) for the detection of bile duct stones, and it is more sensitive for the detection of stones

Atlas of Endoscopic Ultrasonography, First Edition. Edited by Frank G. Gress, Thomas J. Savides, Brenna Casey Bounds, John C. Deutsch.

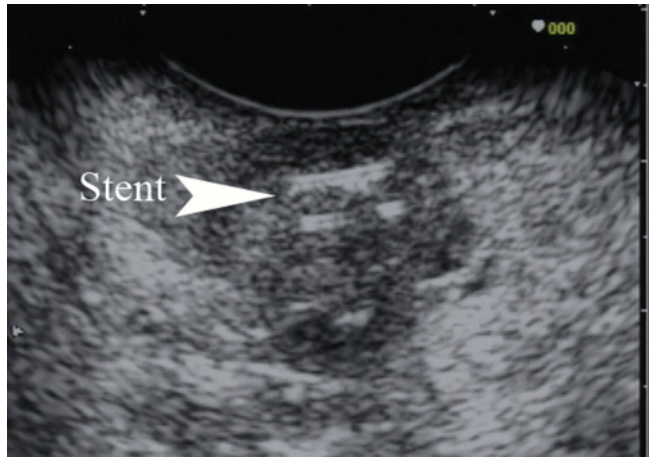

Figure 20.1 In this example of a small bile duct malignancy, a focal hypoechoic mass is seen surrounding the bile duct. A biliary stent is present within the mass.

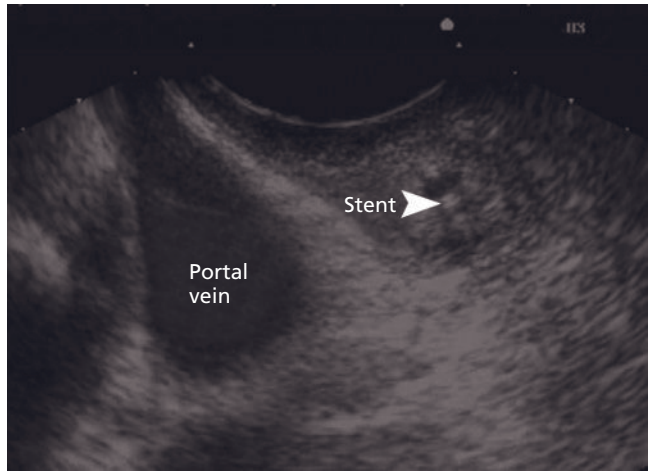

Figure 20.2 The linear array echoendoscope is positioned in the second portion of the duodenum. A hypoechoic mass is seen here within the bile duct surrounding a biliary stent. The portal vein is to the left of the mass and the pancreatic parenchyma can be seen beneath and to the right of the mass.

Figure 20.3 This 78-year-old woman has unresectable pancreatic cancer. Endoscopic ultrasound demonstrates a markedly dilated bile duct containing a large amount of biliary sludge. The patient was treated with biliary stent placement.

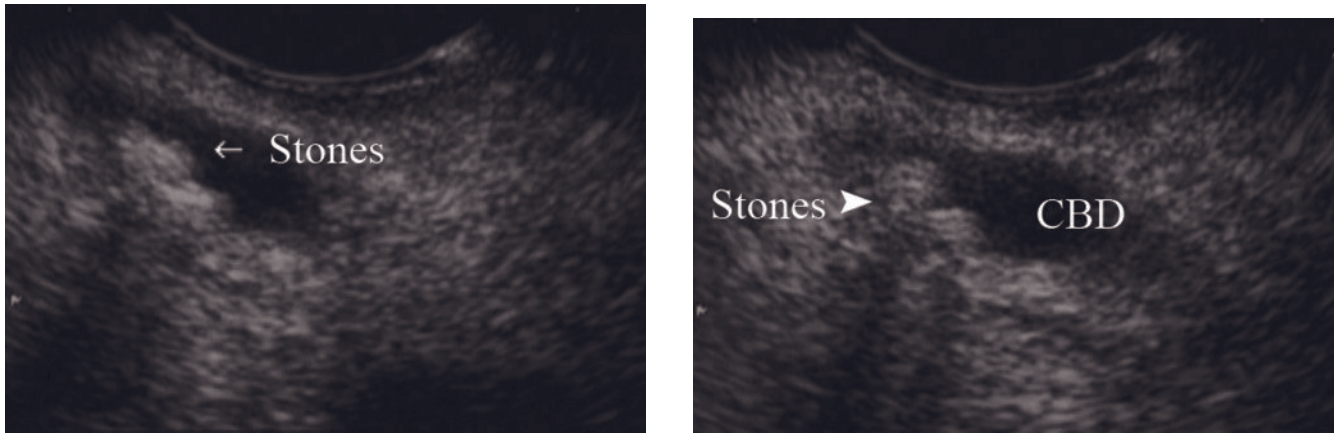

(a) (b)

Figure 20.4 This 46-year-old woman presented with elevated liver function tests and right upper quadrant pain. A magnetic resonance cholangiopancreatography (MRCP) revealed a mildly dilated common bile duct with cholelithiasis but no choledocholithiasis. The surgical service has requested clearance of the common bile duct prior to proceeding to cholecystectomy. Endoscopic ultrasound was performed prior to endoscopic retrograde cholangiopancreatography (ERCP) and two common bile duct stones were revealed (a & b). The patient then underwent therapeutic ERCP with successful stone extraction.

<6 mm than magnetic resonance cholangiopancreatography (MRCP). Choledocholithiasis is easily recognized as curvilinear hyperechoic foci with strong acoustic shadowing using either standard or catheter based EUS. Low amplitude echoes without acoustic shadowing are considered sludge. While ERCP is more accurate for the detection of choledocholithiasis than EUS by a slim margin, it carries significantly higher risk of complications post procedure and is thus no longer desirable as a diagnostic test. Endoscopic ultrasound is a minimally invasive procedure with a procedural risk identical to that of esophagogastroduodenoscopy (EGD). ERCP should be reserved for planned therapeutics. IDUS is useful during ERCP for detecting small stones and sludge that might otherwise go undetected with ERCP alone.

Chapter video clip

Video 20.1 The video demonstrates a cholangiogram which reveals a common bile duct stenosis suspicious for malignancy.

21 Gallbladder Pathology

Sam Yoselevitz and Ann Marie Joyce
Tufts University School of Medicine, Burlington, MA, USA

Introduction

Gallbladder disease is one of the most common gastrointestinal disorders worldwide. It is estimated that there are at least 20.5 million cases of gallbladder disease annually in the United States. Gallbladder pathology encompasses a wide spectrum of disorders including cholelithiasis, cholecystitis, microlithiasis, gallbladder polyps, and carcinoma. Endoscopic ultrasound (EUS) has emerged as a valuable tool in the diagnosis and characterization of gallbladder lesions. EUS is considered to be superior to conventional ultrasound (US) for imaging the gallbladder. With much higher US frequencies, EUS can readily image the structure of the gallbladder and provide high-resolution images of even the smallest of lesions. Clinically, EUS is a useful diagnostic modality for patients who present with suspected gallstone disease despite a normal conventional US. Because EUS can influence clinical management, it is important to understand this technique and to recognize common gallbladder pathology.

Gallbladder stones

Gallstones are the most common biliary pathology. Conventional US is generally considered to be the gold standard for the diagnosis of cholelithiasis, with a sensitivity and specificity of 97% and 95%, respectively. However, multiple studies have demonstrated that EUS is much more sensitive for diagnosing small stones ≤3 mm, particularly in patients who are obese or have other anatomic considerations. In one study of patients with idiopathic pancreatitis by Frossard *et al*., EUS identified cholelithiasis in 30–40% of cases that that had been missed by conventional US.

On EUS, gallstones appear as hyperechoic foci that cast an acoustic shadow and are found in the dependent portion of the gallbladder (Figures 21.1 and 21.2) Two additional clinically significant gallbladder conditions that are frequently described are sludge (Figure 21.3) and microlithiasis (Figure 21.4). These entities are echogenic in appearance but do not cast an acoustic shadow. Sludge also tends to be more viscous and is not necessarily found in the dependent portion of the gallbladder.

Gallbladder polyps

Gallstones must be distinguished from gallbladder polyps, which can have a similar sonographic appearance. Gallbladder polyps represent a heterogeneous group of lesions in the gallbladder, including premalignant adenomas, cholesterol polyps, inflammatory polyps, and adenomyomas. Other lesions of the gallbladder, such as fibromas, lipomas, and leiomyomas are extremely rare. Although most gallbladder polyps are benign, some lesions do have the potential for malignant transformation. Current guidelines suggest that gallbladder polyps >10 mm have a higher incidence of malignancy and should be treated with cholecystectomy. However, recent data has shown that up to 29% of polyps between 5 and 10 mm in size can be premalignant. This underlines the importance of EUS in the proper indentification of these lesions.

Gallbladder polyps appear on EUS as single or multiple echogenic foci protruding into the gallbladder lumen without acoustic shadowing. These polyps do not cause destruction of the normal three-layer pattern of the gallbladder wall (Figures 21.5 and 21.6). Although echogenic patterns are highly variable, neoplastic lesions tend to be more heterogeneous in appearance, while benign lesions such as cholesterol polyps have a more homogeneous echo pattern. In a study by Sugiyama *et al*. in 2000, a total of 194 patients with small gallbladder polyps (<20 mm) underwent both US and EUS. Endoscopic ultrasound correctly predicted the histology in 97% of cases, compared to 76% with conventional

Atlas of Endoscopic Ultrasonography, First Edition. Edited by Frank G. Gress, Thomas J. Savides, Brenna Casey Bounds, John C. Deutsch.

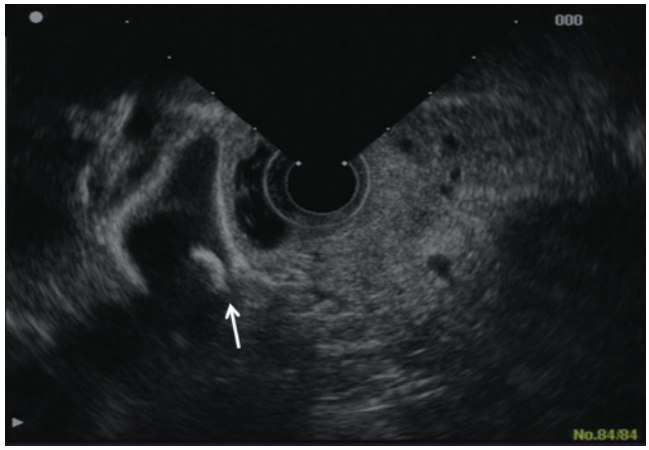

Figure 21.1 Gallbladder stone (arrow) with posterior shadowing.

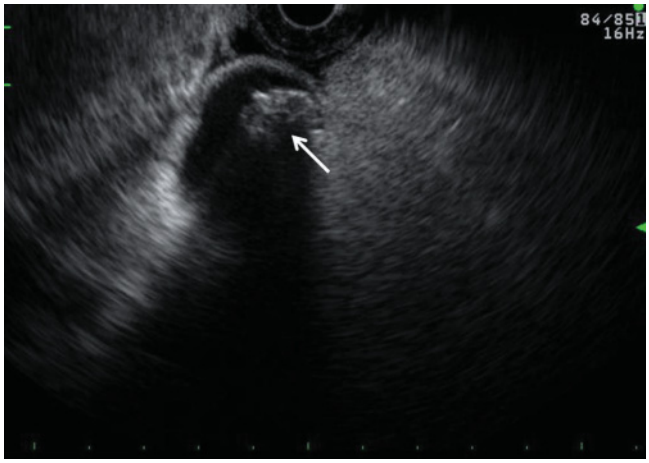

Figure 21.2 Gallbladder stone (arrow) with posterior shadowing.

Figure 21.3 Gallbladder sludge (arrow).

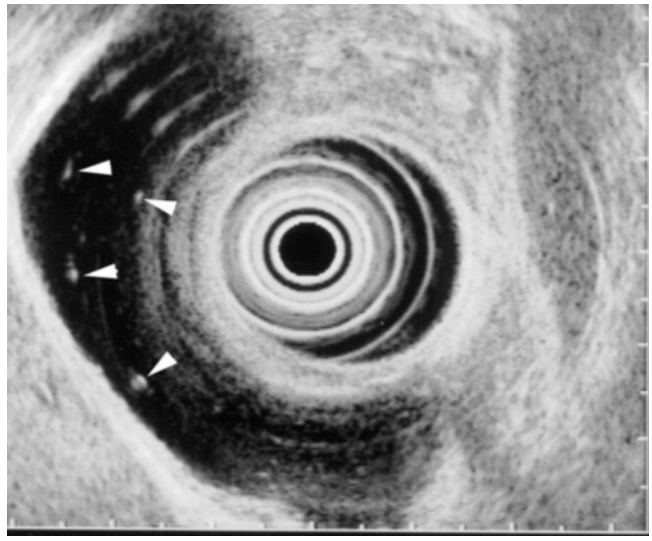

Figure 21.4 Gallbladder microlithiasis (arrows). (Courtesy of Michael L. Kochman, MD.)

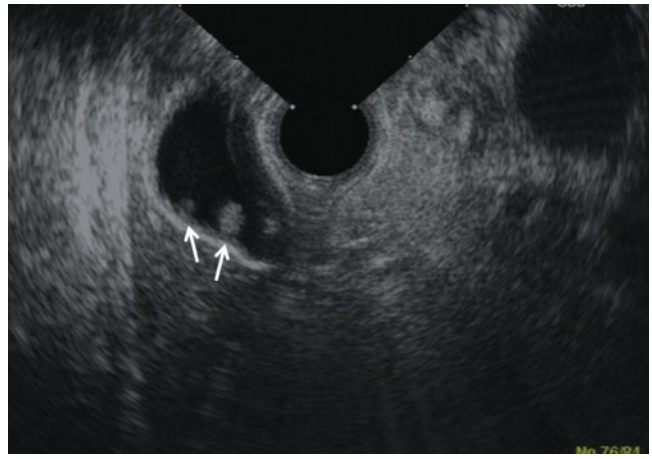

Figure 21.5 Gallbladder polyps (arrows). Notice the lack of shadowing.

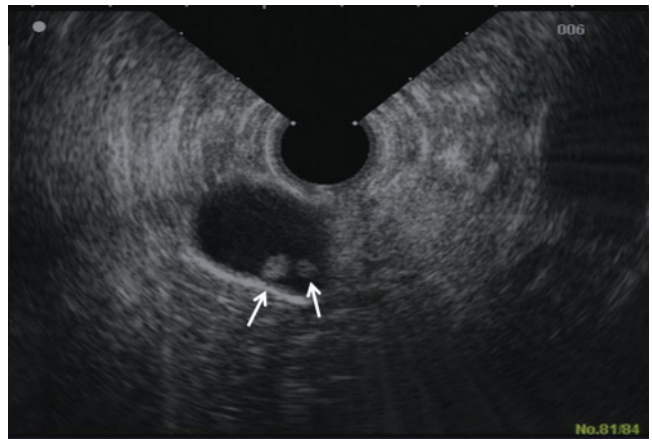

Figure 21.6 Gallbladder polyps (arrows). Notice the lack of shadowing.

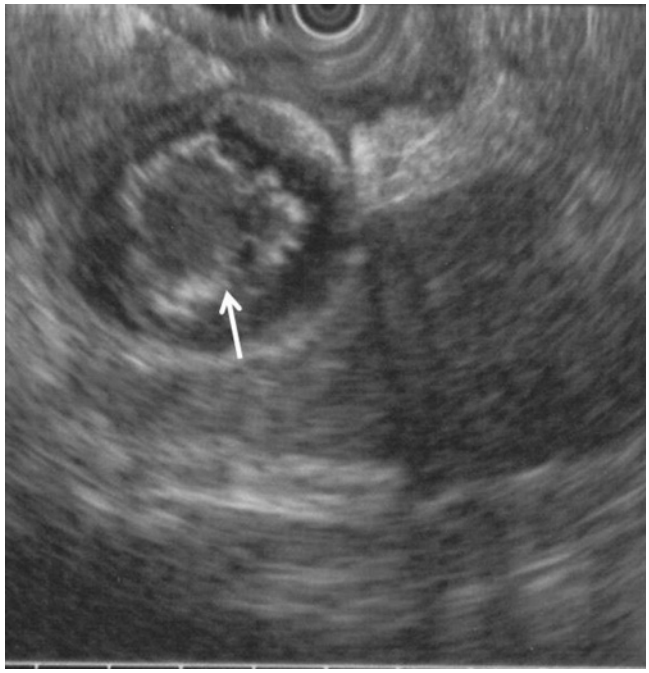

Figure 21.7 Gallbladder carcinoma (arrow).

US. Studies therefore suggest that EUS should be included as part of the standard work-up for gallbladder polyps.

Gallbladder carcinoma

Malignant lesions of the gallbladder are uncommon, yet unfortunately associated with a very poor prognosis. Gallstones and premalignant gallbladder polyps are the strongest risk factors for the development of gallbladder cancer. Endoscopic ultrasound is useful both in the differential diagnosis of gallbladder lesions as well as in staging tumor extent. In a study by Azuma *et al.*, 89 patients with polyps <20 mm underwent both EUS and conventional US. The sensitivity and specificity for the diagnosis of gallbladder cancer were 92% and 88% respectively with EUS, compared to 54% with US.

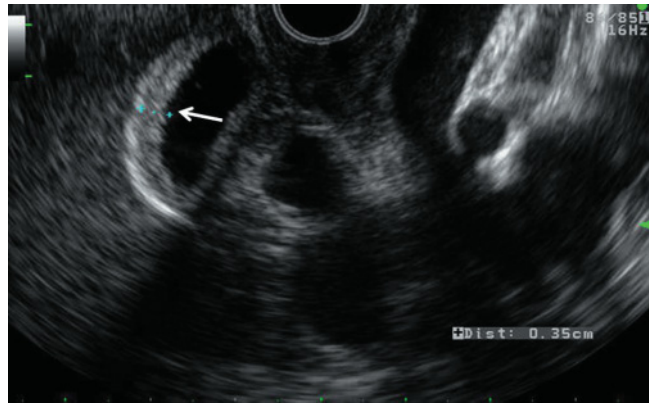

Figure 21.8 Thickened gallbladder wall (arrow).

Carcinoma of the gallbladder is usually seen on EUS as a hypoechoic mass protruding into the gallbladder lumen or completely filling it. These lesions usually have irregular margins and characteristically destroy the normal three-layer structure of the gallbladder wall (Figure 21.7). Other EUS findings that are suggestive but not diagnostic of gallbladder carcinoma include thickening or calcification of the gallbladder wall, and loss of the normal sonographic interface between the gallbladder and liver. Gallbladder wall thickening, however, may also represent other conditions such as acute or chronic cholecystitis (Figure 21.8).

Endoscopic ultrasound is a useful modality to assess the depth of invasion of gallbladder carcinoma as well as to define lymph node involvement. Several recent studies have shown that EUS imaging is quite accurate for TMN staging of gallbladder carcinoma, and correlates strongly with post-operative histopathologic findings. In one study by Mitake *et al.*, 39 patients with gallbladder carcinoma were evaluated preoperatively with EUS. Carcinoma considered to be at an early stage with no lymph node involvement was correctly diagnosed in 87.5% of cases. In another study by Sadamoto *et al.*, 41 patients with gallbladder carcinoma evaluated by EUS were analyzed retrospectively. Endoscopic ultrasound was found to be extremely accurate in determining the stage of the tumor, particularly with T1 and T3–4 lesions.

22 Pancreatic Adenocarcinoma

Douglas G. Adler
University of Utah School of Medicine, Salt Lake City, UT, USA

Introduction

Adenocarcinoma accounts for 90% of all pancreatic tumors. The highest cure rate is seen in patients with lesions that are localized to the pancreas and do not involve significant local vascular structures. Only 15–20% of patients have potentially resectable disease at the time of diagnosis. Surgery has been and remains the most effective treatment for pancreatic cancer, although 5-year survival rates remain low at 18–33% even in patients who progress to surgery. Accurate staging of patients with pancreatic adenocarcinoma is critical and allows patients to be appropriately selected to undergo for surgery, chemotherapy, radiation therapy, or palliative care. Endoscopic ultrasound (EUS) is a minimally invasive technique that has proved invaluable for both accurate locoregional staging of pancreatic adenocarcinoma and as a means of providing tissue from tumors and lymph nodes, thus allowing for a definitive diagnosis.

Tumor identification and diagnosis via fine needle aspiration

The overall staging accuracy of EUS in patients with pancreatic adenocarcinoma is approximately 90–100%. In general, EUS is superior to computed tomography (CT) scans for the detection of pancreatic cancers. For small pancreatic masses (those lesions 16 mm or smaller), EUS sensitivity for tumor detection approaches 100% as compared to 66% using multi-detector computed tomography (CT) scans. As determined by EUS, accuracy for resectability is 88–100%. If CT or magnetic resonance imaging (MRI) scans reveal metastatic disease, then staging is complete (the patient has stage IV disease), and EUS may not be required. In patients with metastatic disease, EUS with fine needle aspiration (FNA) can still be performed if a definitive tissue diagnosis is desired. The sensitivity, specificity, positive predictive value, and negative predictive value of EUS-guided pancreatic FNA for the diagnosis of malignancy in patients with pancreatic cancer has been reported to be 64%, 100%, 100%, and 16% respectively (Figures 22.1 and 22.2).

Evaluation of vascular invasion

As mentioned, detection of vascular involvement in patients with pancreatic adenocarcinomas is critical for staging. Unfortunately, the definition of "vascular involvement" invasion has not been uniformly defined in the literature. When evaluating peripancreatic vessels via EUS, tumor can be seen to contact vessels with or without the loss of a clear tissue plane (a.k.a. echoplane), be adjacent to vessels, invade blood vessels with tumor visualized in the vascular lumen, thrombose vessels, and/or to encase blood vessels. All of these are considered vascular involvement, but individual surgeons may differ on which of these findings may exclude patients for surgery.

If there is vascular involvement/invasion between the tumor and the celiac artery or the superior mesenteric artery (SMA), the patient has unresectable disease (Figure 22.3). Vascular invasion of the splenic artery or splenic vein are typically not contraindications to surgical intervention. With respect to the portal vein and/or the superior mesenteric vein, vascular invasion into the portal vein, the superior mesenteric vein, or the confluence of these vessels is not a contraindication to surgery, but advanced surgical techniques such as vascular grafting and/or reconstruction may be required for successful pancreaticoduodenectomy (Figures 22.4 and 22.5; and Video 22.1).

In patients with pancreatic adenocarcinoma, vascular staging accuracy for EUS has been reported to be 100% vs. 81% for CT in one study. Another similar study found EUS to have a sensitivity, specificity, positive predictive value,

Atlas of Endoscopic Ultrasonography, First Edition. Edited by Frank G. Gress, Thomas J. Savides, Brenna Casey Bounds, John C. Deutsch.

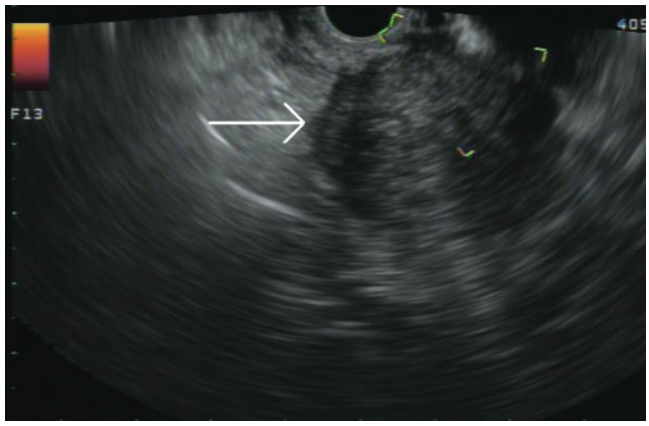

(a)

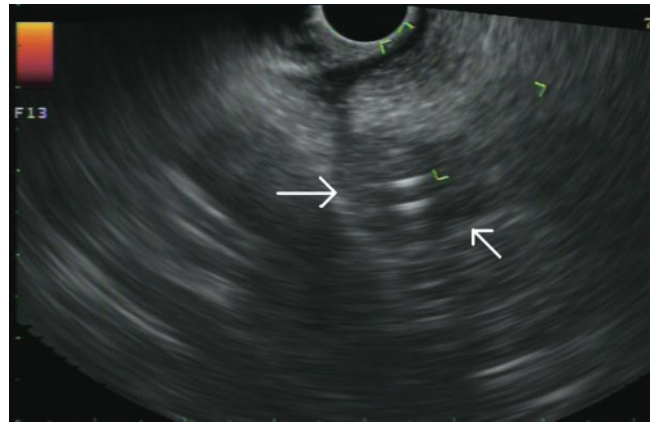

(b)

Figure 22.1 (a) Representative endoscopic ultrasound (EUS) image of a large pancreatic adenocarcinoma (arrow). The tumor is a well demarcated, hypoechoic mass lesion in the body of the pancreas. (b) Representative EUS image of a small pancreatic adenocarcinoma (arrows). The patient has a 1.5 cm lesion in the head of the pancreas surrounding the central bile duct (CBD), which is seen to contain a plastic stent. The walls of the plastic stent appear as bright, hyperechogenic lines.

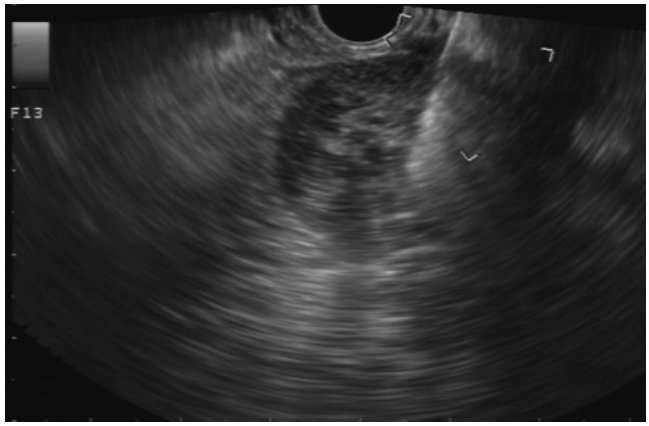

Figure 22.2 Endoscopic ultrasound-guided fine needle aspiration (FNA) of a pancreatic adenocarcinoma with a 22-gauge needle.

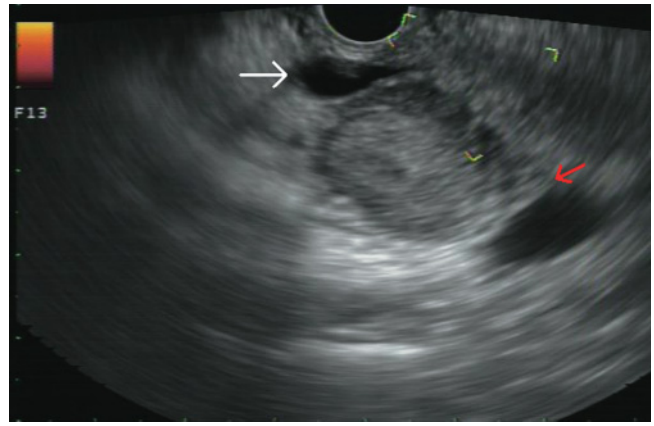

Figure 22.4 A 2-cm pancreatic head mass seen to abut and compress the central bile duct (CBD) (white arrow, top of image) and to abut the portal vein (bottom of image) with intact tissue plane between the mass and the vessel (red arrow).

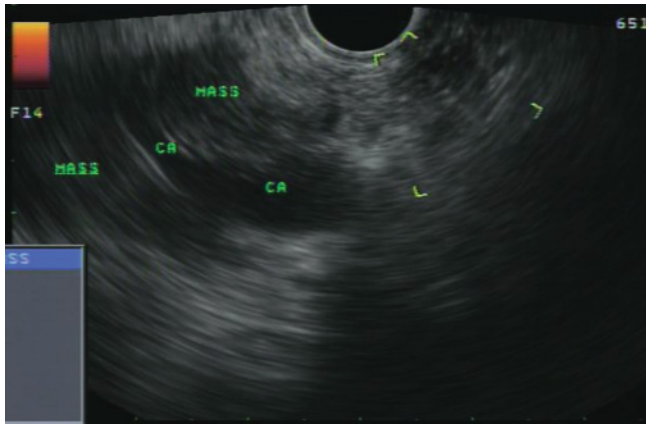

Figure 22.3 Endoscopic ultrasound image of a pancreatic adenocarcinoma in the body of the pancreas encasing the celiac artery (CA).

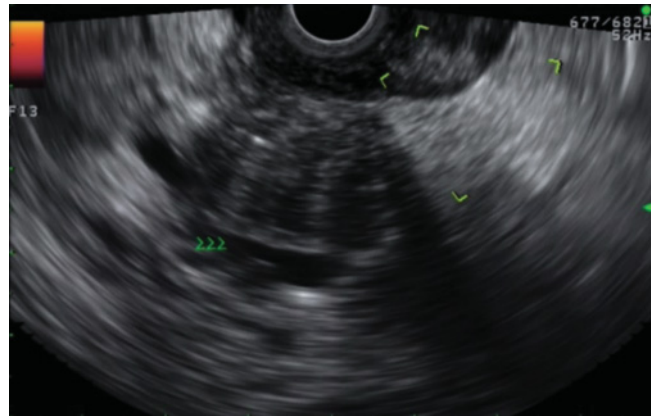

Figure 22.5 Large pancreatic cancer in the head of the pancreas seen to encase the superior mesenteric vein (SMV) (green arrows).

and negative predictive value for determining superior mesenteric vein and portal venous involvement in patients with pancreatic adenocarcinoma to be 81%, 86%, 87%, and 80%, respectively. This same study also demonstrated that for SMA tumor involvement the sensitivity and specificity, positive predictive value, and negative predictive value have been reported to be 17%, 67%, 17%, and 67%, respectively. These lower numbers reflect that the SMA can be difficult to fully track via EUS once it diverges significantly from the aorta. A meta-analysis found the overall sensitivity of EUS for diagnosing vascular invasion overall to be 73% with a specificity of 90%.

Evaluation of peripancreatic lymphadenopathy

The presence or absence of malignant peripancreatic lymphadenopathy does not play a definitive role in determining if a pancreatic cancer is resectable or unresectable, but the presence of malignant adenopathy can have a powerful effect on overall management. If a cancer appears to be potentially resectable, the identification of malignant lymph nodes may be a justification for neoadjuvant therapy.

When imaged via EUS, malignant lymphadenopathy is suggested by the presence of lymph nodes that are greater than 1 cm in size, hypoechoic, have distinct margins, and are round in shape. Individually, none of these characteristics determine the presence of malignant cells, but when all four of the above features are present in the same lymph node, the accuracy for predicting malignant involvement is 80%. Sensitivity, specificity, positive predictive value, and negative predictive value for the detection of celiac axis, portal vein, hepatic artery, and SMA lymph nodes via EUS are 44%, 93%, 80%, and 72%, respectively (Figures 22.6 and 22.7).

Endoscopic ultrasound evaluation of peripancreatic lymphadenopathy is superior to that of CT. While not all malignant appearing nodes are sampled, if the appearance of a lymph node is indeterminate for malignant involvement, EUS-guided FNA of the node in question can be performed for a definitive nodal evaluation. The overall sensitivity, specificity, and accuracy of detection of malignant lymph nodes by EUS are approximately 85%, 100%, and 89%, respectively.

Limitations and complications of EUS in patients with pancreatic cancer

Despite its value in patients with pancreatic adenocarcinoma, EUS has some significant limitations. Pancreatic adenocarcinomas may be difficult to detect via EUS (and, of note, CT or MRI) in patients with chronic pancreatitis (due to baseline tissue distortion) or if the tumor has is isoechoic with the surrounding pancreatic parenchyma. As mentioned above, EUS is relatively insensitive for the detection of SMA involvement. Complete visualization of the entire pancreas can sometimes be difficult. The pancreatic genu and uncinate process can be challenging to completely image, especially in patients with large body habitus.

Potential complications from EUS with or without FNA can include acute pancreatitis (0–2%), perforation (0.03%), infection/febrile episode (1%), and significant hemorrhage (1.3–4.0%).

The number of EUS practitioners, while clearly increasing, remains limited, and some many endosonographers receive only limited training. One study on EUS training volumes revealed that most three-year gastrointestinal fellows and many fourth-year advanced endoscopy fellows are currently receiving insufficient training in EUS. Further limiting the

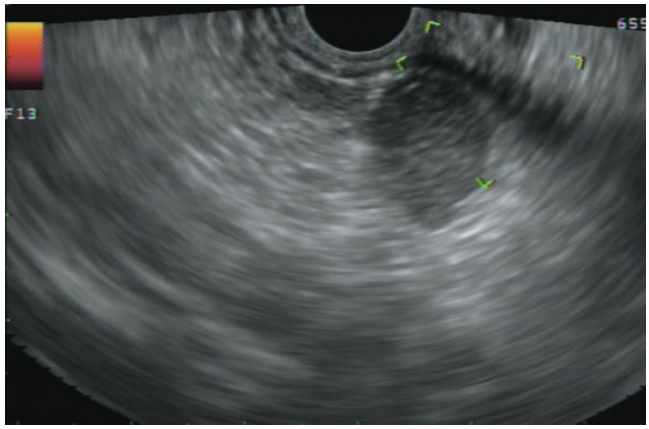

Figure 22.6 A 15-mm peripancreatic lymph node. Node is hypoechoic, round, well demarcated, and greater than 1 cm in size, all of which suggests malignancy.

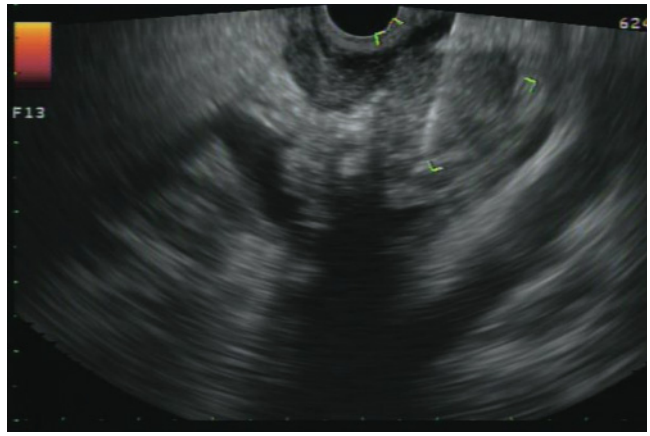

Figure 22.7 Endoscopic ultrasound-guided fine needle aspiration (FNA) of a large, 2.5 cm peripancreatic/celiac node in a patient with pancreatic adenocarcinoma. Cytology revealed malignant cells.

spread of EUS to the general community, training in EUS is not offered at 14% of US gastrointestinal fellowship programs. In general, the best results are obtained from the most experienced operators.

Conclusion

Pancreatic adenocarcinoma remains a commonly encountered clinical entity. Accurate staging and tissue diagnosis are critical for formulation of optimal management plans. Endoscopic ultrasound offers high accuracy for the staging pancreatic adenocarcinoma, provides excellent tissue acquisition, and is essentially unrivaled for the detection of small tumors. It is also highly effective in evaluating patients for the presence of malignant lymphadenopathy and in assessing vascular involvement.

Chapter video clip

Video 22.1 Locally advanced pancreatic cancer.

23 Pancreatic Malignancy (Non-adenocarcinoma)

Michael J. Levy and Suresh T. Chari
Mayo Clinic, Rochester, MN, USA

Introduction

Endoscopic ultrasound (EUS) is routinely employed in the evaluation of solid pancreatic mass lesions to enhance diagnostic accuracy, guide management, and improve patient outcomes. Much has been published regarding the use of EUS for pancreatic adenocarcinoma, which accounts for approximately 95% of all solid pancreatic malignancies. Understandably, there are fewer EUS data concerning endocrine tumors, and even less for lymphoma, solid pseudopapillary tumors, acinar cell carcinoma, and secondary metastatic tumors.

Endocrine pancreatic tumors (Figures 23.1a–c and 23.2)

Endocrine pancreatic tumors (EPTs) are rare with an incidence of less than 1/100 000. Gastrinoma, insulinoma, and non-functioning tumor are most common, with glucagonoma, somatostatinoma, and VIPoma less often reported. Preoperative localization helps guide surgical resection, which offers the only chance for cure and is usually undertaken when possible due to the malignant potential. Endoscopic ultrasound localizes 75–95% of insulinomas. The high EUS detection rate for insulinomas is likely explained by the fact that 99% of insulinomas are contained within the pancreas. Approximately 75–100% of pancreatic gastrinomas are identified by EUS versus only 0–67% of duodenal gastrinomas.

The EUS appearance is similar regardless of the tumor type or functional status, typically appearing as round, well-delineated, homogenous, mildly hypoechoic lesions, often with a surrounding hyperechoic rim. They may also appear isoechoic or hyperechoic, have a hypoechoic border, be cystic or calcified. The EUS technique for localizing these tumors is identical to that of adenocarcinoma, except that a more deliberate exam may be needed to find these often small lesions. The parapancreatic region should also be carefully examined to search for lymphadenopathy and because the primary tumor may be attached by a pedicle or completely separate from the pancreas and are more difficult to locate than intrapancreatic tumors.

Endoscopic ultrasound-guided fine needle aspiration (EUS-FNA) helps differentiate benign parapancreatic lymph nodes from primary endocrine tumor, a distinction that can be difficult, especially for insulinomas. The EUS appearance may also predict the malignant potential, which can be otherwise difficult to discern in the absence of extensive local invasion or distant metastasis. The presence of anechoic regions, an irregular central echogenic area, or pancreatic duct obstruction corresponds with severe hemorrhage, necrosis, or hyaline degeneration, each of which suggests a malignant tumor; although their predictive value is uncertain. EUS-FNA and Tru-cut biopsy (TCB) further increase diagnostic accuracy.

Primary pancreatic lymphoma (Figure 23.3)

Approximately one third of patients with non-Hodgkin's lymphoma (NHL) develop secondary pancreatic involvement. Primary pancreatic lymphoma (PPL) is rare and accounts for fewer than 3% of extranodal NHL, and less than 0.5% of all pancreatic malignancies. It is generally treated with chemotherapy and/or radiation therapy, commonly resulting in disease remission and occasionally cure.

Most tumors appear by EUS as a mildly hypoechoic solid and less often cystic mass that may be single or multiple. It may be difficult to distinguish primary pancreatic mass(es) from commonly accompanying prominent peripancreatic lymphadenopathy. Although the appearance may mimic adenocarcinomas, lymphomas are less hypoechoic, have less

Atlas of Endoscopic Ultrasonography, First Edition. Edited by Frank G. Gress, Thomas J. Savides, Brenna Casey Bounds, John C. Deutsch.

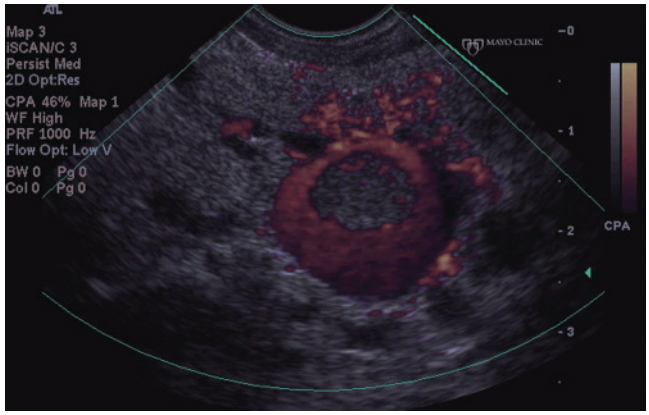

(a)

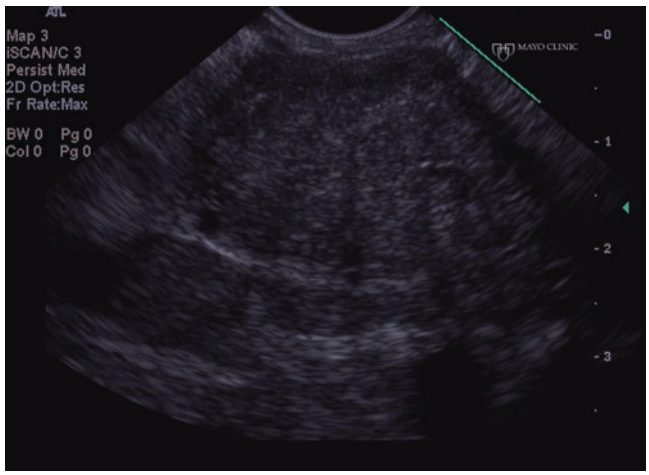

(b)

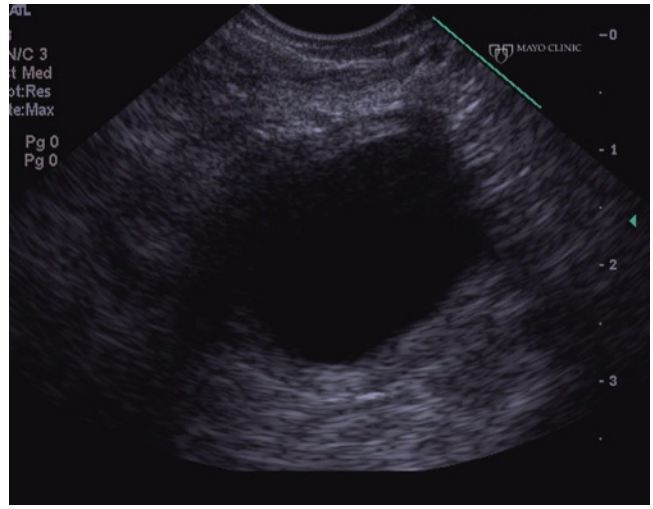

(c)

Figure 23.1 Images obtained from a patient with a gastrinoma following helical computed tomography (CT) that revealed a pancreatic cyst that was not felt to represent a gastrinoma. Linear endoscopic ultrasound identified malignant vascular thrombosis as highlighted with the use of Power Doppler (a). A large endocrine tumor was identified, which appeared more hypoechoic, irregular, and infiltrating than usual. This mass encompassed most of the pancreatic body and tail (b). The tumor also contained a pancreatic tail cystic component that was seen on CT (c).

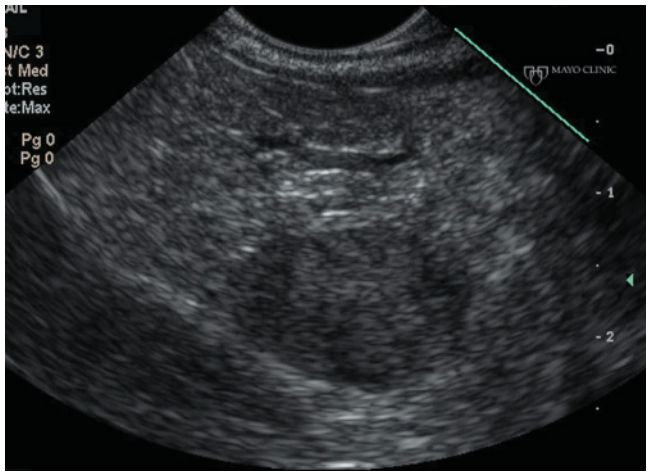

Figure 23.2 Following a negative computed tomography (CT) to search for a presumed insulinoma, linear endoscopic ultrasound identified the insulinoma within the pancreatic body, allowing curative surgical intervention.

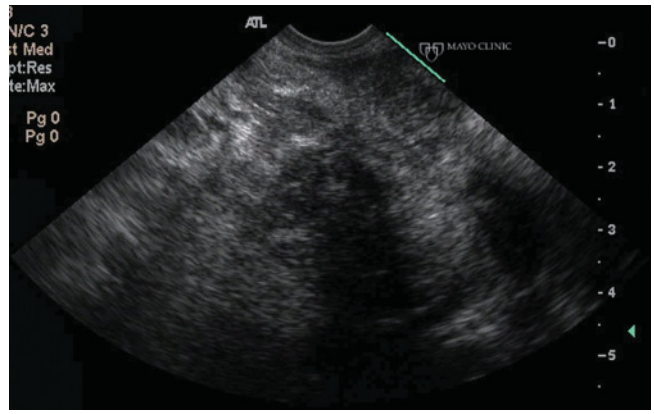

Figure 23.3 Linear endoscopic ultrasound imaging of a patient with a pancreatic lymphoma.

pronounced peritumoral inflammatory changes, and vascular invasion and pancreatic duct dilatation are uncommon. Clinical presentation is of little utility as typical "B-type" symptoms, including fever and night sweats, are seldom present. Non-Hodgkin's lymphoma may be diagnosed by EUS-FNA with immunophenotyping by flow cytometry. The diagnostic accuracy may be further improved by submitting dedicated FNA passes for flow cytometry and obtaining EUS-TCB to further enhance morphologic and architectural assessment.

Solid pseudopapillary tumors (Figure 23.4)

Solid pseudopapillary tumors (SPTs) are rare pancreatic neoplasms that typically develop in young women in the second or third decade of life. They are usually incidentally discovered and typically follow an indolent course. They can be malignant and develop distant metastases. Surgery is the therapy of choice providing curative resection in 95% of patients. Most favor an aggressive resection for malignant disease that includes major venous and even arterial structures and distant metastases. Of note, nodal metastases are unusual, and formal lymphadenectomy is not necessary. Continued surveillance of all patients is recommended, and should metastases appear, surgical resection is indicated.

Imaging typically reveals large well-circumscribed hypoechoic lesions that may be solid to nearly entirely cystic often containing multiple cystic compartments. EUS-FNA permits diagnosis in most patients; however, the cytology may be confused with endocrine tumors and acinar cell carcinoma. Negative chromogranin and synaptophysin staining exclude an islet cell neoplasm, whereas a negative keratin stain excludes acinar carcinoma. Immunohistochemical analysis of SPTs usually shows strong staining for CD56 and vimentin and β-*catenin* gene mutations are common.

Acinar cell carcinoma (Figure 23.5)

Although acinar cells comprise over 80% of all pancreatic cells, acinar cell carcinoma (ACC) accounts for less than 1% of all pancreatic neoplasms. They typically develop in males during the sixth or seventh decade of life. Most patients present with large tumors with associated pain and weight loss. Patients may develop lipase hypersecretion syndrome resulting from systemic secretion of pancreatic enzymes and characterized by fever, polyarthritis, subcutaneous fat necrosis, and eosinophilia. There is some debate as to the clinical course of ACC. While some report poor outcomes, most recent studies have found a better prognosis than for pancreatic adenocarcinoma. Despite the typically large size of ACC, resection margins are usually negative. Surgical resection is the therapy of choice and while nearly all succumb to their disease, the postoperative survival duration is greater (approximately 4–5 years) than for pancreatic adenocarcinoma. Neoadjuvant therapy may provide effective downstaging and allow resection in a small cohort of patients.

Immunohistochemical analysis of ACC usually shows strong staining for trypsin, chymotrypsin, and lipase permitting diagnosis. The most common neoplasm in the differential diagnosis of patients with ACC is well-differentiated pancreatic endocrine tumors. Immunohistochemical stains

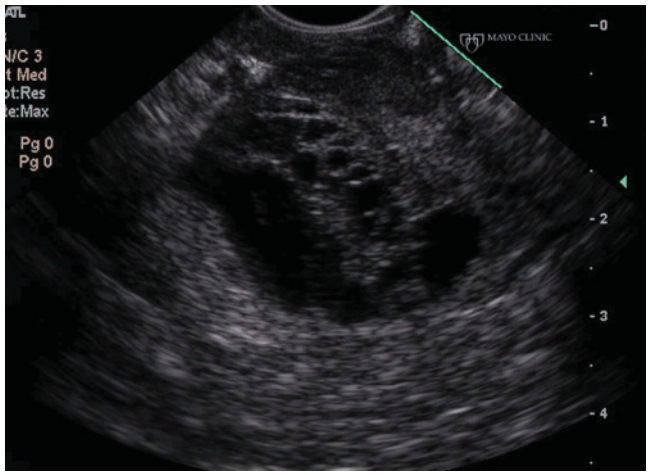

Figure 23.4 Endoscopic ultrasound revealed a large well-circumscribed hypoechoic lesion that contained solid and cystic components with the diagnosis of a solid pseudopapillary tumor established by endoscopic ultrasound-guided fine needle aspiration (EUS-FNA) and later confirmed at surgery.

Figure 23.5 A pancreatic head acinar cell tumor is identified by endoscopic ultrasound and confirmed at fine needle aspiration (FNA) leading to pancreaticoduodenectomy.

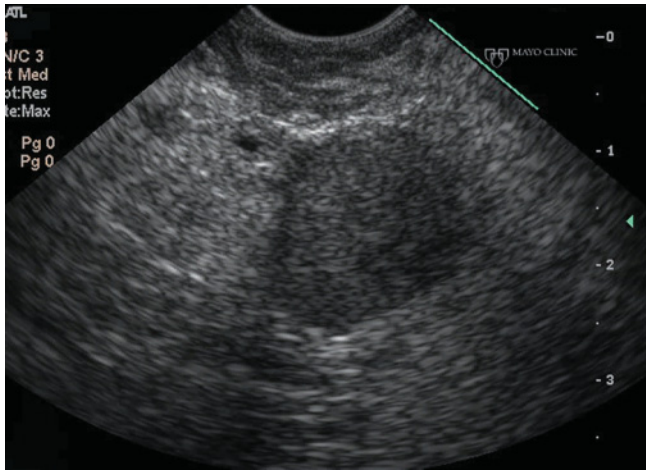

(a)

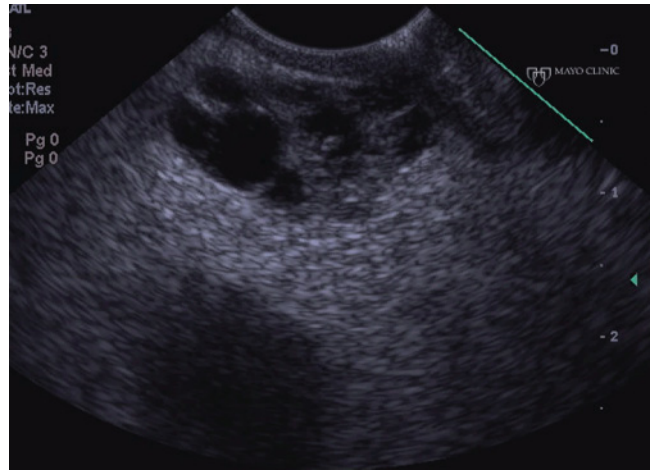

(b)

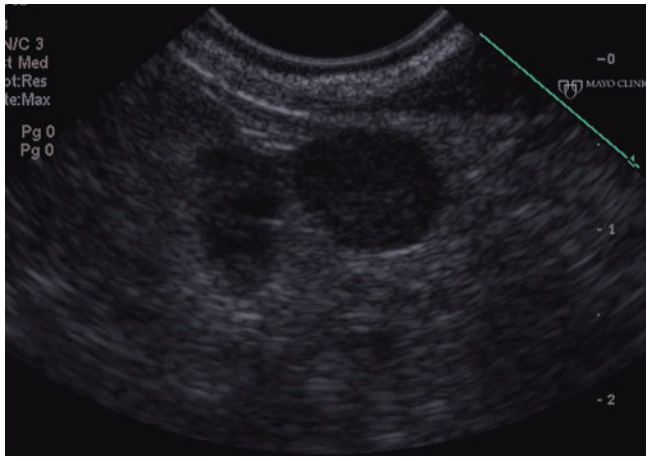

(c)

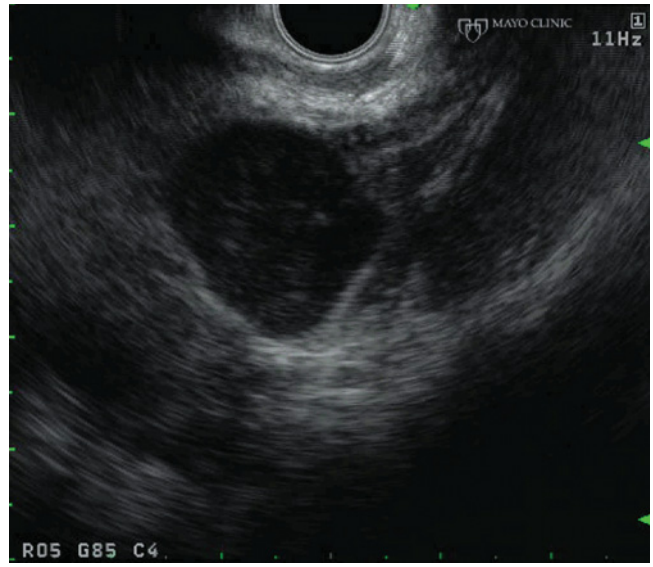

(d)

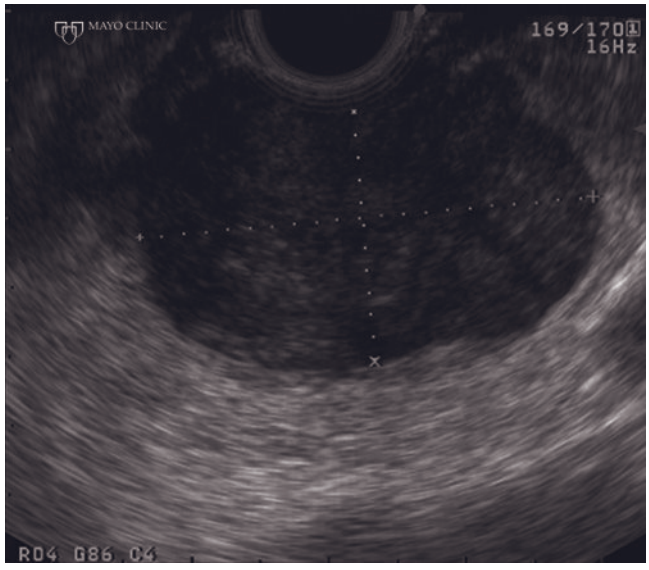

(e)

Figure 23.6 The varied appearance of metastatic tumors to the pancreas is demonstrated (a–e).

for neuroendocrine markers, synaptophysin and chromogranin, help differentiate these neoplasms. However, mixed acinar–endocrine neoplasms occur and are associated with improved prognosis over pure ACC.

Secondary metastatic tumors

(Figure 23.6a–e)

Pancreatic metastases account for approximately 1% of all resected solid pancreatic mass lesions. While over 30 sites of origin have been reported, the most common primary tumors include renal cell carcinoma, lung, breast, colon, melanoma, sarcoma, and ovarian. These tumors are notable for a prolonged delay from initial primary tumor diagnosis until pancreatic metastasis that averages 5–10 years and may occur more than 25 years later. While most metastasize to the pancreatic head, multiple metastases are seen in a third to half of patients, and diffuse infiltration is also reported. Pancreatic metastases are more often resectable and portend a better prognosis than patients with primary pancreatic adenocarcinoma.

Imaging can vary tremendously for these lesions that may be solid and/or cystic, have variable echodensity, and are often hypervascular. EUS-FNA can usually establish the diagnosis, but EUS-TCB and immunostaining may be necessary for definitive diagnosis. Endoscopic ultrasound further impacts patient care through the detection of multifocal disease undetected by non-invasive imaging. Endosonographers should suspect metastatic tumor in patients with a prior diagnosis of distant neoplasia given the relatively indolent course and improved surgical outcomes with postoperative survival of 2–4 years.

Summary

Endoscopic ultrasound is now routinely used to evaluate pancreatic masses. By offering high resolution imaging and tissue sampling, EUS can often establish whether a mass is inflammatory, benign, or malignant, enhance staging accuracy, and determine the tumor type to help guide patient care and improve outcomes.

Chapter video clip

Video 23.1 Pancreatic cancer.

24 Autoimmune Pancreatitis

Michael J. Levy and Suresh T. Chari
Mayo Clinic, Rochester, MN, USA

Introduction

While the first description of autoimmune pancreatitis (AIP) was by Sarles *et al*. in 1961, the term autoimmune pancreatitis was first introduced by Yoshida *et al*. in 1995. In the past year AIP has been subclassified as type 1 and type 2; type 1 being the classic AIP described from Japan. Type 1 AIP is part of a systemic fibro-inflammatory process that afflicts multiple organs including pancreas, bile duct, retroperitoneum, lymph nodes, salivary glands, and kidneys which demonstrate a characteristic IgG_4-rich lymphoplasmacytic infiltrate. Type 2 AIP appears to be a pancreas-specific disorder, sometimes associated with inflammatory bowel disease. Both forms readily respond to steroid therapy. Type 2 can be definitively diagnosed only on histology.

The initial description of AIP highlighted the presence of jaundice secondary to a pancreatic head mass mimicking pancreatic carcinoma. As clinical experience evolved there came a greater understanding of the diverse clinical, laboratory, and histological manifestations of AIP, leading the way to more comprehensive diagnostic criteria such as the Mayo HISORt system that considers the findings of histology, imaging, serology, other organ (non-pancreatic) involvement, and response to steroid therapy. While pancreatic imaging is a key component of the diagnostic systems, notably absent is specific mention of the role for endoscopic ultrasound (EUS). This omission of EUS from diagnostic algorithms likely results from the lack of meaningful studies that document the EUS imaging features and a paucity of data pertaining to the utility and safety of endoscopic ultrasound-guided fine needle aspiration (EUS-FNA) and Tru-cut biopsy (TCB) in this patient cohort. Our aim is to review the spectrum of AIP features identified by EUS and suggest a potential role of EUS-guided tissue sampling.

Endoscopic ultrasound imaging

(Video 24.1)

The characteristic EUS finding is diffuse (sausage-shape) pancreatic enlargement with a hypoechoic, coarse, patchy, heterogeneous appearance (Figures 24.1–24.3) However, there may be significant overlap between the appearance of AIP and other pancreatic disorders. Endoscopic ultrasound may reveal an isolated or multiple mass lesions that can mimic "unresectable" carcinoma (Figure 24.4). Other less common EUS features include glandular atrophy, calcification, cystic spaces, features of usual chronic pancreatitis, or even a normal gland (Figure 24.5). Unfortunately, there are no pathognomonic EUS findings for AIP. While a few features of AIP are characteristic, none are adequate to allow definitive diagnosis of AIP and their presence in other pancreatic disorders is common. The lack of pathognomonic features and diverse spectrum of EUS findings somewhat limits the utility of EUS imaging alone. This has driven the pursuit for safe and reliable methods for obtaining tissue to enhance diagnostic accuracy.

EUS-FNA and EUS-TCB

As per recent expert panel deliberations on AIP held at the 2009 Honolulu (American Pancreatic Association and Japan Pancreas Society) Meeting, pancreatic FNA is inadequate for diagnosing AIP. There was consensus that definitive diagnosis requires pancreatic core biopsy obtained at surgery or by EUS-TCB. The TCB device (Quick-Core, Wilson–Cook, Winston–Salem, North Carolina) incorporates a disposable 19-gauge needle with tissue tray and sliding sheath with a spring-loaded mechanism is contained within the handle.

Atlas of Endoscopic Ultrasonography, First Edition. Edited by Frank G. Gress, Thomas J. Savides, Brenna Casey Bounds, John C. Deutsch.
 Published 2012 by Blackwell Publishing Ltd.

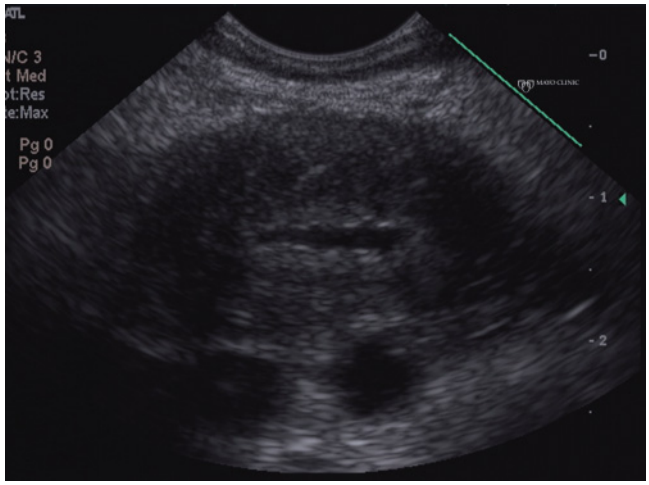

Figure 24.1 Classic endoscopic ultrasound appearance of autoimmune pancreatitis including hypoechoic diffuse (sausage-shape) pancreatic enlargement with hypoechoic, coarse, patchy, heterogeneous parenchyma.

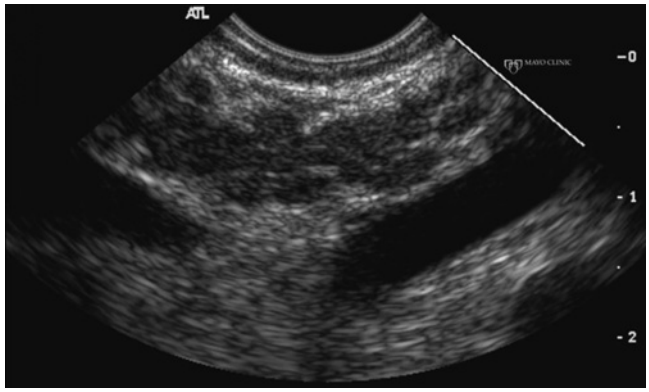

Figure 24.2 Almost classic endoscopic ultrasound appearance of autoimmune pancreatitis with a hypoechoic gland and course, patchy, heterogeneous changes without glandular enlargement.

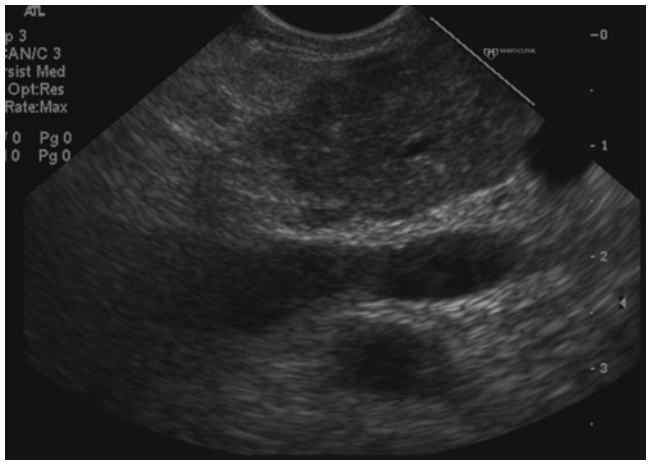

Figure 24.3 Almost classic endoscopic ultrasound appearance of autoimmune pancreatitis with a hypoechoic and enlarged gland without the prominent course, patchy, heterogeneous changes.

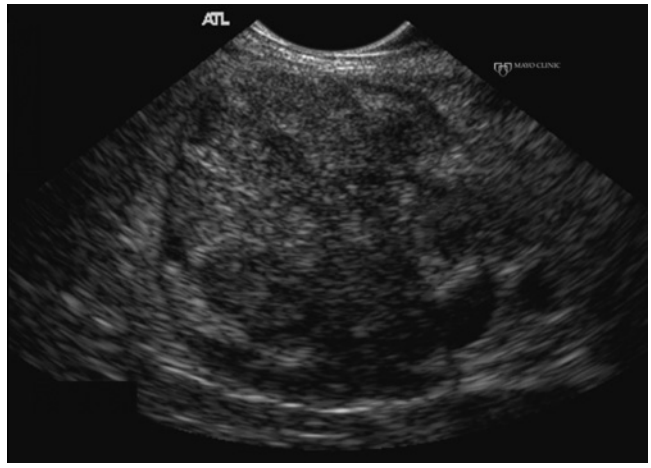

Figure 24.4 Endoscopic ultrasound finding of a mass-like lesion in a patient with autoimmune pancreatitis that may be confused with an "unresectable" pancreatic ductal carcinoma.

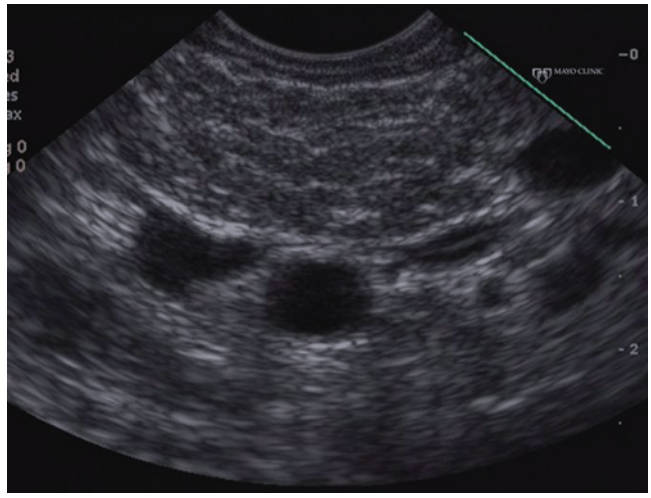

Figure 24.5 Endoscopic ultrasound features of non-specific chronic pancreatitis in a patient with autoimmune pancreatitis.

However, some discouraged the use of EUS-TCB due to the perceived insufficient sensitivity for diagnosis of AIP and the associated risk.

We previously demonstrated that EUS-TCB acquires core specimens with preserved tissue architecture permitting histologic diagnosis of AIP. In updating our initial report, 48 patients (38 male, 10 female; mean age 59.7 years [range 18–87]) with a final diagnosis of AIP have undergone a mean of 2.9 EUS-TCBs (range 1–7). Autoimmune pancreatitis was histologically diagnosed on EUS-TCB in 35 (73%) patients and the diagnostic sensitivity varied among the 5 endosonographers from 33% to 90%. Non-diagnostic cases were found to have chronic pancreatitis ($n = 8$), non-specific histology ($n = 2$), and failed tissue acquisition

($n = 3$). Thirty-seven patients underwent EUS-FNA (mean 3.4 passes, range 1–7 passes) that failed to establish or suggest the diagnosis in any patient. Complications of EUS-TCB included mild transient abdominal pain ($n = 3$) and self-limited intraprocedural bleeding ($n = 1$). No patient required hospitalization or therapeutic intervention. The diagnosis of AIP was strongly suspected prior to EUS in 14 patients as a result of their clinical, laboratory, imaging, and laboratory findings. For 22 patients the diagnosis was considered pre-EUS as part of a broader differential, and in 12 patients the EUS appearance alone led to the initial suspicion of AIP. Serum IgG_4 was >2× upper limit of normal (ULN) in only 23% of patients. No patient with EUS-TCB diagnosis of AIP required surgery. In the patients with false negative EUS-TCB, the diagnosis was made by HISORt criteria. Over a mean follow-up of 2.6 years no false negative diagnoses of pancreatic cancer were identified. Our experience demonstrates that large caliber pancreatic biopsy is safe and provides sufficient material to definitively diagnose AIP obviating the need for surgical resection.

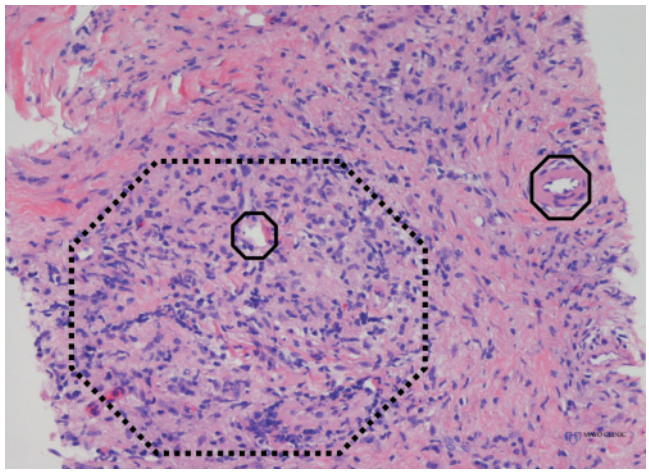

Figure 24.6 Histologic examination of endoscopic ultrasound-guided Tru-cut biopsy (EUS-TCB) specimen reveals an intact artery is seen at the right of the image (single solid marker). In addition, an intense infiltration by lymphocytes and histiocytes results in near complete obliteration of the vein (obliterative phlebitis) shown at the left of the image (dashed marker surrounding solid marker). (H&E, orig. mag. ×300.)

Histologic features

Histologic features of type I AIP (lymphoplasmacytic sclerosing pancreatitis; LPSP) include a lymphoplasmacytic infiltrate that surrounds medium and large-size interlobular pancreatic ducts, and pancreatic venules (obliterative phlebitis) while sparing arterioles, as well as swirling fibrosis centered around pancreatic ducts (storiform fibrosis) (Figure 24.6). Histology accurately distinguishes AIP from other causes of chronic pancreatitis and pancreatic carcinoma. IgG_4 immunostaining of tissue samples identifies IgG_4 positive plasma cells and presence of moderate (11–30 cells/high power field [HPF]) or severe (>30 cells/HPF) is considered diagnostic (Figure 24.7). These findings distinguish AIP from alcohol-induced pancreatitis and the peri-tumoral inflammation associated with carcinoma. Histologic features of type II AIP (idiopathic duct-centric pancreatitis; IDCP) include a lymphoplasmacytic infiltrate with granulocyte epithelial lesions with partial/complete duct obstruction. Tissue immunostaining in IDCP is typically negative, but may reveal mild (1–10/HPF) or moderate (11–20/HPF) IgG_4-positive plasma cell infiltration.

Summary

The difficulty in diagnosing AIP highlights the need for improved understanding its EUS imaging features and development of reliable and safe methods for acquiring core tissue specimens. Until such time, EUS will have a central role in the evaluation of AIP in a minority of centers. We

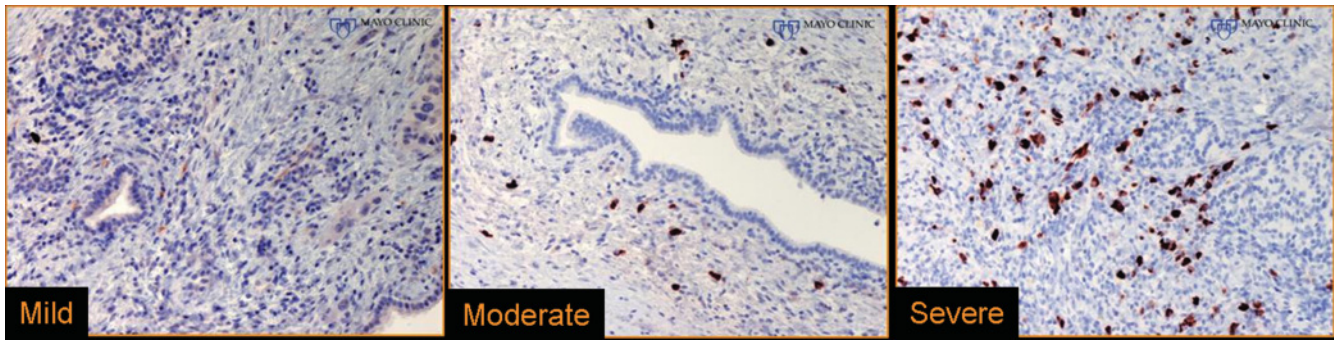

Figure 24.7 IgG_4 immunostaining of the Tru-cut biopsy specimen reveals the findings of mild infiltration (1–10 plasma cells/high power field [HPF]), moderate infiltration (11–30 cells/HPF) and severe infiltration (>30 cells/HPF).

advocate EUS imaging to provide supportive evidence for or against an AIP diagnosis. Because imaging alone cannot firmly establish the diagnosis, FNA is often necessary to exclude underlying malignancy. We recommend EUS-TCB for patients with a compatible clinical presentation in whom there is diagnostic uncertainty and when the finds are likely to alter management. This recommendation assumes the reliable and safe us of EUS-TCB. Further study is necessary to help clarify the diagnostic accuracy and role of EUS imaging and tissue sampling in this patient cohort.

Chapter video clip

Video 24.1 Autoimmune pancreatitis.

25 Pancreatic Cystic Lesions: The Role of EUS

William R. Brugge
Massachusetts General Hospital and Harvard Medical School, Boston, MA, USA

Introduction

The frequent use of cross-sectional radiographic imaging has lead to an increase in the identification of cystic lesions of the pancreas. In asymptomatic patients, the cystic lesion most often represents a form of intraductal malignancy. Fluid collections in patients with acute pancreatitis are usually inflammatory in nature. In the management of patients with a cystic lesion, there are usually two predominant questions: "Is the cyst mucinous or non-mucinous?" and "Is the cyst malignant or benign?" Endoscopic ultrasound (EUS) with fine needle aspiration (FNA) can provide critical data in these diagnostic questions.

Cystic lesions of the pancreas are often readily apparent by EUS. The lesions appear as anechoic against the "salt and pepper" background of the pancreatic parenchyma. Focal fluid collections can simulate a true cyst of the pancreas, but often there are tell-tale signs of pancreatitis. Occasionally, tumor necrosis can simulate a pancreatic cyst because of the presence of fluid in the mass. Endoscopic ultrasound can provide details of the structural characteristics of the cyst, pancreatic parenchyma, pancreatic duct as well as surrounding structures, but is not sufficient to distinguish malignant from benign lesions (Table 25.1).

Fine needle aspiration of the cyst fluid and analysis of cellular material, amylase level, and tumor markers such as carcinoembryonic antigen (CEA) have been shown to assist in narrowing the differential diagnosis. In studies where surgical correlation is available, EUS with FNA and cytopathology has an accuracy of 55–91%. In particular, a cyst fluid CEA concentration of >192 ng/ml is predictive of a mucinous lesion with 79% accuracy. The presence of a kRAS mutation is also indicative of a mucinous lesion.

The diagnostic techniques described above are particularly pertinent in those patients who are not surgical candidates or do not have symptoms attributable to the cyst. Endoscopic ultrasound with FNA should be reserved for those cases in which the results would alter clinical management. If a cyst is found in the setting of recurrent acute pancreatitis in a patient who is fit for surgery, resection should be considered and EUS is not indicated.

Pseudocyst

A pancreatic pseudocyst represents an inflammatory fluid collection. There is no epithelial lining within a pseudocyst and surrounding structures form the borders of a pseudocyst. Imaging findings of chronic pancreatitis, including calcifications, increase the likelihood that a cystic lesion is a pseudocyst.

The EUS features of pseudocysts include a thick-walled, unilocular, fluid-filled cavity (Figure 25.1). Aspiration of a pseudocyst reveals thin, brown, amylase rich fluid. Cytologic examination reveals inflammatory cells and occasionally necrotic debris. The fluid CEA levels should be relatively low and without evidence of mucin.

Serous lesions

Serous cystadenoma is the most common type of non-mucinous cyst (Figure 25.2). These lesions typically have a microcystic morphology creating a honeycomb appearance. The microcysts are divided by thin septations that can become fibrotic and form the classic central stellate scar. Macrocystic morphology is seen in a minority of serous cystadenoma. Microscopically, the cyst lining is composed of

Atlas of Endoscopic Ultrasonography, First Edition. Edited by Frank G. Gress, Thomas J. Savides, Brenna Casey Bounds, John C. Deutsch.

Table 25.1 Demographics and characteristics of pancreatic cystic neoplasms.

Cyst type	Most common location	Gender	Solitary or multi-centric	Morphology	Malignant potential
Serous cystadenoma	Head	Female	Solitary	Microcystic with honeycombing, minority are macrocystic	Very low
Mucinous cystic neoplasm	Tail	Strongly female	Solitary	Macrocystic, can be septated	High
Intraductal papillary mucious neoplasm	Multi-focal	Equal	Multi-centric	Main branch: dilated duct, mixed macro, microcystic Brach duct: cluster of grapes	High
Solid pseudopapillary neoplasm	Body	Strongly female	Solitary	Encapsulated, mixed solid and cystic	Moderate
Cystic endocrine tumor	Tail	Equal	Solitary	Variable	Variable based on type

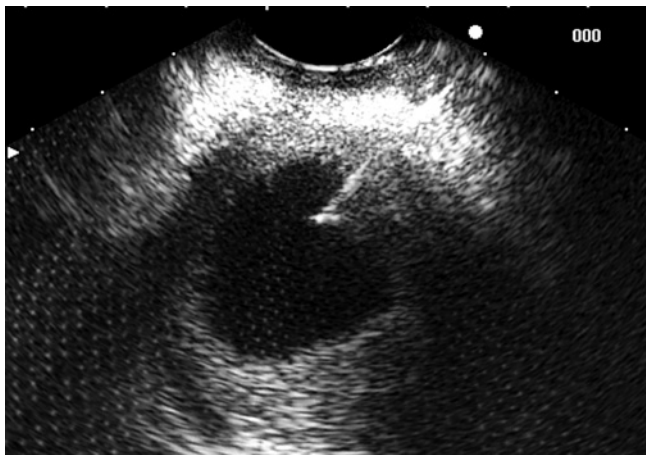

Figure 25.1 Thick-walled cystic lesion undergoing fine needle aspiration (FNA). The lesion was resected and was a pseudocyst.

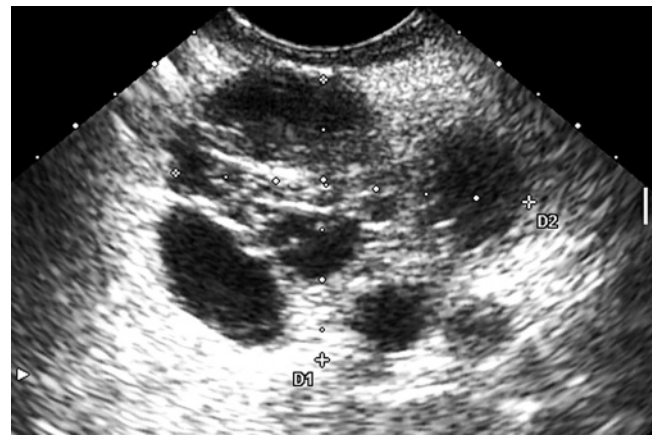

Figure 25.2 Serous cystadenoma. Multicystic lesion in the body of the pancreas with microcystic and macrocystic components and a central scar. The overall size is 2.8 × 3.5 cm.

cuboidal cells with glycogen-rich cytoplasm and dense chromatin.

Mucinous lesions

Mucinous cystic neoplasms (MCN) are a distinct type of mucinous cyst (Figure 25.3a). They occur almost exclusively in women when they are defined by the presence of ovarian stroma. These tumors are principally located in the tail of the pancreas and mucin may be visible within the cyst cavity (Figure 25.3b). Malignant MCNs may have a mural nodule or mass apparent on EUS (Figure 25.3c). Depending on the degree of cellular atypia, MCNs are classified as adenomas, borderline tumors, or carcinomas. The cysts do not communicate with the pancreatic ductal system and the cyst fluid generally contains mucin and a high concentration of CEA.

Intraductal papillary mucinous neoplasm (IPMN) (Figure 25.4a) generally presents in the seventh decade of life. It can be divided into morphologic subtypes: main duct IPMN, branch duct IPMN, and mixed. Main duct IPMN carries a much greater likelihood of malignancy than branch duct IPMN. The characteristic imaging features of branch duct IPMN include multilocular appearance with a cluster of grapes configuration, communication with the pancreatic duct, and dilated ductal structures with filling defects representing mucus. In addition, a dilated main pancreatic duct, cyst size >3.0 cm and mural nodularity are features of IPMN predict an increased likelihood of malignancy (Figure 25.4b,c).

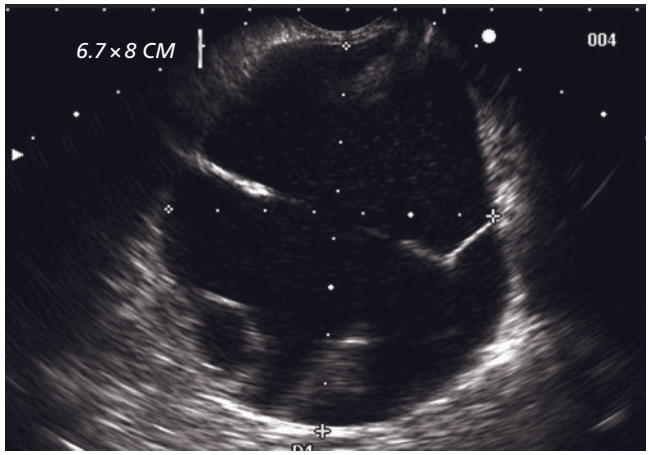

(a)

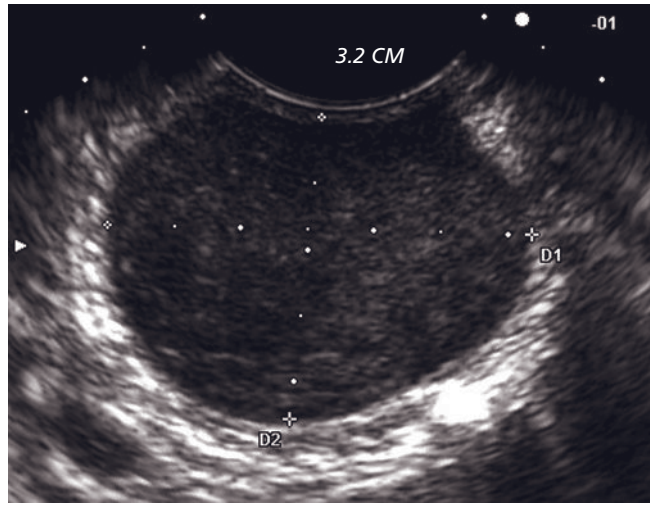

(b)

(c)

Figure 25.3 (a) Mucinous cystic neoplasm with multiple septations. The lesion was benign when surgically resected. (b) Mucinous cystic neoplasm with mucin visible within the cyst cavity. (c) A 1.5 cm malignant cystic lesion with mucin and debris in the lumen of the cyst.

Other cystic neoplasms

Solid pseudopapillary epithelial neoplasm (SPEN) usually occurs in young women. Though this lesion is rare, recognition is important given its malignant potential and very high cure rate with surgical resection. It is typically large with solid and cystic features. Fine needle aspiration cytopathology may demonstrate branching papillae and myxoid stroma.

Pancreatic cystic endocrine tumors have a male to female ratio of 1:1 with a peak incidence in the fifth and sixth decades. Cystic neuroendocrine tumors often have a thick wall (Figure 25.5a). Given their high degree of vascularity, EUS with color flow Doppler may demonstrate increased blood flow within these lesions (Figure 25.5b).

Ductal adenocarcinoma can also present with cystic morphology as a result of tumor necrosis. As with solid adenocarcinoma of the pancreas, there is a male predominance, and the typical age of onset is late 60s to early 70s. Endoscopic ultrasound may demonstrate mixed solid-cystic mass with resultant ductal obstruction and possible invasion of adjacent structures.

Chapter video clip

Video 25.1 Pancreatic cystic lesions.

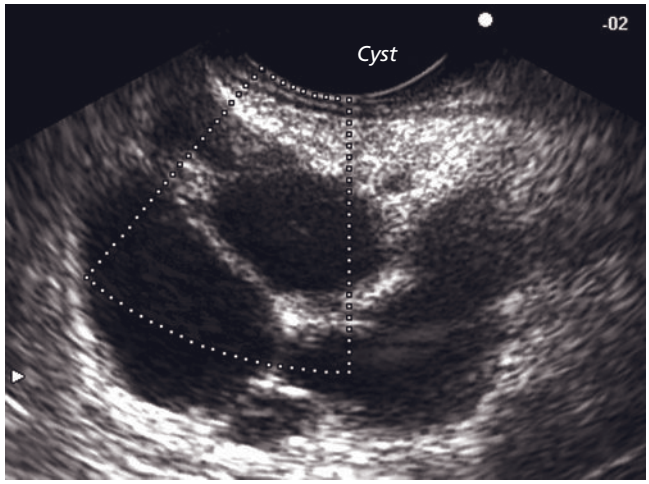

(a)

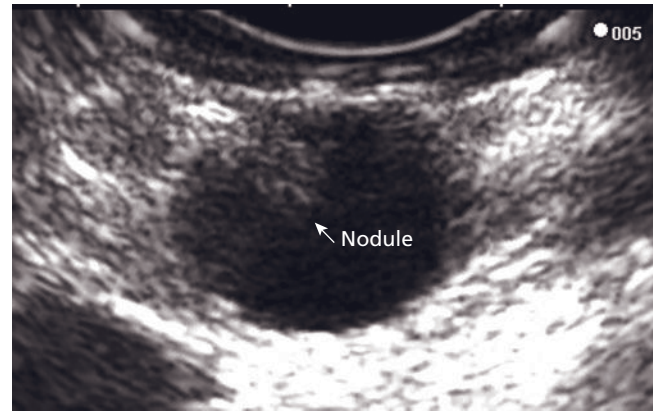

(b)

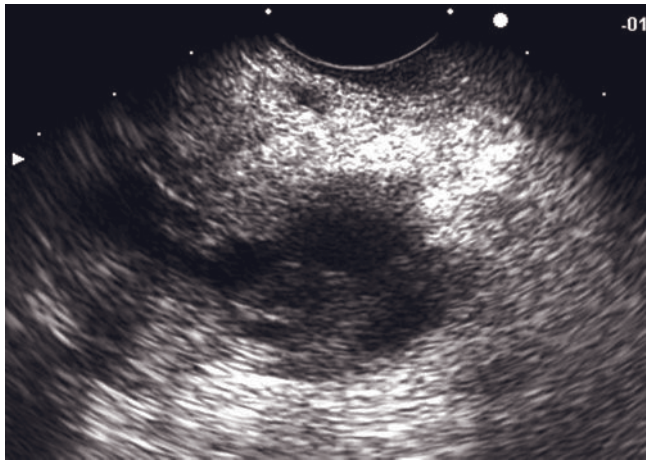

(c)

Figure 25.4 (a) Thinly septated intraductal papillary mucinous neoplasm (IPMN) in the head of the pancreas. (b) IPMN with mural nodule suggestive of malignancy. (c) Malignant IPMN with thick wall and large nodule.

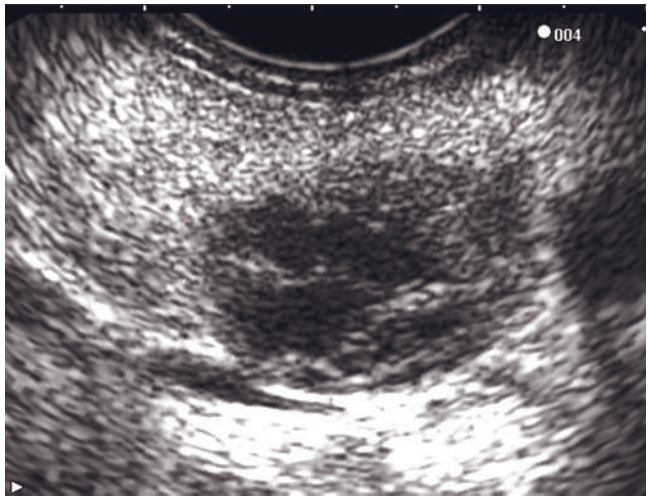

(a)

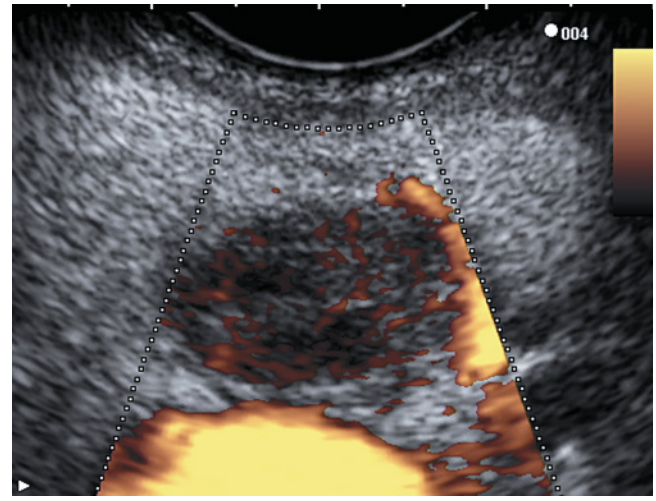

(b)

Figure 25.5 (a) Pancreatic cystic endocrine tumor. Note the presence of the thick wall and complex septations. (b) Pancreatic endocrine tumor. Color flow Doppler demonstrates hypervascularity within the solid portions of the mass.

26 Intraductal Papillary Mucinous Neoplasms: The Role of EUS

William R. Brugge
Massachusetts General Hospital and Harvard Medical School, Boston, MA, USA

Introduction

Intraductal papillary mucinous neoplasms (IPMNs) have emerged as the most common mucinous cystic neoplasm and represent a significant clinical entity. Endoscopic ultrasound (EUS) is an important tool for the diagnosis and management of IPMNs.

IPMNs represent a premalignant pancreatic lesion generally characterized by proliferation of the mucinous epithelium with varying degrees of ductal and cystic dilatation. These papillary lesions typically involve the main pancreatic duct with or without side branch involvement. Based on the differential location of the tumor, they can be classified into three types: branch duct IPMN, main duct IPMN, and mixed IPMN. IPMNs can further be described according to a continuum of cellular atypia similar to that of colorectal cancer: benign (adenoma/low-grade dysplasia), borderline (moderate dysplasia), and malignant (ranging from carcinoma in situ/high-grade dysplasia to invasive carcinoma).

Several studies have suggested that main duct IPMNs are associated with higher grade of histology and more rapid growth, compared with branch duct lesions, which are felt to represent more indolent disease. The exact rate of cell transition from benign to malignant is not clear, although the progression to invasive disease in main duct IPMN has been estimated to range from 5 to 7 years. There have been estimates of the rate of malignant degeneration ranging from 0.5 to 1.0% per year. Overall, invasive carcinoma arising in association with IPMN has a better prognosis than conventional ductal adenocarcinoma; however, when metastatic, its prognosis is as poor as that of pancreatic adenocarcinoma.

Clinical features

Symptoms for IPMN are vague and often non-specific, and most patients are asymptomatic, especially those with small (≤3 cm) lesions. When symptomatic, patients usually present with abdominal pain which may represent recurrent pancreatitis. Patients commonly present in the sixth to seventh decade, with the mean age at diagnosis being 65 years.

Obvious main duct lesions are more likely to present with symptoms masquerading as chronic pancreatitis and other features. Gradual distension of the pancreatic duct due to excess mucin secretion induces recurrent abdominal pain and symptoms of pancreatitis secondary to main duct IPMN. Due to the presentation and appearance, IPMNs have in fact been misdiagnosed as chronic pancreatitis in the past.

Role of imaging

Multiple modalities can be used to image and stage IPMNs, including computed tomography (CT), magnetic resonance cholangiopancreatography (MRCP), endoscopic ultrasound (EUS), and endoscopic retrograde cholangiopancreatography (ERCP). Using any one of the modalities can provide diagnostic features, evidence of malignancy, and staging information.

Cross-sectional imaging

The resolution of multi-detector CT (MDCT) has improved dramatically in the past years. The quality of the digital displays provides excellent imaging of the pancreas and the ductal system. Communication between a cystic branch duct lesion and the main duct is well-visualized on thin-section MDCT. With these improvements, CT provides excellent imaging of IPMN including important features such as septations and nodules (Figure 26.1).

MRCP has also evolved rapidly in the imaging of the pancreas. Breath-hold MRCP is less dependent upon patient cooperation. Studies have shown this technique to be even

Atlas of Endoscopic Ultrasonography, First Edition. Edited by Frank G. Gress, Thomas J. Savides, Brenna Casey Bounds, John C. Deutsch.

more effective in detecting connections with the main pancreatic duct than MDCT (Figure 26.2). The use of intravenous secretin improves the quality of MRCP and visualization of the extent of duct involvement. For IPMN evaluation, whether MDCT or MRCP is used, a dedicated pancreatic imaging protocol should be adhered to.

Endoscopic ultrasound evaluation

Endoscopic ultrasound evaluation can be particularly helpful if there is diagnostic uncertainty, although it is not the preferred first-line imaging modality for IPMN. It is also helpful in cases where surgical risk is high, and verification of malignancy is needed before resection, such as in older patients or those with high comorbidities.

Endoscopic ultrasound can provide detailed imaging of main duct IPMN, side branch disease, and combined duct disease.

The EUS findings of IPMN include cystic lesions, a dilated main pancreatic duct, and/or a parenchymal mass (Figures 26.3–26.5). The diagnosis is usually readily made once multiple cystic lesions have been demonstrated. However, the findings of a viscous fluid during fine needle aspiration (FNA) will confirm the diagnosis. With the diagnosis established, attention should turn towards detection of malignancy. The most obvious targets are a dilated main duct, a nodule arising within a cyst, and a pancreatic mass

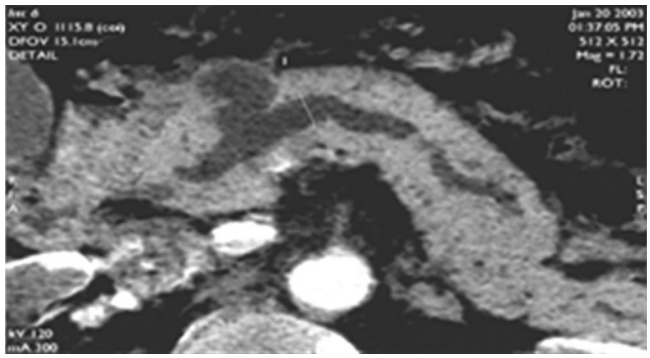

Figure 26.1 Reformatted computed tomography (CT) scan demonstrating a side branch intraductal papillary mucinous neoplasm (IPMN).

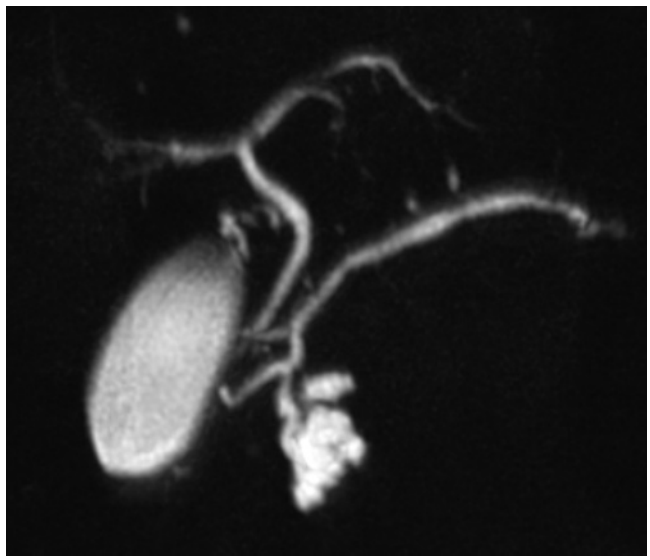

Figure 26.2 Magnetic resonance cholangiopancreatography (MRCP) demonstrating a side branch intraductal papillary mucinous neoplasm (IPMN) in the head of the pancreas.

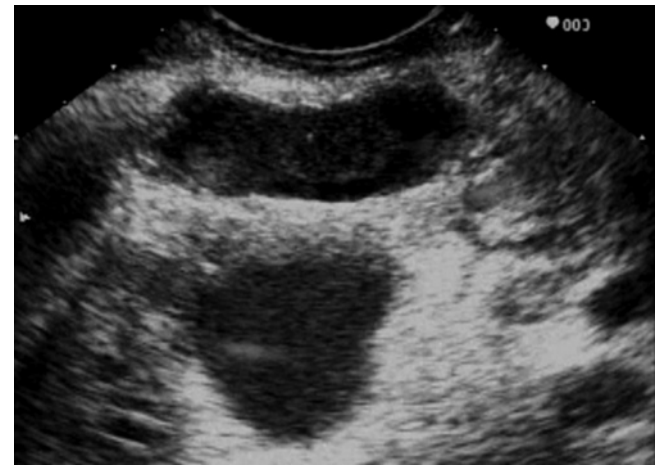

Figure 26.3 Linear endoscopic ultrasound (EUS) image demonstrating a dilated main pancreatic duct, indicative of a main duct intraductal papillary mucinous neoplasm (IPMN).

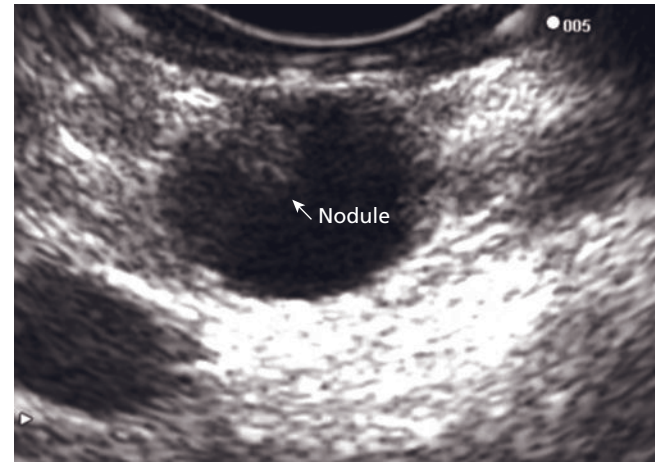

Figure 26.4 Linear endoscopic ultrasound (EUS) image revealing a small cystic lesion with a mural nodule.

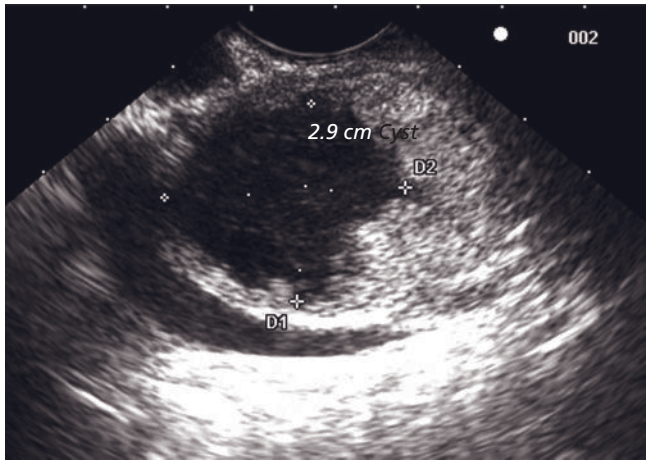

Figure 26.5 Linear endoscopic ultrasound (EUS) image of a malignant appearing 2.9 cm cystic lesion, including an adjacent mass.

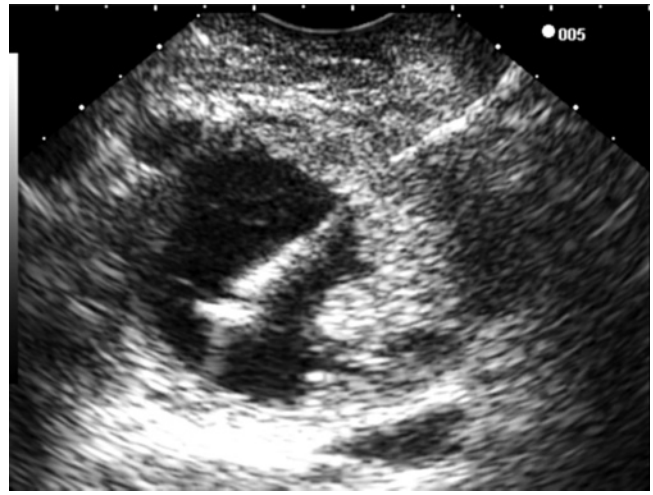

Figure 26.6 Fine needle aspiration (FNA) of a malignant cystic mass.

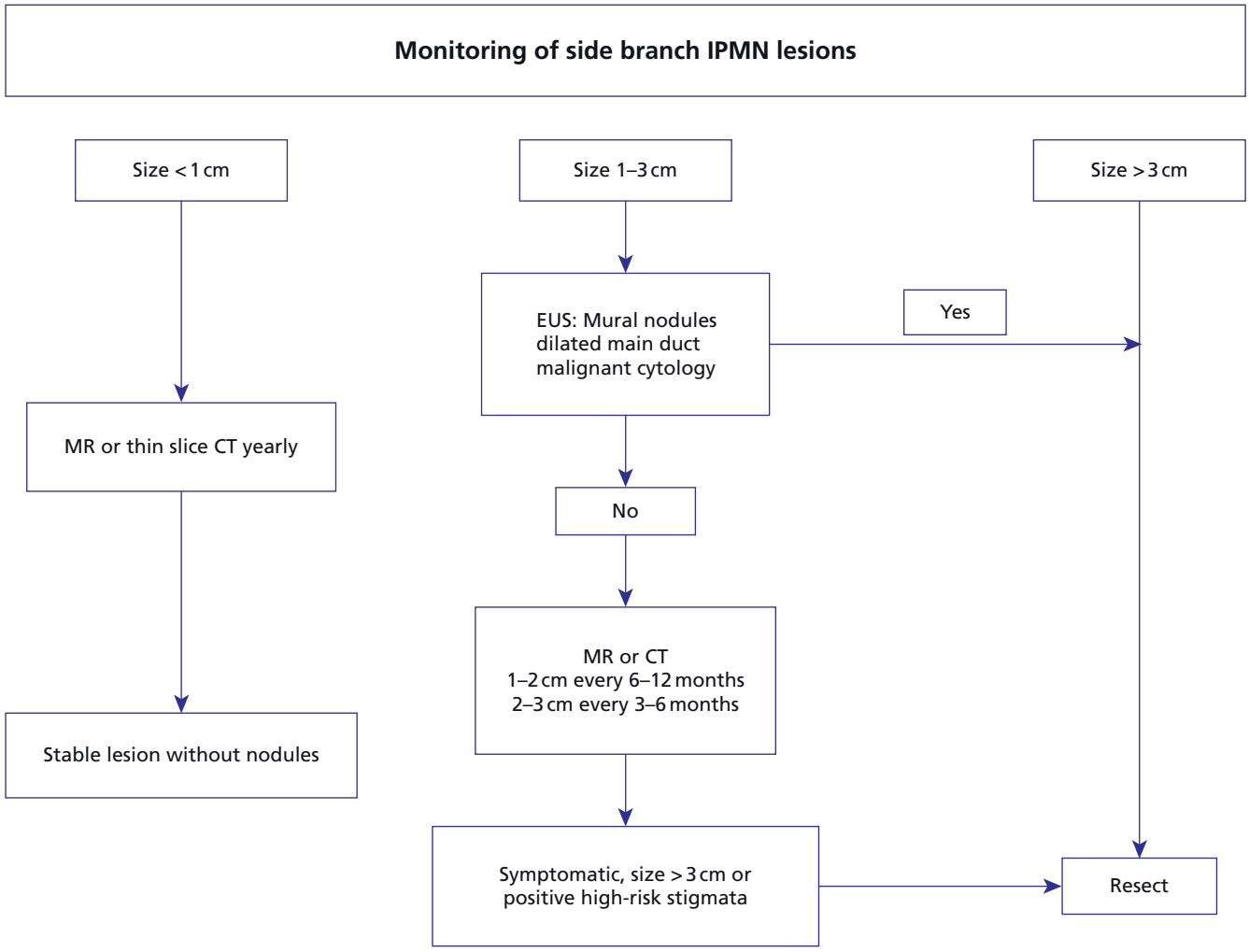

Figure 26.7 International Association of Pancreatology (IAP) algorithm for management of intraductal papillary mucinous neoplasm (IPMN).

(Figure 26.6). Of course, signs of metastatic disease such as liver metastases, lymphadenopathy, and ascites are very important findings. Fine needle aspiration of the main pancreatic duct is performed with a 22-gauge needle usually from the gastric body. Pancreatic duct juice is readily aspirated from the main duct. Care should be taken in the aspiration of nodules, because of the risk of bleeding and contaminating the cytologic specimen. The results of FNA should be used to assist in the planning of resection. For example, in the presence of multiple cysts, representative lesions in the head, body, and tail should be used to determine the type of resection.

Cytologic material from aspiratants is often inconclusive for IPMN. However, cyst fluid tumor markers, such as carcinoembryonic antigen (CEA) and cancer antigen 72–4, are important for establishing the mucinous origin of the cyst. KRAS is also a very useful marker for a mucinous lesion. The diagnosis of malignancy is usually established with the finding of malignant cytology, aspirated from a cyst, nodule, or mass.

Management of small IPMN (≤3 cm)

Many IPMNs need not be resected and can be followed conservatively due to their low risk for malignancy and slow progression toward invasive cancer. These include IPMNs without symptoms, without main duct dilatation (>6 mm), without mural nodules, without thick walls/septations, or <3 cm in size. Consensus follow-up guidelines have been formulated by the International Association of Pancreatology (IAP): yearly follow up is recommended for lesions <1 cm in size; follow up every 6–12 months is advisable for 1–2 cm lesions; and for lesions >2 cm, 3–6 monthly follow up is indicated (Figure 26.7).

If symptoms arise, or if any of the above limits regarding size, dilatation, or solid components are surpassed on follow up, resection is suggested. A >1 cm increase in lesion size over a year is generally considered significant for malignancy. If minimal or no change is observed after two years, then the time frame between follow-up studies can be extended. An algorithm for observing small (≤3 cm) IPMN has been proposed.

When deciding which modality to use, follow-up imaging should be tailored further by considering radiation concerns relative to age. It may be advisable to monitor IPMN patients who are <40 years old with MR and those who are >40 years old with CT. Steps should still be taken to minimize radiation risk since the cumulative exposure from prolonged and repeated radiological follow up may be substantial.

Chapter video clip

Video 26.1 How to perform cyst FNA.

Video 26.2 Intraductal papillary mucinous neoplasms.

27 Chronic Pancreatitis

David G. Forcione
Massachusetts General Hospital and Harvard Medical School, Boston, MA, USA

Introduction

Chronic pancreatitis is defined by irreversible morphologic changes of the pancreas often associated with abdominal pain, and in late stages, endocrine and exocrine insufficiency. Data from the United States and Japan have demonstrated that as many as 3% of US male veterans and 17% of Japanese individuals may be affected. In addition to being associated with significant medical morbidity, care of patients with chronic pancreatitis is costly, with estimates of over 2 billion dollars per year in the United States for the over 100 000 outpatient and 50 000 inpatient annual visits.

As with other diseases, early diagnosis offers a better a chance of effective treatment outcomes. Since Sivak's original description of the use of endoscopic ultrasound (EUS) to evaluate chronic pancreatitis in 1986, there has been increasing interest and data demonstrating the utility of this imaging modality for early diagnosis. The close proximity of the upper gastrointestinal tract to the pancreas provides endosonographers with an ideal imaging modality of the pancreas. In general, EUS appears safer than endoscopic retrograde cholangiopancreatography (ERCP). Furthermore, there is increasing data that both ductal and parenchymal changes of the pancreas associated with chronic pancreatitis may be seen earlier and more accurately with EUS as compared with conventional cross-sectional imaging modalities. Advances in EUS imaging such as sonoelastography and contrast-enhanced EUS are expected to improve the overall accuracy of the examination. Preliminary data using combined contrast-enhanced EUS and real-time sonoelastography demonstrates these modalities may further improve our ability to discern chronic pancreatitis from pancreatic neoplasia.

Threshold diagnostic criteria and interobserver variability are both common issues that may arise when any imaging modality is the predominant diagnostic tool for a specific disease entity. Chronic pancreatitis is particularly challenging given that the gold standard way of diagnosis (i.e. histology) is rarely feasible. Furthermore, EUS is particularly susceptible as an imaging modality to these given the potential subjective nature of the examination. In the past two years, the EUS community has come closer to reducing the potential for this variability through the development of a specific EUS-based criteria. The Rosemont Criteria (2009) is a significant step forward towards unifying the role of EUS in diagnosing chronic pancreatitis.

In this chapter, we will review the utility of EUS as an imaging modality for chronic pancreatitis.

Clinical overview of chronic pancreatitis

The classification and diagnosis of chronic pancreatitis has evolved since the Marseilles conference of 1963 first established the histopathologic paradigm of fibrosis, inflammation, loss of exocrine parenchyma, ductal dilation, and stones. It soon became clear, however, that conventional radiologic diagnosis (transabdominal ultrasound [TUS], computed tomography [CT], magnetic resonance imaging [MRI]) was best suited for diagnosing advanced disease and may not have sufficient accuracy for early or mild chronic pancreatitis.

The role of ERCP was incorporated in 1984 by the Cambridge Classification. The Cambridge Classification incorporates features of both the main pancreatic duct and side branch, including dilation and ductal ectasia, to assess the severity of chronic pancreatitis. Although ERCP appeared to be more accurate than conventional cross-sectional imaging at identifying chronic pancreatitis through ductal changes, it continues to be seen as an imaging modality with limited predictive value. As noted with histopathology, autopsy series have demonstrated age-related ductal changes of chronic pancreatitis without associated symptoms.

Atlas of Endoscopic Ultrasonography, First Edition. Edited by Frank G. Gress, Thomas J. Savides, Brenna Casey Bounds, John C. Deutsch.

Furthermore, as an invasive examination with potential morbidity, the role ERCP for the diagnosis of early or mild chronic pancreatitis remains to be well established.

Pancreatic function testing (PFT) remains an option for the diagnosis of chronic pancreatitis. Currently, this is performed using standard upper endoscopy and secretin stimulation of the exocrine pancreas. Duodenal aspirates are obtained for bicarbonate and enzymatic (lipase) measurements. Some have incorporated PFT in the diagnostic criterion for chronic pancreatitis Nonetheless, the role of PFT remains uncertain due to limited availability, patient intolerance, and uncertain validation across larger, more diverse patient populations. Furthermore, patients may have exocrine changes without associated morphologic changes and it is unclear if these patient subsets truly have chronic pancreatitis.

The gold standard for the diagnosis of chronic pancreatitis remains histopathology. Typical morphologic changes include chronic inflammation, fibrosis, and glandular atrophy. These findings may be uniform or patchy in the pancreas. Autopsy series have identified "asymptomatic/normal" individuals with significant atrophy and fibrosis. Furthermore, variation in pathologist interpretation of these findings adds to the potential difficulties in accurate diagnosis using these criteria.

There is increasing data that a wide array of insults may be associated with the development of chronic pancreatitis. Whitcomb *et al*. established the TIGAR-O classification in 2001 to incorporate the roles of Toxic (ethanol), Idiopathic, Genetic (SPINK-1, PRSS, and CFTR), Autoimmune, Recurrent severe acute pancreatitis, and Obstructive etiologies. All of these entities should be carefully considered in patients being evaluated for chronic pancreatitis. Despite an exhaustive search, the etiology remains idiopathic in up to 20% of patients.

Endoscopic ultrasound imaging of the normal pancreas

In order to best understand the role of EUS in imaging of chronic pancreatitis, it is useful to review some of the fundamentals of normal pancreas imaging with EUS. Data from large series of "normal" TUS and EUS examinations from the 1990s have provided some useful imaging parameters.

Wiersema *et al*. characterized the normal pancreas parenchyma to have uniformly echogenicity, typically brighter than the liver. The mean ductal diameters were 2.4 mm in the head (range 0.8–3.6 mm), 1.8 mm in the body (0.9–3.0 mm), and 1.2 mm in the tail (0.5–2.0 mm). Catalano *et al*. made endosonographic observations of the pancreas in 25 "normal" patients. The normal pancreas parenchyma was described to be homogeneous with identification of variable echotexture separating the ventral and dorsal anlage of the pancreas in 68%. The mean ductal diameter in the body was 1.7 mm (range 1–3 mm), and side branches could be appreciated in 32%.

Some studies have also provided some interesting insight into the wide spectrum of findings that may be seen in otherwise healthy individuals. A large TUS series from Japan (130 951 patients) identified that pancreatic duct dilation (>3 mm) may be seen in 0.49% of individuals and tended to be found in older men. In addition, calcifications and cysts were found in 0.05% and 0.22% of patients, respectively.

In summary, these data provide endosonographers with a basic framework for normal parenchymal and ductal imaging and set the basis for establishing some threshold criteria for the diagnosis of chronic pancreatitis.

EUS imaging in chronic pancreatitis – historical perspectives

Since the original description of the role of EUS imaging in chronic pancreatitis by Sivak in 1986, a number of studies have tried to define appropriate criteria for diagnosis. Early classifications incorporated nine criteria for chronic pancreatitis, including five parenchymal and four ductal. These data were almost exclusively derived using radial EUS imaging performed by experts in academic practices. The parenchymal changes included hyperechogenic foci, hyperechogenic strands, lobulation, cysts, and calcifications. Histopathologic correlates of the former three were felt to represent focal fibrosis and glandular atrophy. Ductal changes included a dilated main pancreas duct (>3 mm head, >2 mm body, >1 mm tail), ductal irregularity ("chain of

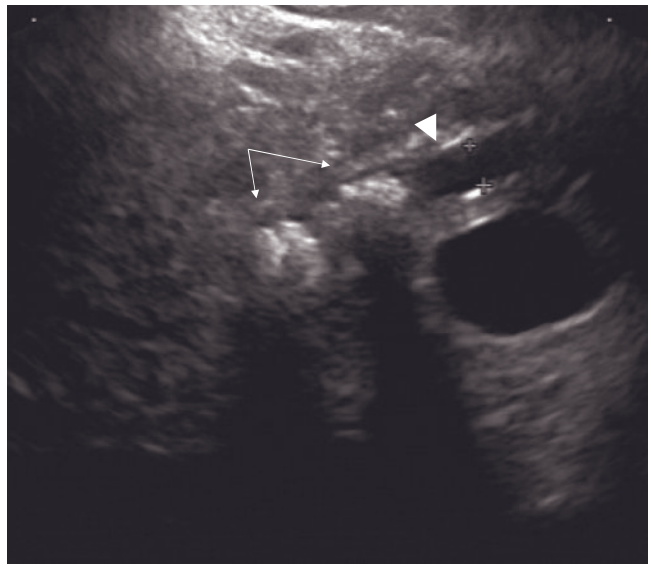

Figure 27.1 Endoscopic ultrasound (linear) showing features of chronic pancreatitis: a dilated pancreatic duct (arrow head) and two intraductal stones (arrows).

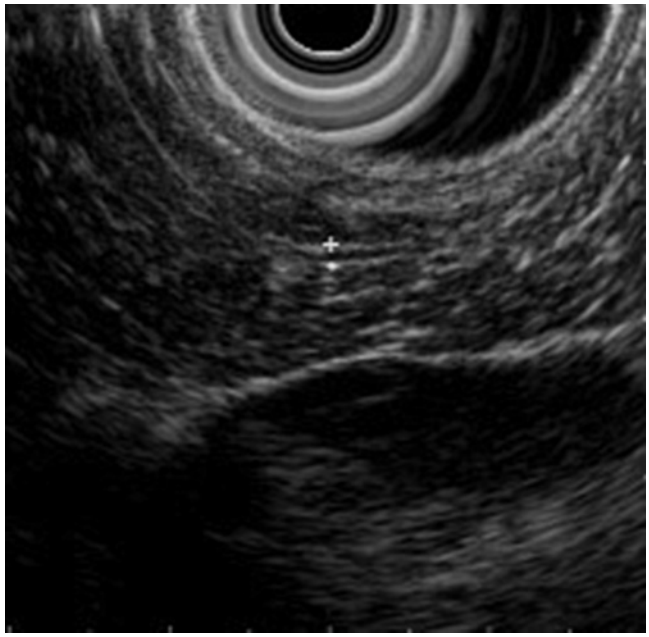

Figure 27.2 Endoscopic ultrasound showing a hyperechoic duct wall (crossmark) in chronic pancreatitis.

lakes" appearance), hyperechoic ductal margins, and side branch ectasia (Figures 27.1 and 27.2).

Clearly, the number of threshold criteria selected will determine how sensitive and specific the imaging test may be – fewer (<2) threshold criteria are associated with higher sensitivity but lower specificity, and more (>6) are associated with a lower sensitivity and higher specificity. Since these criteria were developed, several studies have been done to define the appropriate threshold criteria. Initial attempts at this defined chronic pancreatitis to be "unlikely" if 0/9 criteria were noted, "likely" if >5/9 were noted, and "uncertain" if between 1 and 5 criteria were noted.

Both comparative and receiver operator curve studies have been done to further define the role of EUS and the number of threshold criteria. Stevens *et al*. compared EUS and ERCP with a threshold of six criteria and found statistical equivalence with ERCP in terms of sensitivity and specificity (68%, 79%, respectively). The authors also considered secretin stimulation pancreatic function testing (SS-PFT). This did not appear to add to the diagnostic accuracy over ERCP and EUS. Furthermore, SS-PFT was felt to be not widely available and potentially inconvenient for patients. Varadarjulu *et al*. evaluated patients with non-calcific chronic pancreatitis going to surgery and identified >4 EUS criteria as 91% sensitive and 86% specific for the diagnosis. Pungapong *et al*. identified the combination of EUS and secretin stimulated magnetic resonance cholangiopancreatography (MRCP) to have a very high sensitivity and specificity at 98% and 100%, respectively. These authors also identified pancreatic juice interleukin-8 levels (after secretin stimulation) to add diagnostic value. Finally, over the last five years, it also has become clear that age and other factors (gender, alcohol use, tobacco, body mass index) may affect the diagnostic threshold and that certain criteria, such as calcifications, may carry greater weight towards a diagnostic endpoint.

As noted, histopathology remains the diagnostic gold standard for chronic pancreatitis. Unfortunately, this is rarely available outside of surgical or autopsy specimens. Biopsy techniques of the pancreas are limited by the often patchy nature of chronic pancreatitis, safety, availability, and limited tissue acquisition. Linear echoendoscopy provides an opportunity to perform biopsy (fine needle aspiration [FNA] for cytology and core biopsy for histology) of the pancreas using a transgastric or transduodenal technique, and this option has been evaluated for chronic pancreatitis. Hollerbach *et al*. evaluated EUS-FNA in 27 patients with suspected chronic pancreatitis and found a surprisingly high specificity of 67%. Dewitt *et al*. evaluated the use of EUS Tru-cut biopsy for core specimen acquisition in 16 patients with chronic pancreatitis. In this study, diagnostic confirmation was achieved in 5.6%. Fourteen of sixteen were either normal or non-diagnostic and one was associated with equipment malfunction. The authors noted a complication frequency of 11%, including acute pancreatitis and pain requiring hospitalization in two patients. The overall kappa value in this study was only 0.25. At this time, the role of EUS-FNA or Tru-cut biopsy remains uncertain and limited by accuracy and technical factors (safety and availability).

EUS imaging in chronic pancreatitis – the Rosemont Criteria

Over the last decade, the true role of EUS for the diagnosis of chronic pancreatitis has been hampered by a number of factors including interobserver variability, lack of standardization in technique, and nomenclature. There has also been disagreement in the number and appropriate validaton of threshold criteria. Furthermore, expense and availability of EUS has limited its impact for routine use in chronic pancreatitis.

In 2007, a group of 37 expert endosonographers from North America and Japan convened in Rosemont, Illinois to review the literature and develop updated diagnostic criteria using EUS for chronic pancreatitis. The group evaluated three areas: parenchymal criteria, ductal criteria, and correlation with histology, and, from these, established an EUS-based diagnostic system. For the first time, attention was also placed on relative weight of various factors (i.e. major and minor criterion, and rank). Consensus for criteria was established when greater than two-thirds agreement was found. It is important to note that similar to previous classification systems, the criteria were based on radial EUS

Table 27.1 The Rosemont Criteria (adapted from Catalano *et al. Gastrointestinal Endoscopy,* 2009).

Features	Definition	Location	Major criteria Minor criteria		Rank	Histologic correlate
Parenchymal						
Hyperechoic foci with shadowing	Echogenic structures >2 mm in length and width that shadow	Body, tail	Major A		1	Parenchymal Calcifications
Lobularity	Well circumscribed, >5 mm Structures with enhancing rim and relatively echo-poor center				2	Unknown
A. With honeycombing	Contiguous >3 lobules	Body, tail	Major B			
B. Without Honeycombing	Non-contiguous lobules	Body, tail		Yes		
Hyperechoic foci wthout shadowing	Echogenic structures/foci >2 mm in both length and width without shadowing	Body, tail		Yes	3	Unknown
Cysts	Anechoic round/elliptical structures without septations	Head, body, tail		Yes	4	Pseudocysts
Stranding	Hyperechoic lines >3 mm in length in at least 2 different directions	Body, tail		Yes	5	Unknown
Ductal						
MPD calculi	With acoustic shadowing	Head, body, tail	Major A		1	Stones
Irregular MPD	Uneven or irregular MPD	Body, tail		Yes	2	Unknown
Dilated side branches	>3 tubular anechoic structures each >1 mm width budding from MPD	Body, tail		Yes	3	Side branch ectasia
MPD dilation	>3.5 mm body, or >1.5 mm tail	Body, tail		Yes	4	MPD dilation
Hyperechoic MPD margin	Echogenic, distinct structure >50% entire MPD	Body, tail		Yes	5	Ductal fibrosis

imaging. This classification system (denoted the "Rosemont Criteria") was formally published in *Gastrointestinal Endoscopy* in 2009.

The Rosemont Criteria are demonstrated in Table 27.1. Many of the previously described criteria were again found to be important imaging characteristics in diagnosing chronic pancreatitis. Hyperechoic foci with shadowing, cysts, and intraductal calculi were felt to be relevant if found anywhere in the pancreas, whereas all other findings required demonstration in the body and/or tail. After an extensive review of the literature and consensus discussions, the overall kappa for findings in this group of experts was quite good (>0.7). Some of the advantages of the Rosemont Criteria include differential weighting, stricter definitions, and a four-level diagnostic stratification (Table 27.2).

Table 27.2 The Rosemont diagnostic stratification (adapted from Catalano *et al. Gastrointestinal Endoscopy,* 2009).

Stratum	Criteria
Consistent with chronic pancreatitis	1 major A + >3 minor features 1 major A feature + a major B feature 2 major A features
Suggestive of chronic pancreatitis	1 major A feature + <3 minor features 1 major B feature + >3 minor features >5 minor features
Indeterminate of chronic pancreatitis	3 or 4 minor features, no major features Major B alone or with <3 minor features
Normal	<3 minor features*, no major features

*Except non-shadowing foci, cysts, main pancreas duct dilation, and dilated side branches.

Since the publication of the Rosemont Criteria in 2009, one multi-center comparison study has been reported evaluating standard criteria versus Rosemont Criteria for chronic pancreatitis (Stevens *et al.*). In this study, 50 video clips (all radial EUS) were evaluated by 14 experts, equally divided into those with extensive experience (>1000 cases) and those with moderate experience (500–999 cases). In this series of clips, 13 had established chronic pancreatitis. The standard criteria threshold was >4/9 findings. Interestingly, the use of the Rosemont Criteria did not significantly increase interobserver agreement for EUS diagnosis of chronic pancreatitis compared with standard scoring. One would therefore conclude that high interobserver agreement is critical for the reliability of any diagnostic test.

The Rosemont Criteria have initiated important steps in the right direction for the EUS diagnosis of chronic

pancreatitis – a common nomenclature. Ideally, the system will be further validated in larger patient populations prospectively and against the gold standard, which is histopathology.

Endoscopic ultrasound imaging in chronic pancreatitis – the future

The utility of EUS as a diagnostic modality for chronic pancreatitis holds great promise. Improvements in imaging quality will continue to evolve. Additional studies are clearly necessary to validate the Rosemont Criteria. Minimally invasive ways of pancreatic tissue acquisition will likely develop and will be an important part of the evaluation of these patients. As with many other complex diseases where tissue acquisition is challenging, multimodal evaluation may be optimal. It is likely that combination evaluation with high resolution EUS imaging, secretin stimulated MRCP, and exocrine function testing will provide the most accurate means of morphologic and physiologic assessment.

Chapter video clips

Video 27.1 Chronic pancreatitis.

Video 27.2 Pancreatic duct stones.

28 Liver Pathology

Indraneel Chakrabarty and Ann Marie Joyce
Tufts University School of Medicine and Lahey Clinic Medical Center, Burlington, MA, USA

Introduction

The most common liver pathology seen using endoscopic ultrasonography (EUS) includes cirrhosis, fatty liver, hepatic cysts, and neoplasms. Dilated intrahepatic, extrahepatic, and common bile ducts with or without stones are often seen as well. Endoscopic ultrasonography of the liver can be frustrating as it is often difficult to determine if the liver was viewed in its entirety depending on the patient's body habitus and anatomy. For optimal imaging, the echoendoscope should be set to the lowest possible frequency for maximal hepatic penetration. There are three primary positions for viewing the liver. The duodenal bulb is the best position to evaluate the right lobe of the liver. The balloon over-inflation technique can be used to help lock the scope into the duodenal bulb. From here the scope should be advanced and withdrawn and torque clockwise and counterclockwise accordingly for maximal views of the right lobe. This should be repeated until the ultrasonographer feels that he or she has viewed the liver to the best of their ability given the patient's size and anatomy. After completion of this exam, the balloon should be deflated and the scope positioned in the antrum. This will give views of both the right and left hepatic lobes. The same technique of torque and advancing the scope forward and backwards should be applied until all views of the liver have been exhausted. The last position is the gastric fundus, which gives optimal views of the left hepatic lobe. It is usually initiated from the gastroesophageal (GE) junction using the same techniques as in the latter position until all views are achieved to the ultrasonographer's satisfaction. The endosonographic description of liver pathology will be reviewed in this chapter.

Cirrhosis

The two leading causes of cirrhosis in the United States is alcohol abuse followed by hepatitis C. Combined they are the twelfth leading cause of death in the United States as of 2000, accounting for over 25 000 deaths. In addition, approximately 75–85% of acutely infected hepatitis C individuals progress to chronic infection, with up to 20% developing cirrhosis over 20–25 years. Other etiologies include hepatitis B, non-alcoholic steatohepatitis, primary biliary cirrhosis, primary sclerosing cholangitis, autoimmune hepatitis, hereditary hemochromatosis, Wilson's disease, and alpha 1-antitrypsin deficiency. All patients with cirrhosis are at increased risk of developing hepatocellular carcinoma. In general, cirrhosis is characterized by the replacement of normal hepatic tissue with permanent scar tissue which leads to disruption of organ function and blocks portal blood flow through hepatic parenchyma leading to the various clinical features of cirrhosis. This scar tissue can often be visualized under EUS as nodular tissue characterized by coarse diffuse heterogeneous echoic parenchyma (Figure 28.1a). The outer wall of the liver often loses its smooth border and can appear irregular or nodular (Figure 28.1b). One of the complications related to cirrhosis is ascites. Ascites can be seen as anechoic areas adjacent to intra-abdominal organs (Figure 28.1c). A sample of the fluid can be obtained through a fine needle aspiration (FNA).

Fatty liver disease

Fatty liver disease (FLD) is an accumulation of large vacuoles of triglyceride or fat within the hepatic parenchyma via the

Atlas of Endoscopic Ultrasonography, First Edition. Edited by Frank G. Gress, Thomas J. Savides, Brenna Casey Bounds, John C. Deutsch.

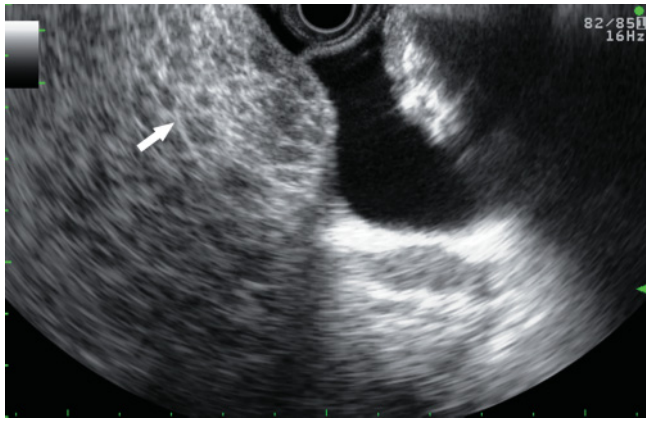

(a)

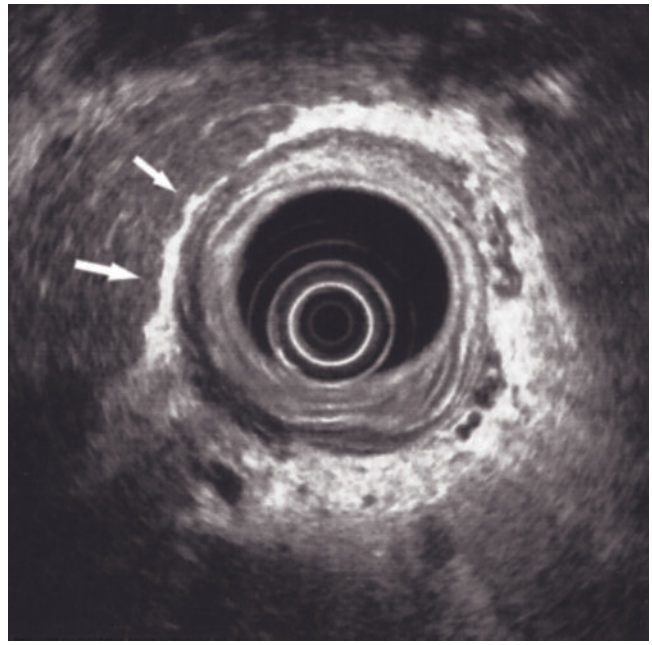

(b)

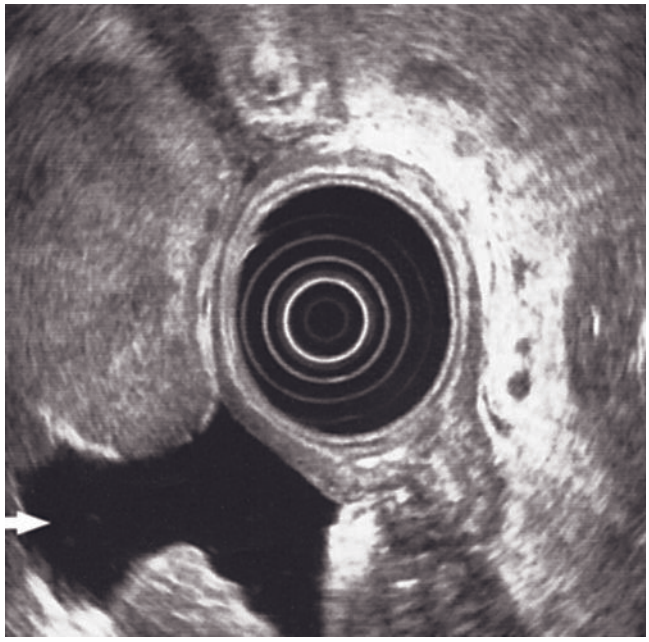

(c)

Figure 28.1 (a) Cirrhosis. The cirrhotic liver is characterized by diffuse coarse nodular heterogeneous echoic parenchyma (arrow). (b) Cirrhosis with nodular surface. The smooth border of the liver is often lost in cirrhotics and can appear irregular or nodular as in this image (arrows). (c) Cirrhosis with ascites. Ascites is often seen in cirrhotics as anechoic regions surrounding intrabdominal organs (arrow).

process of steatosis and is normally reversible. This deposition can often be seen via EUS and is described as hyperechoic or bright parenchyma secondary to fat deposition when compared to normal parenchyma (Figure 28.2). It is usually diffuse but can also be seen in patches as in focis of hyperechoic parenchyma surrounded by normal echoic parenchyma. There are multiple causes for fatty liver, the most common being alcohol abuse (alcoholic fatty liver disease or AFLD) and non-alcoholic fatty liver disease (NAFLD) such as from obesity with or without diabetes. Consequently FLD is very common in the United States, and it can be difficult to distinguish between AFLD and NAFLD without a proper history. Chronic AFLD is the precursor to developing cirrhosis; however, a small percentage of individuals with NAFLD can also progress to cirrhosis.

Hepatic cysts

Hepatic cysts are fluid-filled spaces found within the hepatic parenchyma. There are three main types of hepatic cysts, which include hydatid cysts, fibrocystic disease of the liver,

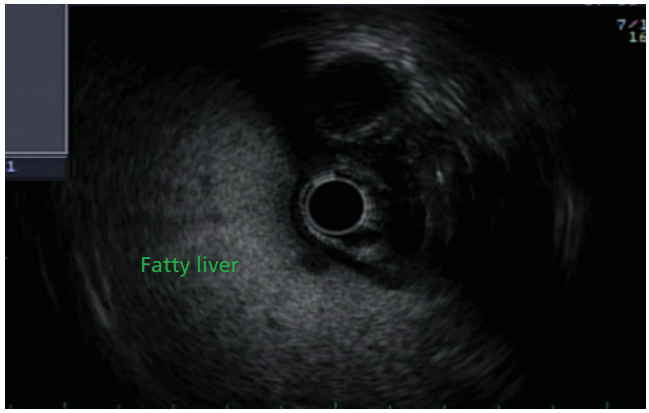

Figure 28.2 Fatty liver. Fatty liver is described as diffuse or focis of hyperechoic or bright parenchyma secondary to fat deposition when compared to normal parenchyma.

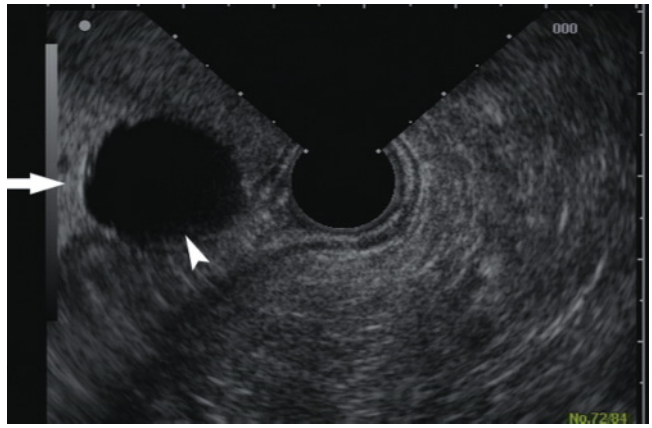

Figure 28.3 Simple hepatic cyst. Simple hepatic cysts can be seen as an anechoic fluid-filled structure within the hepatic parenchyma (arrow head), which demonstrates through transmission beyond the cyst relative to the probe (arrow).

and solitary congenital cysts or simple hepatic cysts. Hydatid cysts are caused by various parasitic infections, are often numerous, and often accompanied by right upper quadrant abdominal pain and fever. Fibrocystic disease is a group of rare conditions that result in abnormal remodeling of the ductal plate that give rise to multiple cystic formations within the liver, most commonly seen in polycystic liver disease and often associated with polycystic kidney disease. Simple hepatic cysts are congenital in origin, benign, occur in little over 3% of the population, occur more frequently in woman, and are generally <5 cm in diameter. They are usually asymptomatic and are often found incidentally. Under endosonography, they are described as anechoic fluid-filled structures within the hepatic parenchyma and normally demonstrate through transmission beyond the cyst relative to the probe. Through transmission is increased enhancement beyond a fluid-filled structure because the intensity of the transmitted ultrasound undergoes less attenuation as it propagates through the cyst and as the reflected signal returns to the transducer. Observing through transmission is helpful in diagnosing whether an anechoic structure is a cyst (Figure 28.3). Doppler endosonography may be necessary to exclude a vessel.

Neoplasms

Malignancy involving the liver is either due to primary liver cancer or secondary to metastatic liver disease. The most common form of primary liver cancer in adults is hepatocellular carcinoma and is the fifth most common cancer in men, eighth in women, and ranks fourth in annual cancer mortality rates. Cholangiocarcinoma is rarer accounting for only 7% of liver tumors in the United States. Even rarer is fibrolamellar hepatocellular carcinoma accounting for only 0.85% of all primary liver cancers. However, metastatic liver disease is more common than primary liver cancer and is mostly associated with pancreatic, colon, breast, lung, and other cancers that originate from the gastrointestinal tract. The endosonographic findings of metastatic liver disease are similar to that of hepatocellular carcinoma. They are often described as a lesion within the hepatic parenchyma with an outer hypoechoic border and a heterogeneous echogenic center (Figure 28.4a,b). This hypoechoic border is normally referred to as acoustic shadowing, which occurs secondary to refraction from the interface between normal tissue and neoplasm. Hepatic metastases are generally echo poor and without a distinct border (Figure 28.4a). In addition, hypoechoic to anechoic regions within a tumor could also represent necrosis. Suspicious lesions in the liver can be aspirated using EUS (Figure 28.4b) for diagnostic purposes.

Cavernous hemangiomas are the most common benign tumors of the liver and are thought to be a congenital malformation or a hamartoma that increases in size as the liver grows from birth. Cavernous hemangiomas can be difficult to diagnosis with ultrasonography as the appearance is quite variable and nonspecific by ultrasound. They can appear as irregular echogenic to hypoechoic lesions surrounded by normal hepatic parenchyma (Figure 28.4c). A computed tomography (CT) scan confirmed this lesion as a hemangioma.

(a)

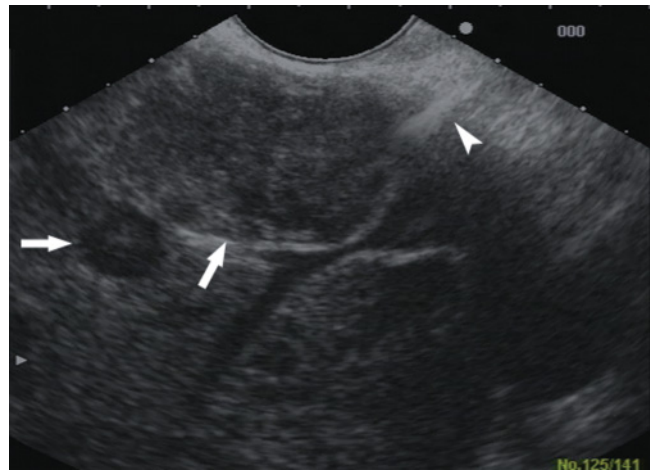

(b)

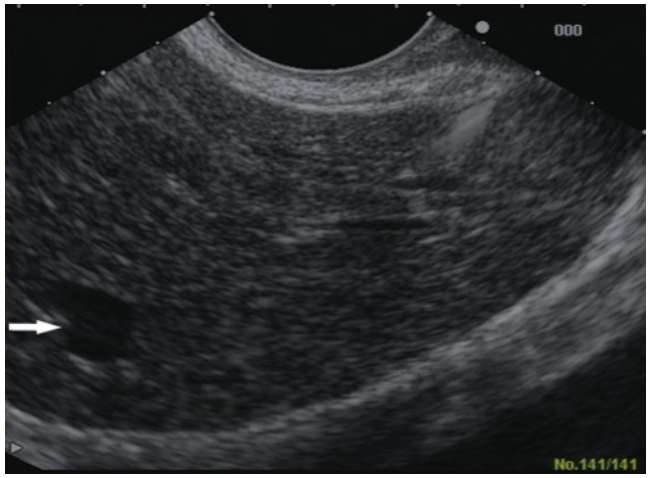

(c)

Figure 28.4 (a & b) Metastatic liver disease. Lesions found within the hepatic parenchyma with an outer hypoechoic border and a heterogeneous echogenic center demonstrating acoustic shadowing (arrows). A fine needle aspiration (FNA) needle is seen in part (b) (arrow head). (c) Cavernous hemangioma. An irregular hypoechoic lesion seen within the hepatic parenchyma (arrow). Note the lack of through transmission. A computed tomography (CT) scan confirmed this lesion as a hemangioma.

Figure 28.5 Dilated intrahepatic ducts. Dilated intrahepatic ducts (arrows) are visualized here and are >1.5 mm in diameter.

Dilated intrahepatic ducts

Dilated intrahepatic ducts can also be seen on endosonography. There are numerous causes for dilated intrahepatic ducts ranging from a distal obstruction secondary to stones or from strictures secondary to anastomotic stricture post liver transplant, primary sclerosing cholangitis, or from cancers such as cholangiocarcinoma. Smaller intrahepatic ducts eventually give rise to the main left and right hilar intrahepatic ducts, which are normally 1.0–1.5 mm in diameter. These eventually become the left and right hilar external hepatic ducts, which eventually merge to form the common hepatic duct that flows into the common bile duct. Extrahepatic ducts are discussed in more detail in Chapter 2. Thus, dilated hilar intrahepatic ducts >1.5 mm (Figure 28.5) may be concerning for a pathological process in the right clinical setting and should be worked up.

4 How to Section

29 How to Interpret EUS-FNA Cytology

Cynthia Behling
Pacific Rim Pathology Group, Sharp Memorial Hospital, San Diego, CA, USA

Introduction

Endoscopic ultrasound (EUS) is an ideal method for obtaining tissue from submucosal lesions in the gastrointestinal (GI) tract or from organs near the gastrointestinal tract. A pathologic interpretation of the tissue biopsy in addition to the EUS characteristics helps to accurately determine the nature of the lesion. The pathologist represents an important member of the patient care team, since microscopic evaluation is a key in determining the nature of the sampled lesion. This chapter illustrates some common lesions as well as technical issues. This chapter is divided into three sections which relate pathology and EUS: the technical quality of the material; the quality of interpretation; and the integration of pathologic and clinical information. The goal of the pathologist is to contribute to a successful EUS service by providing accurate and precise diagnostic information.

Although EUS-guided sampling is a relatively newer way of obtaining tissue, the means of preparing the cells or tissue, obtained from endoscopic ultrasound-guided fine needle aspiration (EUS-FNA), referred to in general as a "biopsy", are well developed and standardized procedures in most cytology/anatomic pathology laboratories. In this chapter, the term "biopsy" will refer to any tissue sample obtained via EUS guidance. A "biopsy" could be an FNA representing cells obtained through a small needle and dispersed onto slides, or a core, representing an intact piece of tissue. Discussion of the advantages and disadvantages of each type of biopsy will be discussed later.

Technical quality of EUS biopsy material

There are a number of techniques and strategies which can optimize the technical quality of EUS biopsy material.

Personnel

Before developing an EUS service, it is important to involve a pathologist or cytotechnologist in planning for specimen handling. Selection of biopsy type and other procedures depend on the personnel and laboratory resources available. Use of a liquid-based cytologic preparation such as ThinPrep™ or SurePath™, direct smears, core biopsy, or some combination of these methods depends on the lesion, pathologist and endoscopist preference, staffing, location of the endoscopy suite in relation to the laboratory, and the relative sensitivity, specificity, and diagnostic accuracy of the various technical choices.

Personnel issues are key in planning for the actual EUS service. For example, at some institutions, the laboratory is physically close to the endoscopy suite and a laboratory technologist travels to the site to prepare aspirate smears, while in other practices, the GI endoscopy staff are trained to make slides. If laboratory personnel will help prepare specimens, the scheduling of procedures should be done in consideration of the laboratory schedule and any ancillary tests such as flow cytometry, which might require special processing.

Biopsy type: aspirate or core

There are two ways of obtaining biopsy material from a lesion. One is to cut out a small piece of the lesion with a cutting needle and the other to aspirate individual cells and small fragments of tissue. Core biopsies provide tissue architecture including, that is, the relationship of the lesional cells and their surrounding stroma are maintained. In core biopsies, vascular and duct structures usually remain intact (Figure 29.1a). In an aspirate sample, the cells are dispersed and evaluated primarily for their individual characteristics although some microarchitecture remains (Figure 29.1b).

Three-to-five micron hematoxylin and eosin-stained sections are cut from tissue obtained with a core biopsy, and

Atlas of Endoscopic Ultrasonography, First Edition. Edited by Frank G. Gress, Thomas J. Savides, Brenna Casey Bounds, John C. Deutsch.

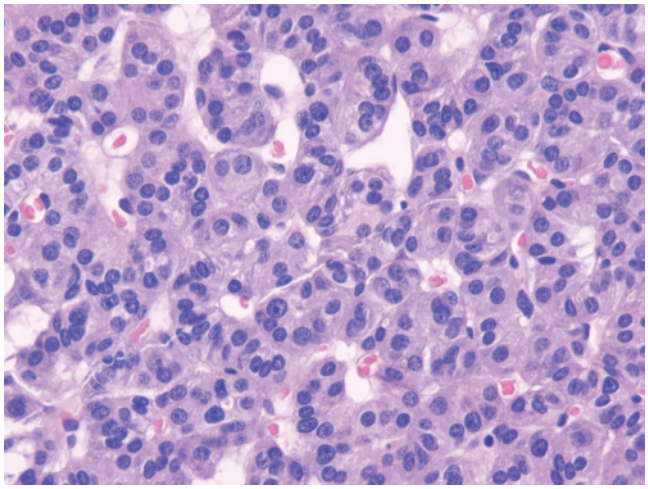

(ai)

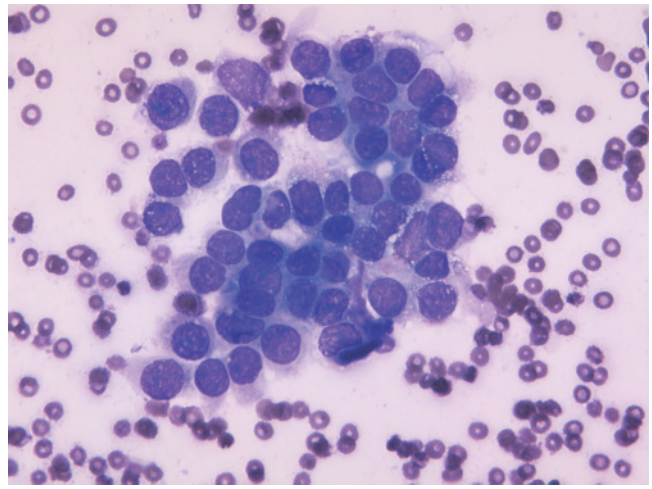

(bi)

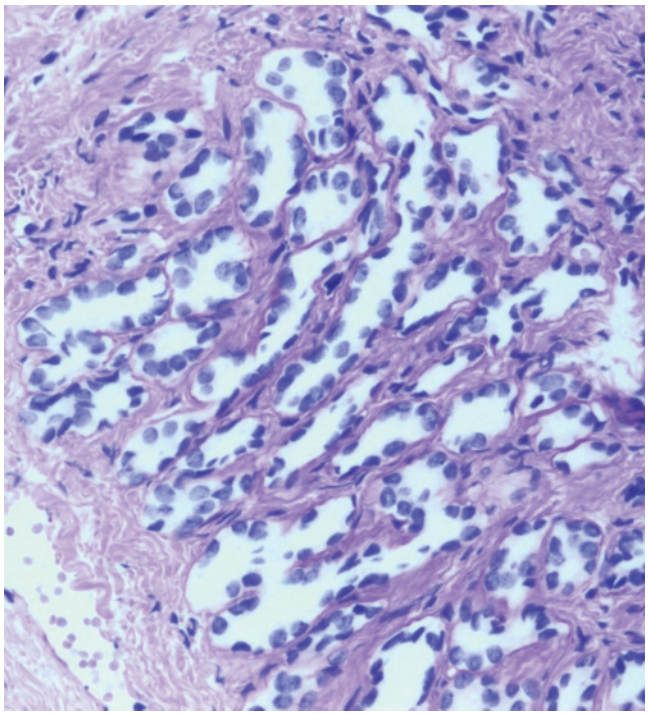

(aii)

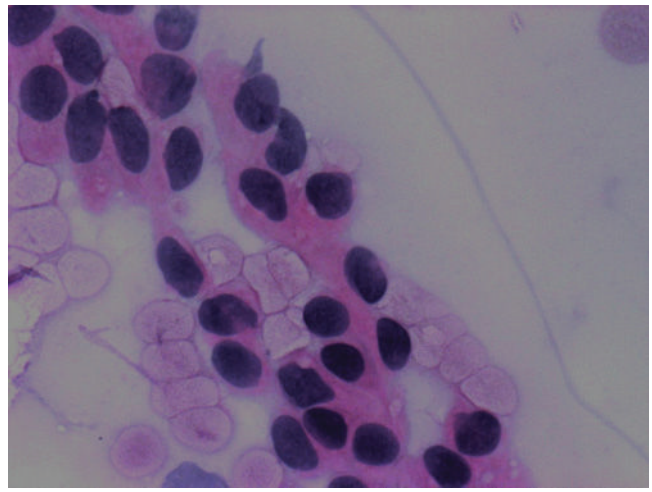

(bii)

Figure 29.1 (a) Core biopsies demonstrate intact tissue architecture and structures such as ducts, vessels, and stromal relationships. (ai) Pancreatic neuroendocrine tumor showing fine vascular structures and rosette formation. (aii) Diastase digested PAS stain of a serous cystadenoma of the pancreas showing small cysts in a fibrous stroma. (b) The dispersed preparation of cells from a fine needle aspirate allow evaluation of individual nuclear and cytoplasmic features as well as microarchitecture. (bi) Pancreatic neuroendocrine tumor cells have finely dispersed chromatin, small nucleoli, and little cytoplasm. (bii) Fine needle aspirates from serous tumors usually contain few cells with oval nuclei arranged in small glandular structures.

are typically fixed in formalin, processed, and embedded in a paraffin-embedded block. The procedure is essentially identical to the way in which mucosal biopsies from the GI tract are processed. These are the familiar blue and pink, hematoxylin and eosin slides with which all pathologists and gastroenterologists are familiar. For FNA biopsies are dropped onto a glass slide and then dispersed as a monolayer by drawing a second slide over the fluid drop.

An aspirate biopsy is usually obtained with a "fine" needle which is 22 gauge or smaller. In this type of biopsy, the material flows or is actively aspirated into the needle and then dispersed onto a slide or placed directly into a preservative or fixative for processing. Smears are prepared in a manner similar to that used in making blood smears. A small drop of the aspirate is placed on one end of the slides and then carefully pulled along the slide to make a dispersed layer of

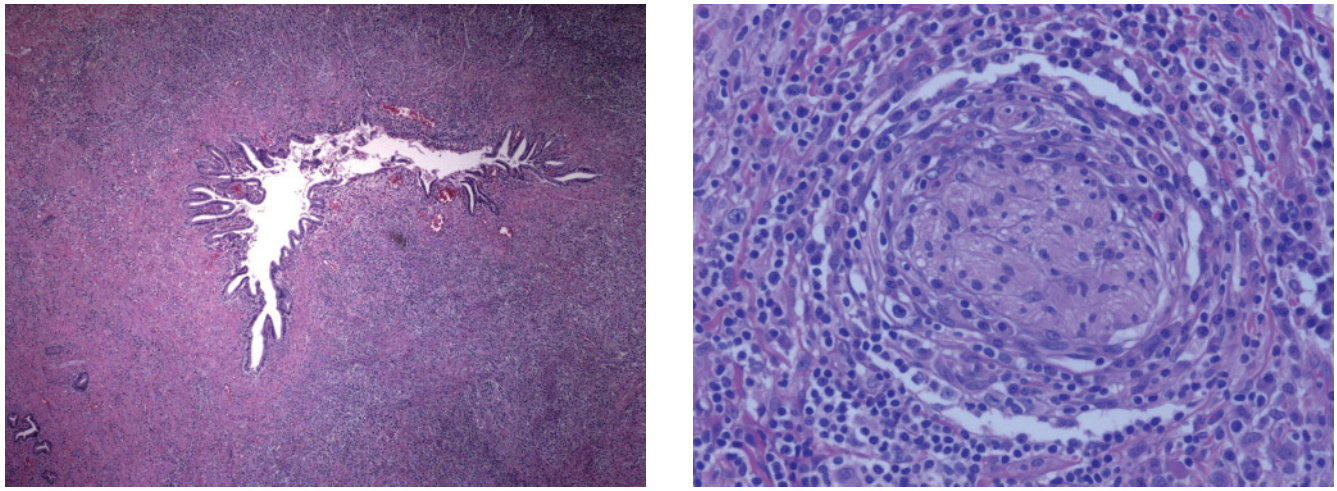

(a) (b)

Figure 29.2 Diagnostic features of autoimmune pancreatitis rely on the demonstration of duct centric inflammation (a), and a dense plasmacytic infiltrate, often surrounding nerves (b).

individual and small groups of cells. The features of the cells appear somewhat different in smears than in tissue sections and also depend on the type of smear preparation and staining. In many pathology laboratories, aspirate smears are prepared as both air-dried and alcohol-fixed smears.

Different criteria are used in interpreting tissue sections and cytology smears. In the tissue sections evaluable features include formation of structures such as glands, invasion of stroma or nerves, inflammatory changes in ducts structures, and many others (Figure 29.2a,b). Preservation of the architecture allows observation of features such as the shape of glands, quality of the surrounding stroma, and the presence of vasculitis. Aspirate smears rely on visualization of nuclear and chromatinic detail, nuclear membrane contour, and cytoplasmic quality (Figure 29.3a–c), emphasizing features of individual cells.

Endoscopic ultrasound-guided sampling lends itself to either aspiration or acquisition of a tissue core (with few exceptions). In some procedures both types of biopsy are obtained, in order to capitalize on the advantages of both preparations. However, for some diseases such as autoimmune pancreatitis or lymphoma, diagnostic criteria may be dependent on features of intact tissue.

Core biopsy tissue remaining in the paraffin block after the intial sections are taken can be used for special stains. Special stains are not limited to tissue biopsies; however, since a portion of the aspirated material from each needle pass can be aliquoted into cell culture media such as RPMI or into a preservative and the sample centrifuged and the pellet processed, embedded, and sectioned. This cell block made from aspirated material can be similarily used for ancillary studies (Figure 29.4a,b).

While examination of tissue sections is the core practice of pathologists, not all pathologists practice cytopathology and, in general, more pathologists are comfortable interpreting tissue sections. For this reason and others, some believe that a tissue core is a better choice. The issue of core versus aspirate can be debated, however, the two methods are complimentary. Various strategies of "dual sampling" or sequential sampling, that is, using FNA when the core is macroscopically inadequate have been examined. For some situations, such as autoimmune pancreatitis, a core biopsy may provide better diagnostic material. The tissue architecture of a core biopsy may be useful for traditional diagnostic criteria for lymphomas, and can help distinguish invasive and in situ malignancies or very well differentiated malignancies such as some pancreatic carcinomas. In addition, core biopsy may require fewer needle passes for diagnostic material. Endoscopic ultrasound-guided core biopsies are a recent technical development and have not been studied as completely as EUS-FNA, so the true diagnostic accuracy remains to be determined.

A potential advantage of core biopsy is that tissue remains in the paraffin block and is available for special stains or other studies as needed. Core biopsy may lead to a more confident benign diagnosis when used in combination with FNA for mediastinal lesions but may be less sensitive in pancreas.

Potential disadvantages to core biopsy include more tissue damage. Deployment of a Tru-cut or other needle for core biopsy may also depend on characteristics and location of the lesion as well as clinical and imaging differential diagnosis.

Cell block

Preparation of a cell block from aspirate material can preserve material for special studies in a manner similar to a core biopsy. A cell block is made by placing the aspirate in

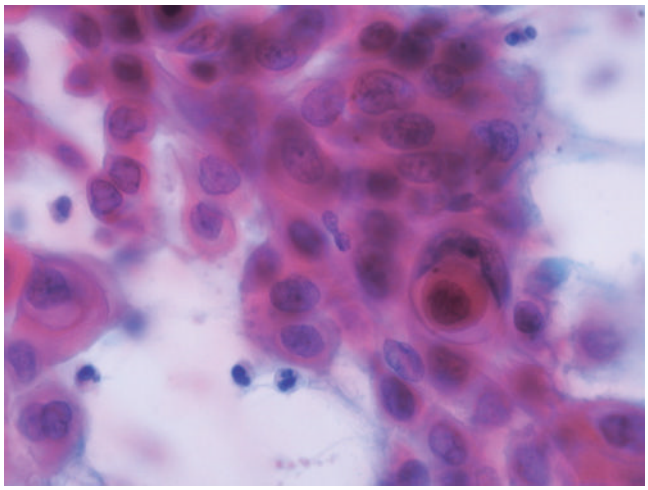

(a)

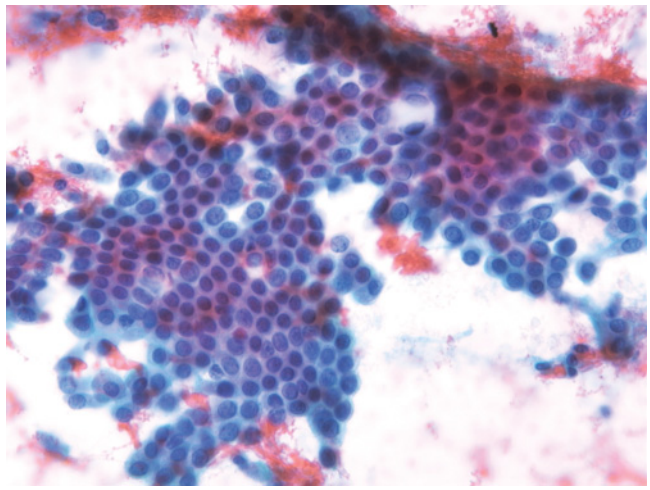

(b)

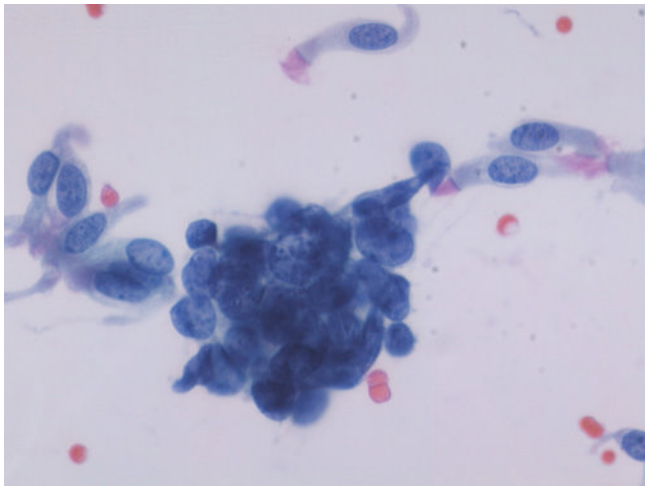

(c)

Figure 29.3 Aspirate smears demonstrate fine cellular detail such as squamous differentiation (a), uniform sheets of epithelium with goblet cells from the duodenum (b), or nuclear molding in a small cell carcinoma (c).

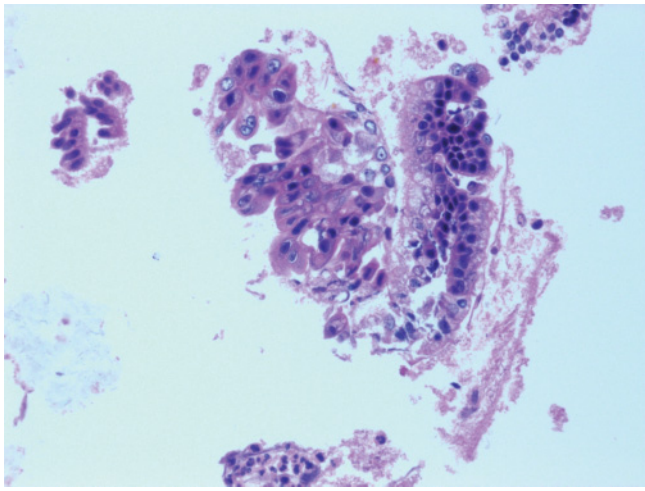

(a)

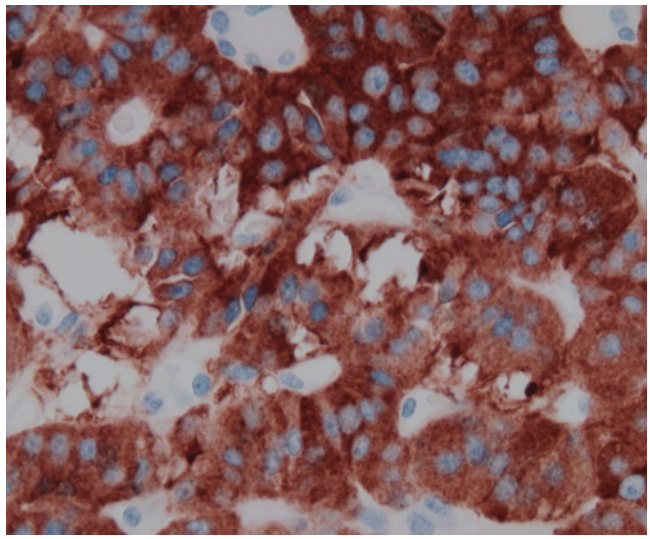

(b)

Figure 29.4 Cell blocks, prepared from fine needle aspirate (FNA) material and placed in liquid-based cytology media or RPMI, can be used both for pathologic interpretation or special stains. Part (a) demonstrates atypical tufting, hyperplastic epithelium (left) adjacent to benign ductal epithelium (right). Part (b) demonstrates neuroendocrine staining of an islet cell tumor.

a preservative media such as RPMI, centrifuging the media to create a cell pellet, and then fixing the cells in formalin and then processing the pellet as a tissue biopsy.

A cell block has some but not all the attributes of a biopsy. While the sections may seem more familiar to pathologists, formalin fixation and paraffin embedding is not optimal for preserving cytologic detail and cell block is not usually a "stand-alone" preparation. Cell blocks are however useful as a repository of lesional tissue on which special stains can be performed.

Technical aspects of the needle can influence the quality of the biopsy. Smaller needle sizes (such as 25 gauge) yield adequate numbers of cells. Larger biopsies (22 gauge) may increase the number of cells but at the expense of tissue trauma and bleeding. In general, minimal heparinization of the needle before passes reduces clotting of the material (Figure 29.5a,b).

At some institutions a cell block is made from leftover material rinsed from the needle and may not contain cells from the lesion. One way to ensure that the cell block contains useful material is to aliquot drops of material to the cell block media at the same time the slides are made. This procedure is discussed below.

A new method is that of brush cytology performed through the FNA needle. In a preliminary study, this method showed promise for cystic pancreatic lesions because it yielded more cellular specimens, but will require more testing and validation.

Ideal aspirate smears are thin, well dispersed, and do not have large clotted material or clumps. Also ideal is the preparation of both air-dried and alcohol-fixed slides, since the former lend themselves to quick modified Romanowsky stains, such as Diff-Quik™ for immediate cytologic evaluations, exaggeration of any nuclear pleomorphism, and help identify intra or extracellular mucin while the latter (alcohol-fixed) allow evaluation of nuclear detail, chromatin quality, and keratinization of cells (Figure 29.6a,b).

Needle size

Needle size for core biopsy is limited by compatibility with the endoscope. Needle size for aspirate is also limited by availability, but the choice of needle size can influence the cytology preparation. Needles as small as 25 gauge have been shown to produce adequate numbers of cells for diagnosis. Furthermore, small needle sizes theoretically produce less tissue injury and less bleeding, decreasing the risk that diagnostic cells will be obscured by blood.

Smaller needle size may also be beneficial in patients with coagulopathy to reduce the risk of bleeding in organs where air or fluid leak may occur or in organs where tissue trauma

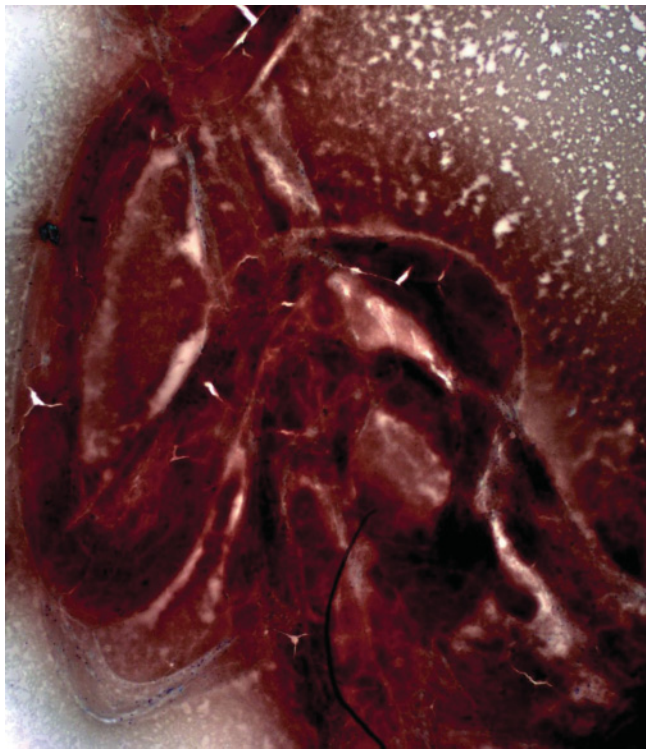

(a)

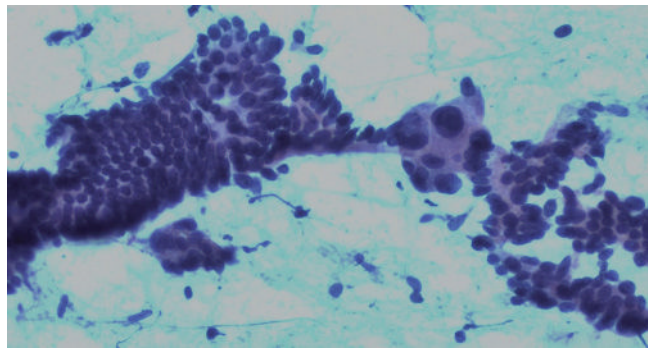

(b)

Figure 29.5 Clotted blood within the needle obscures lesional tissue (a). Optimally heparinized aspirates allow lesional cells to distribute themselves on the slide as an easily visualized monolayer (b).

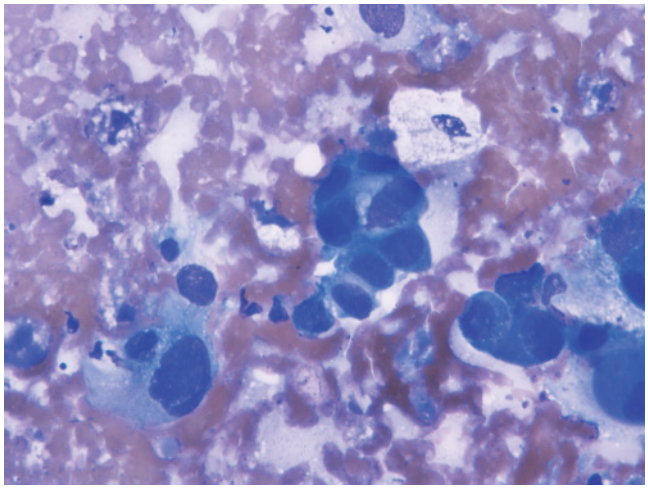

(a)

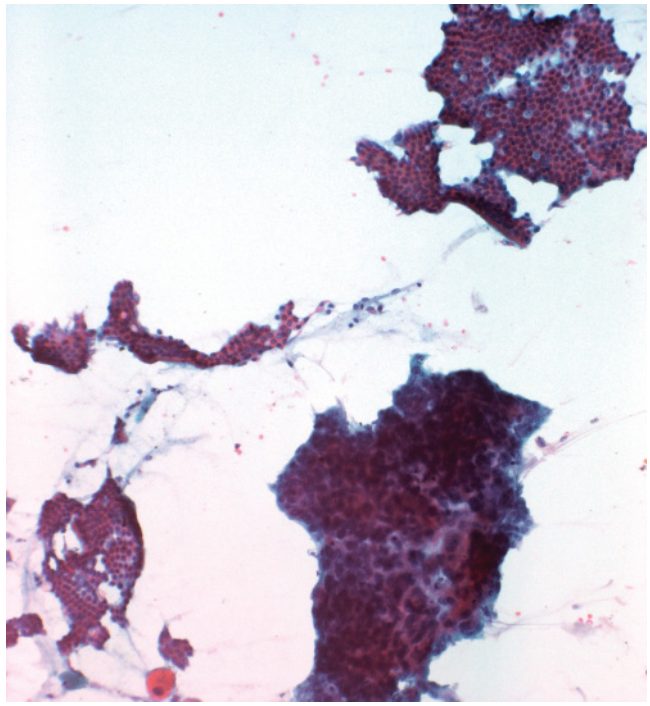

(b)

Figure 29.6 Air-dried slides stained with a modified Romanovsky stain demonstrate cellular pleomorpism as in this pancreatic adenocarcinoma. (a) Squamous differentiation, also from a pancreatic tumor is highlighted by the bright orange staining of keratin by a Papanicolau (Pap) stain (b).

could increase complications. Larger gauge needles can be used where a larger volume of cells is needed such as a work-up for lymphoma.

Needle preparation

Heparin may be used in aspirate procedures to decrease clot formation in the needle lumen. Typically, the stylet is completely removed from the needle and then the needle flushed with heparin. Air is then flushed through the needle to expel out the excess heparin. The stylet is then replaced and the needle is ready for use. Use of heparin may have particular application to EUS aspirates in which the needle is extremely long. Clotting can interfere with the preparation of aspirate smears and lead to artifacts such the as clumping of cells. Too much heparin however can also distort the cells, and thus flushing excess heparin from the needle with air is a necessary step in the procedure.

If clots do form, the material trapped inside can be salvaged by gentle microdissection or by scraping the clotted material from the slide and placing it in media for the cell block.

Suction

Application of suction during fine needle biopsy serves to hold the tissue against the cutting edge of the needle. This may increase the number of cells that are sampled for some lesions. Before withdrawing the needle, however, suction should be released to prevent the air drying of cells when air rushes into the needle as it is removed, and also to prevent the theoretical risk of contamination of the needle tract. However, not all studies document an increased diagnostic yield when suction is used, and, for vascular organs, use of suction may increase blood contamination of the specimen. In addition to increasing the blood in a specimen, suction can induce cytologic artifact. This is rarely a problem in practice however and, in general, fewer insufficient specimens are obtained when suction is used.

Slide preparation and staining

Technical aspects of the slide preparation can influence specimen quality and ultimately adequacy. The manner in which material is expressed onto the slide helps ensure optimal slide preparations. A trained technical assistant (nurse, laboratory technician, or other person) holds the tip of the catheter needle over the end of a labeled glass slide while the needle is advanced approximately 1 cm from the catheter by another assistant (often the endoscopy technician). The stylet is slowly advanced into the needle. This causes a very controlled passage of single drops of material out of the tip. Alternate drops of the material are placed on a slide and into RPMI-1640 medium. The optimal distribution of the material for both cell block and smears is ensured by this technique but it requires a very controlled expulsion of the material from the needle to avoid large "globs" of material

on the slides. If there is too much material on a slide, the diagnostic cells could be obscured or, worse, drip off of the slide. After several slides are prepared the remaining material is placed into media for cell block. After all the slides are prepared the remaining material is rinsed from the needle with a few cc of saline and then air to expel any remaining material into the RPMI. The medium RPMI-1640 is a cell culture media that is used as transport media to preserve the cells until they are made into a cell block or sent for flow cytometry or other special study.

Usually between two and six slides are prepared from each pass, depending on the amount of material obtained. More than six slides usually add little to the diagnostic yield and make the cytotechnologist and pathologist unhappy, since screening and then reviewing many slides containing only one or two cells of interest is quite time consuming and inefficient.

After the material is placed onto the slides, the drops of aspirated material are quickly spread downward onto the slides using another clean glass slide. This method is identical to that used to prepare a blood smear and requires practice. Too much pressure destroys the cells, while too little causes the cells to remain clumped or be obscured by blood or mucus. Ideally, half of the slides are air-dried and the remainder immediately immersed in 95% ethyl alcohol for later Papanicolaou (Pap) staining. The air-dried slides can be stained with a Diff-Quik stain for immediate cytologic evaluation by the pathologist, if available. Immediate cytologic evaluation is discussed below. When the procedure is finished, the alcohol-fixed slides and RPMI-cell suspension are transported to the laboratory for standard Pap staining and cell block preparation respectively. To prepare a cell block, thrombin is added to the material in RPMI and the mixture centrifuged into a pellet. The pellet is resuspended and then the resulting clot removed, wrapped in lens paper, placed in a tissue cassette, fixed in formalin, and routinely processed for paraffin embedding and H&E or immunostaining. If indicated, material for flow cytometric immunophenotyping or other studies is removed from the RPMI before adding the thrombin.

Although the preparing both air-dried and alcohol-fixed slides may seem like extra work, the two preparations are complimentary and are used to demonstrate different cytologic features of lesions. Air-dried smears are stained using a modified Romanowsky stain, such as Diff-Quik. As the cells dry, they spread over the glass and there is an exaggeration of pleomorphism if present. Air-dried smears also highlight intracytoplasmic material, and extracellular substances such as mucin. Air-dried, Diff-Quik-stained smears are also ideal for evaluating lymphoid lesions.

Alcohol fixation preserves nuclear features. Alcohol-fixed slides can be stained with H&E or Pap stains. The Pap stain highlights nuclear detail, chromatin quality, and, if present, keratinization of squamous cells.

Liquid-based preparations

Liquid-based cytology is becoming a standard means of preparing many cytology samples, and has been especially successful in gynecologic practice. Its use for other samples, including those derived from EUS-FNA, is increasing. In this method, the sample is placed into a proprietary fixative and slides prepared by an automated process. The automated sampling and slide preparation is designed to minimize technical problems associated with manual preparation of smears. Two methods are US Food and Drug Administration (FDA) approved. The first is produced by Cytyc Co., Marlborough, MA (ThinPrep™) and the second by TriPath Inc., Burlington, NC (SurePath™). The advantages of a liquid-based preparation are the very consistent and high quality preservation of the cells and improved screening, since the cells are dispersed in a monolayer and are confined to a smaller area of the slide than conventional smears. Another advantage is the decreased technical effort involved in slide preparation. Smears do not have to be made at the time of aspiration, rather the material from the aspirate can be entirely placed into the fixative and transported to the laboratory. This method is especially appealing if the laboratory or the pathologist are located at a distance from the endoscopy suite.

Liquid-based cytology is more expensive due to the use of proprietary media for fixation however, and the method causes some alterations in cytologic detail that need to be considered in interpretation. For example, the procedure decreases the mucin in a specimen. Although for some specimens this is a desirable effect, mucin can be a helpful background feature in the interpretation of mucinous pancreatic neoplasms. The liquid-based preparation techniques may also cause disaggregation of cells and cause loss of microarchitecture. Finally, because the fixative is alcohol based, there may be some degredation of antigens, making immunohistochemistry less reliable.

Interpretation of the cells which are obtained by EUS-FNA or core biopsy procedures is made by a pathologist. Some cytology specimens are first screened by a cytotechnologist and then reviewed by a pathologist. A persistent and known pitfall of interpretation of the aspiration specimens is the frequent presence of contaminating cells from the tubular GI tract. An easy distinction is not always possible but awareness of the issues should help in interpretation.

Quality of the interpretation

Pathologists are becoming more familiar with EUS-obtained material; however, most have limited experience with these specimens. Fortunately, there are a number of courses pertaining to EUS-FNA which can serve to educate pathologist or endoscopist about pathology issues.

Just as the endoscopist's ability to perform EUS-FNA rises on a steep learning curve, so does the pathologist's ability to interpret the material obtained via EUS biopsy. Endoscopic ultrasound-guided biopsies provide access to material organs and tissues which were previously uncommonly sampled, and therefore the pathologist may have little experience in interpreting these specimens. There are some peculiarities of samples obtained via EUS such as "noise" or contaminating cells from the digestive system which need to be distinguished from lesional cells.

Characteristics features of all of the possible lesions in the organs amenable to sampling by EUS-guided biopsy is beyond the scope of this chapter, but a few of the distinctive or commonly sampled lesions are illustrated (Figure 29.7a–e). Review of cytologic diagnosis of mediastinal lymph nodes obtained from EUS-FNA shows good reproducibility between pathologists. Performance is better for pathologists with more experience.

At centers with experience, false negative and false positive diagnoses are rare. In general, a false negatives result occurs when the lesion is not sampled, while false positive results are due to the pathologist's interpretive error or contamination of the extraluminal aspirate with luminal tumor. Adherence to criteria for diagnosis of malignancy and basic cytologic principles can minimize the possibility of false positive diagnoses, although in published studies false positive diagnoses are minimal.

Integration of pathologic and clinical information

Rapid cytologic evaluation

In an ideal situation, a rapid cytologic evaluation is performed during the procedure to assess the adequacy of each pass and to determine if other studies are needed. During immediate cytologic evaluation, a pathologist microscopically examines the air-dried Diff-Quik stained slides prepared at the site. If the material is adequate for diagnosis, then the procedure is stopped. If there is necrosis or no material, then the endoscopist can redirect the needle to another part of the lesion. The goal of rapid evaluation is to optimize the procedure by reducing the number of unsatisfactory or atypical diagnoses as well as reduce the overall number of passes. Rapid evaluation may provide a preliminary diagnosis and reduces the number of false negative procedures due to inadequate sampling.

The literature supports a role for rapid evaluation in optimizing EUS-FNA; however, the practice is variable among institutions. Although rapid evaluation improves diagnostic yield, some pathologists are reluctant to provide rapid evaluation due to inadequate reimbursement for the increased amount of pathologist time. On an institutional level, however, there may be significant cost savings by reducing the number of repeat procedures due to inadequate specimens. Ways to minimize cost include calling the pathologist after several passes have been prepared instead of having them present for the whole procedure, using a cytotechnologist to assess adequacy instead of a pathologist, having the slides transported to the pathologist in real time, or making a gross assessment of the slides without microscopic evaluation.

The ability to redirect the needle during an EUS procedure is one of the chief advantages of FNA with rapid evaluation over a single needle core. The real time image of EUS-FNA allows the needle to be placed directly in the tissue of interest. For some tumors, it may be useful to target the edge of the lesion in order to avoid a necrotic center, while for other lesions the center may have a better yield of tumor cells. For example, an aspirate at the edge of a pancreatic cancer may yield only chronic pancreatitis. While precise direction of the needle isn't always necessary, a thoughtful approach coupled with rapid interpretation may increase yield in difficult lesions.

Role of the laboratory in EUS

It is important for the pathologist to understand that, in many instances, the EUS procedure is intended to be a diagnostic test rather than a screening test.

Education of the pathologist and laboratory about the direct role they play in the EUS procedure and the patient care algorithm will help ensure the success of the EUS biopsy service. The indications for the procedure and pertinent clinical and imaging details for each patient should be discussed. It is important to know if the procedure is performed for screening, diagnosis, or to obtain material for culture or flow cytometry of genetic testing.

Archiving of slides and reports, and the creation of a database containing pathology and EUS information should be considered as part of a quality assurance and competency program. Records of clinical information, EUS features of a lesion, diagnosis, and other data can allow assessment of individual practitioner competency (endosonographer and pathologist), diagnostic accuracy of the service, and the utility of various techniques such as immediate cytologic evaluation.

Pathologists and their staff should understand the limitations of EUS biopsy, know the technical aspects of their part of the process, and be well trained. Laboratory services in the United States are regulated at state and national levels by the Clinical Laboratory Improvement Amendments of 1988 (CLIA '88), the Laboratory Accreditation Program of the College of American Pathologists (CAP), and others. A high quality laboratory provides the best possible service to the patient. Specific details of practice guidelines and other standards are available from the College of American Pathologists and the American Society of Cytopathology.

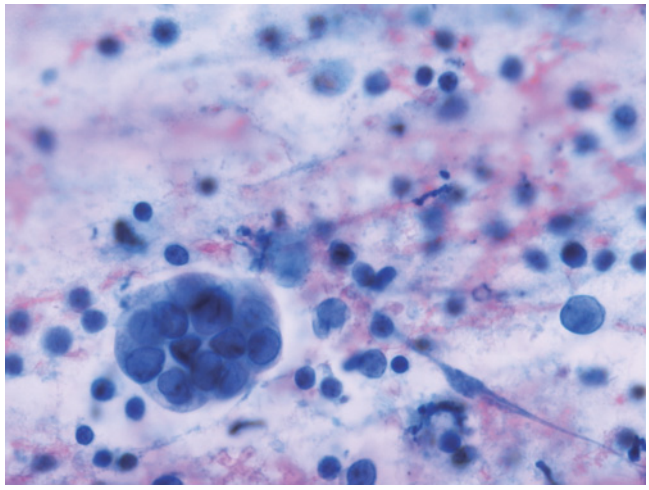

(a)

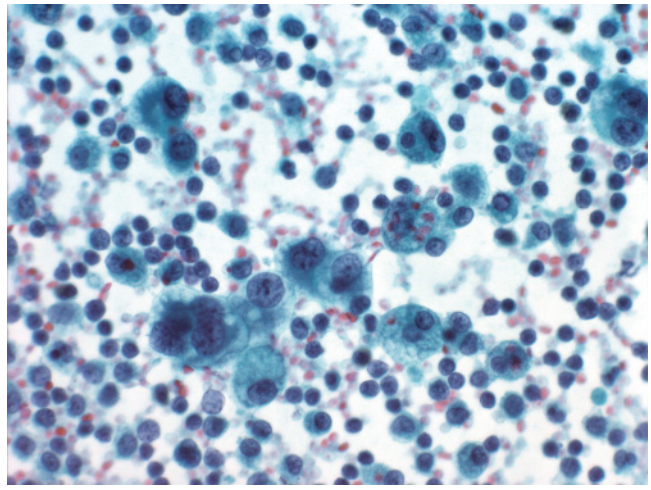

(b)

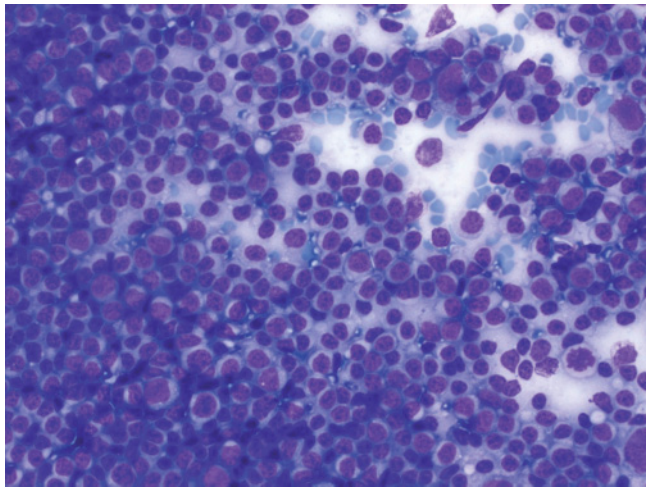

(c)

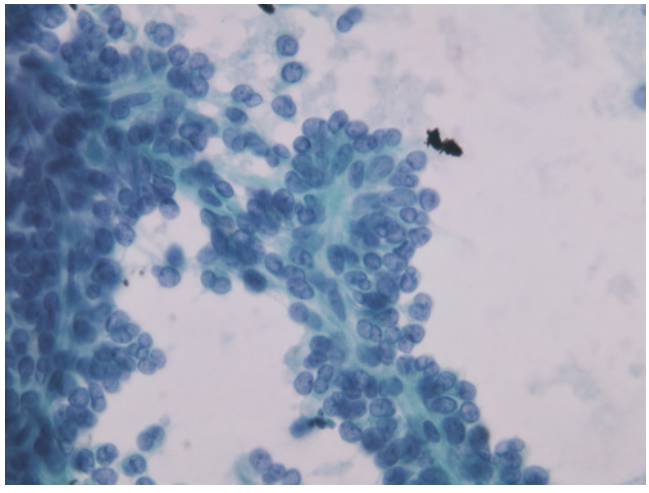

(e)

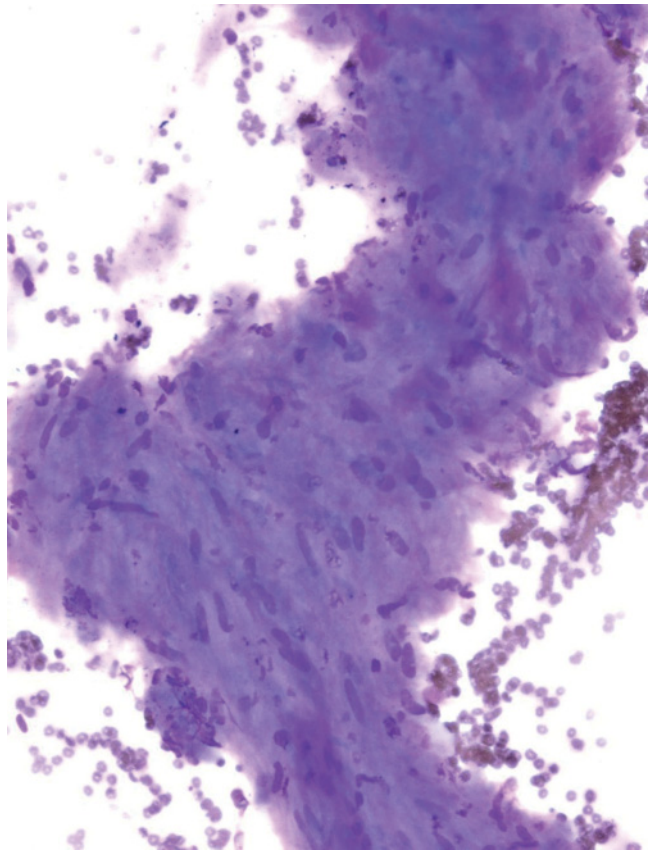

(d)

Figure 29.7 Distinctive or commonly encountered in endoscopic ultrasound-guided fine needle aspiration (EUS-FNA) biopsies include: (a) metastatic adenocarcinoma in mediastinal lymph nodes; (b) metastatic renal cell carcinoma; (c) lymphoma; (d) gastrointestinal stromal tumors; (e) pancreatic solid pseudopapillary tumor.

30 How to do Mediastinal FNA

Sammy Ho
Montefiore Medical Center/AECOM, Bronx, NY, USA

The approach to biopsy lesions in the mediastinum has changed over time. Invasive mediastinoscopy and thoracotomy have limited role for tissue acquisition, particularly in the posterior mediastinum, due to the increased use of endoscopic ultrasound-guided fine needle aspiration (EUS-FNA). Most recent literature has demonstrated its overall safety, reliability, and accuracy. There is convincing evidence that EUS-FNA is an accurate method for mediastinal staging in patients with non-small cell lung cancer (NSCLC), which has become the main indication for transesophageal EUS-FNA (Table 30.1).

Attempts should be made to review cross-sectional imaging prior to EUS-FNA, often using a computed tomography (CT) scan of the thorax, to help formulate a plan for targeted tissue acquisition as well as characterizing any anatomic aberrancies.

Due to the duration of the time spent with echoendoscope in the esophagus during mediastinal FNA, proper sedation is imperative as is vigilance for peri-procedural aspiration. Sudden movements have to be avoided to prevent injuries. Suctioning of the stomach for secretions and minimal use of air and water instillation within the esophagus should reduce the risk of aspiration.

The same linear-array echoendoscope equipment that is used in other parts of the gastrointestinal (GI) tract is utilized for the assessment of mediastinal lesions. The transducer is positioned in the esophagus to examine the posterior mediastinum. Tip of the echoendoscope is adjusted to view the ventral aspect toward 12 o'clock, the dorsal aspect toward 6 o'clock, the cranial toward 9 o'clock, and the caudal toward 3 o'clock position on the screen.

Evaluation of the mediastinum using the linear-array echoendoscope should follow a standardized approach. Beginning with the tip of the echoendoscope in the proximal stomach, the celiac nodes and left adrenal gland can be inspected. The mediastinum is surveyed by first finding the descending aorta. Slow withdrawal of the echoendoscope in 3–4 cm increments and 360-degree rotations can encompass the entire posterior mediastinum. When the transducer is positioned on the posterior and left side of the esophagus, it is possible to examine the thoracic aorta, the left pleura, and the left lung. When the transducer is positioned on the right side of the esophagus, one can visualize the azygous vein as far as its arch, situated between 24 and 25 cm from the incisors. By having the transducer pointing toward the anterior side of the esophagus in the middle part of the posterior mediastinum, the cardiac region can be examined, including the left atrium, the left ventricle, the pulmonary artery, and the aortic root.

Most of the mediastinal lesions are in close proximity to the esophageal wall. Hence, positioning of the echoendoscope to enable visualization and sampling is relatively easier than in other areas of the GI tract. It is important to have an excellent apposition of the tip of the instrument with the wall of the esophagus to avoid "recoil" of the echoendoscope. The actual EUS-FNA technique is similar to the one used in other areas in the GI tract. Generally, in the medistinum, one to three needle passes are sufficient to obtain adequate material. Presence of vessels in the needle path is a contraindication to EUS-FNA, and this possibility can be effectively excluded using color or power Doppler.

Lymph nodes in the mediastinum are classified according to the American Thoracic Society mediastinal staging map for lymphadenopathy (Figure 30.1). The nodal stations amendable to EUS-FNA from inferior to superior include the pulmonary ligament (stations 9R and 9L), lower paraesophageal (stations 8R and 8L), subcarinal (station 7), AP window (station 5), and para-aortal (station 6) nodes. When more

Atlas of Endoscopic Ultrasonography, First Edition. Edited by Frank G. Gress, Thomas J. Savides, Brenna Casey Bounds, John C. Deutsch.

Table 30.1 TNM staging system for lung cancer (7th edition). (Adapted from Goldstraw *et al*. *J Thorac Oncol* 2007; *2*: 706.).

Primary tumor (T)			
T1	Tumor ≤3 cm diameter, surrounded by lung or visceral pleura, without invasion more proximal than lobar bronchus		
T1a	Tumor ≤2 cm in diameter		
T1b	Tumor >2 cm but ≤3 cm in diameter		
T2	Tumor >3 cm but ≤7 cm, or tumor with any of the following features: Involves main bronchus, ≥2 cm distal to carina Invades visceral pleura Associated with atelectasis or obstructive pneumonitis that extends to the hilar region but does not involve the entire lung		
T2a	Tumor >3 cm but ≤5 cm		
T2b	Tumor >5 cm but ≤7 cm		
T3	Tumor >7 cm or any of the following: Directly invades any of the following: chest wall, diaphragm, phrenic nerve, mediastinal pleura, parietal pericardium, main bronchus <2 cm from carina (without involvement of carina) Atelectasis or obstructive pneumonitis of the entire lung Separate tumor nodules in the same lobe		
T4	Tumor of any size that invades the mediastinum, heart, great vessels, trachea, recurrent laryngeal nerve, esophagus! vertebral body, carina, or with separate tumor nodules in a different ipsilateral lobe		
Regional lymph nodes (N)			
N0	No regional lymph node metastases		
N1	Metastasis in ipsilateral peribronchial and/or ipsilateral hilar lymph nodes and intrapulmonary nodes, including involvement by direct extension		
N2	Metastasis in ipsilateral mediastinal and/or subcarinallymph node(s)		
N3	Metastasis in contralateral mediastinal, contralateral hilar, ipsilateral or contralateral scalene, or supraclavicular lymph node(s).		
Distant metastasis (M)			
M0	No distant metastasis		
M1	Distant metastasis		
M1a	Separate tumor nodule(s) in a contralateral lobe; tumor with pleural nodules or malignant pleural or pericardial effusion		
M1b	Distant metastasis		
Stage groupings			
Stage IA	T1a–T1b	N0	M0
Stage IB	T2a	N0	M0
Stage IIA	T1a, T1b, T2a	N1	M0
	T2b	N0	M0
Stage IIB	T2b	N1	M0
	T3	N0	M0
Stage IIIA	T1a, T1b, T2a, T2b	N2	M0
	T3	N1,N2	M0
	T4	N0,N1	M0
Stage IIIB	T4	N2	M0
	Any T	N3	M0
Stage IV	Any T	Any N	M1a or M1b

Adapted from: Goldstraw, P, Crowley, J, Chansky, K, et al. The IASLC Lung Cancer Staging Project: Proposals for the revision of the TNM stage groups in the forthcoming (seventh) edition of the TNM classification of malignant tumours. J Thorac Oncol 2007; 2:706.

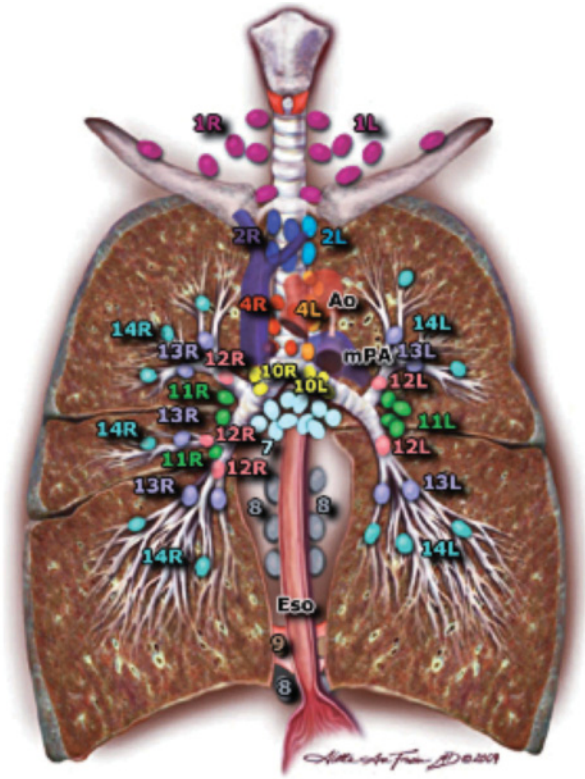

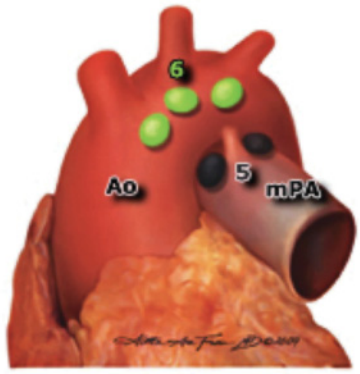

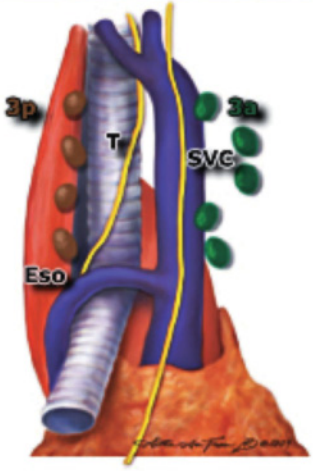

Supraclavicular zone

1 Low cervical, supraclavicular, and sternal notch nodes

Superior mediastinal nodes

Upper zone

2R Upper paratracheal (right)
2L Upper paratracheal (left)
3a Prevascular
3p Retrotracheal
4R Lower paratracheal (right)
4L Lower paratracheal (left)

Aortic nodes

AP zone

5 Subaortic
6 Para-aortic (ascending aorta or phrenic)

Inferior mediastinal nodes

Subcarinal zone

7 Subcarinal

Lower zone

8 Paraesophageal (below carina)
9 Pulmonary ligament

N1 nodes

Hilar/interlobar zone

10 Hilar
11 Interlobar

Peripheral zone

12 Lobar
13 Segmental
14 Subsegmental

Figure 30.1 The International Association for the Study of Lung Cancer (IASLC) lymph node map, including the proposed grouping of lymph node stations into "zones" for the purposes of prognostic analyses. (Reproduced with permission from Rusch *et al*. *J Thorac Oncol* 2009; 4:568. Copyright ©2009 Lippincott Williams & Wilkins.)

than one lymph node group is present, the clinically most important location that is also accessible is selected. If two lesions in anatomically different areas are to be sampled, it is advisable to use two different needles, to avoid cross-contamination and possible misinterpretation of results.

Chapter video clips

Video 30.1 EUS-FNA of a small subcarinal node.

Video 30.2 EUS-FNA of a subcarinal node in conjunction with elastography.

31 How to do Pancreatic Mass FNA

Michael D. Harris and Jonathan M. Buscaglia
State University of New York at Stony Brook, Stony Brook University Medical Center, Stony Brook, NY, USA

Introduction

Gastrointestinal (GI) specialists are frequently consulted for the diagnosis and management of solid lesions within the pancreas. These masses are often malignant and include pancreatic ductal adenocarcinoma, neuroendocrine tumors, lymphoma, and metastatic disease presenting as a solid pancreatic lesion (e.g. renal cell carcinoma). Some benign lesions include focal chronic pancreatitis and autoimmune pancreatitis (AIP). Endoscopic ultrasound (EUS) is the most sensitive imaging modality of the pancreas and remains pivotal for the evaluation of these solid masses. It allows for safe, minimally invasive characterization of pancreatic pathology with the ability for tissue acquisition in the form of ultrasound guided fine needle aspiration (FNA). Large prospective studies have demonstrated the safety of EUS-FNA with overall complication rates of approximately 1–2%. The major risk is acute pancreatitis and occurs in 1% of patients undergoing FNA of solid masses.

Prior to endoscopy it is important to carefully review the patient's history, physical exam findings, and pertinent blood work. It is often especially important to review all relevant cross-sectional imaging such as a computed tomography (CT) scan or magnetic resonance imaging (MRI). This provides the endosonographer with specific clues that may facilitate a more thorough and complete examination, such as the exact location of a lesion or its relationship with major vascular structures. Furthermore, knowledge of additional pathologic features such as hepatic metastases or abdominal ascites may be important if FNA results are non-diagnostic, and they can frequently influence intra-procedural decision making. Figures 31.1–31.7 demonstrate typical examples of the sonographic appearance of masses in the pancreas during EUS evaluation.

The technique

We begin our examination with a radial echoendoscope and image the pancreas from the uncinate process to the tail of gland. This allows for a more thorough examination of the pancreas given its 270–360 degree imaging capability. It also facilitates a more complete evaluation of the pancreatic neck and tail, as well as the mediastinum. After the location of the mass is identified, we then introduce the curved linear array echoendoscope. Depending on the lesion location, FNA is performed transgastrically for lesions of the pancreatic genu, body, and tail; while transduodenal FNA is generally performed for lesions in the uncinate process and head of the pancreas. Transduodenal FNA is often more technically difficult due to the torque on the echoendoscope and the use of extreme upward tip deflection necessary for masses involving the uncinate process.

Once the lesion is positioned favorably in a 5–7 o'clock position below the EUS probe, FNA is performed with the appropriate needle under constant EUS guidance. Multiple needles are available for FNA and include a 19-gauge (G), 22-G, and 25-G needle. The choice of needle is based on the type of lesion targeted. For solid mass lesions, a 19-G needle is generally discouraged due to the potential risk for bleeding, as well as the lack of data demonstrating a diagnostic advantage with larger caliber FNA needles. In general, we prefer to use the 25-G needle because of its flexibility and thus ease-of-use in difficult positions with excessive torque on the echoendoscope, such as inside the first and second portion of the duodenum. In straighter positions, such as within the stomach, we often use a 22-G needle. Prior to FNA, the tip of the EUS probe is positioned in a fashion to minimize the distance between the lesion and the probe itself. This allows for greater precision when advancing the

Atlas of Endoscopic Ultrasonography, First Edition. Edited by Frank G. Gress, Thomas J. Savides, Brenna Casey Bounds, John C. Deutsch.

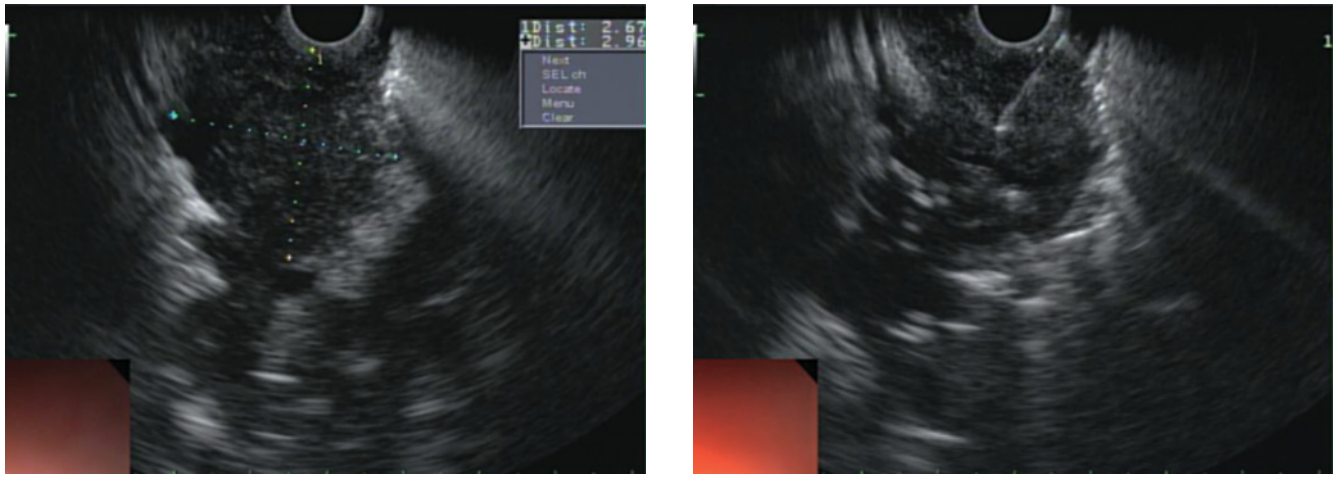

(a) (b)

Figure 31.1 (a) Hypoechoic, irregular, 3 cm adenocarcinoma in the head of pancreas (HOP). (b) Mass positioned in the 6–7 o'clock position during fine needle aspiration (FNA).

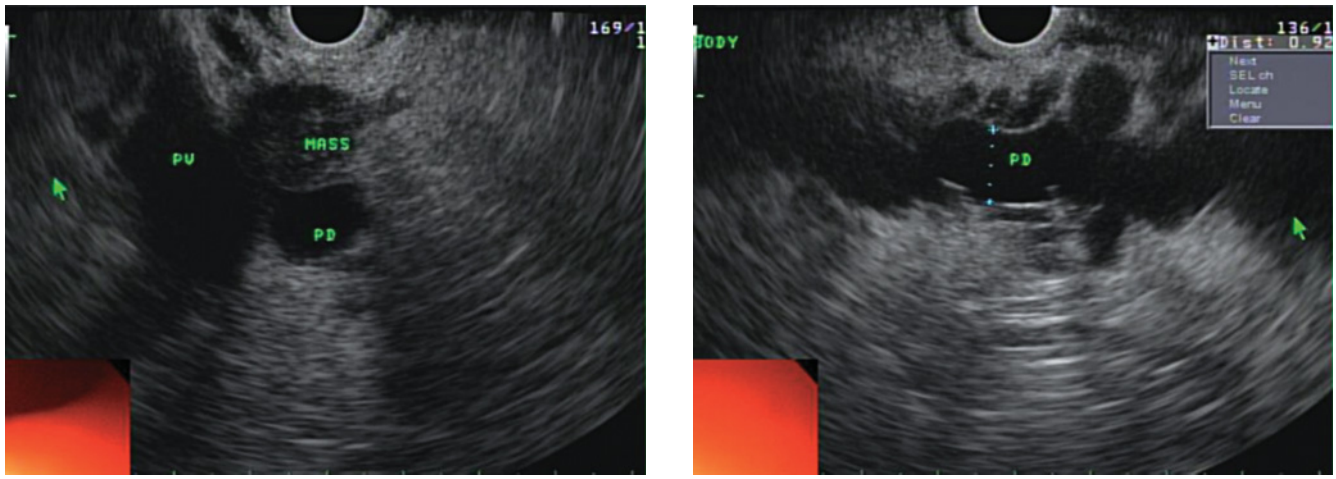

(a) (b)

Figure 31.2 (a) Small adenocarcinoma in the head of pancreas (HOP) adjacent to the portal vein (PV) and a dilated pancreatic duct (PD). (b) Downstream dilation of the PD in the body of the pancreas.

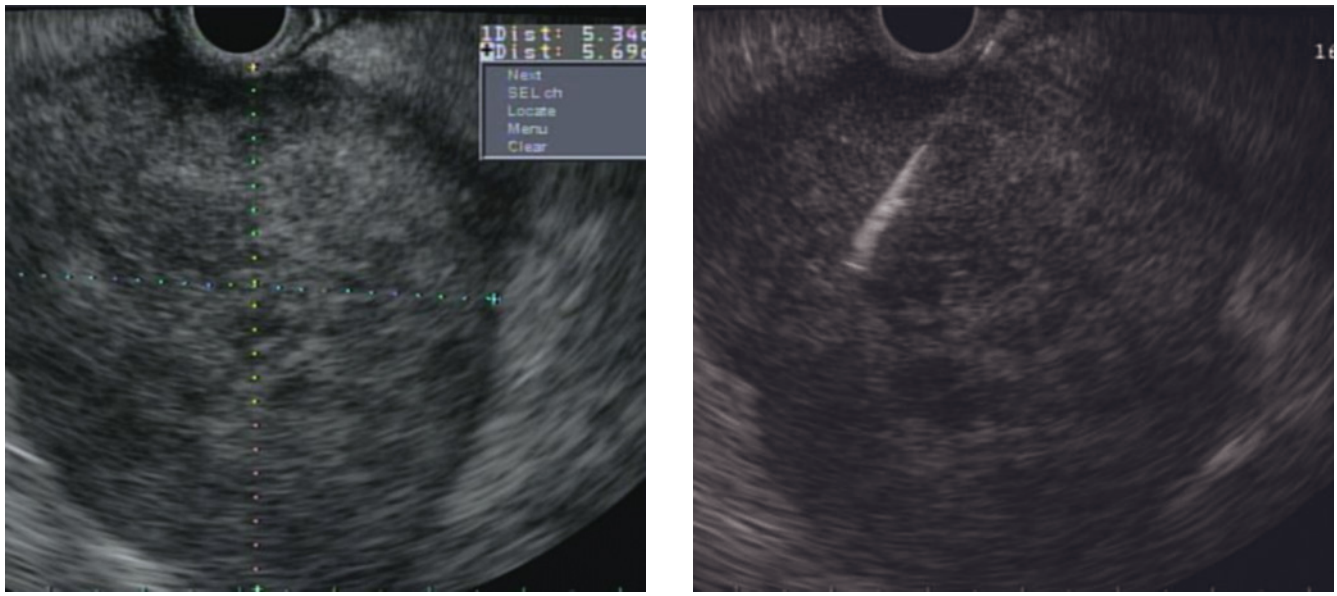

(a) (b)

Figure 31.3 (a) Large 5 cm adenocarcinoma in the tail of pancreas. (b) Mass positioned at the 6 o'clock position during fine needle aspiration (FNA) with a 25-gauge needle.

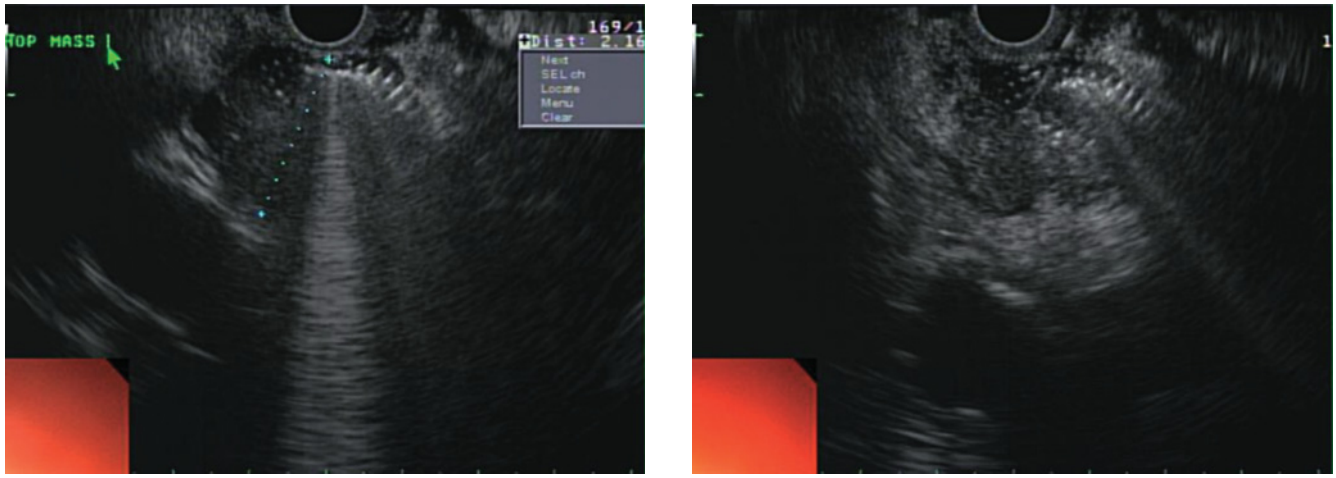

(a) (b)

Figure 31.4 (a) A 2 cm mass in the head of pancreas (HOP) with acoustic interference from a metal stent within the common bile duct. (b) Fine needle aspiration (FNA) through the metal stent to sample tissue from the inferior portion of the mass.

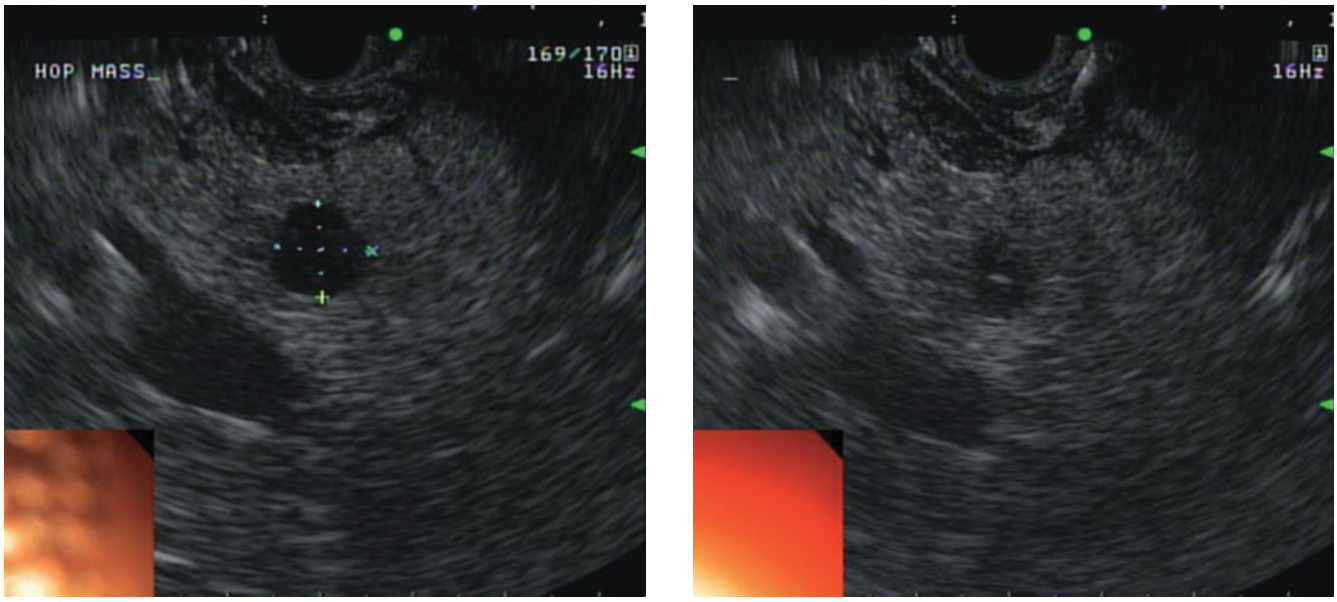

(a) (b)

Figure 31.5 (a) Small 1 cm hypoechoic neuroendocrine tumor in the head of pancreas (HOP). (b) Fine needle aspiration (FNA) needle tip visible in the center of the mass.

needle through the GI wall and into the pancreas. Color Doppler is often used to exclude any intervening vessels just before FNA.

When the FNA needle is in place inside the echoendoscope channel and appropriately fastened at the end of the scope, the stylet is pulled back approximately 1 cm to create a sharpened needle tip. Both dials controlling tip deflection on the echoendoscope are locked to ensure scope stability. Next, the needle is introduced into the mass with a quick thrust and sufficient force to penetrate the GI wall without causing tenting of the lumen. This assures accurate entrance of the needle tip into the lesion. Once the FNA needle tip lies sufficiently within the center of the lesion, the stylet is pushed forward to purge any GI contaminant obtained at

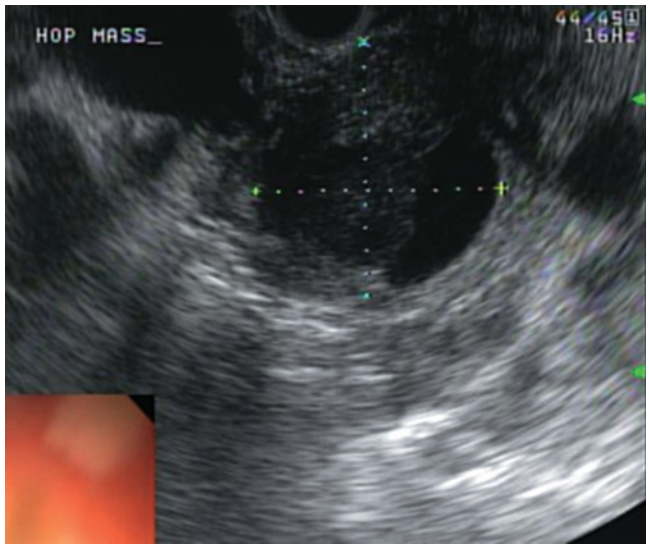

(a)

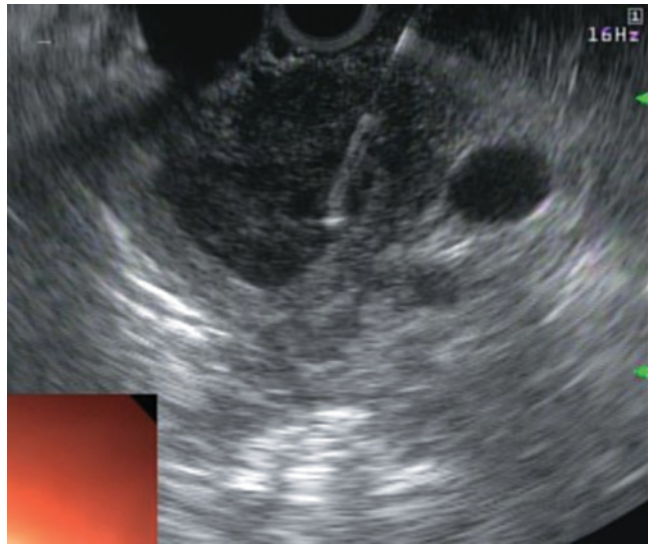

(b)

Figure 31.6 (a) Cystic neoplasm with malignant degeneration in the head of pancreas (HOP). (b) Fine needle aspiration (FNA) targeting the solid components of the mass for higher diagnostic yield.

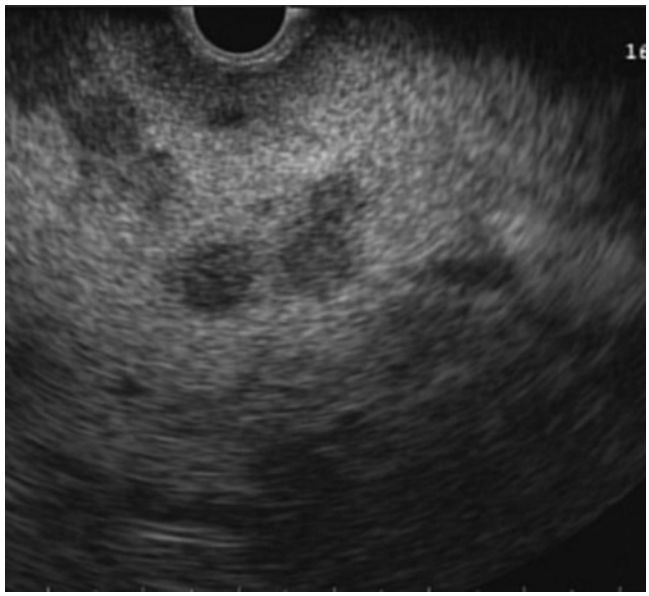

Figure 31.7 Hepatic metastases visualized during endoscopic ultrasound (EUS) examination for a pancreas mass.

the time of wall puncture. The stylet is then completely removed, and a 10–20 ml syringe may be fastened to the operator end of the needle in order to apply suction to the needle's lumen. The needle is then passed back and forth swiftly (multiple rapid thrusts) within the mass along separate linear planes while keeping the needle tip visible at all times. The trajectory of the needle can be changed with the elevator or subtle tip deflection using the large endoscope dial (Video 31.1).

In solid masses, the center of the lesion is often soft and necrotic; therefore, the margin of the mass (or the firm portions of the mass) should be aspirated to maximize the cytological yield. Prior to removal of the needle from inside the mass, suction should be turned off to again prevent intestinal contamination. The needle is then removed completely from the echoendoscope channel, and an air-filled syringe is used to flush the aspirated material onto glass slides. If clot is present within the needle, the stylet is inserted to push the material forward. A thin smear is then made and immediately rinsed with an alcohol fixative. For in-room staining, a separate thin smear may be made and then air-dried. Next, a Diff-Quik™ stain is usually performed which allows for immediate evaluation either by the endosonographer or the cytotechnician.

The number of passes with the FNA needle depends on the presence of rapid on-site evaluation of cytology (ROSE). If ROSE is present, additional passes with the needle is dependent upon the adequacy of the specimen delivered to and assessed by the cytotechnician. When ROSE is not available, we generally perform three separate passes with the needle, and then await a future and final cytopathological interpretation. If para-tumor or celiac axis lymph nodes are noted, FNA with a separate needle can be performed in a similar fashion. This may be especially important in making an accurate diagnosis for a necrotic mass lesion in which adequate tissue acquisition is often difficult.

Summary

Fine needle aspiration is an important aspect in the diagnosis

and management of pancreatic masses. Studies have shown the overall accuracy of EUS-FNA ranges between 71% and 90% in this setting. It is important to review all pertinent clinical data (especially cross-sectional imaging) prior to performing endoscopy. The choice of the needle may depend on the location and size of the lesion. Once the lesion is targeted and placed in optimal position, FNA is performed under total EUS-guidance while visualizing the needle tip at all times. Factors that may increase the diagnostic yield of FNA include sampling the lesion in multiple planes, targeting the margins or firmer ends of a necrotic mass, and arranging for ROSE or rapid on-site evaluation of cytology (Table 31.1).

Table 31.1 Tips for EUS-FNA of solid pancreatic masses.

- Review clinical data prior to endoscopy
- Choose appropriate needle size
- Sample lesion with quick "thrusts" in multiple linear planes
- Aim for margins of necrotic masses
- Arrange for on-site cytopathology if possible

Chapter video clip

Video 31.1 EUS-FNA of a pancreatic mass.

32 How to do Pancreatic Mass Tru-cut Biopsy

Michael J. Levy[1] and Maurits J. Wiersema[2]

[1] Mayo Clinic, Rochester, MN, USA
[2] Lutheran Medical Group, Fort Wayne, IN, USA

Indications

Since introduction in 2002, there has been much debate as to the need and role of Tru-cut biopsy (TCB) and use has varied tremendously among endosonographers. Technical difficulties associated with the device arise from a steep learning curve particularly for pancreatic biopsy, thereby limiting experience to few centers. Furthermore, histologic interpretation of core biopsies requires expertise not widely available. Due to the paucity of well-designed studies, there are insufficient data to firmly establish the accuracy and safety of endoscopic ultrasound-guided Tru-cut biopsy (EUS-TCB) and a lack of broadly accepted practice guidelines. Many endosonographers deny any role for EUS-TCB. This view is often expressed by individuals with limited experience and/or success using this device. Others are enthusiasts who freely advocate EUS-TCB often when fine needle aspiration (FNA) would suffice or even be favored. The ideal approach lies likely somewhere between these disparate points of view.

We recommend use of EUS-TCB to evaluate a variety of pancreatic disorders and categorize the indications as those where TCB has a clear role and distinct advantage over EUS-FNA versus those for where TCB and FNA provide complementary information (Table 32.1). The clearest advantage of TCB is in the evaluation of autoimmune pancreatitis because of the need for histology to establish the diagnosis. Although some perform FNA in this setting, there are no accepted criteria for cytologic diagnosis and pathologists prefer to examine surgical or core specimens that preserve tissue architecture. For cystic pancreatic tumors (CPTs), islet cell tumors, secondary "metastatic" pancreatic tumors, lymphoma, and primary solid pancreatic tumors, EUS-TCB and FNA may provide complementary information. For instance, while EUS-FNA allows cystic fluid analysis, definitive diagnosis of CPTs is uncommon. Instead, the findings merely suggest whether a cyst in mucinous or non-mucinous. Conversely, histologic review of core specimens obtained from the cyst wall and underlying pancreatic parenchyma can provide a definitive diagnosis in a subset of patients.

The vascularity of islet cell tumors and metastatic pancreatic tumors may lead to bloody, non-diagnostic cytology even in the absence of negative pressure (i.e. when performing the FNA no suction is applied). For these patients, TCB may be particularly useful and often diagnostic following false negative FNA. A point of contention is the use of TCB for pancreatic lymphoma or suspected ductal carcinoma. While EUS-FNA may establish the diagnosis, TCB may be of use when FNA fails to establish the diagnosis or may do so with fewer passes. The technical ease and reasonable diagnostic accuracy of EUS-FNA makes it the favored means of biopsy. One must also consider patient and lesion specific characteristics, cytopathologist expertise, and endosonographer success and safety with TCB when selecting the biopsy device.

Device design and preparation

The TCB device contains a spring-loaded firing mechanism within the handle. As with EUS-FNA needles, an adjustable "screw-stop lock" is incorporated in the handle (Figure 32.1). The handle also includes an "adjustment wheel" that rotates the device into the proper orientation and slightly varies the length. A "spacer" may be added to help account for the varied echoendoscope length among manufacturers. The non-handle portion of the device consists of an outer "catheter sheath", an internal 19-gauge "cutting sheath", an 18 mm long "specimen tray", and a 5 mm long "stylet tip." The spring-loaded mechanism rapidly fires the cutting sheath over the specimen tray to sever the tissue (Figure 32.2).

To initially prepare the TCB device the handle is retracted into the "firing position" which retracts both the cutting

Atlas of Endoscopic Ultrasonography, First Edition. Edited by Frank G. Gress, Thomas J. Savides, Brenna Casey Bounds, John C. Deutsch.
 Published 2012 by Blackwell Publishing Ltd.

Table 32.1 Indications for pancreatic EUS-TCB.*

TCB favored over FNA	Autoimmune pancreatitis
TCB and FNA have complementary roles	Cystic pancreatic tumor Islet cell tumor Lymphoma Secondary "metastatic" solid pancreatic tumor Primary solid pancreatic tumor

EUS = endoscopic ultrasound; FNA = fine needle aspiration; TCB = Tru-cut biopsy.
*Assumes target lesion is located in a site that is readily accessible to EUS-TCB and that tissue acquisition is clinically indicated.

sheath and specimen tray (Figure 32.3). The inner needle remains in the withdrawn position until the biopsy is performed. Next, the needle is advanced until the tip is nearly flush with the catheter sheath (Figure 32.4). Under advancement of the needle tip may result in inadvertent puncture of the catheter and echoendoscope, whereas over advancement risks damage to the echoendoscope accessory channel.

Biopsy technique (Figure 32.5)

Due to the stiffness of the TCB needle, the distal endoscope must be maintained in a fairly straight position thereby limiting use of this device to within the stomach when biopsying the pancreas.

Figure 32.1 The various components of the endoscopic ultrasound-guided Tru-cut biopsy (EUS-TCB) device handle are demarcated. They include the spring-loaded mechanism that permits automated collection of a tissue specimen, a "screw-stop lock" that when unlocked allows advancement of the needle up to 8 cm and protects against inadvertent advancement, an "adjustment wheel" that rotates the device into the proper orientation, and a "spacer" that may be used depending on the length of the manufacturer of the linear echoendoscope.

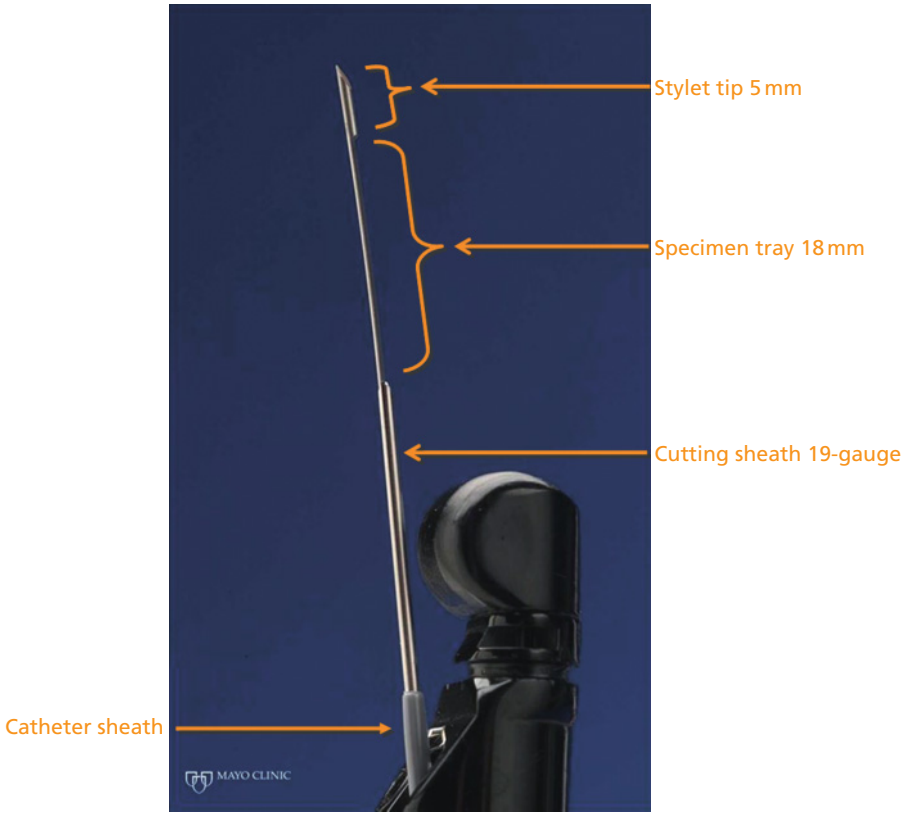

Figure 32.2 The various components of the endoscopic ultrasound-guided Tru-cut biopsy (EUS-TCB) needle tip are demarcated. They include a "catheter sheath", an internal 19-gauge "cutting sheath" that shaves off the tissue specimen, an 18 mm long "specimen tray" that contains the tissue core, and a 5 mm long "stylet tip".

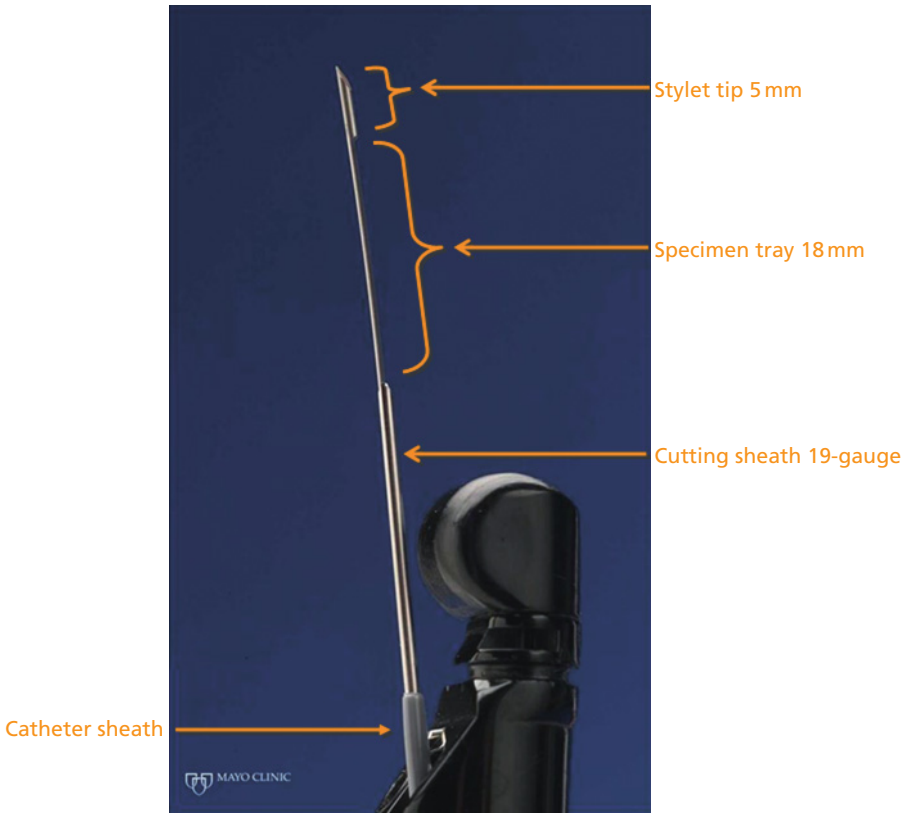

Figure 32.3 The handle is retracted into the "firing position" which retracts both the cutting sheath and specimen tray.

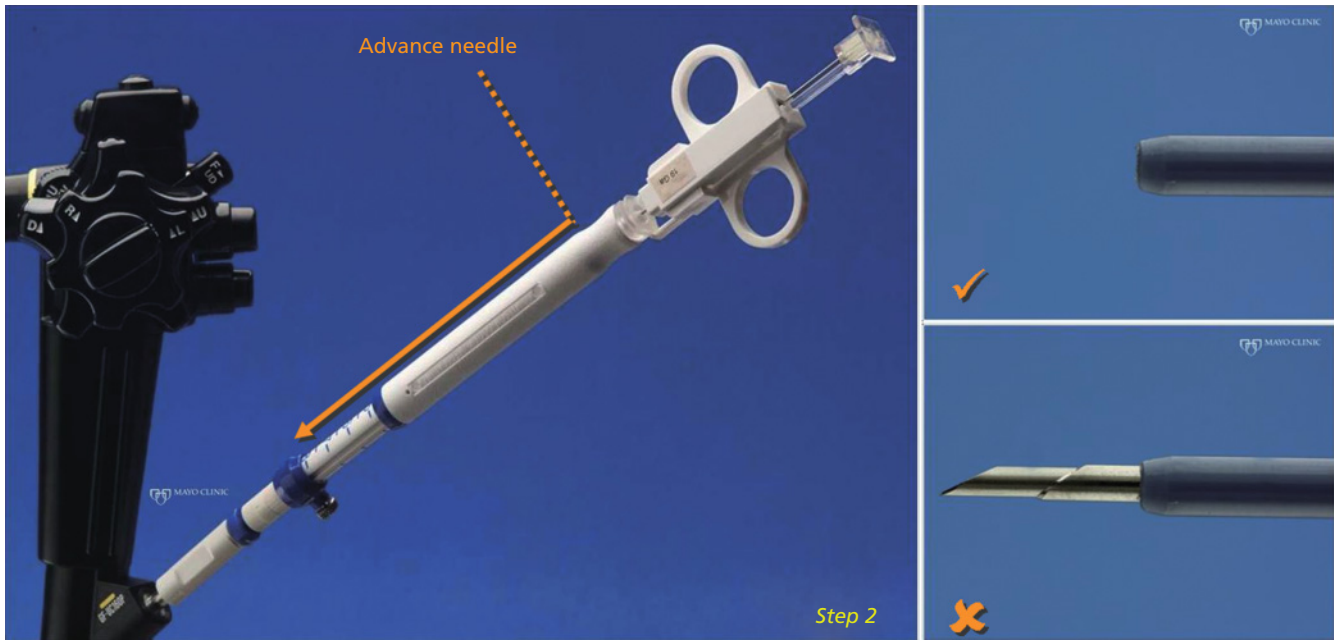

Figure 32.4 The needle is advanced until the tip is nearly flush with the catheter sheath. Under advancement may result in inadvertent puncture of the catheter and echoendoscope, whereas over advancement risks damage to the echoendoscope accessory channel.

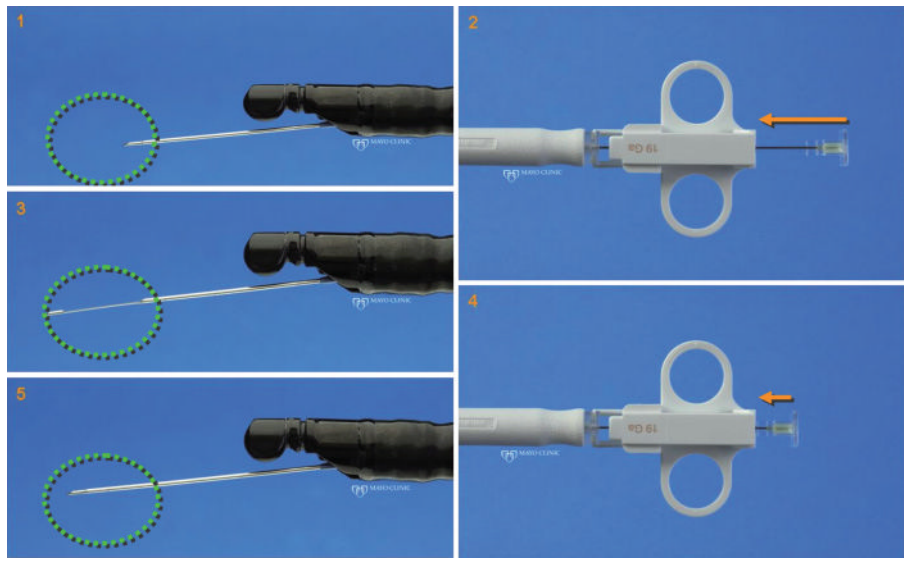

Figure 32.5 The needle is advanced into the target lesion with the spring handle in the retracted "firing" position. The spring handle is then pressed forward until resistance is felt. Doing so advances the specimen tray into the target lesion. Further pressure on the spring handle will fire the device and obtain a biopsy.

The needle is advanced into the target lesion under EUS guidance with the spring handle in the retracted "firing" position. The spring handle is then pressed forward until resistance is felt. Doing so advances the specimen tray into the target lesion. When targeting the biopsy, one should realize that the specimen tray will extend approximately 20 mm beyond the needle tip. Further pressure on the spring handle will fire the device and obtain a biopsy. All controls (up–down and left–right) and the elevator should be released into a "relaxed" position and the echoendoscope should be straightened. Failure to do so results in sluggish advancement of the cutting sheath over the specimen tray. The needle assembly is withdrawn into the catheter, the screw-stop is locked and the entire TCB device is removed from the endoscope. The tissue is carefully removed from the specimen tray and submitted in formalin for processing and review (Figure 32.6). Proper orientation of the echoendoscope may assist tissue sampling. One may utilize the orientation adjuster to rotate the handle in a particular manner that places the needle tip in an ideal orientation. As the

handle is rotated, so too is the needle tip orientation. The handle is ideally rotated to allow the specimen tray to face the transducer (Figure 32.7).

Pancreatic TCB is most difficult in patients with a relatively normal size gland without a mass lesion, such as in patients with autoimmune pancreatitis. We favor TCB of the pancreatic neck to help avoid main pancreatic duct injury (Figure 32.8). One may also sample other areas of the pancreas with care to rotate away from the main duct. When sampling a CPT we position the specimen tray so that it overlaps the solid portion of the cyst thereby improving ones' chances of acquiring epithelial cells (Figure 32.9).

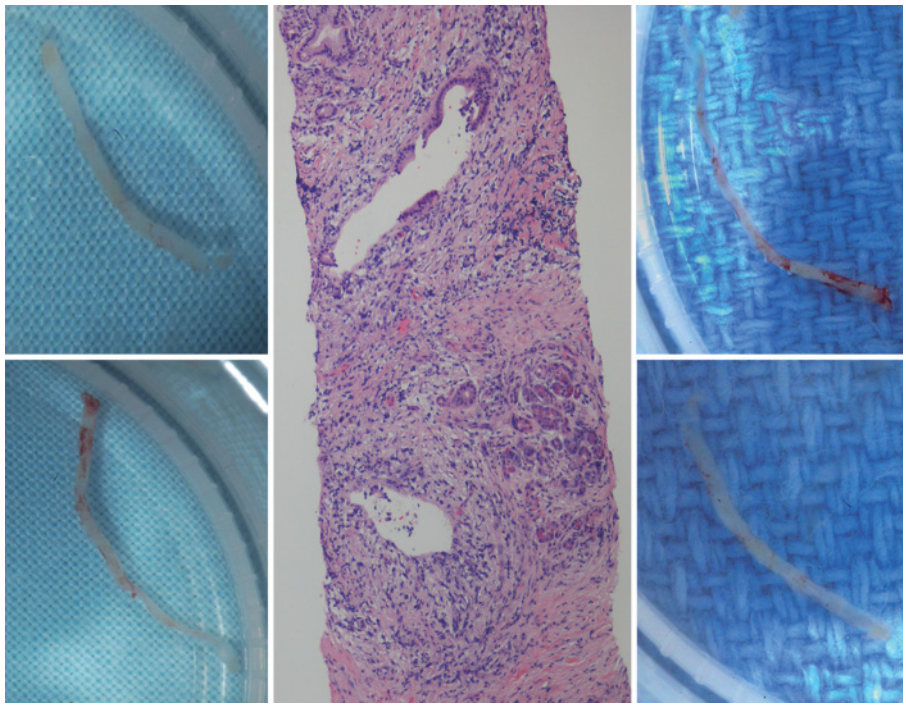

Figure 32.6 The tissue is carefully removed from the specimen tray and submitted in formalin for processing and review.

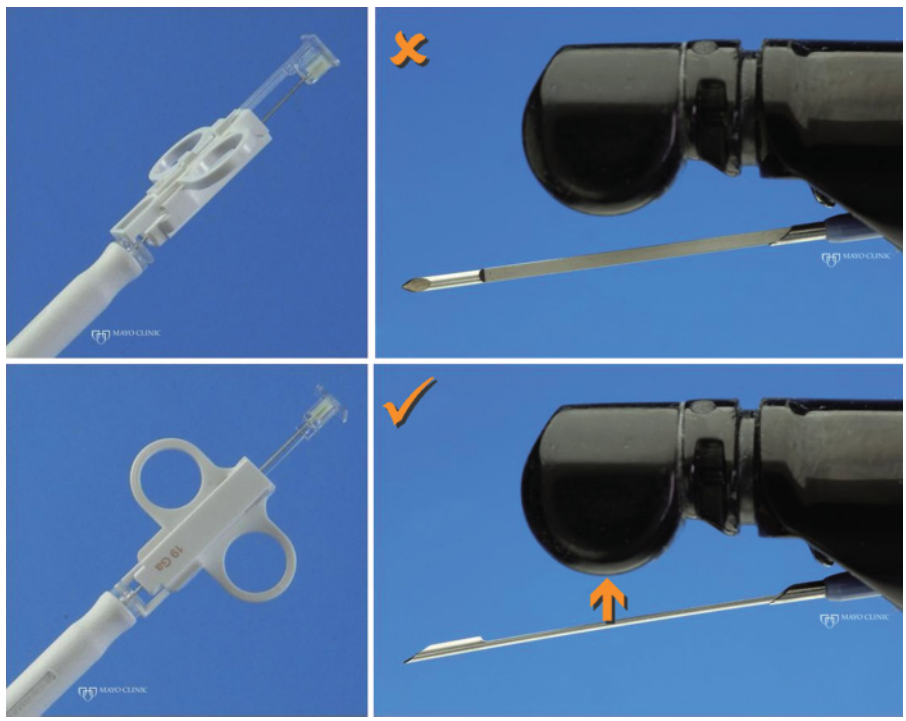

Figure 32.7 As the handle is rotated, so too is the needle tip orientation. The handle is ideally rotated to allow the specimen tray to face the transducer.

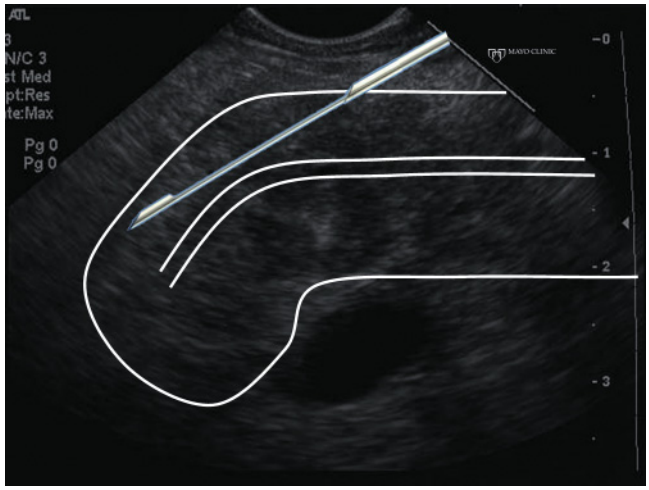

Figure 32.8 We favor Tru-cut biopsy (TCB) of the pancreatic neck to help avoid main pancreatic duct injury.

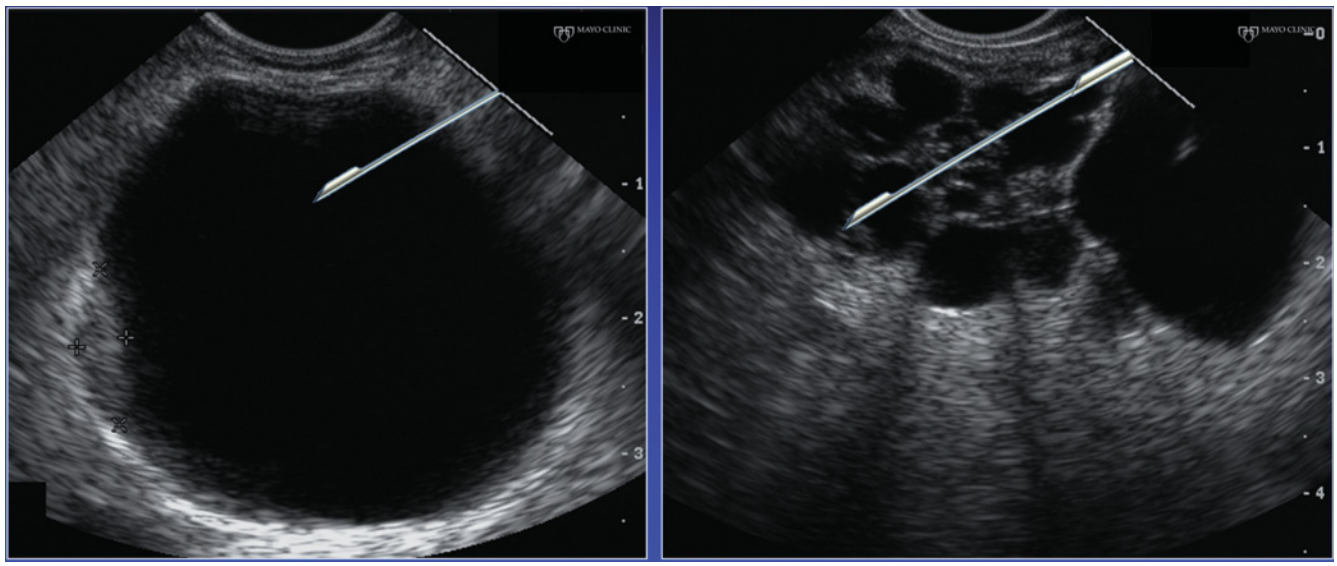

Figure 32.9 When sampling a cystic pancreatic tumor we position the specimen tray so that it overlaps the solid portion of the cyst thereby improving acquisition of epithelial cells.

Summary

EUS-FNA allows easy and safe pancreatic tissue sampling and provides high diagnostic accuracy in most settings. However, limitations associated with FNA reduce accuracy for several pancreatic disorders, in particular autoimmune pancreatitis, but also CPTs, vascular tumors, and occasionally lymphoma and carcinoma. EUS-TCB design allows acquisition of larger tissue samples permitting histologic examination. EUS-FNA and TCB should be considered complimentary as failure with one method is often remedied by use of the alternate device. Issues of device safety, accuracy, and cost must be further clarified to refine the role of EUS-TCB.

Chapter video clip

Video 32.1 Pancreatic EUS-TCB.

33 How to do Pancreatic Cyst FNA

Aman Ali[1] and William R. Brugge[2]

[1] Massachusetts General Hospital, Boston, MA, USA
[2] Massachusetts General Hospital and Harvard Medical School, Boston, MA, USA

Pancreatic cystic lesions pose a unique diagnostic and therapeutic challenge in day to day clinical practice. With improved cross-sectional imaging, incidental pancreatic cysts are increasingly encountered. This chapter will focus on the technique of performing fine needle aspiration (FNA) of pancreatic cysts. The differential diagnosis, cyst fluid analysis and management of pancreatic cystic lesions are discussed elsewhere.

It is important to understand the limitations of pancreatic cyst FNA before undertaking this task. When considered individually, the diagnostic accuracy of endoscopic ultrasound (EUS) morphological features, pancreatic cyst fluid analysis (for carcinoembryonic antigen [CEA], amylase) and cytology is limited. However when combined, these features might be useful in detecting the (potentially) malignant cysts. For an accurate diagnosis and appropriate treatment of pancreatic cysts, it is imperative that the endosonographer fully understands the clinical setting, reviews the available imaging and takes a multidisciplinary team approach in making appropriate treatment recommendations.

It is important to note the clinical features of the patient and the clinical condition. If there is a history of pancreatitis, altered surgical anatomy, coagulopathy, portal hypertension, gastric varices with or without splenic vein thrombosis, and other underlying co-morbidities, the increased risks should be discussed with the patient and family. In patients with acute or recent pancreatitis, pancreatic cyst FNA should be avoided. It is important to note that in patients with history of recurrent or chronic pancreatitis, the presence of a pancreatic cyst does not necessarily appoint towards the diagnosis of a pseudocyst. The presence of a cystic lesion in an index computed tomography (CT) scan obtained during the first episode of pancreatitis or a history of a pre-existing pancreatic cyst raises the suspicion of a cystic neoplasm. This is especially true when such a lesion can itself lead to pancreatitis, e.g. an intraductal neoplasm. Obstruction of the main pancreatic duct by mucin or the presence of a mass may be an important factor in the pathogenesis of pancreatitis. Anticoagulants that are stopped in consultation with patient's internist or cardiologist are usually resumed shortly after an uneventful procedure. All available cross-sectional imaging should be reviewed before the procedure. It not only aids in selecting the approach for FNA (e.g. second duodenum for uncinate lesions vs. gastric body for tail cysts) but also highlights the individual patient's anatomy and relevant important findings, e.g. communication of cyst with pancreatic duct (PD), presence of peri-gastric varices, pseudoaneurysms, etc.

Adequate sedation is critical for optimizing patient cooperation during FNA. In the initial evaluation, a detailed examination of the entire pancreas with the linear array echoendoscope is performed. The size and exact location of the pancreatic cyst(s) is noted along with its relationship to the adjacent vessels, organs and lymph nodes. A focused cyst exam also includes documenting cyst wall thickness, number and thickness of septae, presence of focal mural irregularity and masses (Figure 33.1). The cyst fluid cavity is examined for debris, blood, and mucin (Figure 33.2). The proximity of the cyst with the main pancreatic duct and/or side branches should be documented. The presence of chronic pancreatitis should be noted by examining the pancreatic parenchyma carefully for calcifications, hyperechoic foci and lobularity. An oblique viewing echoendoscope also allows an endoscopic view of the ampulla to exclude mucin protruding from the ampulla (fish mouth deformity) suggestive of a main branch intraductal papillary mucinous neoplasm (IPMN).

Once the target cyst has been identified, it should be positioned in such a way that the transducer is in close proximity to the cyst, providing a short needle path. Also positioning the lesion in the natural pathway of the needle with a relatively straight scope position allows an easier needle passage (Figure 33.3). There is usually some compromise between achieving the proximity to the cyst and ease of the needle

Atlas of Endoscopic Ultrasonography, First Edition. Edited by Frank G. Gress, Thomas J. Savides, Brenna Casey Bounds, John C. Deutsch.

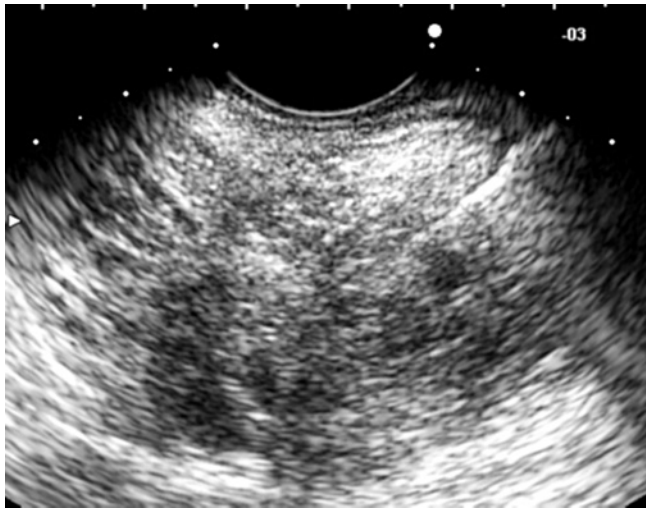

Figure 33.1 Fine needle aspiration (FNA) of microcystic serous cystadenoma.

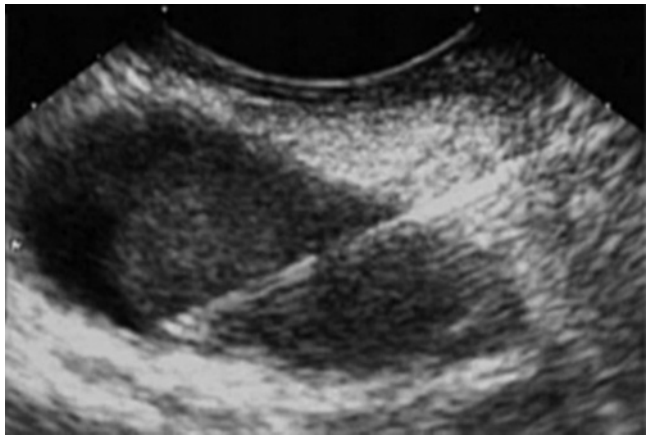

Figure 33.2 Intraductal papillary mucinous neoplasm (IPMN) with evidence of mucin floating within the cyst cavity.

Figure 33.3 Fine needle aspiration (FNA) of a complex cyst. Note the straight needle trajectory.

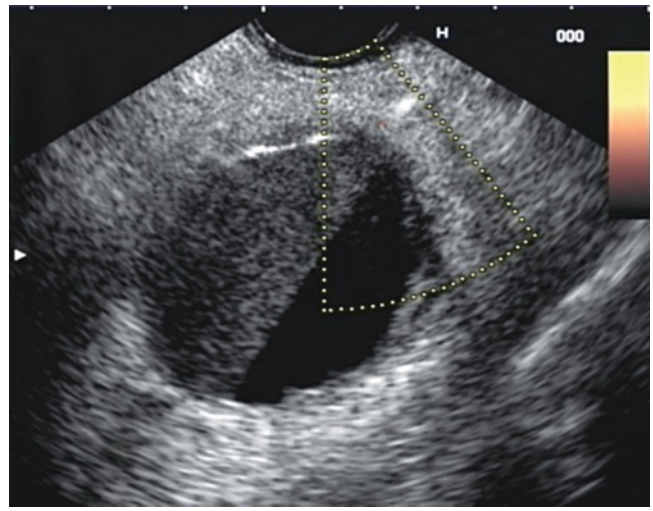

Figure 33.4 Evidence of intra-cystic bleeding with layering of hyperechoic material.

pass. The approach should be individualized, e.g. in accessing some pancreatic head or neck lesions, the best approach may be from the gastric body. Also not infrequently while performing a transduodenal FNA for a pancreatic head or uncinate cyst, there may be resistance as the needle is advanced out of the sheath. The needle should never be forced out of echoendoscope as this may result in damage to the instrument channel. In order to remedy the excessive resistance, the echoendoscope, the elevator and scope angulation should be minimized in order to allow the needle to exit from the scope. After advancement of the needle out of the sheath, the echoendoscope should be repositioned. Once an adequate position is achieved, the echoendoscope control knobs are locked. Just prior to needle passage, the needle pathway is scanned with color Doppler, looking for intervening vessels. Then while keeping the needle in the visual plane at all times, the needle is passed through the cyst wall at a 90-degree angle with one quick motion. With the needle clearly in the cyst cavity, the stylet is removed and suction is turned on. The cyst should be completely evacuated, ideally with only one cyst puncture in order to minimize the risk of infection. The needle position is adjusted by slowly withdrawing the needle tip as the cyst cavity collapses. Needle suction is eliminated before withdrawing the needle back in to the echoendoscope.

A 22-gauge needle is routinely used for pancreatic cyst aspiration. While fluid yield is low for serous cystadenomas due to their microcystic nature, mucinous cysts with high viscosity fluid or pseudocysts might require the use of a 19-gauge needle to allow complete cyst evacuation. If only a small amount of cyst fluid is available, the priority should be focused on a cytologic diagnosis. CEA determination is requested for unknown types of cysts (usually 1 ml is required). Mural nodules should be targeted for cytology

during cyst aspiration. After complete aspiration of the cyst, the area is carefully examined for a mass so that it can be targeted for FNA. Acute cyst cavity hemorrhage is the most common complication but rarely results in any symptoms (Figure 33.4). The blood in the cyst cavity should not be reaspirated. Aspiration (Figure 33.5) of the cyst wall increases the risk of bleeding and leaks. Antibiotics should be given to minimize the infection risk. The reported incidence of post pancreatic cyst FNA infection and bleeding is <1% and pancreatitis is 2–3%. When appropriate technique is utilized, pancreatic cyst FNA is a safe and effective procedure that helps in making an accurate diagnosis and selecting appropriate treatments.

Chapter video clip

Video 33.1 How to do pancreatic cyst FNA.

Figure 33.5 Malignant mucinous cyst with evidence of wall nodularity.

34 How to do Pancreatic Pseudocyst Drainage

Shyam Varadarajulu[1] and Vinay Dhir[2]

[1] University of Alabama at Birmingham Medical Center, Birmingham, AL, USA
[2] Institute of Advanced Endoscopy, Mumbai, India

Introduction

Pseudocysts (PCs) are fluid-filled cavities surrounded by a non-epithelial wall composed of inflammatory material. Drainage is required for large PCs that are persistent and symptomatic. Historically, PCs that produce a luminal compression on the stomach or duodenal wall are treated endoscopically by transmural drainage and those not causing a luminal compression by surgery or percutaneous techniques. Accumulating evidence over the past decade suggests that endoscopic ultrasound (EUS) is a safe and effective modality for drainage of PCs, irrespective of the presence or absence of a luminal compression. Unlike conventional transmural drainage which is a relatively "blind" technique, EUS-guidance enables the puncture of a PC under real-time imaging thereby minimizing the potential for complications such as bleeding and perforation. Also, unlike percutaneous techniques, the procedure does not predispose to fistula formation or restrict patient mobility. Compared to surgery, EUS-guided drainage is less invasive, less costly, and is associated with shorter length of hospital stay.

Patient selection

The majority of the PCs larger than 4 cm in size and located adjacent to the gastric or duodenal wall are suitable for EUS-guided drainage. Pseudocysts located in the tail region of the pancreas do not cause a luminal compression and may require puncture from unusual locations such as the distal esophagus. Although hitherto considered a relative contraindication, multiple, large PCs can be accessed individually and drained successfully under EUS-guidance when located close to the gastrointestinal (GI) lumen. Cysts smaller than 4 cm in size are not suitable for stent placement. If treatment is required in such cases, complete cyst aspiration under EUS guidance can be undertaken in one session Alternatively, if the PC communicates with the main pancreatic duct, transpapillary stenting may be appropriate. Multi-septated cysts in general do not respond well to endotherapy as the non-evacuated portions of the cyst tend to persist and suboptimal drainage predisposes to infection. Also, the presence of large amounts of necrotic debris warrants endoscopic necrosectomy or surgery. Transluminal stenting per se is inadequate therapy for necrotic fluid collections.

Requisite instruments and accessories

A curvilinear array echoendoscope with a channel diameter of 3.7 mm or more is needed for stent depolyments. A 19-gauge endoscopic ultrasound-guided fine needle aspiration (EUS-FNA) needle is required for passing a 0.035-inch guidewire into the PC. Pseudocyst puncture can also be performed with a needle knife catheter, or with a one-step needle wire device (available in Europe), or a cystotome. Over-the-wire balloon catheters are required for dilation of the transmural tract and double pigtail plastic stents for facilitating drainage of cyst contents. Nasocystic catheters may be required for continuous irrigation of the abscess cavity or necrotic contents. It is important to perform the procedures in a room equipped with fluoroscopy to monitor guidewire exchange and stent deployment.

Assessment of the pseudocyst by EUS

A careful evaluation of the PC should be undertaken prior to puncture. The size, location, and number (single or multiple) of PCs should be determined. Most PCs are unilocular with predominantly clear contents and well defined walls (Figure 34.1). Multilocular cysts and those with mucinous

Atlas of Endoscopic Ultrasonography, First Edition. Edited by Frank G. Gress, Thomas J. Savides, Brenna Casey Bounds, John C. Deutsch.

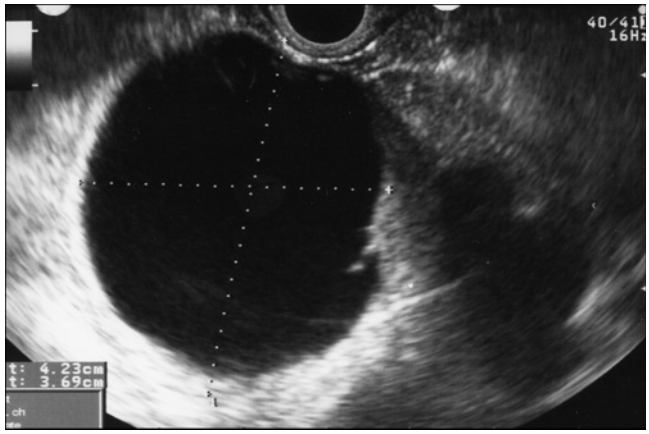

Figure 34.1 A large, unilocular, pseudocyst with clear contents as visualized under endoscopic ultrasound (EUS) guidance.

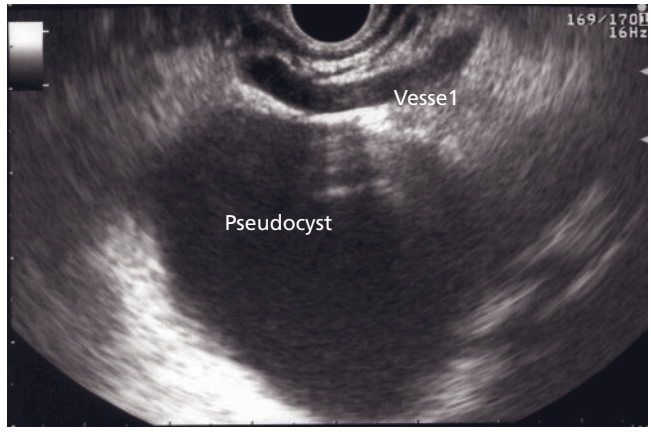

Figure 34.3 Presence of intervening vasculature between the endoscopic ultrasound (EUS) transducer and the pseudocyts.

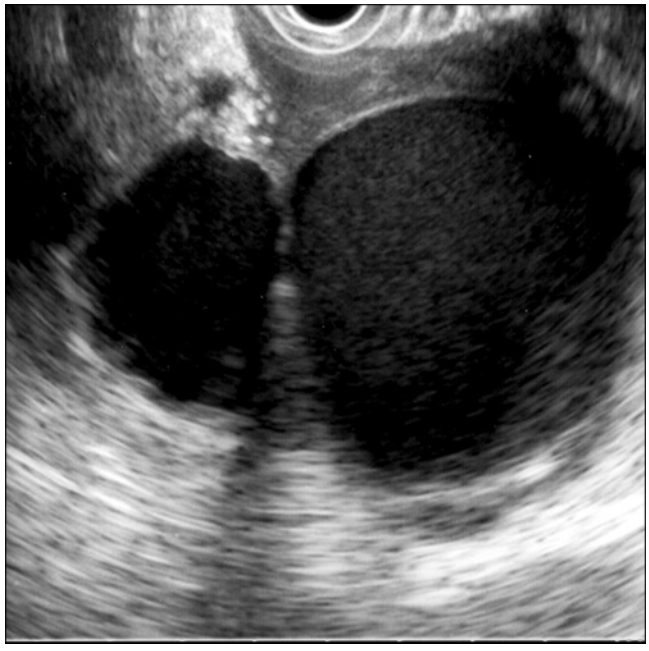

Figure 34.2 Two pseudocysts are seen at endoscopic ultrasound (EUS), the promixal lesion on fine needle aspirate (FNA) analysis was a mucinous neoplasm and the distal lesion a reactive pseudocyst.

Figure 34.4 Endoscopic ultrasound (EUS) guidance enables access to the pseudocyst by providing an appropriate window in a patient with gastric varices.

contents or thick nodular walls need to be aspirated to rule out a neoplastic process (Figure 34.2). Also, a thorough survey of the pancreatic gland must be undertaken prior to drainage as a proximal tumor can cause a reactive PC. Some PCs located in the distal body or tail of the pancreas may cause splenic vein thrombosis and collaterals may be present between the cyst and gastric wall (Figure 34.3). In such cases, a puncture site should be chosen after excluding the presence of intervening vasculature (Figure 34.4). It is important that the PC is located within 1–2 cm of the GI lumen to avoid perforation or stent migration.

Pseudocyst puncture

Antibiotic prophylaxis is recommended prior to puncture of any cystic lesions. Pseudocyst puncture can be done with a 19-gauge needle (Video 34.1) without the need for cautery (Figure 34.5). Alternatively, cautery-assisted cyst puncture can be performed with help of a needle knife catheter or the Giovannini one-step needle wire device. Puncture should preferably be done at a site where the echoendoscope is relatively straight. An angulated echoendoscope may cause

resistance to passage of accessories and stents. As angulation is sometimes unavoidable when accessing a PC from the fundus of the stomach, we prefer not to use electrocautery in such situations as it may result in tangential catheter passage and perforation. The use of fluoroscopy aids in maintaining a straight position of the tip of the echoendoscope (Figures 34.6a,b).

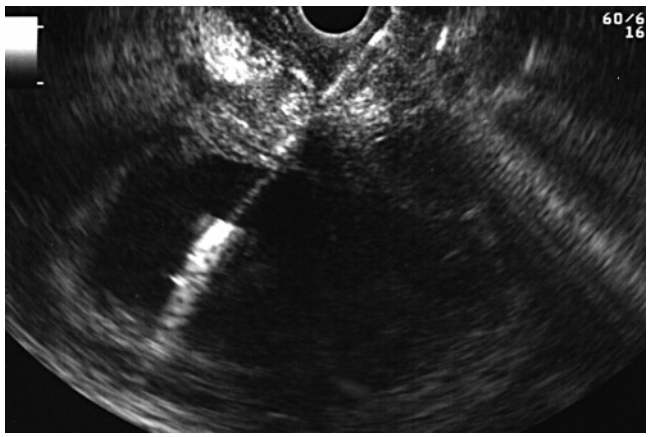

Figure 34.5 Pseudocyst accessed with a 19-gauge fine needle aspirate (FNA) needle.

Transmural tract dilation

Once the needle is seen in the PC, fluid should be aspirated for analysis (Gram stain, culture, chemistry, or tumor marker studies). A 0.035-inch guidewire is then coiled within the PC (Figure 34.7). The tract can then be dilated sequentially using a 5-French (Fr) endoscopic retrograde cholangiopancreatography (ERCP) catheter (Figure 34.8), Soehendra biliary dilator, 5.5-Fr inner catheter of the Giovannini one-step system or the inner catheter of the cystotome. It is important to keep the guidewire taut as otherwise there may be resistance to passage of dilators. Subsequent dilation is then undertaken using an 8–15 mm over-the-wire balloon dilator (Figure 34.9). Large diameter balloons can be used when the cyst contents are turbid to facilitate better drainage. When using large diameter balloons it is important to ascertain that there is proper effacement between the PC and the GI lumen so as to avoid perforation.

Stent deployment

Depending on the fluid consistency, a 7 or 10-Fr double pigtail stent is deployed after transmural tract dilation (Figure 34.10). It is preferable to place more than one stent in large cysts. Multiple wires can be placed at one time if

(a)

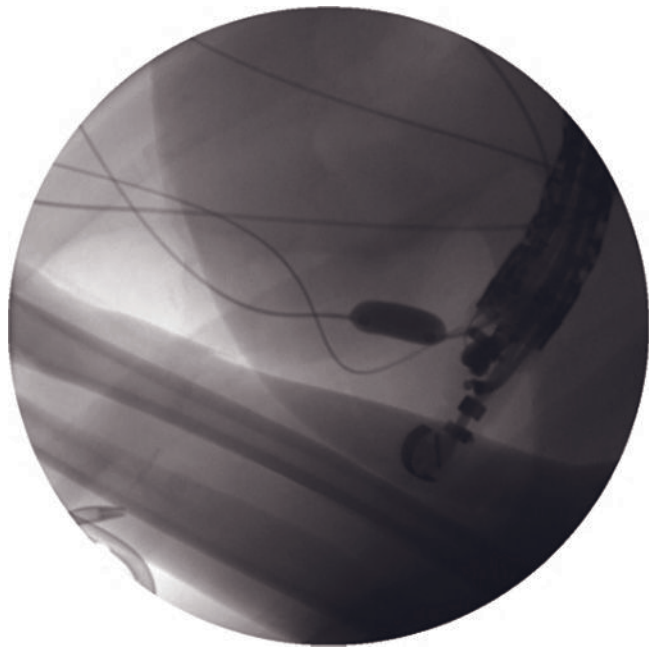

(b)

Figure 34.6 (a) Acute angulation encountered when the echoendoscope is located in the gastric fundus. (b) The tip of the echoendoscope is subsequently straightened with aid of fluoroscopy to facilitate passage of accessories.

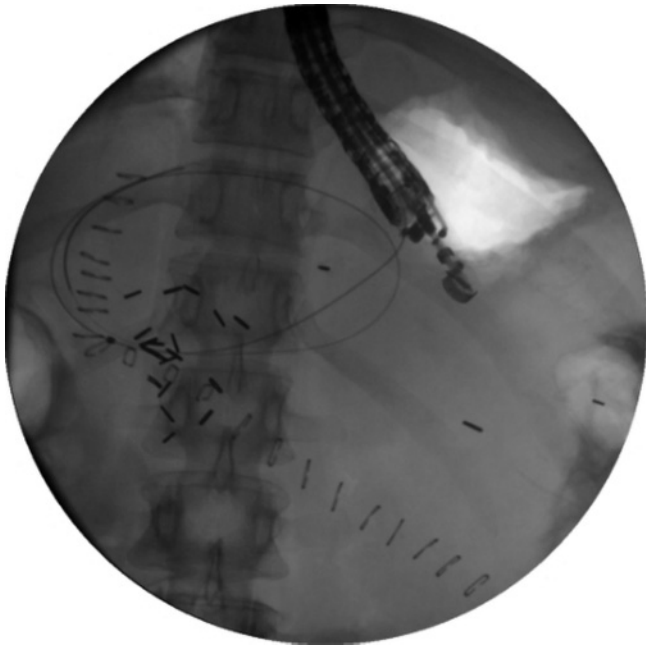

Figure 34.7 A 0.035-inch guidewire is coiled within the pseudocyst under fluoroscopic guidance.

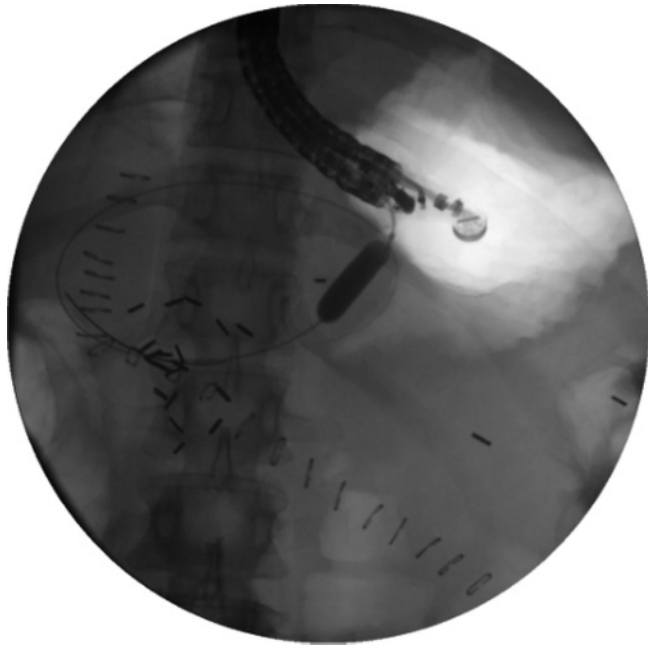

Figure 34.9 The transmural tract is subsequently dilated using a 8 mm over-the-wire biliary balloon dilator.

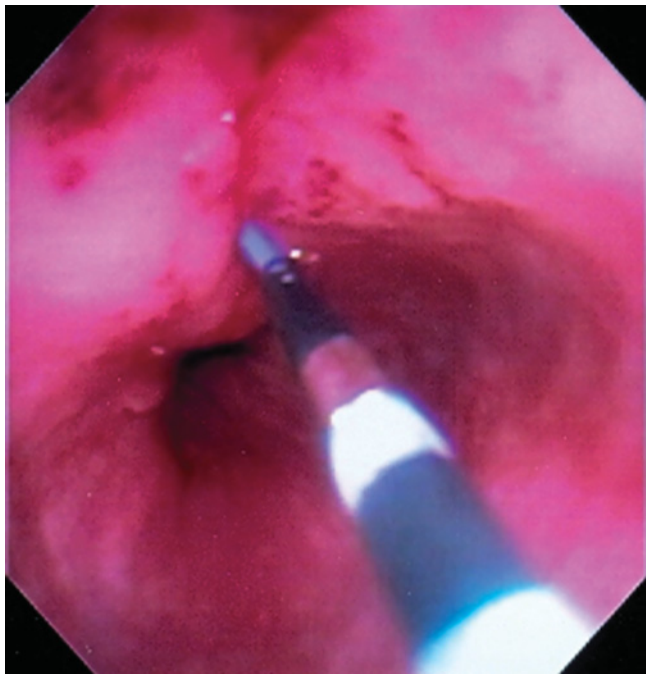

Figure 34.8 The transmural tract is dilated using a 5-French (Fr) endoscopic retrograde cholangiopancreatography (ERCP) cannula.

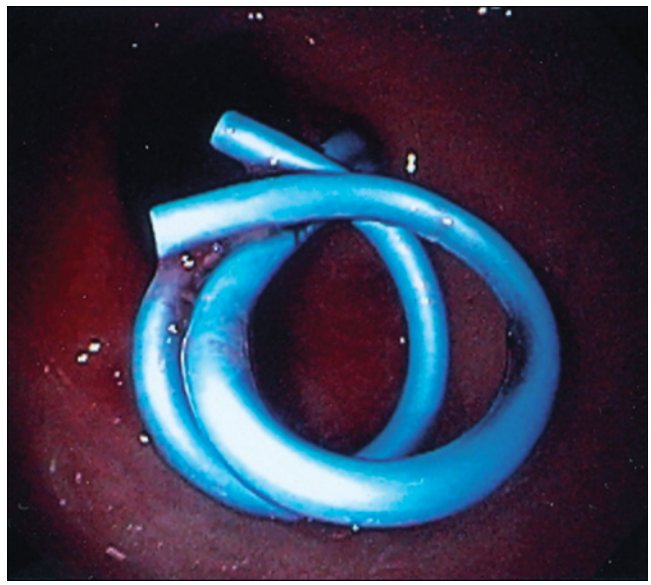

Figure 34.10 Multiple 7-French (Fr) transmural stents are deployed (fluoroscopy view) to facilitate drainage of pseudocyst contents.

7-Fr stents are being deployed. Multiple wires should not be placed when 10-Fr stents are deployed due to small diameter of the echoendoscope channel. In such cases, it is better to cannulate again for subsequent deployment of individual 10-Fr stents. During stent deployment, it is vital to keep the tip of the echoendoscope straight to avoid resistance. Sometimes, the thick viscous fluid from the PC can clog the biopsy channel and create friction during stent passage. This can be minimized by spraying PAM® (a cooking lubricant) through the biopsy channel prior to stent passage. Pseudocysts with large amount of debris may require placement of a nasocystic drainage catheter (in addition to stents) to facili-

tate continuous irrigation and evacuation of cyst contents over a few days.

Post-procedure follow up

After the procedure, the patient is observed for signs of infection, bleeding, or pancreatitis. Majority of patients can resume oral intake the same day. Antibiotics are continued for 48 hours. A follow-up computed tomography (CT) is usually undertaken in 6–8 weeks to assess response to therapy. However, following the procedure, if a patient develops persistent pain, unremitting fever, chills or leucocytosis, a CT scan should be obtained to rule out procedural complications.

Chapter video clip

Video 34.1 Video demonstrating the technique of EUS-guided pseudocyst drainage.

35 How to do Pancreatic Cyst Ablation

John DeWitt
Indiana University Medical Center, Indianapolis, IN, USA

Pancreatic cysts may be benign (pseudocysts) or have a negligible malignant potential (serous cystadenomas) while others represent premalignant (i.e. intraductal papillary mucinous neoplasms [IPMNs] or mucinous cystic neoplasms [MCNs]), or malignant (i.e. invasive IPMNs or mucinous cystadenocarcinomas) tumors. Due to significant morbidity and rare mortality associated with pancreatic surgery, a minimally invasive technique for pancreatic cyst ablation would be an attractive option for premalignant lesions, particularly in high-risk patients with multiple preoperative comorbidities. The premalignant potential of pancreatic cysts arises from the epithelial cells that line the cyst. The theoretical benefit of cyst ablation therefore arises from destruction of these cells and perhaps the malignant potential. Because of the close apposition between the endoscope and the pancreas, endoscopic ultrasound (EUS) would seem to be an ideal minimally invasive technique for guiding pancreatic cyst and tissue ablation. Ethanol is a commonly used ablative agent for solid and cystic tumors in a variety of sites. It is widely available, inexpensive, often effective, and relatively easy to administer. For EUS-guided cyst ablation, ethanol has been the most commonly used agent and concentrations up to 100% have been utilized. Recent studies have reported the additional use of dilute (3 mg/ml) paclitaxel which is injected and left within the cyst after ethanol lavage has been completed.

Prior to EUS cyst ablation, baseline characteristics of the cyst with regard to location (head, body, tail, neck, or uncinate), maximal diameter, wall thickness, number of septations, and presence of any internal debris or associated mass should be recorded. Cysts that have been treated in published studies are generally clinically suspected mucinous cysts that measure between 1 and 5 cm in diameter. These are usually found incidentally or possibly in patients with minimal nonspecific abdominal pain believed to be unrelated to the cyst. Patients with previous acute pancreatitis or worrisome symptoms such as weight loss or jaundice should not be treated. Complex cysts associated with a hypoechoic mass are also not candidates for ablation due to the possibility of underlying malignancy. Round unilocular cysts with well-defined margins are the easiest cysts to treat. Branched duct IPMNs while often treatable may have complex morphologies or three-dimensional orientations that preclude safe treatment. Recent studies suggest that the presence of septations and mural nodules should not prevent attempted ablation.

All studies published to date on EUS-guided pancreatic cyst ablation have used a 22-gauge needle; the safety of a 19-gauge needle has not been evaluated. Preloading a needle with the ablative agent is generally not recommended due the possibility of deposition of the agent in an unintended site should more than one pass into the cyst be required to optimally orient the needle. If analysis of the cyst fluid is not required, then use of a stylet prior to cyst ablation is not essential. The technique of cyst ablation begins with transgastric or transduodenal passage of a fine needle aspirate (FNA) needle into a cyst using a linear echoendoscope. A 10-ml syringe is then attached to the proximal end of the needle and near complete evacuation of the cyst is attempted. It is critical that the cyst is not completely collapsed in order to assure the endosonographer that the needle remains within the cyst prior to injection of the ablative agent. If little to no fluid is obtained in the syringe during initial cyst aspiration of viscous cyst fluid and/or a small cyst cavity, then 0.5 ml of saline or the ablative agent can be injected into the cyst to decrease the viscosity of the cyst fluid or expand the small cyst cavity to confirm proper needle placement. If aspiration of cyst fluid can be performed, then the amount of aspirated fluid, the viscosity, and the color of the cyst fluid should be noted. With the needle in the nearly collapsed cyst, the ablative agent is injected in the cyst by using a volume equal to that initially aspirated in the syringe from the cyst (Video 35.1). Studies to date have performed cyst lavage for 5 minutes, alternately filling and emptying the cavity. For

Atlas of Endoscopic Ultrasonography, First Edition. Edited by Frank G. Gress, Thomas J. Savides, Brenna Casey Bounds, John C. Deutsch.

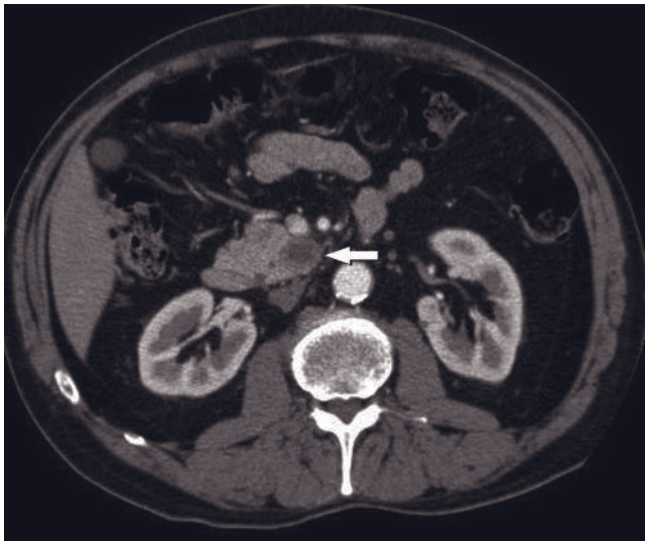

(a)

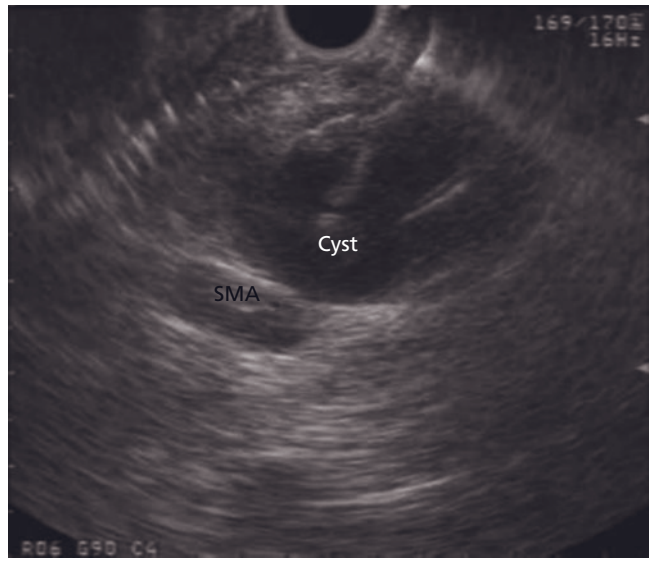

(b)

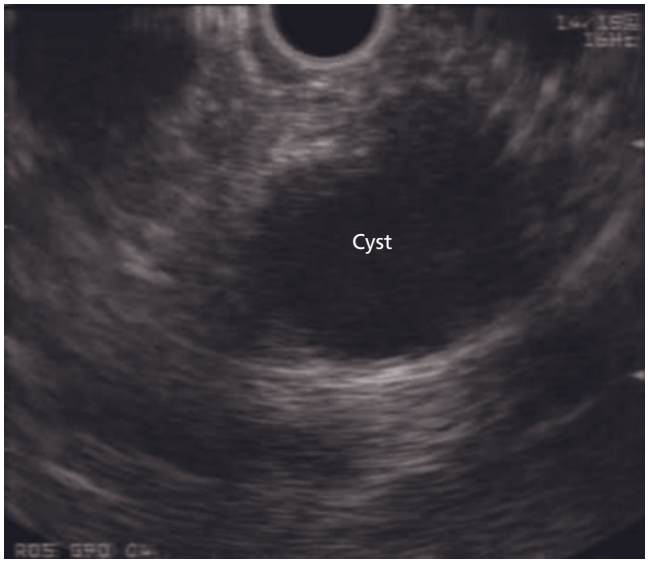

(c)

(d)

Figure 35.1 a: Baseline axial computed tomography (CT) scan with intravenous (IV) contrast in a 79 year-old asymptomatic male demonstrating a 22 × 21 mm cyst (white arrow) in the uncinate process of the pancreas. (b) Linear endoscopic ultrasound (EUS) demonstrating the corresponding cyst between the duodenal wall and the superior mesenteric artery (SMA). EUS-FNA of the pancreatic cyst is performed with a 22-gauge needle. Cyst fluid analysis before ablation demonstrated: CEA 22 040 ng/ml (normal <2.5), amylase 93 U/L (normal 25–161), and cytology demonstrating benign cyst contents. The clinical diagnosis was a mucinous cystic neoplasm. Ethanol cyst ablation was performed. (c) Linear EUS 3 months after initial EUS-ablation showing little change in the cyst which now measured 19 × 16 mm in diameter. A second ethanol lavage was performed. Final cytology from EUS-FNA before the second ablation showed atypical mucinous epithelial cells therefore surgery was recommended. (d) Gross specimen obtained following enucleation of the uncinate cyst. (e) Photomicrograph of surgical histopathology (H&E; 2×) demonstrating complete ablation of the mucinous epithelial cells lining the pancreatic cyst. (f) Higher power view of enucleated specimen demonstrating absence of epithelial cells and replacement with fibrosis (H&E; 4×). There is an infiltration of chronic inflammatory cells.

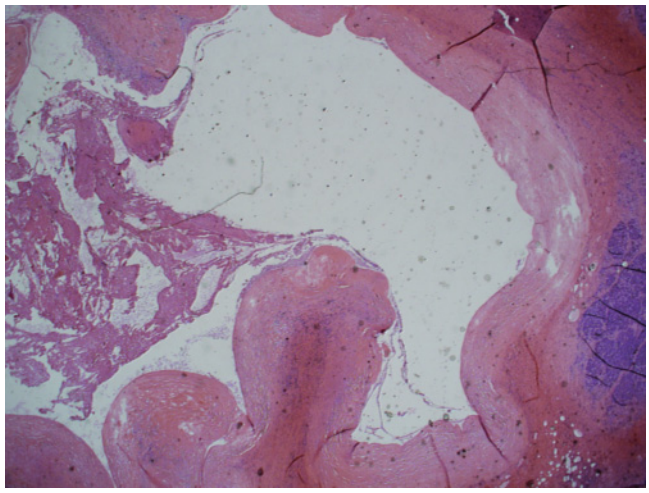

(e)

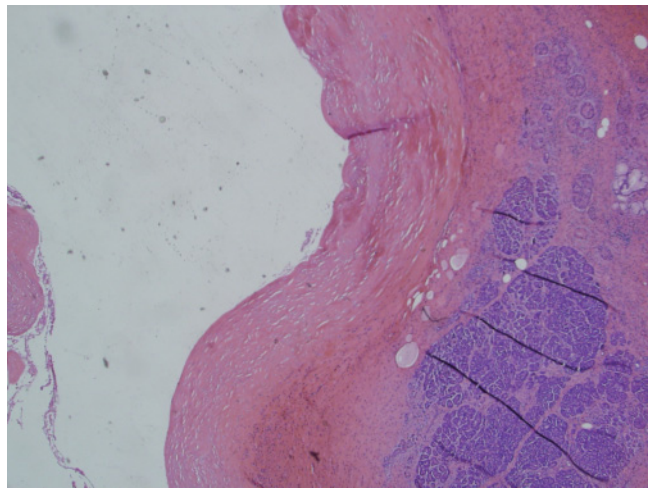

(f)

Figure 35.1 (*Continued*)

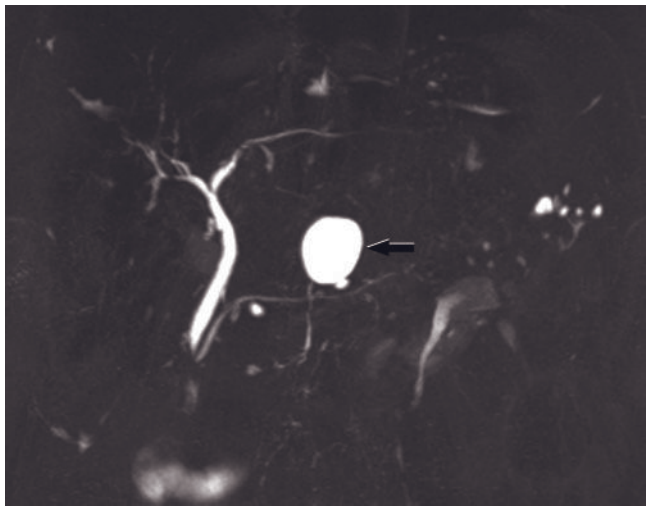

(a)

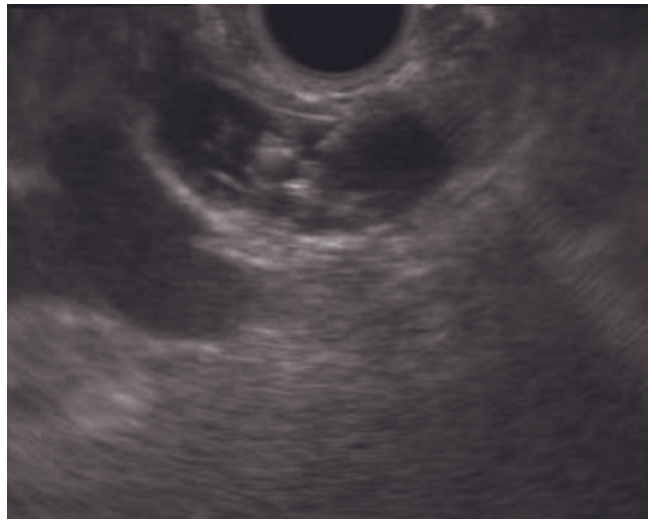

(b)

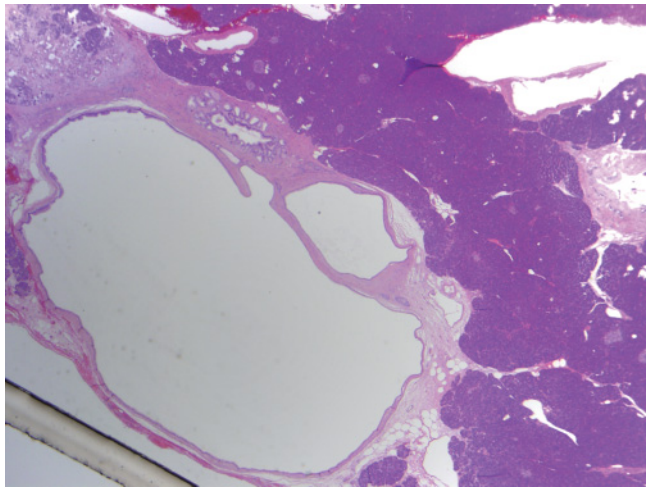

(c)

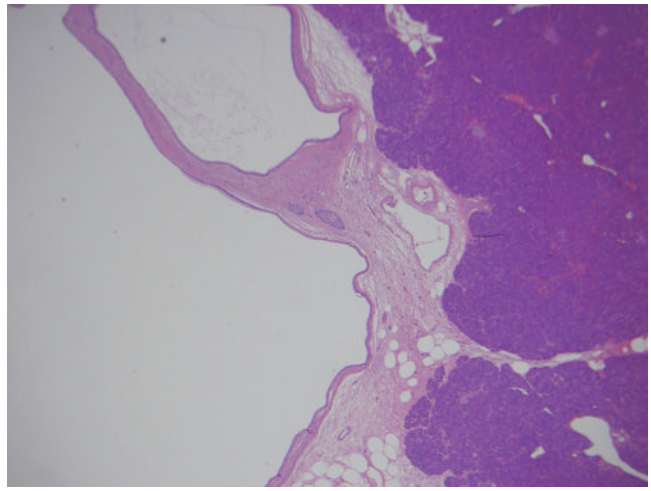

(d)

Figure 35.2 (a) Baseline magnetic resonance image (MRI) in a 63-year-old female with non-specific abdominal pain demonstrating a 2.2 cm cyst (black arrow) in the body of the pancreas in continuity with a normal diameter main pancreatic duct. There are other smaller cysts in the pancreatic tail. The findings are consistent with a multifocal branched duct intraductal papillary mucinous neoplasm (IPMN). The patient participated in a randomized trial and was assigned to saline lavage. (b) Endoscopic ultrasound (EUS) -guided saline lavage of the cyst. Follow up computed tomography (CT) 3 months later demonstrated no significant change in the size of the cyst and the patient refused consideration of further treatment. About 15 months later, the patient chose to undergo surgical resection due to enlargement of the cyst. (c) Low power photomicrograph of surgical pathology from central pancreatectomy demonstrating an IPMN-adenoma (H&E; 4×). No epithelial ablation was observed. (d) Higher power photomicrograph demonstrating intact columnar epithelium (H&E; 10×).

cysts with viscous fluid, this averages 3–4 lavages over the 5-minute period, whereas thin fluid would allow 7–8 lavages over the same period. At the conclusion of the lavage, the injectate/cyst fluid mixture should be completely drained of fluid as much as possible. Patients should be monitored in a recovery unit for at least 2 hours after EUS for the development of abdominal pain, hypotension, and nausea or vomiting. One dose of an intravenous antibiotic (i.e. ampicillin/sulbactam or ciprofloxacin) should be given and a prescription for an additional 3 days of an oral antibiotic (i.e. amoxicillin/clavulinic acid or ciprofloxacin) to be taken after discharge. Follow up intravenous contrast pancreas protocol computed tomography (CT) or EUS is recommended 2–3 months after initial ablation to assess treatment response.

As with any ablative technique, safety and treatment success are important initial parameters for assessment. Initial published experience has shown complications from EUS-guided pancreatic cyst ablation with ethanol and/or paclitaxel have included acute pancreatitis in 4.5–10.0% and abdominal pain in up to 20%. Complications do not appear to be higher in cysts that communicate with the main pancreatic duct (i.e. branched IPMNs) compared to those which

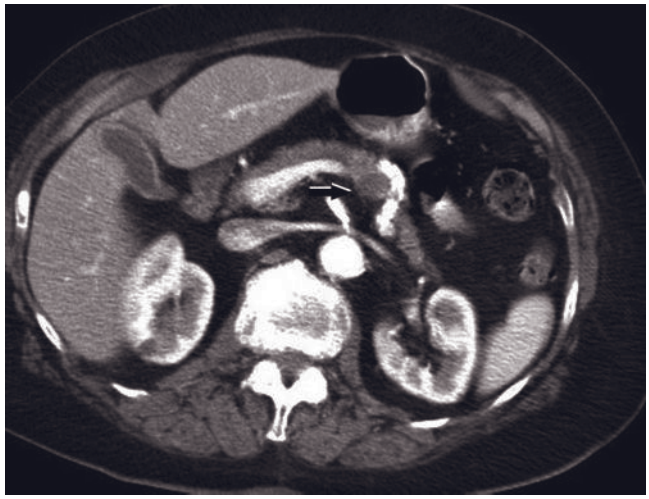

(a)

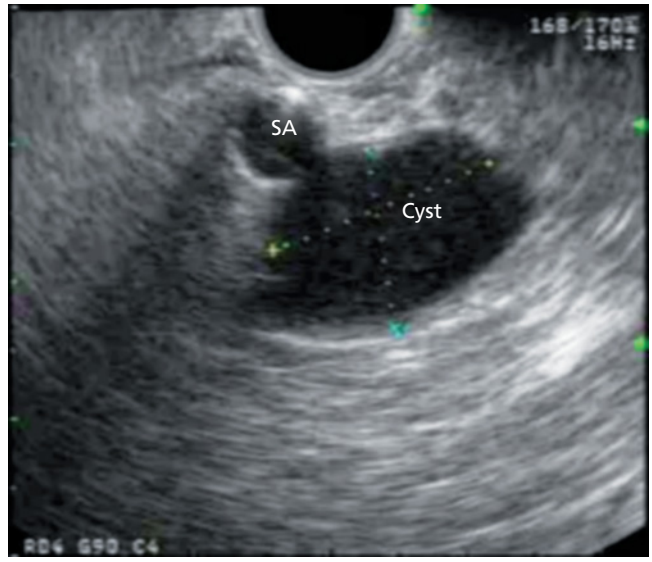

(b)

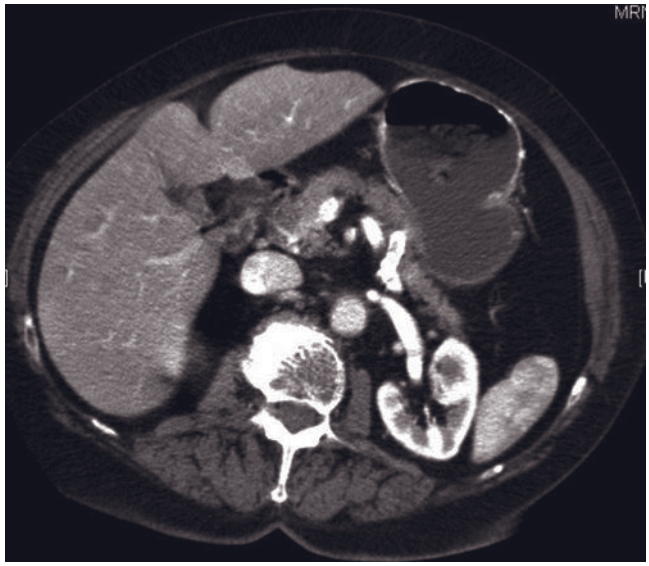

(c)

Figure 35.3 (a) Baseline axial computed tomography (CT) scan in an asymptomatic 82-year-old female demonstrating a 17-mm cyst (black arrow) in the body of the pancreas. (b) Corresponding linear endoscopic ultrasound (EUS) in the same patient demonstrating the cyst adjacent to the splenic artery (SA). The patient underwent two ethanol lavages; follow up CT scan 6 months after the second lavage demonstrated resolution of the cyst. (c) Axial CT 32 months after initial CT documentation of cyst resolution demonstrating continued absence of any pancreatic cyst.

rarely communicate (MCNs). Data published to date has demonstrated that patients undergoing surgical resection of pancreatic cysts following one or two ethanol ablations have cyst epithelial ablation ranging from 50% to 100% (Figure 35.1). This is in contrast to saline ablation which offers no cyst epithelial destruction (Figure 35.2). Reported short term, CT-defined cyst resolution rates with this technique reportedly range from 33% to 79%. Recent studies also suggest that this short term, imaging-defined cyst resolution is durable with longer term follow up (Figure 35.3).

Chapter video clip

Video 35.1 Ethanol lavage of a pancreatic tail cyst.

36 How to do Celiac Plexus Block

Adam J. Goodman and Frank G. Gress
SUNY Downstate Medical Center, Brooklyn, NY, USA

Introduction

Pain that develops as a result of pancreatic cancer (Figure 36.1) or chronic pancreatitis (Figure 36.2) is often difficult to manage. Various methods have been used to treat these patients including narcotic analgesia, antidepressants, pancreatic enzymes, octreotide, denervation procedures, and palliative or decompression/drainage procedures. Opioid analgesics can effectively treat pain, but are associated with numerous side effects including constipation, delirium, nausea, and the potential for addiction in patients with chronic pancreatitis. Non-pharmacologic methods of pain control may improve quality of life and minimize drug-related side effects.

The celiac plexus lies anterior to the aorta at the level of the celiac artery (Figure 36.3). Most of the sensory nerves returning from the pancreas and other intra-abdominal viscera pass through the celiac ganglion and splanchnic nerves and interruption of these fibers may lessen pain in pancreatic malignancies and chronic pancreatitis. Celiac plexus block (CPB) is a temporizing treatment where a steroid and long-acting local anesthetic are injected into the celiac plexus to control pain associated with chronic pancreatitis. Celiac plexus neurolysis (CPN) is used in patients with pancreatic cancer and refers to the injection of alcohol or phenol, a more permanent agent, into the celiac plexus in attempt to ablate the nerve fibers that transmit pain.

The efficacy of CPN for the treatment of cancer pain has been demonstrated in a number of studies with pain control in 70–90% of patients up to 3 months after the procedure. CPB may have a role in the treatment of pain related to chronic pancreatitis. One study consisting of 18 patients with chronic pancreatitis noted a reduction in pain in 50% (5/10) of patients undergoing endoscopic ultrasound (EUS) -guided CPB compared with 25% (2/8) of patients undergoing computed tomography (CT) -guided blocks. The benefit persisted for up to 24 weeks in 30% of responders. Other studies have demonstrated significant improvement in overall pain scores in approximately 55% of patients at up to 8 weeks of follow up; however, only 10% of patients noted a persistent benefit beyond 24 weeks.

Technique (Video 36.1)

Patients with inoperable pancreatic cancer and pain requiring narcotic analgesics are potential candidates for CPN. Selection of patients with pain related to chronic pancreatitis for CPB is less clear; however, patients wishing to avoid narcotics or those with pain refractory to high doses of narcotics may be appropriate candidates.

Prior to the procedure the patient is hydrated with intravenous saline (500–1000 ml). Then the patient is placed in the left lateral decubitus position and sedation is administered. The linear array echoendoscope is advanced to just below the gastroesophageal (GE) junction where a sagittal view of the aorta is obtained through the posterior gastric wall. The aorta is traced to the celiac trunk, the first large vessel emerging off the aorta, and the second branch is usually easily identified as the superior mesenteric artery (Figure 36.4). Identifying both the celiac and superior mesenteric artery helps to confirm correct location. Color flow Doppler should be used to exclude any intervening vessels.

The stylet is removed from the 22-gauge FNA needle and the entire system is flushed with normal saline to remove any air as this can interfere with imaging. Using real-time imaging, the FNA needle is inserted immediately lateral and anterior to the aorta at the level of the celiac trunk via a transgastric approach (Figure 36.5). A small amount (2 ml) of 0.9% saline is injected to clear the needle. An assistant then aspirates a 10-ml syringe filled with 0.9% saline for

Atlas of Endoscopic Ultrasonography, First Edition. Edited by Frank G. Gress, Thomas J. Savides, Brenna Casey Bounds, John C. Deutsch.

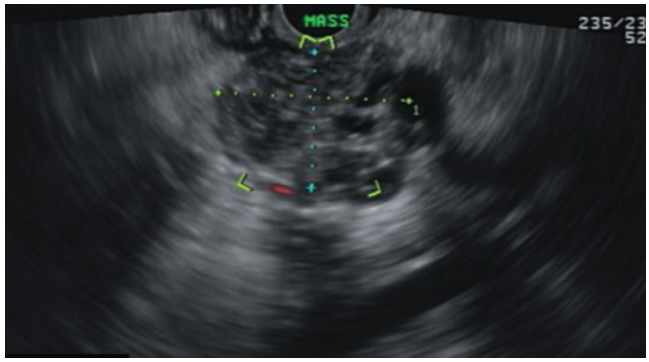

Figure 36.1 Hypoechoic pancreatic mass as seen by endoscopic ultrasonography.

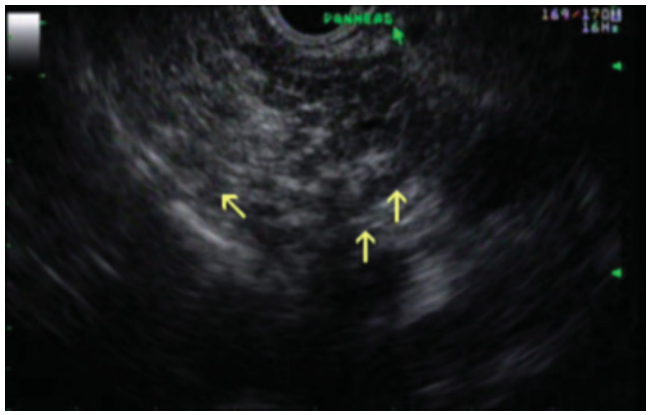

Figure 36.2 Endoscopic ultrasound demonstration of lobularity; one of the major criteria to help diagnose chronic pancreatitis by endoscopic ultrasonography.

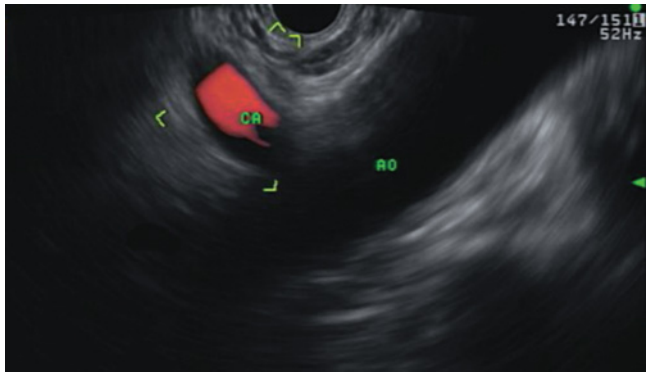

Figure 36.3 Celiac axis as seen by endoscopic ultrasonography.

approximately 10 seconds. This is to confirm that the needle is not within any of the regional blood vessels.

Injections into the celiac axis can be performed in two ways: one in which the injection is performed with the entire amount of medication infused at a single site at the base of the celiac artery takeoff, and one in which injections are performed by rotating to each side of the celiac trunk.

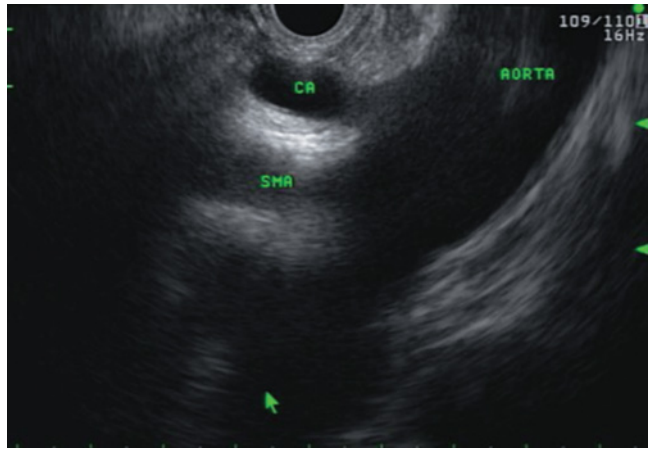

Figure 36.4 Celiac axis confirmed by the aorta, celiac artery and superior mesenteric artery.

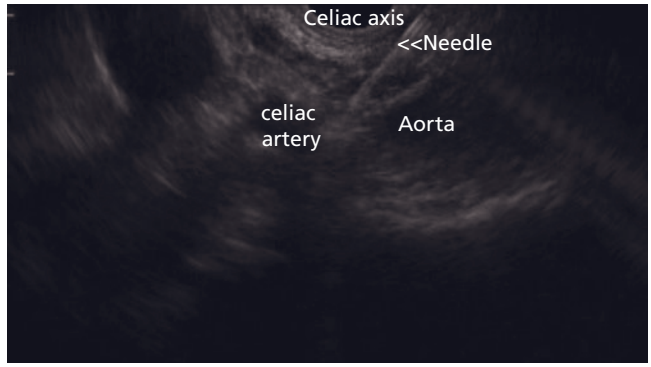

Figure 36.5 Insertion of the endoscopic ultrasound-guided fine needle aspiration (EUS-FNA) needle into the area of the celiac axis.

For CPB, 20 ml of preservative-free bupivacaine (0.25%) followed by 80 mg of triamcinolone is injected followed by 3–5 ml of saline. For CPN, 20 ml of bupivacaine (0.25%) followed by 20 ml of dehydrated alcohol is injected at the base of the celiac artery. After alcohol injection the needle is flushed with 3 ml of saline prior to withdrawal.

Alternatively, two separate injections are performed by rotating to each side of the celiac trunk. With this technique, 10 ml of bupivacaine (0.25%) and 10 ml of dehydrated alcohol in CPN and 10 ml of bupivacaine (0.25%) followed by 40 mg (1 ml) of triamcinolone in CPB are injected on each side of the celiac trunk. The aspiration test is repeated before each injection. It is believed that the two techniques have similar results.

The examination usually takes 30 minutes and is performed on an outpatient basis. Recovery time is usually 2 hours. Before discharge, orthostatic blood pressure changes should be checked, and patients should be counseled regarding potential complications.

Complications

Endoscopic ultrasound-guided CPB and CPN are generally effective, safe, and well-tolerated procedures. The three most common complications are transient hypotension (20–40%), transient diarrhea (4–38%), and transient increase in pain (9%). These symptoms are usually limited to 2 days post-procedure. Less common complications include unilateral paresis or paraplegia, pneumothorax, loss of sphincter function, retroperitoneal bleeding, renal puncture, and prolonged gastroparesis. In addition, cephalic spread of the neurolytic agent may result in involvement of the cardiac nerves and plexus. Infectious complications are uncommon but potentially serious. In a series of 90 patients, only one patient (1/90) developed an infectious complication (a peripancreatic abscess), which resolved with a 2-week course of antibiotics.

Chapter video clip

Video 36.1 How to do celiac plexus block.

37 How to Place Fiducials for Radiation Therapy

Satish Nagula[1] and Christopher J. DiMaio[2]

[1] SUNY Stony Brook School of Medicine, Stony Brook, NY, USA
[2] Mount Sinai School of Medicine, New York, NY, USA

Introduction

Traditional radiation therapy (RT), involving the delivery of high doses of toxic radiation to a target field, is wrought with the unfortunate consequence of acute and chronic injury to healthy tissue adjacent to the tumor. The development of real-time image-guided radiation therapy (IGRT) systems allows for the safe delivery of focal, high-dose RT to target lesions while minimizing the amount of collateral damage to normal tissue. These techniques, such as stereotactic radiosurgery and intensity-modulated RT, allow for the precise delivery of RT by being able to verify the target location and track its movement during the respiratory cycle. IGRT is dependent on reference points by which the target lesion can be identified and tracked. Fiducials are inert radiographic markers which are implanted into the target lesion for this purpose. Given the ability of endoscopic ultrasound (EUS) to allow for close proximity to structures in the mediastinum, abdomen, and pelvis that may not otherwise be accessible by percutaneous approaches, the use of EUS-guided fiducial placement into both luminal and extraluminal targets has become an accepted technique.

Equipment

Fiducials

Standard fiducial markers are cylindrical gold seeds. These markers measure 0.8 mm in diameter and 3–5 mm in length (Northwest Medical Physics Equipment Inc., Lynnwood, WA), and fit easily into the needle channel of the 19-gauge EUS needle. A newly available gold coil fiducial (Core Oncology, Santa Barbara, CA) has recently been introduced. These flexible gold coil fiducials are 0.35 mm in diameter and are available in lengths of 1 cm, 2 cm, and 3 cm (Figure 37.1; Video 37.1). Given their smaller diameter compared to standard fiducials, the coil fiducials can readily fit into the needle channel of a 22-gauge EUS needle.

Needles

Endoscopic ultrasound-guided fiducial placement can be performed with either a 19-gauge or 22-gauge EUS needle (Cook Medical, Winston-Salem, NC; Olympus, Center Valley, PA) depending on the diameter of the fiducial being used. Either method is acceptable. However, the size and stiffness of the 19-gauge EUS needle can restrict scope tip deflection and prevent close approximation of the tip to the luminal surface. This may result in suboptimal target lesion visualization. In addition, given the relatively larger diameter of the 19-gauge needle compared to the 22-gauge needle, difficulty may be encountered when attempting to penetrate a fibrotic tumor using the 19-gauge needle. For these reasons, EUS-guided fiducial placement using the 22-gauge needle may be preferable.

Techniques

Loading the needle

The stylet is retracted from the needle channel approximately 3 cm. The needle is then manually back-loaded with one fiducial marker. When using the gold cylindrical seeds with a 19-gauge needle, a pair of forceps is used to handle the fiducial and insert it into the needle channel. The gold coil fiducials come pre-loaded on a needle carrier delivery device, which facilitates back-loading into the 22-gauge needle (Figure 37.2; Videos 37.1 and 37.2). The delivery device consists of an outer trocar, through which the needle carrier passes. The fiducial sits on the tip of the needle carrier, and is held in place by a red retention marker. The diameter of the fiducial is larger than that of the outer trocar,

Atlas of Endoscopic Ultrasonography, First Edition. Edited by Frank G. Gress, Thomas J. Savides, Brenna Casey Bounds, John C. Deutsch.
 Published 2012 by Blackwell Publishing Ltd.

(a)

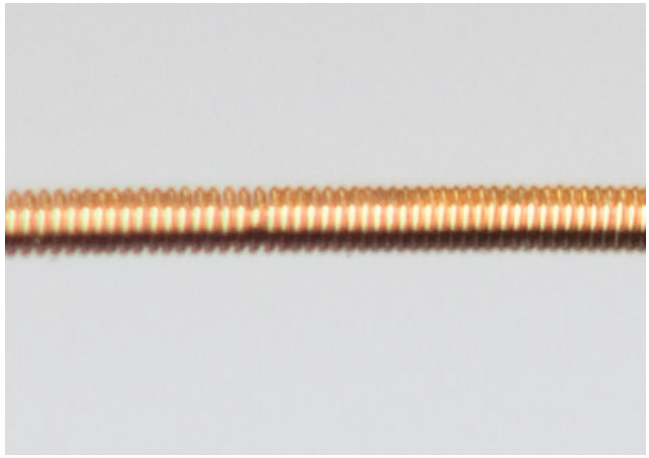

(b)

Figure 37.1 Gold coil fiducial marker is (a) flexible and (b) has a coiled design.

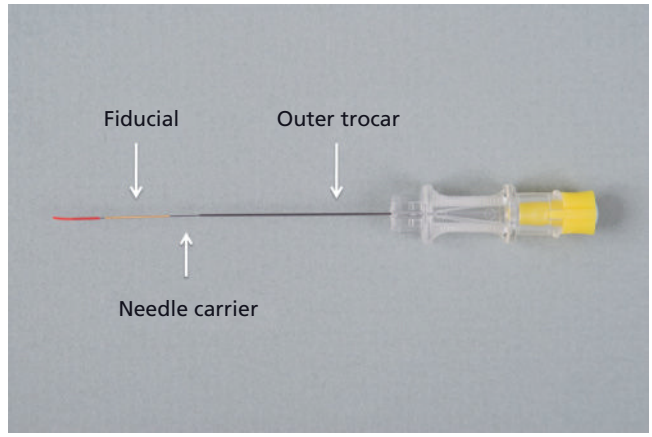

Figure 37.2 Gold coil fiducial pre-loaded on needle–carrier delivery device.

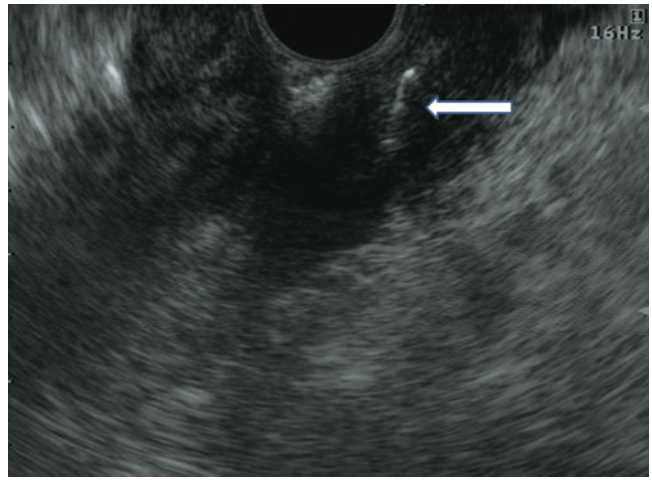

Figure 37.3 Endoscopic ultrasound image (linear array) of fiducial within an adenocarcinoma of the gastroesophageal junction.

such that when the needle carrier is withdrawn through the trocar, the fiducial is pushed off the needle carrier by the trocar. Thus, the pre-loaded needle carrier delivery device can be inserted into the tip of the 22-gauge needle and the fiducial can be deployed by withdrawing the needle carrier as described. Finally, the needle tip is sealed with a small amount of sterile bone wax, in order to prevent inadvertant loss of the fiducial while advancing the EUS needle down the accessory channel of the scope.

EUS-guided fiducial placement (Video 37.3)

Standard EUS evaluation is performed using a curvilinear array echoendoscope. Upon visualization of the target lesion, color Doppler imaging should be performed to ascertain for any intervening vascular structures. Once a safe window has been identified, the pre-loaded EUS needle is then inserted into the target lesion under EUS guidance. The stylet of the needle is then advanced to maximal insertion, effectively pushing the fiducial out of the EUS needle tip and into the target lesion (Figure 37.3). The EUS needle is withdrawn from the scope, re-loaded with a new fiducial, and the sequence repeated until the desired number of fiducial markers have been placed.

The number of fiducials placed is dependent on the size and location of the lesion. For small lesions measuring 1–3 cm (e.g. gastroesophageal junction tumors), a minimum of 2 fiducials should be placed to define the proximal and distal margins of the tumor. For larger lesions (e.g. pancreatic tumors) 3–6 fiducials should be placed in varying locations to define tumor borders and planes. Different IGRT protocols may call for specific fiducial locations, thus pre-procedure planning with a radiation oncologist is critical.

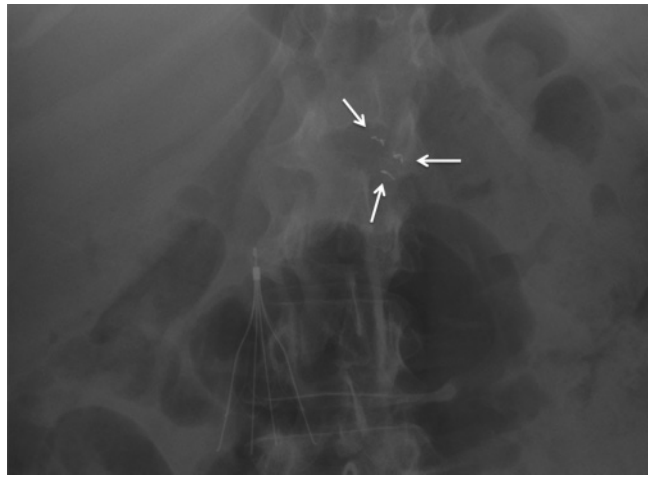

Figure 37.4 Abdominal radiograph (anteroposterior view) demonstrating three fiducials (arrows) located in an adenocarcinoma of the pancreatic head.

Peri-procedural care

Prophylactic antibiotics should be administered pre-procedure, however the benefit of this practice is unknown. The use of either sterile or clean non-sterile technique is acceptable when handling the fiducial markers, EUS needle, and bone wax.

Standard post-procedure monitoring of the patient should be employed. Complications related to EUS-guided fiducial placement are rare. However, site-specific pain, infectious, and inflammatory complications have been reported. Fiducial migration into adjacent soft tissue and vascular structures has also been reported. However the clinical significance of these rare events is unknown. Post-procedure radiographs can be obtained to confirm placement and location of the fiducial markers (Figure 37.4).

Chapter video clips

Video 37.1 EUS-guided insertion of a gold coil fiducial: device design.

Video 37.2 EUS-guided insertion of a gold coil fiducial: loading the fiducial.

Video 37.3 EUS-guided insertion of a gold coil fiducial: case examples.

38 How to Inject Chemotherapeutic Agents

V. Raman Muthusamy and Kenneth J. Chang
University of California, Irvine, Orange, CA, USA

Endoscopic ultrasound (EUS) -guided fine needle injection (FNI) has been used to directly administer chemotherapeutic agents within pancreatic and esophageal tumors. Agents used to date include an allogenic mixed lymphoctye culture and anti-tumor viral therapy using viral vectors encoding tumor necrosis factor-alpha (TNFα) or granulocyte-macrophage colony stimulating factor (GM-CSF). These agents can directly or synergistically assist in achieving tumor lysis. We describe below our specific technique for performing such procedures in pancreatic tumors using TNFerade™ (GenVec Inc., Gaithersburg, MD), a replication deficient adenovector encoding human TNFα and regulated by a radiation inducible promoter Egr-1, although the technique is similar for other anti-tumor agents.

Prior to each TNFerade injection, which requires five weekly injections in conjunction with chemoradiation therapy, attire approved by the institutional biosafety committee should be worn by all personnel involved in the procedure, given that a viral vector is being utilized. Typical gear includes material that achieves complete head covering, safety goggles, specially fitted masks to form a complete oral/facial shield, a gown, and gloves. The TNFerade solution is prepared by the pharmacy and is provided to the gastrointestinal (GI) laboratory immediately prior to the procedure. We typically use a 22-gauge fine needle aspiration (FNA) needle (EchoTip™, Cook Medical, Bloomington, IN) to administer the anti-tumor agent. Prior to inserting the FNA needle into the biopsy channel of the echoendoscope, we remove the stylet within the needle. For TNFerade, in which 2.0 cc is actually injected into the tumor, a total of 2.6 cc is usually provided in a 3.0 cc syringe by the pharmacy so that the entire needle channel can be primed prior to intratumoral injection. This is accomplished by attaching the 3.0 cc syringe to the FNA needle via the Luer-lock on the handle. The needle is then primed by injecting the therapeutic agent into the needle until the entire dead-space of the needle (usually 0.2–0.4 cc) contains fluid and fluid is witnessed exiting the needle tip. Fluid injection is then continued until exactly 2 ml remains in the syringe, at which point the needle is ready for use. Once the needle enters the tumor, the remainder of the fluid in the syringe is injected so that exactly 2 ml is delivered intratumorally.

We use a standard linear array echoendoscope (GFUC-140P, Olympus America, Center Valley, PA), operating at a 5 MHz frequency to achieve maximal imaging depth, to perform all EUS-guided FNI procedures. Prior to FNI of the tumor, we routinely assess the lesion at its maximal cross-section and measure its size, circumference, area, and estimate tumor volume (Figure 38.1). This is important initially to set a baseline tumor size and during subsequent weekly injections to assess tumor response or progression. We also perform a careful standard EUS exam to assess for the presence or development of metastatic disease. A detailed review of previous images/videos is critical to ensure comparable regions are measured during subsequent exams being done to measure tumor response. We have noted that as therapy progresses, the echotexture within the tumor may become brighter, possibly indicating the development of fibrosis within the treated lesion. We believe this finding corresponds to a region of the tumor that has achieved a good response to therapy. Areas that are anechoic often indicate a region of tumor necrosis. In contrast, we believe that portions of the lesion that are hypoechoic represent residual areas of viable tumor.

Our technique of EUS-guided FNI involves identifying the most hypoechoic area(s) of the lesion to inject. Once the target has been identified, we place the 22-gauge needle into the biopsy channel of the echoendoscope and Luer-lock it in place. We then line up the needle-tip to the targeted (hypoechoic) area of the lesion. Having an assistant hold the echoendoscope to stabilize its position at this juncture is often helpful. We then slowly advance the needle deep into the lesion using standard EUS-guided FNA technique. Upon reaching the deepest portion of the lesion, we slowly

Atlas of Endoscopic Ultrasonography, First Edition. Edited by Frank G. Gress, Thomas J. Savides, Brenna Casey Bounds, John C. Deutsch.

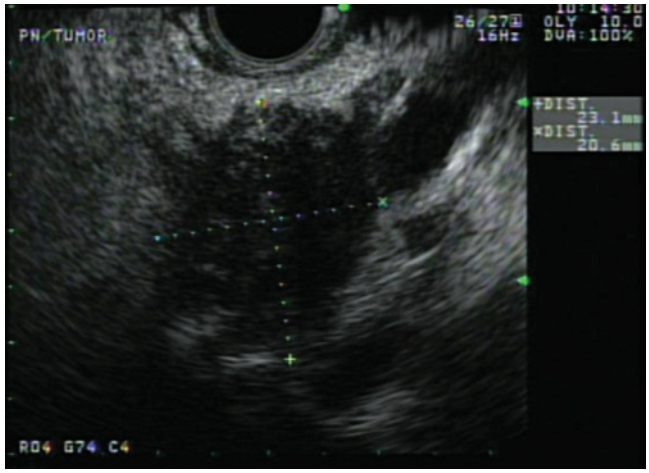

(a)

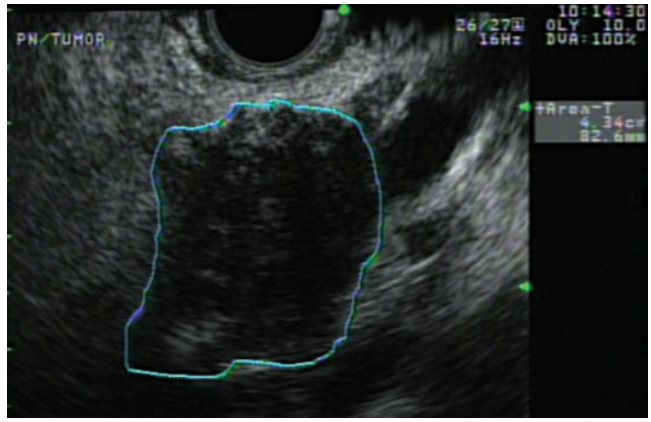

(b)

Figure 38.1 Initial assessment of tumor size by endoscopic ultrasound (EUS) imaging. (a) This figure illustrates the measurement of the tumor in maximal cross-section on EUS-imaging prior to injection therapy. (b) This figure highlights the ability of EUS to measure tumor area, circumference, and using this data, even estimate volume. (From: Chang *et al*. 2008. *Nature Clinical Practice Gastroenterology and Hepatology*, 5: 107–11.)

withdraw the needle and slowly inject the therapeutic agent into the well created by the FNA needle. A gradual, methodical withdrawal and injection is recommended to keep the entire injected solution within the tumor. We avoid injecting into anechoic (necrotic) regions and only inject on withdrawal (Figure 38.2). The needle can be realigned and redirected into other hypoechoic areas of the tumor in a fan-like fashion (Video 38.1). This is done by changing the angle of the elevator when the needle has reached the superficial portion of the tumor (that closest to the GI lumen on imaging) and re-advancing the needle into a new portion of the tumor. Again, withdrawal is done slowly and injection is performed during needle withdrawal only. This process can be repeated until the entire 2 cc in the syringe has been injected, at which time the needle is removed from the lesion and withdrawn from the echoendoscope and the procedure is complete. A typical intratumoral injection lasts only 2–3 minutes in duration.

Antibiotics are administered orally 3 hours pre-procedure and at 12 and 24 hours post-procedure. We typically administer a 500 mg dose of oral ciprofloxacin at these time points. The patient is recovered in a standard fashion in the endoscopy unit and then discharged to receive chemoradiation therapy. We believe that careful attention to chemotherapeutic injection technique is essential to achieving maximal results with these agents. An example of a vigorous response to such therapy is illustrated in Figures 38.3–38.5, which show a dramatic weekly reduction in size of a pancreatic tumor (Figure 38.3), with no residual tumor present in the gross resected specimen (Figure 38.4), or on histology (Figure 38.5).

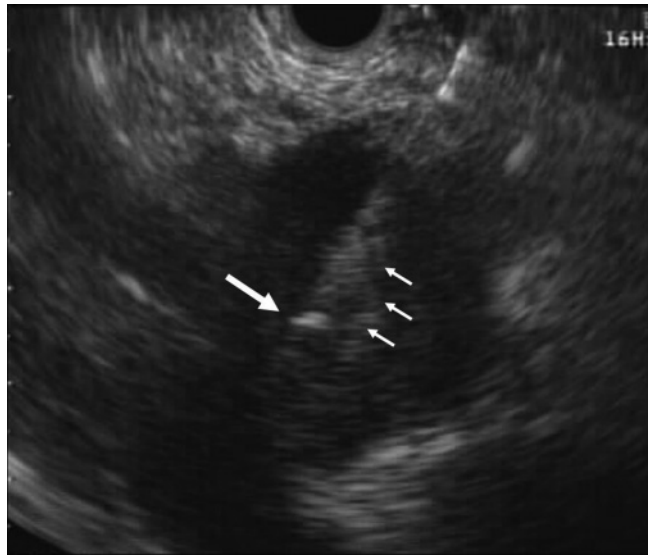

Figure 38.2 Endoscopic ultrasound (EUS) -guided fine needle injection (FNI) of a pancreatic lesion using a 22-gauge needle. The needle tip (large arrow) and the blush resulting from the injection of the chemotherapeutic agent around the needle (small arrows) can be seen. (From: Chang *et al*. 2008. *Nature Clinical Practice Gastroenterology and Hepatology*, 5: 107–11.)

Chapter video clip

Video 38.1 EUS-guided FNI of TNFerade into a pancreatic adenocarcinoma.

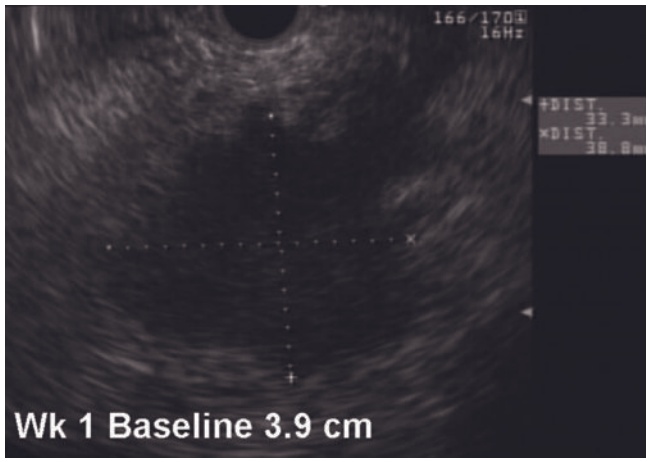

(a)

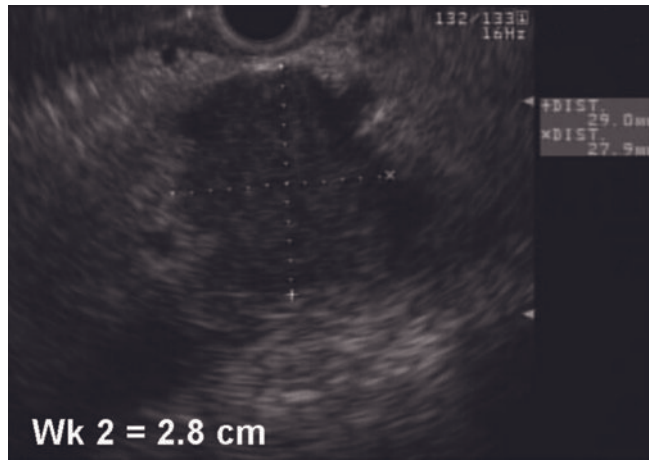

(b)

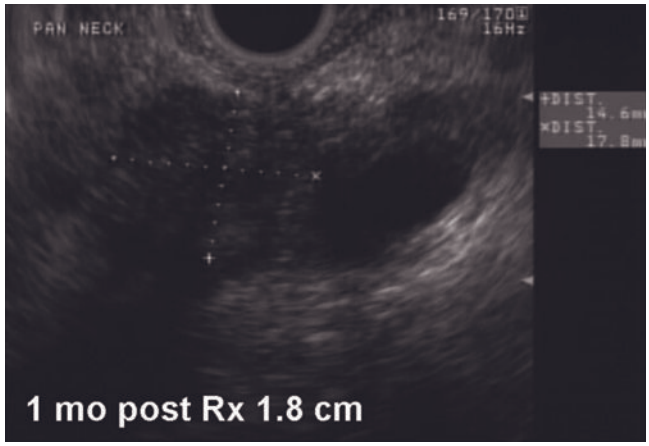

(c)

(d)

Figure 38.3 Tumor assessment during weekly injections of chemotherapeutic agents. These images show the assessment of tumor response at baseline: (a) week 1; (b) week 2; and (c) 1 month after completion of therapy (5 weekly injections). (d) Figure shows a fine needle aspiration (FNA) being performed of the residual lesion 1 month after therapy. (From: Chang *et al*. 2008. *Nature Clinical Practice Gastroenterology and Hepatology*, 5: 107–11.)

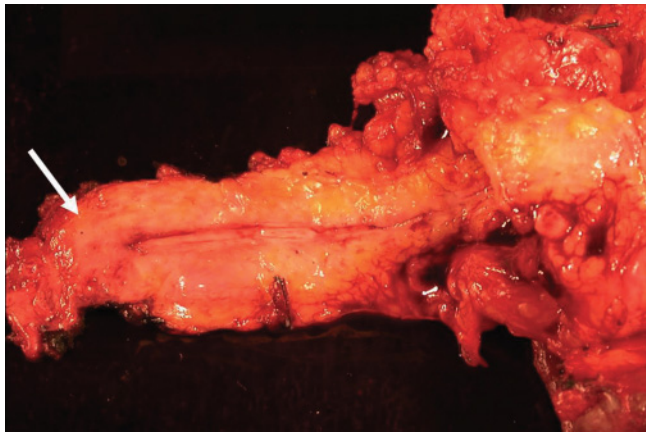

Figure 38.4 Gross specimen of the resected pancreas in Figure 38.3 revealing no residual tumor remaining. The area of the treated tumor can be seen (arrow). (From: Chang *et al*. 2008. *Nature Clinical Practice Gastroenterology and Hepatology*, 5: 107–11.)

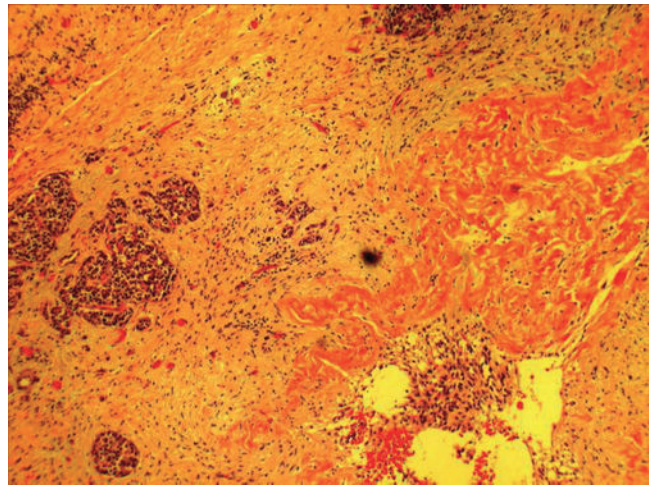

Figure 38.5 Histology from the specimen in Figure 38.4 demonstrating a complete pathologic response. (From: Chang *et al*. 2008. *Nature Clinical Practice Gastroenterology and Hepatology*, 5: 107–11.)

39 How to do EUS-guided Biliary Drainage

Jennifer Maranki and Michel Kahaleh
University of Virginia Health System, Charlottesville, VA, USA

Introduction

Endoscopic retrograde cholangiography (ERC) with stent placement has become the standard of care for biliary drainage in patients with obstructive jaundice. Biliary decompression in expert hands is successful in 90–95% of cases. Failure to cannulate the bile duct may be related to prior surgery, periampullary diverticula, tortuous ducts, impacted stones, or tumor infiltration. Most experts agree that after failed initial ERC, the next step is a referral to a tertiary care center. Alternative means of achieving biliary decompression include percutaneous transhepatic drainage (PTC), and surgical intervention. However, both are associated with significant morbidity.

The evolution of the linear-array echoendoscope has greatly increased the therapeutic potential of endoscopic ultrasound (EUS). It has become a crucial tool for fine needle aspiration (FNA), pancreatic pseudocyst drainage, and celiac plexus block and neurolysis. Anatomically, the biliary tree is in close approximation to the stomach and duodenum, thereby allowing its visualization. The next step was to offer EUS-guided drainage of the biliary system. Initial EUS-guided cholangiography was reported by Wiersema and colleagues in 1996 and involved 10 patients who failed standard biliary decompression. Today, this technique has been well established in achieving biliary drainage.

Techniques

Endoscopic ultrasound-guided biliary drainage (EUBD) is typically attempted with either a transenteric–transcholedochal (extrahepatic) or transgastric–transhepatic (intrahepatic) approach.

Extrahepatic approach

The echoendoscope is typically positioned in the duodenum or the distal antrum, depending on the anatomy. After color Doppler is used to identify adjacent vasculature (Figures 39.1 and 39.2), the EUS needle is then inserted into the bile duct and contrast injection is performed (Figure 39.3). The guidewire is advanced in an antegrade fashion and manipulated beyond the biliary obstruction and across the ampulla into the duodenum (Figure 39.4). At this point, a rendezvous is required to place a transpapillary stent. The echoendoscope is removed while leaving the guidewire in place (Figure 39.5). A duodenoscope is inserted and advanced to the duodenum, with visualization of the ampulla (Figure 39.6). The wire is then grasped with a snare and withdrawn through the accessory channel (Figure 39.7). The rest of the procedure can be completed using standard ERC with stent placement (Figure 39.8). If the guidewire cannot be advanced into the duodenum, a transenteric fistula can be created by dilating the tract with a 4–6 mm wire-guided balloon catheter or a 6–7 French (Fr) bougie, followed by stent placement.

Intrahepatic approach

The intrahepatic approach is performed with the echoendoscope positioned in the cardia or lesser curvature of the stomach to allow visualization of the dilated left intrahepatic biliary system. Once color Doppler has excluded overlying vasculature (Figure 39.9), the EUS needle is advanced into the intrahepatic duct, and contrast is injected to opacify the biliary tree (Figures 39.10 and 39.11; Video 39.1). A guidewire is then advanced in an antegrade fashion into the bile duct (Figure 39.12). The guidewire is manipulated beyond the biliary obstruction and across the ampulla into the duodenum. At this point, the procedure can be completed in either an antegrade fashion (Figures

Atlas of Endoscopic Ultrasonography, First Edition. Edited by Frank G. Gress, Thomas J. Savides, Brenna Casey Bounds, John C. Deutsch.

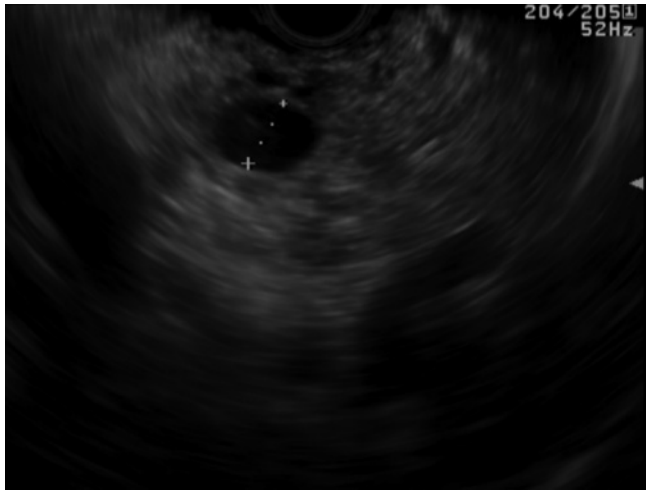

Figure 39.1 Ultrasonographic view with flow Doppler of a dilated common bile duct before endoscopic ultrasound-guided puncture during an extrahepatic approach.

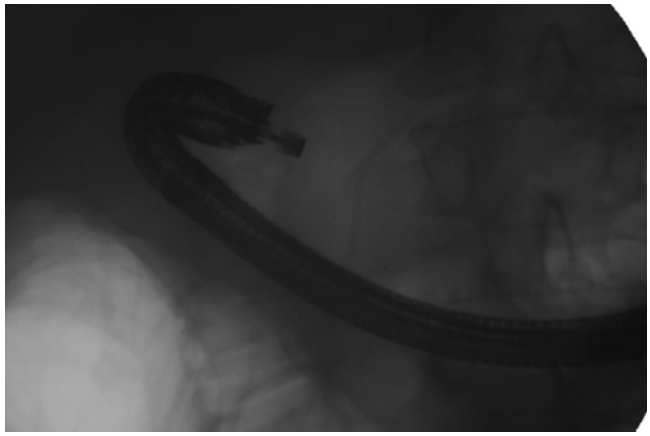

Figure 39.2 Fluoroscopic position of the echoendoscope in the bulb facing the dilated common bile duct after failed endoscopic retrograde cholangiography, pre-cut and pancreatic stent placement.

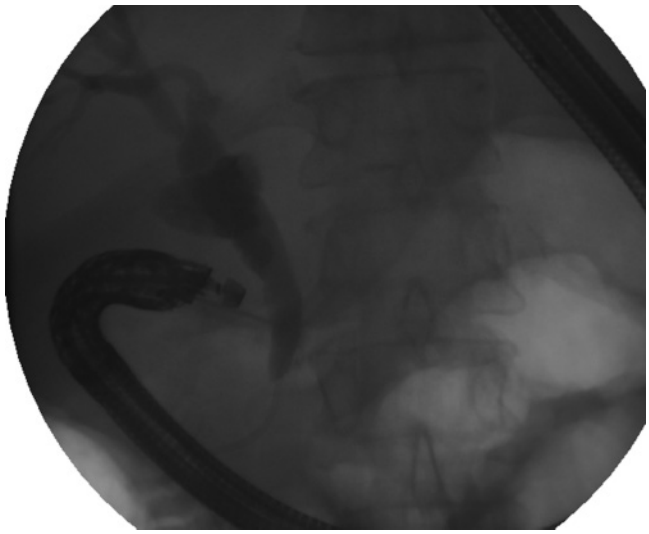

Figure 39.3 Injection of contrast through the endoscopic ultrasound needle, demonstrating dilated common bile dust above a distal stricture during an extrahepatic approach.

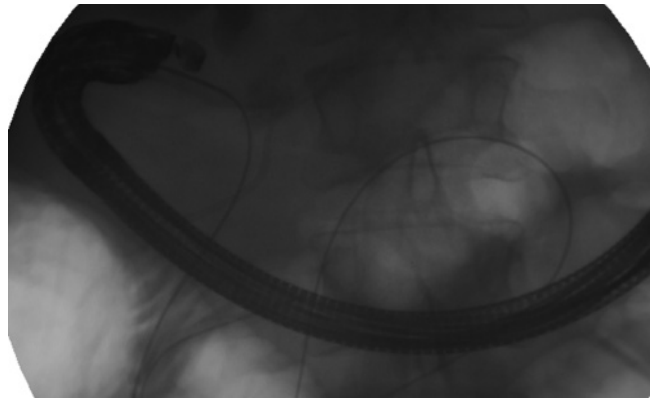

Figure 39.4 A guidewire is advanced into the bile duct across the stricture and into the duodenum during an extrahepatic approach.

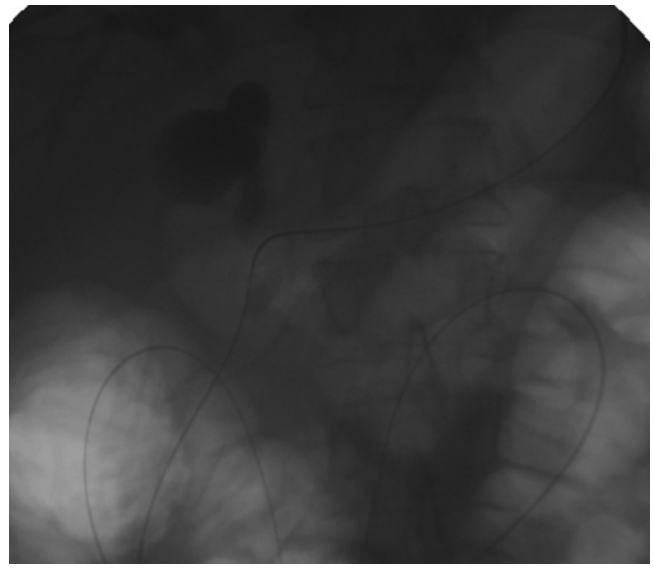

Figure 39.5 Removal of the echoendoscope leaving the guidewire in place across the stricture during an extrahepatic approach with rendezvous.

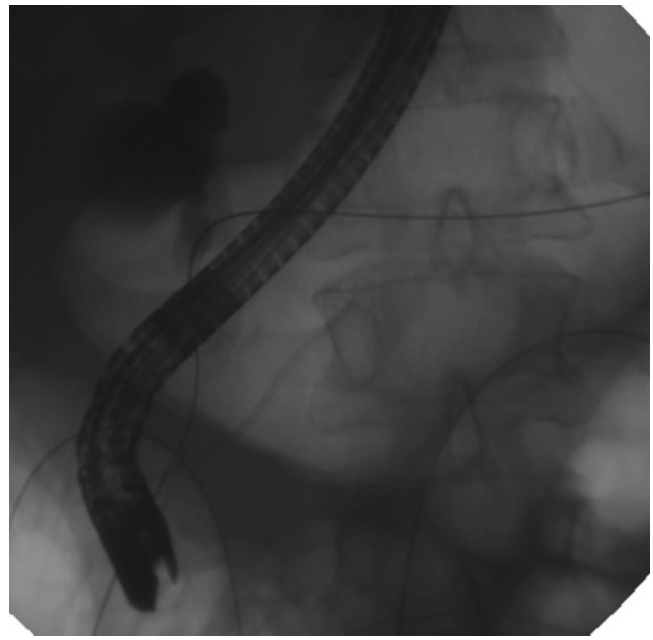

Figure 39.6 Advancement of the duodenoscope alongside the guidewire, up to the second portion of the duodenum, facing the wire protruding from the ampulla.

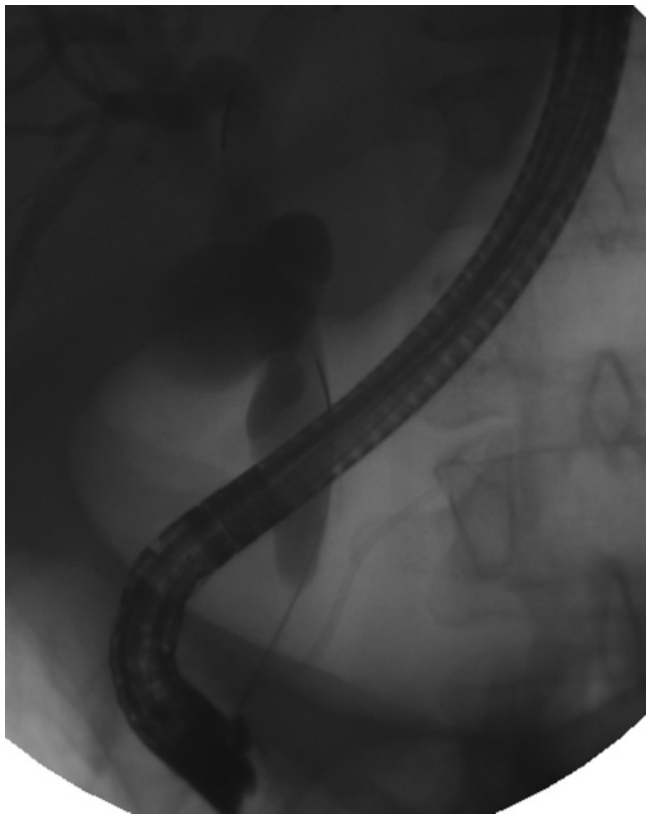

Figure 39.7 Rendezvous with access in the bile duct using the wire placed by ultrasonography.

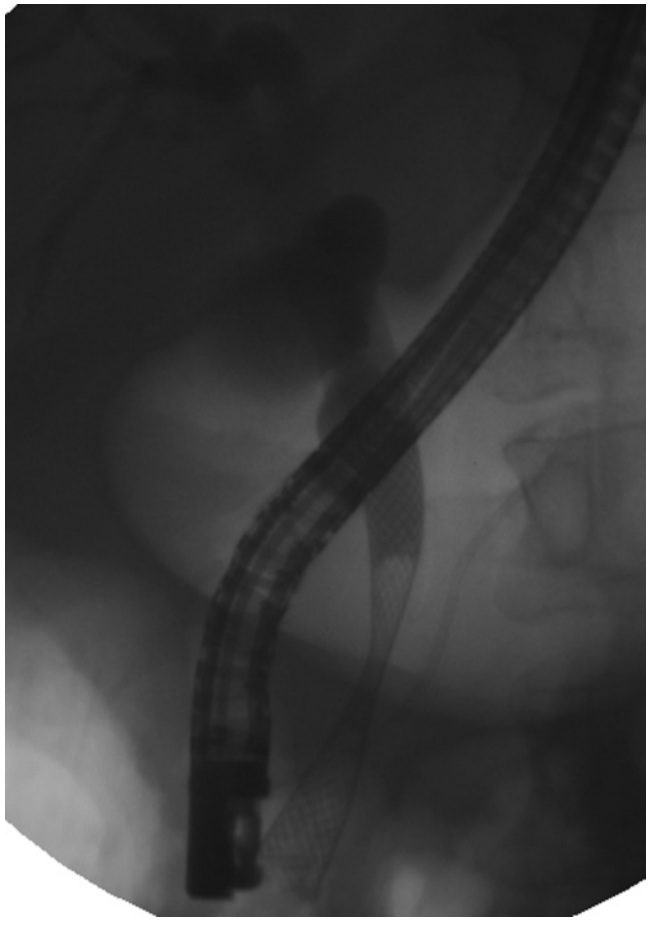

Figure 39.8 Placement of a metal stent across the distal stricture using endoscopic retrograde cholangiography.

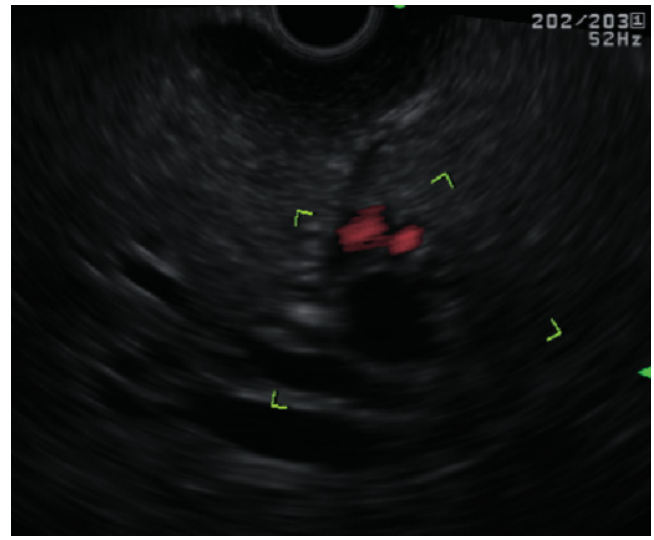

Figure 39.9 Ultrasonographic view with color flow Doppler of a dilated left hepatic before EUS-guided puncture during an intrahepatic approach.

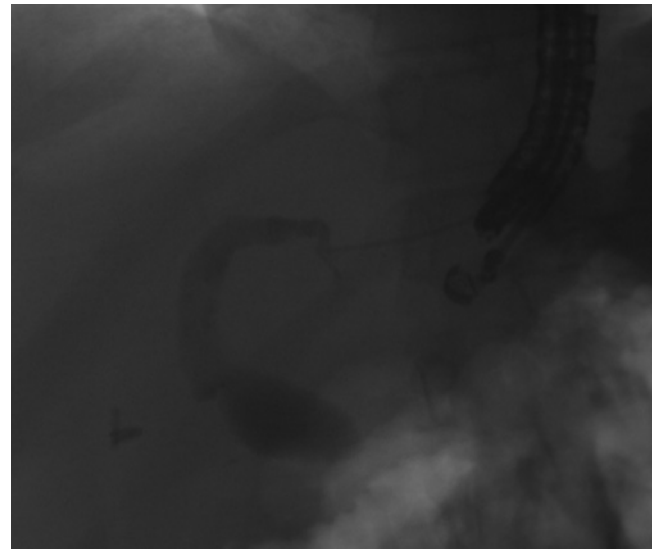

Figure 39.10 Injection of contrast through the endoscopic ultrasound needle, demonstrating successful opacification of the intrahepatic duct.

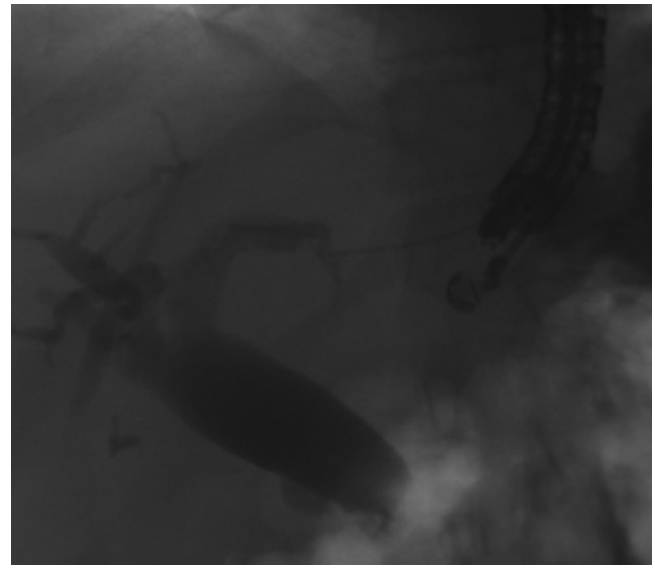

Figure 39.11 Further opacification demonstrating biliary dilation above a distal obstruction during an intrahepatic approach.

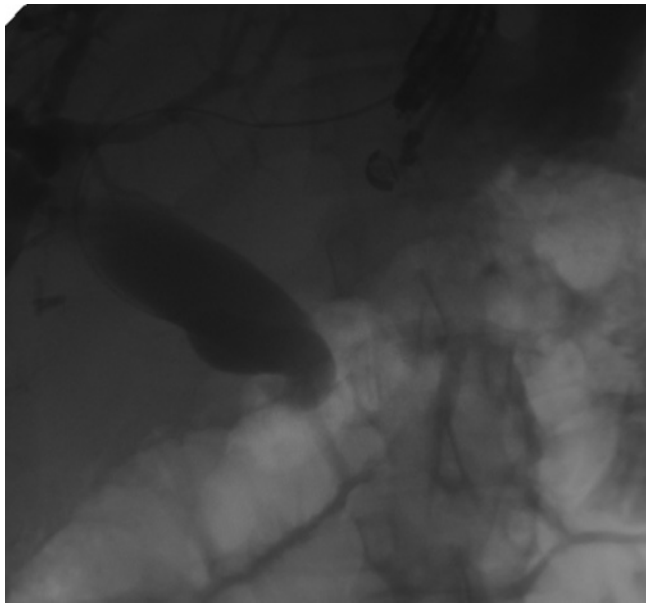

Figure 39.12 Advancement of the guidewire from the left hepatic duct in an antegrade fashion during an intrahepatic approach.

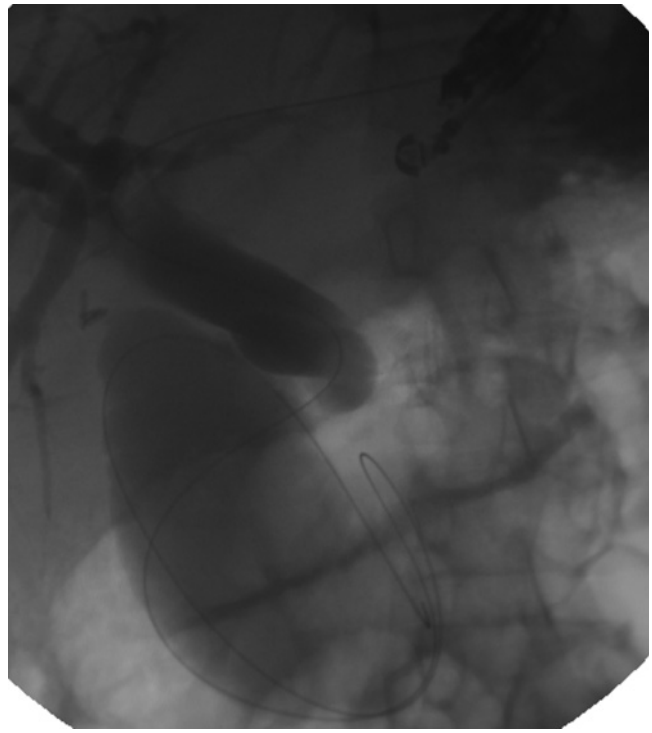

Figure 39.13 Advancement of the guidewire across the distal stricture and into the duodenum during an intrahepatic approach without rendezvous.

39.13 and 39.14) or with a rendezvous technique as described above.

Discussion

Wiersema *et al*. described the use of EUS-guided cholangiography guiding repeat successful ERC in seven patients. In 2003, Burmester *et al*. reported a series of four patients, undergoing creation of EUS-guided enterobiliary fistulas in three patients. Endoscopic ultrasound-guided drainage of obstructed biliary ducts via a rendezvous technique was first described in two patients by Mallery *et al*. Most recently, our group has reported the largest study of EUS-guided ERC performed in 49 patients. The overall success rate was 84% (41/49), with an overall complication rate of 16%. Thirty-five patients underwent the intrahepatic approach, with a success rate of 83% (29/35). Fourteen patients underwent the extrahepatic approach, with success in 12/14 patients, or 86%. Table 39.1 summarizes the published literature of EUS-guided biliary drainage to date with a cumulative success and complication rate of 122/135 (90%) and 25/135 (19%), respectively.

The main complications associated with EUS-guided biliary drainage include pneumoperitoneum, post-procedure pain, and bleeding; most of which tend to be managed conservatively. The risk of bile leak and perforation leading to biliary peritonitis was found to be fairly small based on the reported case series. Of the 135 cases reported, there were seven cases of pneumoperitoneum, one biliary leak, three

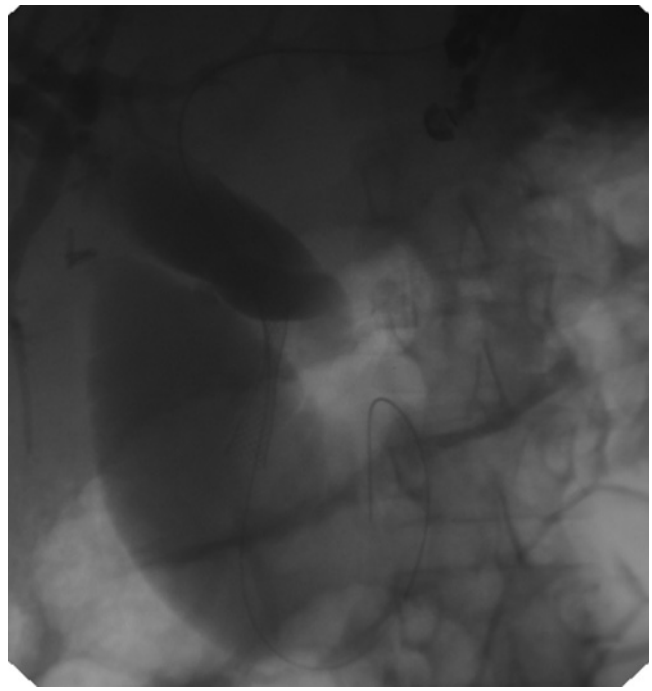

Figure 39.14 Placement of a metal stent across the distal stricture during an intrahepatic approach without rendezvous.

Table 39.1 Published series of endoscopic ultrasound-guided biliary drainage.

Author	Year	No. of patients	Technique	Complications	Rate of success*
Burmester *et al.*	2003	4	Intrahepatic (1) Extrahepatic (2)	Bile leak (1)	75% (3/4)
Mallery *et al.*	2004	2	Extrahepatic (2)	Wire perforation (1)	100% (2/2)
Puspok *et al.*	2005	6	Extrahepatic (6)	None	83% (5/6)
Bories *et al.*	2007	11	Intrahepatic (11)	Ileus (1), Stent shortening (2) Early blockage (1)	91% (10/11)
Will *et al.*	2007	8	Intrahepatic (7) Extrahepatic (1)	Slight pain (2), Cholangitis (1)	88% (7/8)
Tarantino *et al.*	2008	8	Extrahepatic (8)	Death from cirrhosis (1)	100% (8/8)
Yamao *et al.*	2008	5	Extrahepatic (5)	Pneumoperitoneum (1)	100% (5/5)
Brauer *et al.*	2009	12	Extrahepatic (12)	Peritonitis (1) Respiratory failure (1)	92% (11/12)
Park *et al.*	2009	14	Intrahepatic (9) Extrahepatic (5)	Pneumoperitoneum (2)	100% (14/14)
Horaguchi *et al*	2009	16	Intrahepatic (7) Extrahepatic (9)	Peritonitis (1) Stent migration (1)	100% (16/16)
Maranki *et al.*	2009	49	Intrahepatic (35) Extrahepatic (14)	Peritonitis (1), Pain (1), pneumoperitoneum (4), aspiration pneumonia (1), self-resolving bleeding (1)	84% (41/49)

cases of biliary peritonitis, and one case of bile perforation. There was also one case of ileus, three cases of stent malfunction, one early blockage, one death from complications of cirrhosis, three episodes of pain, one case of cholangitis, one aspiration pneumonia, and one case of self-resolving bleeding. The overall complication rate in these 135 cases was 19% (25/135).

Endoscopic ultrasound-guided biliary drainage has several advantages over percutaneous drainage, including the ability to visualize overlying vascular structures in real-time using color Doppler while attempting puncture of the biliary tree. It allows drainage without the need for an external drain, which can be a source of infection and discomfort. It should be performed by trained interventional endoscopists at a tertiary care center, with experienced pancreatobiliary surgeons and interventional radiologists available in the event of complications.

Chapter video clip

Video 39.1 Endoscopic ultrasound-guided drainage of malignant distal biliary stricture.

40 How to do EUS-guided Pelvic Abscess Drainage

Shyam Varadarajulu[1] and Sandeep Lakhtakia[2]

[1] University of Alabama at Birmingham School of Medicine, Birmingham, AL, USA
[2] Asian Institute of Gastroenterology, Hyderabad, India

Introduction

Development of pelvic abscess is a well-recognized complication in patients undergoing low anterior resection for rectal cancer or following medical conditions like inflammatory bowel disease. Traditionally, these abscesses are drained surgically or image guided (ultrasound or computed tomography [CT]) via the percutaneous, transrectal, or transvaginal routes. Although effective, surgical drainage is associated with a prolonged hospital stay, particularly when performed to manage a postoperative complication. The percutaneous drainage technique is less invasive than surgery but limits patient mobility and predisposes to fistula formation and infection. Also, the complex anatomy of the pelvis with surrounding bones, vascular structures, and other organs makes percutaneous access to the abscess cavity a technical challenge. By virtue of its ability to image and access extraluminal lesions, endoscopic ultrasound (EUS) has emerged as a minimally invasive therapeutic alternative for drainage of pelvic abscesses.

Patient preparation

A CT of the pelvis must be obtained to get a clear understanding of the abscess location prior to performing pelvic abscess drainage (Figure 40.1). Patients should be administered prophylactic antibiotics prior to the intervention and continued on oral antibiotics for 2–3 days. Bowel preparation with polyethylene glycol solution or enema is mandatory to minimize the chance of contamination and for adequate visualization. The procedure is best performed under fluoroscopy to visualize guidewire exchange and placement of stent or drain within the abscess. Patients should be instructed to void urine before the procedure as a distended bladder may impair visualization of small abscesses during EUS.

Devices and accessories

A therapeutic linear array echoendoscope with a working channel of 3 mm or more should be used to facilitate deployment of transluminal stents or drainage catheter. A 19-gauge endoscopic ultrasound-guided fine needle aspiration (EUS-FNA) needle is required for transluminal puncture into the abscess cavity, followed by passage of a 0.035 inch guidewire allowing it to coil inside the abscess cavity. A standard 4.5/5.0 French (Fr) endoscopic retrograde cholangiopancreatography (ERCP) cannula or a needle knife catheter is then railroaded over the guidewire into the abscess cavity. An over-the-wire balloon dilator (8–15 mm) is needed for subsequent dilation of the transmural tract. A double pigtail plastic stent (7 or 10 Fr) or drainage catheter is required to facilitate evacuation of the abscess cavity.

Procedural technique

The following steps are undertaken in sequence (Video 40.1):

- A rectal EUS examination is first undertaken to locate the pelvic abscess.
- After ensuring the absence of intervening vasculature using color Doppler, under EUS-guidance, a 19-gauge needle is used to puncture the abscess cavity to gain access into the fluid collection (Figure 40.2). Normal saline is used to flush the abscess cavity using a 20-ml syringe and re-aspirated to clean out the cavity of as much pus as possible. A sample of the aspirate should be sent for gram staining and culture.

Atlas of Endoscopic Ultrasonography, First Edition. Edited by Frank G. Gress, Thomas J. Savides, Brenna Casey Bounds, John C. Deutsch.

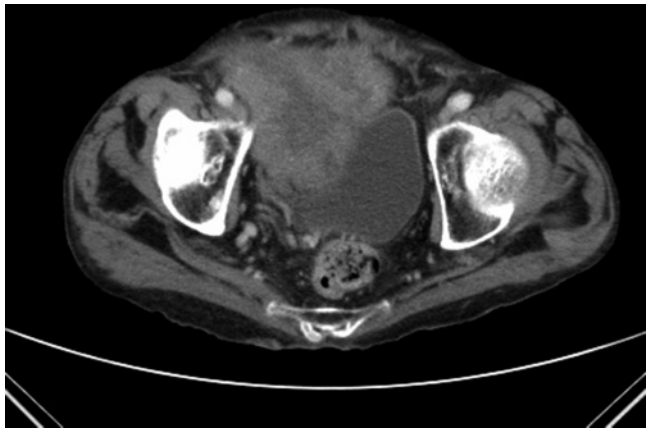

Figure 40.1 Computed tomography (CT) scan of the pelvis revealing an 8 × 7 cm abscess cavity.

Figure 40.2 Passage of a 19-gauge fine needle aspirate (FNA) needle into the pelvic abscess under endoscopic ultrasound (EUS) guidance.

(a)

(b)

Figure 40.3 A 0.035 inch guidewire is then coiled within the abscess cavity (a, endoscopy view) and this can be confirmed by fluoroscopy (b).

• An 0.035 inch guidewire is then passed via the 19-gauge needle and coiled within the abscess cavity (Figure 40.3a,b).
• The transmural tract is then first dilated by passing a tapered tip ERCP cannula (4.5/5.0 Fr) or a needle knife catheter through the working channel of the echoendoscope. The tract is further dilated using an 8–15 mm over-the-wire balloon (Figure 40.4a–c). The presence of a large opening will facilitate better drainage of the abscess and provide easy access for future interventions.
• A 7 or a 10-Fr double pigtail stent is then deployed over the guidewire into the abscess to establish complete drainage (Figure 40.5).
• In patients with pelvic abscesses measuring more than 8 cm in diameter or having thick content, a 10 Fr single pigtail drain may be placed in addition to the stent. To place a drain, guidewire (within cannula) is passed through the created opening, adjacent to the previously placed stent and then the drainage catheter is passed. The drain is secured to

(a)

(b)

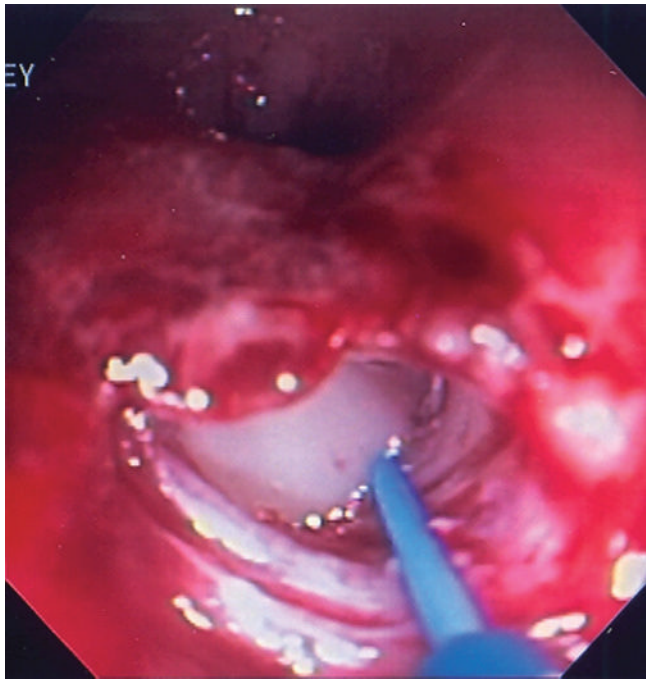

(c)

Figure 40.4 Fluoroscopy view revealing dilation of the tract by using an endoscopic retrograde cholangiopancreatography (ERCP) cannula (a) and then an over-the-wire balloon dilator (b). Pus is seen to extrude following dilation of the transmural tract (c).

the gluteal region by application of tape. The drain is then flushed with 50 cc of normal saline, every 4 hours, until the abscess is completely evacuated.

• A CT scan of the pelvis is obtained at 48 hours to assess response to therapy. If the abscess has decreased in size by more than 50%, the drain is discontinued and the patient is discharged home. After obtaining a follow-up CT at 2 weeks to confirm complete resolution of the abscess, the transrectal stent is removed by sigmoidoscopy.

Figure 40.5 Fluoroscopic view revealing the presence of a stent within the pelvic abscess cavity.

Clinical outcomes

In our experience with a carefully selected cohort of 25 consecutive patients, i.e. those with unilocular collections adjacent to the rectum or left colon, EUS-guided pelvic abscess drainage yielded a successful outcome in 96% of cases. No procedural complications were encountered and, unlike surgical or percutaneous techniques, patients were discharged home within 2–3 days following their procedures. In contrast to surgery and percutaneous techniques, EUS-guided drainage of pelvic abscess is less invasive, less costly, and is associated with minimal patient discomfort.

Technical limitations

Drainage of pelvic abscess cannot be undertaken when the wall of the abscess cavity is more than 20 mm from the EUS transducer. Also, the presence of multiple cavities in an abscess precludes successful drainage. It is important to carry out a helical CT scan before embarking on this procedure because poorly defined or multilocular fluid collections are not suitable for this non-surgical method of drainage. Also, stent deployment may not be possible in patients with pelvic abscess that measure less than 4 cm in size. As the linear array echoendoscope can be advanced only up to 40 cm in the colon, only those fluid collections adjacent to the rectum or left colon can be drained using this technique. Peri-anal fluid collections are not suitable for EUS-guided drainage.

Conclusions

Endoscopic ultrasound-guided drainage can be an effective treatment modality for management of patients with abscesses or fluid collections in the pelvis that are within the reach of the echoendoscope. Comparative studies with other treatment modalities that include a larger number of patients will help identify cases that will benefit the most from this technique.

Chapter video clip

Video 40.1 Video demonstrating the technique of EUS-guided pelvic abscess drainage.

41 How to do Doppler Probe EUS for Bleeding

Richard C. K. Wong
Case Western Reserve University and University Hospitals Case Medical Center, Cleveland, OH, USA

Background and equipment

Doppler ultrasound, in particular, use of the endoscopic Doppler ultrasound (DopUS) probe is quite different from traditional endoscopic ultrasound (EUS) and miniature EUS probes inasmuch that the currently available DopUS probe is non-imaging, the equipment is portable and significantly less expensive than EUS systems, and advanced endoscopic training in traditional EUS is not required. In addition, because the DopUS probe makes direct physical contact with the gastrointestinal (GI) tract lesion of interest, acoustic coupling with instilled water or with a water-filled balloon are not required. Signal output from the non-imaging DopUS probe system is in the form of an audible Doppler US signal with or without graphic display of the acoustic Doppler US waveform.

Within the last decade, two DopUS systems have been utilized in published studies: Endo-Dop (DWL GmbH, Singen, Germany) and VTI Endoscopic Doppler System (Vascular Technology Inc., Nashua, NH) (Figures 41.1 and 41.2). However, only the VTI system has received US Food and Drug Administration (FDA) clearance for use in GI endoscopy in the United States. Both systems are AC powered.

Practical application of DopUS probe

Advanced endoscopic training, detailed knowledge of EUS, or specific training in EUS is not required to use DopUS. The technique of DopUS can be readily acquired by most GI endoscopists in a relatively short time.

Modern DopUS probe systems utilize pulsed-wave ultrasound technology – this allows the endoscopist to vary scanning depth, to select the most appropriate depth for the specific bleeding lesion of interest, and to exclude deep serosal vessels ("innocent bystanders") that are not involved in the bleeding process. Available DopUS systems are small and portable, and can be easily placed on an emergency endoscopy cart for patients located in intensive care units or in operating rooms.

With current DopUS probe technology, a 16- or 20-MHz pulsed-wave ultrasound beam is emitted in a linear fashion from the distal tip of a small, flexible probe that is passed down the accessory channel of a standard diagnostic (or therapeutic) forward-viewing (or side-viewing) endoscope to make direct physical contact with the GI tract lesion of interest. It is important to select the scanning depth based on the lesion of interest: shallow (0–1.5 mm) for peptic ulcers versus mid (0–4 mm) for varices. Depending on the manufacturer, DopUS probes are marketed either as disposable, single-use only, or reusable after gas sterilization or high-level liquid disinfection.

Pre-procedure system check

Before each use, it is important to perform a pre-procedure check to ensure that the DopUS system is functioning appropriately. This is done by first connecting the DopUS probe to the base unit, turning the power on, and tapping the distal probe tip gently with an ungloved finger. In an appropriately functioning system, a corresponding tapping sound should be heard. In units that allow for adjustment of sound volume, this should be kept at maximum. The pre-procedure system check is then completed. Note that the system should be turned off before passing the probe through the accessory channel of the endoscope.

Doppler ultrasound signals

- Positive vs. negative vs. artifact:
  - Positive signal: A repetitive and similar audible and/or visual signal of at least three consecutive cycles duration.
  - Negative signal: Absence of a positive signal.

Atlas of Endoscopic Ultrasonography, First Edition. Edited by Frank G. Gress, Thomas J. Savides, Brenna Casey Bounds, John C. Deutsch.
 Published 2012 by Blackwell Publishing Ltd.

(a)

(b)

Figure 41.1 VTI endoscopic Doppler system. (a) A 20-MHz pulsed-wave Doppler ultrasound system. Doppler ultrasound output signal: audible only. Weight: 1.18 kg. United States Food and Drug Administration (FDA) clearance: yes. (Reproduced by permission of Vascular Technology, Inc., Nashua, NH.) (b) Doppler ultrasound probe: single-use, probe diameter 2.5 mm, lengths 165 cm and 245 cm. (Reproduced by permission of Vascular Technology, Inc., Nashua, NH.)

Figure 41.2 Endo-Dop, 16-MHz pulsed-wave, multigated Doppler ultrasound (DopUS) system with reusable DopUS probe and optional foot pedal. Doppler US output signal: visual and audible. Weight: 6.76 kg. United States Food and Drug Administration (FDA) clearance: no. (Reproduced by permission of Elsevier.)

  - Artifact signal: Simple movement of the probe tip against mucosa will produce a false, artifact signal – this can be readily differentiated from a positive signal by the fact that physical movement is required. In addition, artifact signals can occur if the probe tip is placed in an area where there are naturally transmitted pulsations, e.g. transmitted cardiac pulsations in the fundus of the stomach.
- Arterial vs. venous blood flow:
  - Arterial blood flow: Spiking, high-pitch sound and/or waveform.
  - Venous blood flow: Continuous, low-pitch sound and/or waveform.

Peptic ulcer (Figures 41.3–41.7)

- Irrigate the base of the ulcer with water to clear away any fibrinopurulent exudate.
- Position the DopUS probe in direct physical contact with the ulcer base using moderate pressure, at multiple points, including immediately adjacent to any stigmata of recent hemorrhage (SRH).
- The endoscopist should vary the angle of the probe with the ulcer base so as to minimize the chance of a false-negative Doppler signal. Note that a false-negative Doppler

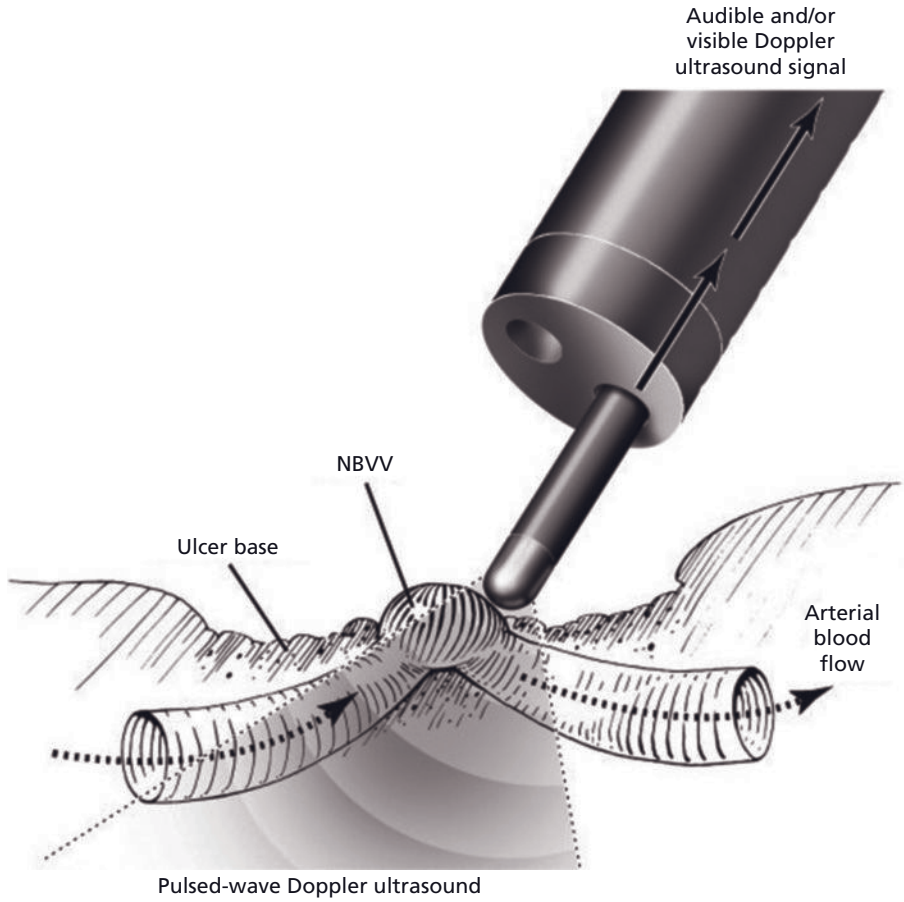

Figure 41.3 Illustration of a bleeding peptic ulcer with a non-bleeding visible vessel undergoing Doppler ultrasound (DopUS) examination using an endoscopic DopUS probe that was passed via the accessory channel of a standard endoscope. (Reproduced by permission of Elsevier.)

signal can occur if the ultrasound beam is directed at a right angle (90 degrees) to the subsurface blood vessel.

• Scanning depth: In peptic ulcer hemorrhage, the selection of scanning depth is dependant on whether there is increased physical distance between the ulcer base and the subsurface vessel of interest. For untreated ulcers, the scanning depth should be kept shallow (0–1.5 mm). For treated ulcers, selection of scanning depth depends on whether injection therapy was performed and whether a subsurface cushion (or bleb) of injectate (fluid) is still present at the time of the DopUS examination. Thus, if injection therapy is performed alone (monotherapy), scanning depth should be increased to mid-range (0–4 mm) because of the existence of the subsurface fluid bleb. On the other hand, if dual combination therapy is performed (injection therapy first followed by thermal-contact therapy with a heat probe or bipolar probe), then the subsurface fluid bleb has been eliminated by the cratering effect of the thermal-contact treatment and scanning depth can be kept shallow (0–1.5 mm).

◦ Shallow (0–1.5 mm):
  (a) Untreated peptic ulcer.
  (b) Injection followed by thermal-contact therapy.
  (c) Thermal-contact therapy alone.
  (d) Endoclip therapy alone.

◦ Mid (0–4 mm):
  (a) Firmly adherent clot.
  (b) Injection therapy alone.
  (c) Injection followed by endoclip.

◦ Deep (0–7 mm):
  (a) Usually not needed.

Published studies

Published studies using the DopUS probe in acute peptic ulcer bleeding have demonstrated the following:

1. Recurrent bleeding is significantly more likely to occur in ulcers that are Doppler positive than in those that are Doppler negative.

2. Ulcers that remain Doppler positive immediately after endoscopic therapy are at significantly increased risk of recurrent bleeding than in those where the Doppler signal is abolished.

3. Positive correlation exists between endoscopic SRH and Doppler signal (Table 41.1).

Clinical scenarios

Clinical scenarios where use of the endoscopic DopUS probe could be useful include the evaluation of uncertain visual SRH, in the assessment of adequacy of endoscopic

(a)

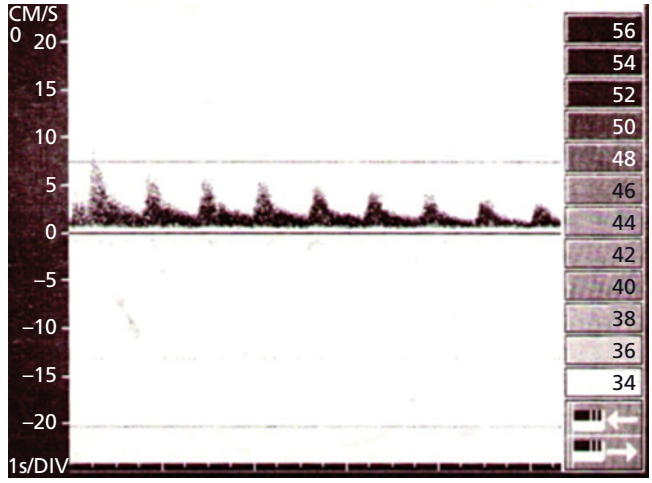

(b)

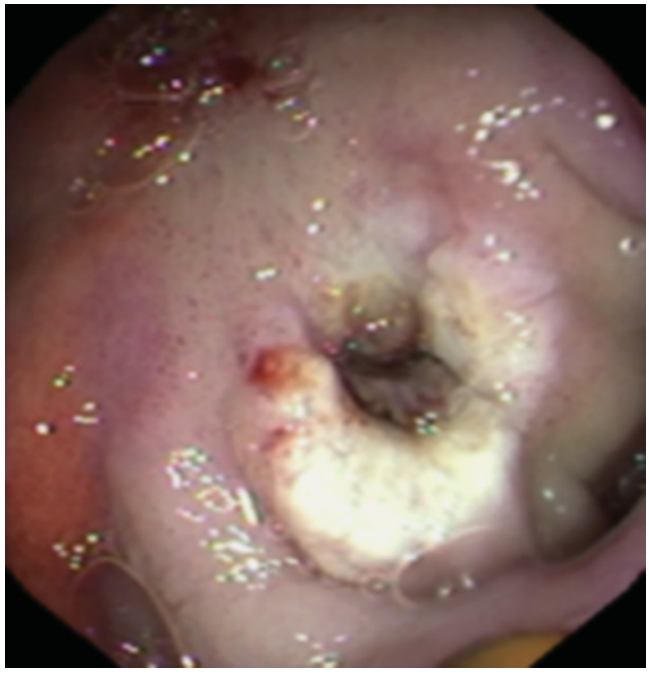

(c)

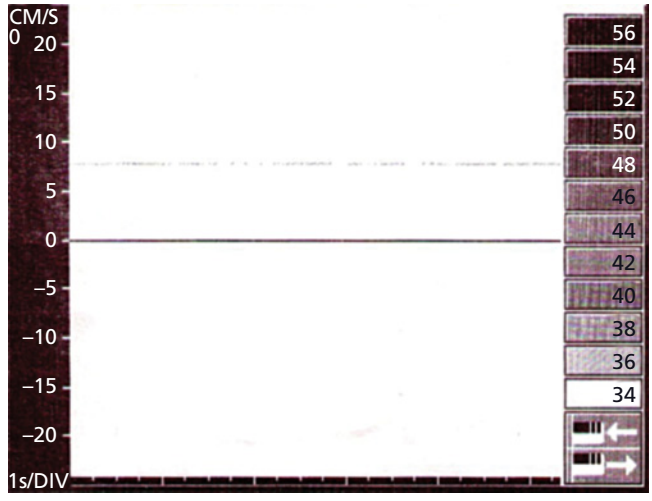

(d)

Figure 41.4 Doppler ultrasound (DopUS) in acute peptic ulcer bleeding. (a) Endoscopic image of a DopUS probe on a bleeding duodenal ulcer with a non-bleeding visible vessel: Doppler positive. (b) Visual graphic display of the corresponding positive DopUS signal (*y* axis: frequency shift [kHz]; *x* axis: time [s]). (c) Endoscopic image of the same ulcer after combination endoscopic therapy with epinephrine injection and heat probe: Doppler negative. (d) Visual graphic display of the corresponding negative DopUS signal. (Reproduced by permission of Elsevier.)

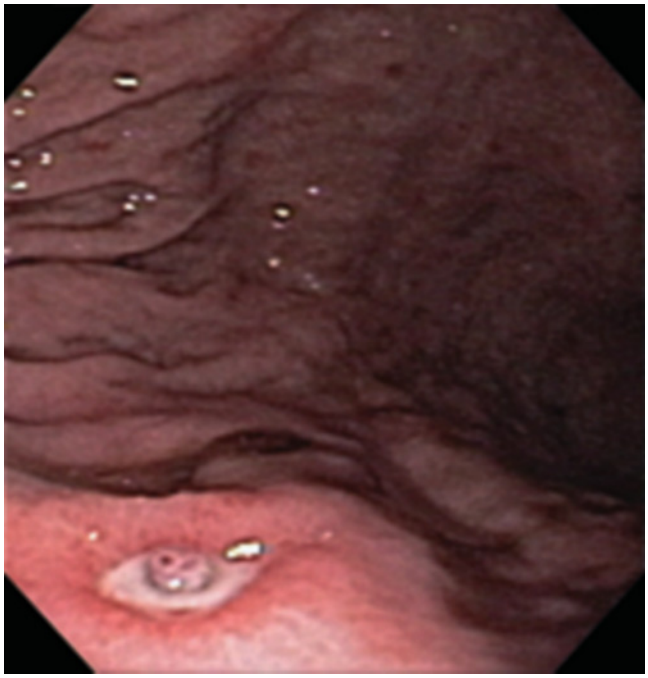

(a)

(b)

(c)

Figure 41.5 Doppler ultrasound-guided hemostasis in acute peptic ulcer bleeding. (a) Gastric ulcer with a non-bleeding visible vessel: Doppler positive. (b) Immediately following dual combination endoscopic therapy with epinephrine injection and heat probe: Doppler positive. (c) Targeted, additional heat probe application to location of positive Doppler signal: Doppler negative. No recurrent bleeding at 30 days.

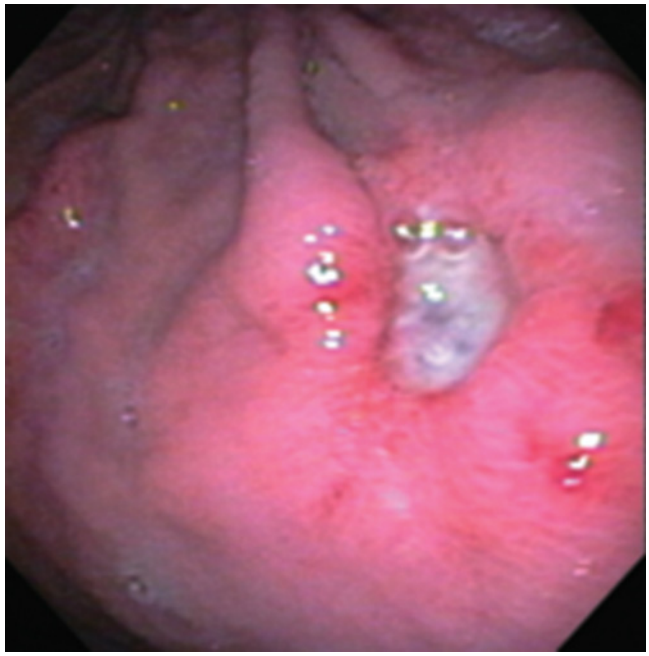

Figure 41.6 Atypical peptic ulcer bleeding – recurrent, major bleeding from a gastric ulcer, clean base, without stigmata of recent hemorrhage (it required a 7 unit blood transfusion in a healthy 23-year-old man). Doppler ultrasound (DopUS) localized a strongly positive arterial Doppler at the 11 o'clock position, targeted DopUS-guided hemostatic therapy was performed with no recurrent bleeding at 30 days.

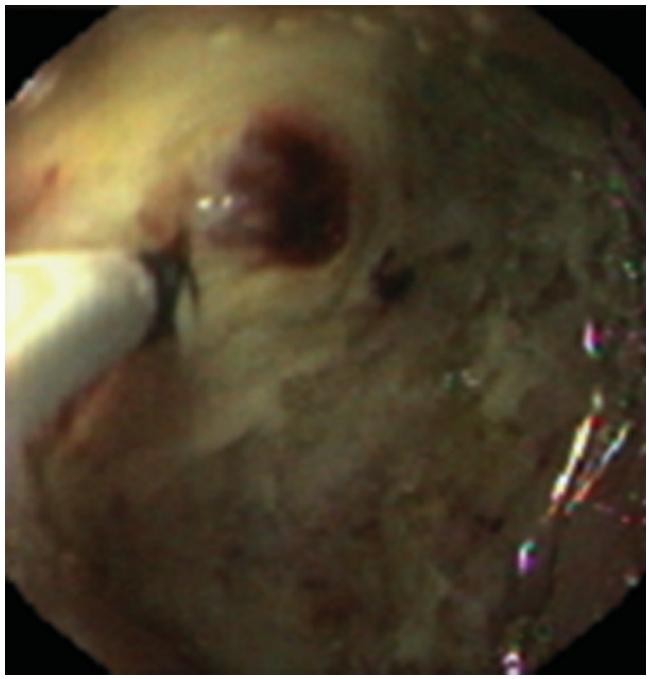

Figure 41.7 Doppler-negative non-bleeding visible vessel. Endoscopic image of a Doppler ultrasound (DopUS) probe being placed on an untreated bleeding duodenal ulcer. (Reproduced by permission of Elsevier.)

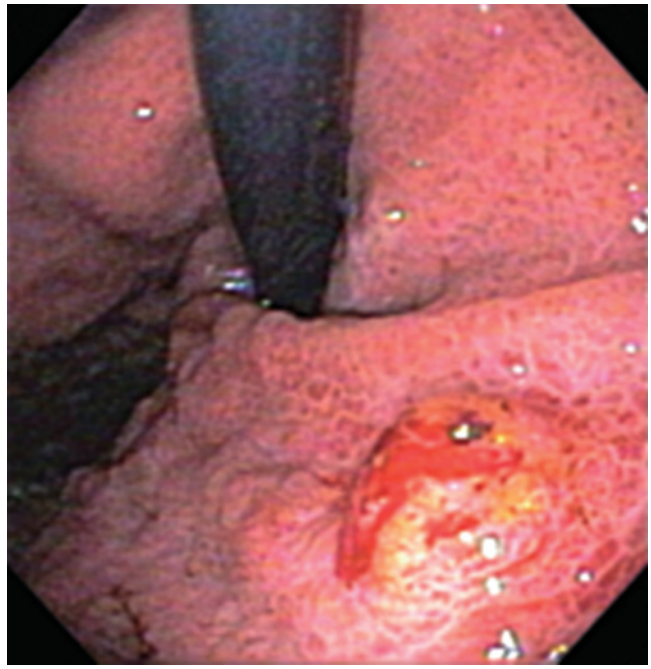

Figure 41.8 Atypical appearance of a bleeding gastric varix. Mild active oozing of blood from a single, small, yellowish submucosal lesion in the gastric fundus, Doppler positive. (Reproduced by permission of Elsevier.)

Table 41.1 Correlation of endoscopic appearance of peptic or anastomotic ulcers with endoscopic Doppler ultrasound signal.

Endoscopic appearance	Doppler (+) (%)
Active bleeding (spurting)	100
Active bleeding (oozing)	60
Non-bleeding visible vessel	44
Adherent clot	14
Flat pigmented spot	9
Clean base	11

hemostatic therapy, and in the evaluation of bleeding ulcers that behave functionally as high risk but which appear to be low risk by visual stigmata alone (e.g. recurrent bleeding from a clean-based ulcer or ulcer with flat pigmented spot).

Gastric varices vs. thickened gastric folds vs. GI stromal tumor (GIST) (Figures 41.8 and 41.9)

- Place probe tip on lesion of interest using light pressure.
- Scanning depth: Mid (0–4 mm).
- Vary incident angle.
  - Gastric varices: Continuous, low-pitch sound and/or waveform. Consistency: soft.
  - Thickened gastric folds: No Doppler signal. Consistency: soft.

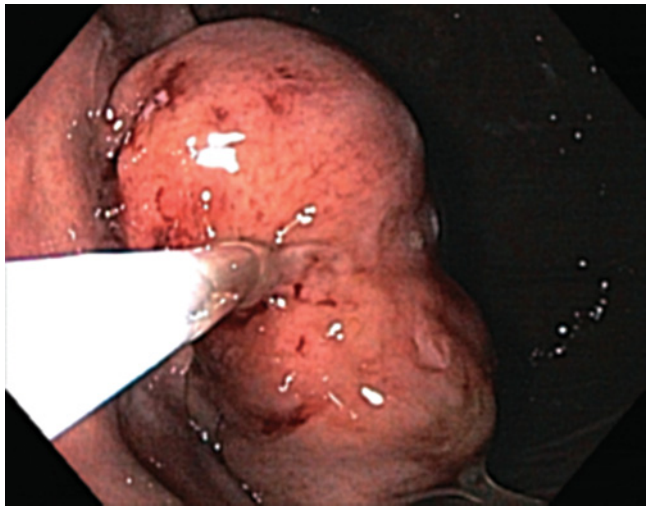

Figure 41.9 Doppler ultrasound examination of a gastrointestinal stromal tumor (GIST) in the gastric fundus, Doppler negative. (Reproduced by permission of Elsevier.)

Figure 41.11 Dieulafoy lesion in rectum, Doppler with strong arterial signal.

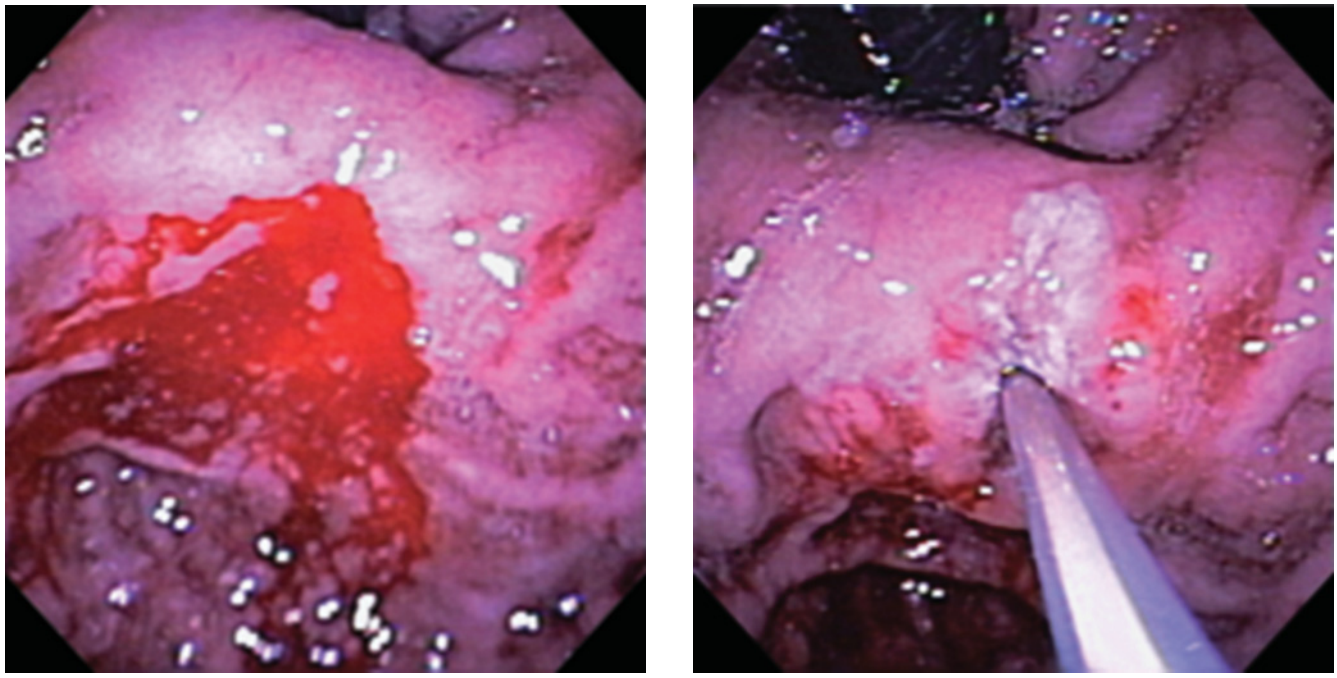

(a) (b)

Figure 41.10 Dieulafoy lesion in gastric cardia. (a) Active bleeding. (b) Doppler ultrasound (DopUS) probe examination immediately following dual combination hemostatic therapy.

  - GIST: ± Doppler signal, but only at base of lesion. Consistency: firm.

- DopUS probe-guided glue injection of bleeding gastric varices. Although there are reports of this technique being used, further studies are required to evaluate its clinical utility.

Miscellaneous disorders

DopUS probe has been used in the following disorders – further studies are required to evaluate clinical utility.

- Dieulafoy's lesion (Figures 41.10 and 41.11).
- Diverticular bleeding.

- Colonic polyps.
- Esophageal varices.
- Major papilla before endoscopic retrograde cholangiopancreatography (ERCP) with sphincterotomy.
- Post-endoscopic submucosal dissection (ESD) ulcer.

Conclusions

The endoscopic DopUS probe allows the endoscopist to determine the presence or absence of subsurface blood flow in bleeding lesions, to differentiate between arterial and venous blood flow, to estimate depth of the subsurface blood vessel, and to estimate location of the subsurface blood vessel. Being able to generate such a subsurface map of blood flow could potentially allow for precise targeting and titration of endoscopic hemostatic therapy based, not on visual surface stigmata alone, but with additional knowledge of subsurface blood flow.

Conflicts of interest disclosure

The author has received research funding from Vascular Technology, Inc.

Chapter video clips

Video 41.1 Peptic ulcer bleeding.

Video 41.2 Gastric varices.

Index

Note: page numbers in *italics* refer to figures and those in **bold** refer to tables

Atlas of Endoscopic Ultrasonography, First Edition. Edited by Frank G. Gress, Thomas J. Savides, Brenna Casey Bounds, John C. Deutsch.